THE UNIVERSITY OF HULL

Positron emission tomography imaging agents with gallium-68:

bifunctional chelators and multimodality

being a Thesis submitted for the Degree of

Doctor of Philosophy in the University of Hull

by

Benjamin Peter Burke, BSc (Hons)

August 2013

Abstract

Positron emission tomography (PET) as a nuclear medicine technique offers very high sensitivity compared with other imaging modalities. PET is often combined with computed tomography (CT) to offer structural information. Incorporation of a positron emitting metal radioisotope such as ^{68}Ga requires a bifunctional chelator (BFC) to form a stable complex *in vivo* and for covalent bond formation (conjugation) with a targeting moiety. In this work, the routinely used macrocyclic BFC DOTA has been modified to replace an acetate arm with a benzimidazole unit to give an alternative BFC structure. It does not affect coordination number, has a secondary amine for bioconjugation and is a chromophore, therefore increasing the number of potential applications beyond DOTA to include optical properties (fluorescence and lanthanide luminescence sensitisation). Four benzimidazole DO3A derivatives have been synthesised and radiolabelled with ^{68}Ga in comparable radiochemical yields to the structurally similar DOTA. Reaction conditions of *ca.* 5 minutes at room temperature are shorter and milder than those required for DOTA, which can cause degradation of conjugated biomolecules.

Magnetic resonance imaging (MRI) can replace CT as the structural partner in clinical PET imaging and has many advantages including the potential for use of MRI contrast agents. PET/MRI is an emerging field and there is scope for the development of multimodal imaging constructs combining a PET radioisotope with a MRI contrast agent. In this work, super-paramagnetic iron oxide nanoparticles (SPIONs) as T_2 MRI contrast agents have been functionalised with a range of macrocyclic derivatives and radiolabelled with ^{68}Ga in near quantitative yields to form PET/MRI multi-modal imaging agents which have been shown to be stable to EDTA competition and in serum over four hours. Modification of the surface of the SPIONs was shown to have no detrimental effect to their clinical applicability by size variation (aggregation).

The use of the chelators synthesised in the work for other applications is also of interest, with preliminary studies carried out towards the development of ^{86}Y and ^{90}Y agents for PET and radioimmunotherapy respectively. Benzimidazole DO3A, along with the corresponding yttrium(III) and europium(III) complexes were studied by potentiometric titration, luminescent lifetime measurements and variable temperature NMR to fully characterise the coordination sphere and gain insight into their physicochemical characteristics.

Risk Assessment

All experiments were carried out in accordance with the University of Hull's Health and Safety guidelines. A full COSHH and risk assessment was carried out for each new experiment, signed by the undertaking student, supervisor (Dr S.J. Archibald) and the departmental safety officer (Dr T. McCreedy) before any practical work started. The COSHH forms carry the reference numbers BPBSJA1-BPBSJA32. Radiochemistry experiments were assessed using the PET Research Facility Risk Assessment Form, signed by the undertaking student, supervisor (Dr S.J. Archibald) and the radiation protection supervisor (Dr S.J. Archibald) before radiochemical experiments were carried out, with the forms carrying the reference numbers BPBRU1-BPBRU3.

Acknowledgements

First of all I would like to thank Dr. Steve Archibald, for his scientific ideas, personal supervision, patience and enthusiasm. I could not be more grateful that he even entertained my idea of doing a PhD under him when I was a third year undergraduate student, since then he has supported my goals and pushed me to be the best researcher I can be without me noticing I was being pushed.

To all past and present members of the Archibald group, I enjoy being in the group immensely. I think I have every emotion every day except boredom; humour, anger, confusion, delight, frustration and joy. All of which make my life eventful and entertaining and all are better than the dreaded feeling of being bored. In no particular order (except chronological) I would like to thank: Rachel, Neazar, Seraj, Ali, Kati, Mustafa, Bassim and Shubhanshi.

I would like to also thank all the people who helped me during my PhD: Carol Kennedy for running CHN samples; Dr. Kevin Welham for running MS samples; Neazar Baghdadi for help with NTA; Dr. Bob Knight for ICP analysis; Prof. Françoise Chuburu's group for potentiometric titrations; Dr. Mark Lorch's group for T_2 measurements; Prof. Stephen Faulkner's group for lanthanide luminescent measurements; Prof. Raphaël Tripier and his group for PET/MRI collaboration and welcoming me in Brest to do some chemistry along with the COST programme for funding the visit. I also offer special thanks to Gonçalo Clemente for immeasurable help and advice with radiochemistry.

Finally and most importantly I would like to thank my parents. Not only for supporting me through my PhD but more significantly for setting me up to be in a position to have the opportunity. Your ability to have the strength to trust me to make my own decisions and mistakes puts me in the situation I am in today. Without your parenting I would be at Prospect.

Abbreviations

3D	Three dimensional
ATSM	Aromatic bis(thiosemicarbazonates)
$\beta+$	Positron (beta plus)
$\beta-$	Electron (beta minus)
B_0	Magnetic field direction
BFC	Bifunctional chelator
Boc_2O	Di-*tert*-butyl dicarbonate
BODIPY	Boron dipyrromethene
BP	Bisphosphonate
Bq	Becquerel's
CB	Cross bridged
CB-MP	Cross bridged mono picolinate
CB-TE2A	2,2'-(1,4,8,11-Tetraazabicyclo[6.6.2]hexadecane-4,11-diyl)diacetic acid
CT	Computed tomography
C-TETA	Carbon functionalised TETA
CuAAC	Copper(I)-catalysed azide-alkyne cycloaddition
DCM	Dichloromethane
DMA	Dimethylacetamide
DMF	Dimethylformamide
DMPTACN	1,4-Bis(2-pyridylmethyl)-1,4,7-triazacyclononane
DOPA	3,4-Dihydroxyphenylalanine
DOTA	1,4,7,10-Tetraazacyclododecane-1,4,7,10-tetraacetic acid
DOTP	1,4,7,10-Tetraazacyclododecane-1,4,7,10-tetra(methylenephosphonic acid)
DO3A	1,4,7-Tris(*tert*-butoxycarbonylmethyl)-1,4,7,10-tetraazacyclododecane
DTPA	Diethylene triamine pentaacetic acid
EC	Electron capture
EDTA	Ethylenediamine tetraacetic acid
ESI	Electrospray ionization
EtOH	Ethanol

FDA	Food and drug administration
FDG	2-Fluoro-2-deoxy-D-glucose
GPTES	(3-Glycidyloxypropyl)triethoxysilane
HPLC	High performance liquid chromatography
HRMS	High resolution mass spectrometry
ICP	Inductively coupled plasma
ICP-OES	Inductively coupled plasma optical emission spectroscopy
keV	Kilo electron volt
logP	Partition coefficient
MALDI	Matrix-assisted laser desorption/ionisation
MeCN	Acetonitrile
MeOH	Methanol
MRI	Magnetic resonance imaging
MS	Mass spectrometry
NIR	Near-infared
NMR	Nuclear magnetic resonance
NMV	Net magnetisation vector
NOTA	1,4,7-Triazacyclononane-1,4,7-triacetic acid
NTA	Nanoparticle tracking analysis
PEG	Polyethylene glycol
PET	Positron emission tomography
ppm	Parts per million
RCY	Radiochemical yield
RGD	Arginylglycylaspartic acid
RES	Reticuloendothelial system
rf	Radio frequency
RT	Room temperature
SD	Size distribution
SM	Starting material
SPECT	Single photon emission computed tomography
SPION	Super-paramagnetic iron oxide nanoparticle

τ	Luminescence lifetime
$t_{1/2}$	Half-life
T_1	Longitudinal or spin-lattice relaxation
T_2	Transverse or spin-spin relaxation
TACN	1,4,7-Triazacyclononane
*t*Bu-DO3A	1,4,7-Tris(*tert*-butoxycarbonylmethyl)-1,4,7,10-tetraazacyclododecane
TEA	Triethylamine
TFA	Trifluoroacetic acid
THF	Tetrahydrofuran
TETA	2-[4-nitrobenzyl]-1, 4, 8, 11-tetraazacyclotetradecane N,N',N'',N'''-tetraacetic acid
TLC	Thin layer chromatography
TMS	Tetramethylsilane
TRAP	1,4,7-Triazacyclononane-1,4,7-tris[(2-carboxyethyl)methylenephosphinic acid]
UV	Ultra-violet
US	Ultrasound
ω	Larmors frequency

Table of Figures

IX

Table of Schemes

Table of Contents

XIX

Chapter 1

Introduction

1. Introduction

1.1. Medical Imaging

Medical imaging is a broad term which relates to the imaging of the intact human body for clinical reasons such as medical diagnosis or the study of disease physiology. The term 'medical imaging' encompasses, amongst many others, nuclear medicine techniques such as positron emission tomography (PET) and single-photon emission computed tomography (SPECT), along with structural techniques such as computed tomography (CT) and magnetic resonance imaging (MRI) and imaging modalities with more niche uses such as optical and ultra-sound (US). Each individual technique has specific advantages, disadvantages and situations in which is it used clinically, see Figure 1.
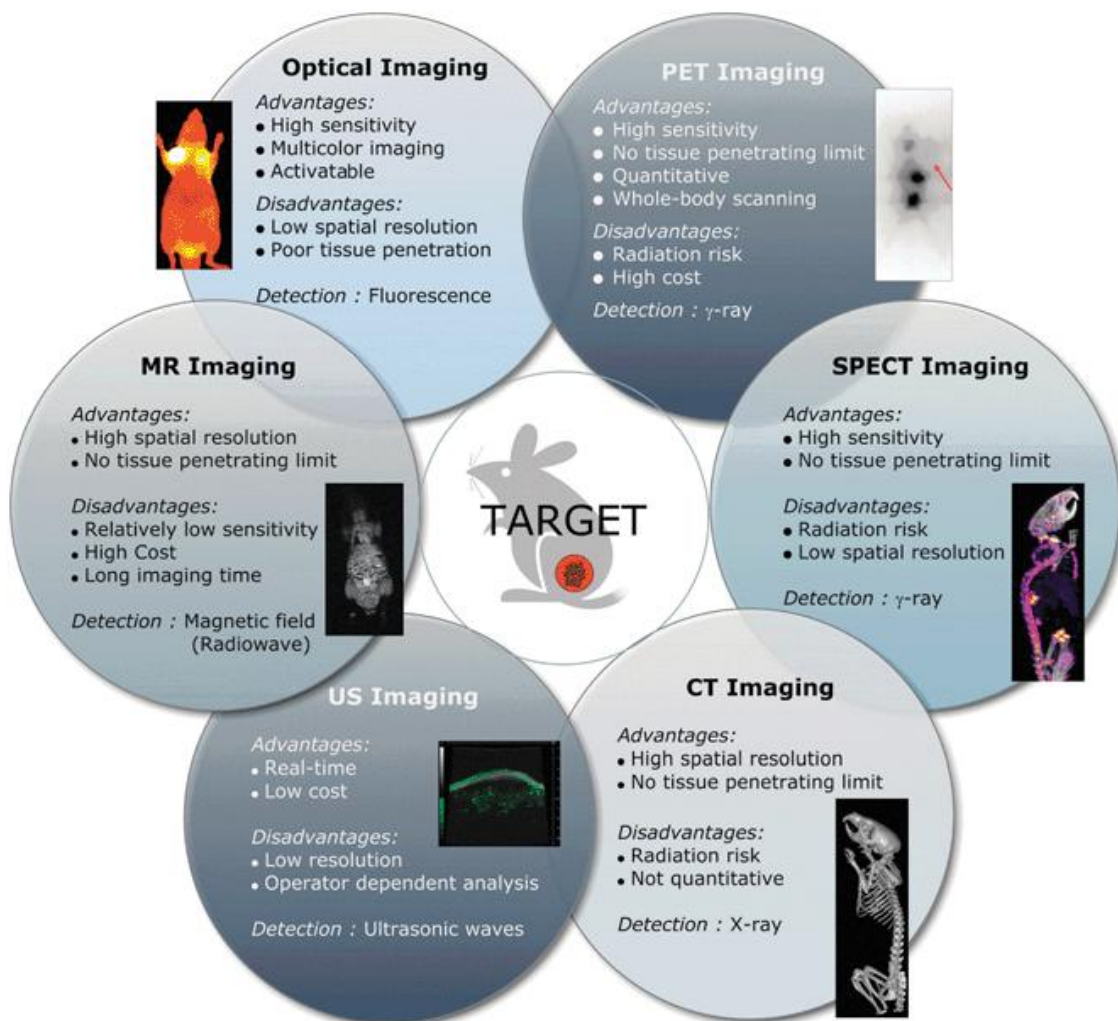
Figure 1 – Characteristics of the medical imaging modalities.[1]

1.1.1. Molecular imaging

Molecular imaging studies cellular and molecular events of a living organism in a non-invasive manner, giving the potential to study biological processes such as tumour receptor overexpression or intracellular protein interactions in their natural state without causing a biological response. Imaging biological responses, such as tumour receptor overexpression, gives information about disease states and aids in clinical diagnosis or the monitoring of disease progression.

1.1.1.1. Nuclear Medicine

Diagnostic nuclear medicine deals with the use of radionuclides and relies on the process of radioactive decay to give an *in vivo* image of the radiopharmaceutical distribution, with the most common types being single-photon emission computed tomography (SPECT) and positron emission tomography (PET).

Figure 2 – The Siemens Biograph mMR PET/MRI scanner.[2]

1.1.1.1.1. Single photon emission computed tomography (SPECT)

Single photon emission computed tomography (SPECT) is a nuclear medicine technique which relies on the detection of gamma ray producing radionuclei. SPECT as an imaging technique grew out of the use of planar imaging for gamma rays, and was developed into a 3D system. SPECT is routinely combined with CT for structural information, and SPECT/CT is routinely used in myocardial perfusion, bone and brain imaging.[3,4]

The gamma emitting radionuclides used for SPECT imaging usually have either long enough half-lives to be easily transported to clinics (^{111}In), or use a generator based system (^{99m}Tc), thus eliminating the need for an on-site cyclotron, saving significant structural costs for the facility. Radiotracers for SPECT are routinely synthesised using radiochemical 'kits' via relatively straightforward procedure. Syntheses which can be carried out by a radiopharmacist eliminate the need for a radiochemist on site. In general therefore, infrastructure costs for SPECT are much lower than for PET.[4]

^{99m}Tc is the most widely used SPECT radioisotope, with a half-life of 6 hours allowing multi-step syntheses to be undertaken if required. ^{99m}Tc SPECT scans form the large majority of nuclear medicine images collected, with 85% of all diagnostic radionuclear scans in the United States in 2007.[5] Its popularity is due largely to it being produced on a generator from the parent isotope ^{99}Mo. ^{99}Mo has a half-life of 66 hours, which allows daily production on a generator and the routine use of ^{99m}Tc clinically. There are a large number of radiopharmaceuticals used clinically with ^{99m}Tc,[6] one example is ^{99m}Tc-sestamibi which is used for myocardial perfusion and breast tumour imaging.[7]

Behind ^{99m}Tc, ^{111}In is the most widely used SPECT radioisotope.[8] ^{111}In has a half-life of 2.8 days which makes it useful for antibody radiolabelling in imaging.[8] Two ^{111}In radiopharmaceuticals are FDA approved and several more are in late stage clinical trials.[9] In aqueous media, ^{111}In is only stable in the oxidation state III and is a hard Lewis acid, preferring hard Lewis bases such as oxygen and nitrogen.[9] Its large size means it can reach coordination numbers of up to eight; a description which is similar to the characteristics of larger lanthanides. These characteristics mean that chelators which are used for gadolinium(III) as MRI contrast agents, including some chelators regularly used for ^{68}Ga and ^{64}Cu, namely DOTA and TETA, are also suitable for ^{111}In. This eliminates the need to develop

specialised chelators to use ^{111}In SPECT as is to produce highly stable ^{99m}Tc complexes with suitable characteristics for imaging.

1.1.1.1.2. Positron emission tomography (PET)

Positron emission tomography (PET) is a non-invasive functional imaging technique with high sensitivity and accurate quantification.[10] PET also has the advantage of being able to detect molecular events and physiological processes in living subjects. Molecular imaging of this nature has distinct advantages over medical imaging techniques such as magnetic resonance imaging (MRI), computed tomography (CT) and X-ray that are inadequate for early stage disease diagnosis. These techniques provide mostly organ structure and detailed anatomical images, giving little or no information about metabolic or molecular events, making detection limited to structural abnormalities. PET can measure chemical changes before macroscopic anatomical signs and patient symptoms are observed.[11-12]

Radiopharmaceuticals only have to be administered at nanomolar/picomolar levels which are sufficient for good detection levels but low enough not to interfere with biological processes, this is known as the true tracer principle. PET radionuclides are limited to isotopes which decay, in some or all parts, by positron emission and have a long enough half-life to be practically useful, either for use directly as produced, or by incorporation into more complex molecules using synthetic procedures.

The choice of PET radionuclide is determined by its physical and chemical characteristics, availability, and maybe most importantly its decay half-life.[13] The half-life must be long enough to allow chemical incorporation of the radionuclide in the target compound, and match the biological half-life of the corresponding tracer to avoid unnecessary irradiation. The labelled probe must be synthesised, purified and analysed usually within a few half-lives for there to be enough radiolabelled material to administer to a patient to obtain a good quality PET scan.[10] PET radionuclides are broadly separated into two groups, non-metals and metals, see Table 1, with each group generally used for a different purpose. Non-metallic elements generally used for small organic molecule labelling and radiometals used when labelling biomolecules (*vide infra*).

Radionuclide	Half-life	Method of production	Decay characteristics
^{11}C	20.3 mins	Cyclotron	β^+ 98%
^{13}N	9.97 mins	Cyclotron	β^+ 100%
^{15}O	2.04 mins	Cyclotron	β^+ 100%
^{18}F	110 mins	Cyclotron	β^+ 97%
^{64}Cu	12.7 hours	Cyclotron	β^+ 19%
			EC 41%
			β^- 40%
^{68}Ga	1.1 hours	Generator	β^+ 90%
			EC 10%
^{86}Y	14.7 hours	Cyclotron	β^+ 33%
			EC 67%
^{89}Zr	78.5 hours	Cyclotron	β^+ 23%
			EC 77%

Table 1 – Properties of commonly used PET radioisotopes.[8,11]

Radioisotope production begins with either a generator, a nuclear reactor or a cyclotron. A generator system is used when the parent isotope of the desired PET isotope is an unstable, but slow decaying isotope, for example ^{68}Ge/^{68}Ga generators use the half-life of ^{68}Ge (271 days). A cyclotron is a compact particle accelerator which generates a proton or deuteron beam. The beam is directed onto the target material which is suitable for the production of the required isotope.[11]
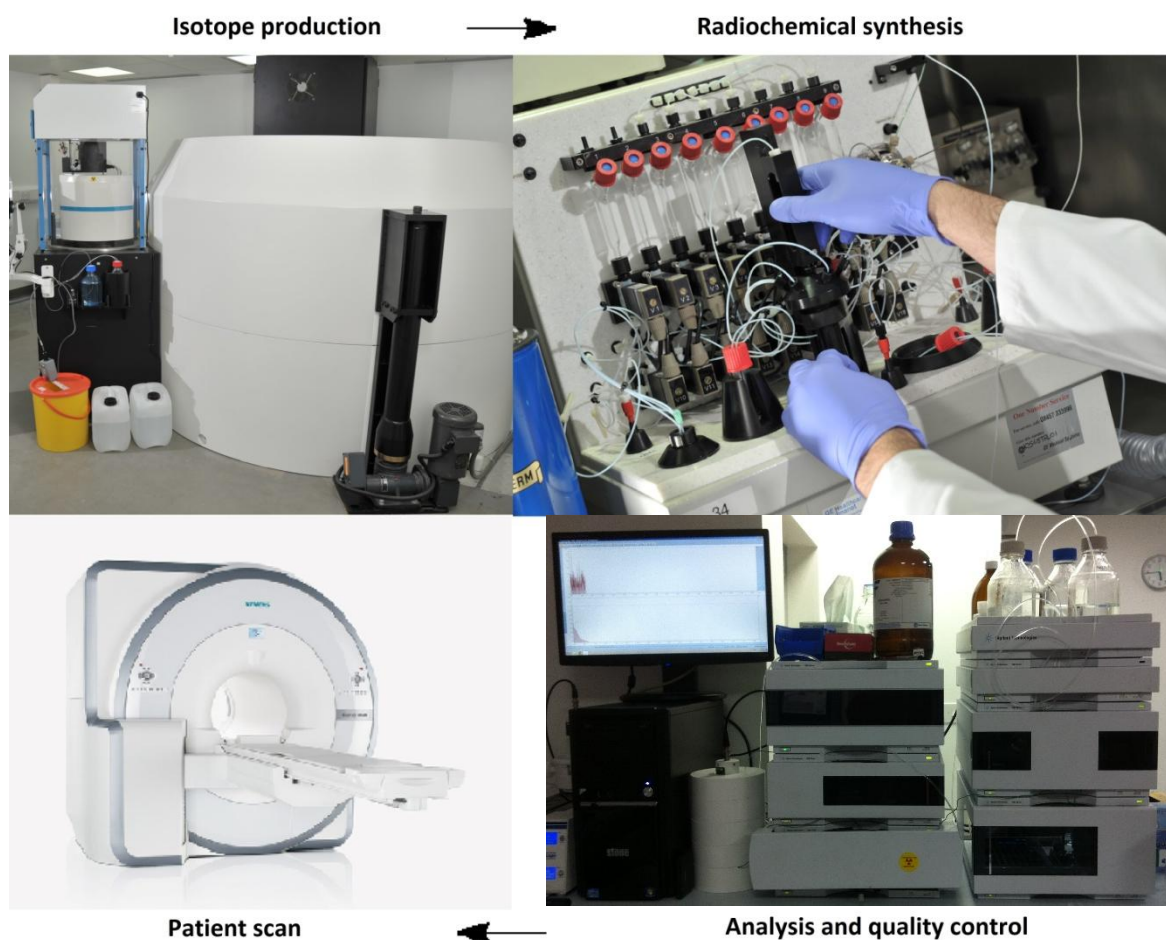
Figure 3 – "Bench-to-bedside" radionuclide production from cyclotron to patient.

Standard bench-top chemistry is not an option when working with radioactive isotopes and the use of thick lead-lined 'hot cells' is widespread in radiosynthetic laboratories, the fresh radiolabelled product is transferred directly from the cyclotron to the hot cell usually using an inert gas stream where it can be used in further synthesis, a process which is usually either computer controlled or automated. Once synthesis is completed, a number of rigorous quality control measures must be followed to ensure the radiopharmaceutical is pure and sterile, amongst other things. Finally, the radiotracer can be distributed for patient use, see Figure 3.

PET is a way of indirectly detecting levels of radioactivity. A fragment of decay is positron emission (β^+), which then travels a short distance (1-2 mm) until the positron encounters an electron. The distance positrons travel before annihilation is directly related to its kinetic energy, with ^{18}F and ^{68}Ga having mean positron ranges of 0.27 mm and 1.05 mm respectively, leading to a slightly lower sensitivity when using ^{68}Ga.[14] The annihilation results in two γ ray photons with energy of 511 KeV at close to 180° to each other. Simulation detection via a circular ring of detectors around the patient gives the location of the radiolabel, see Figure 4, with each detector connected in a coincidence circuit with a detector located on the opposite side of the ring. A large amount of computing power using complex mathematical models is needed to process the raw data into quantified data to build a 3D volume for the whole body or studied organ.[15]
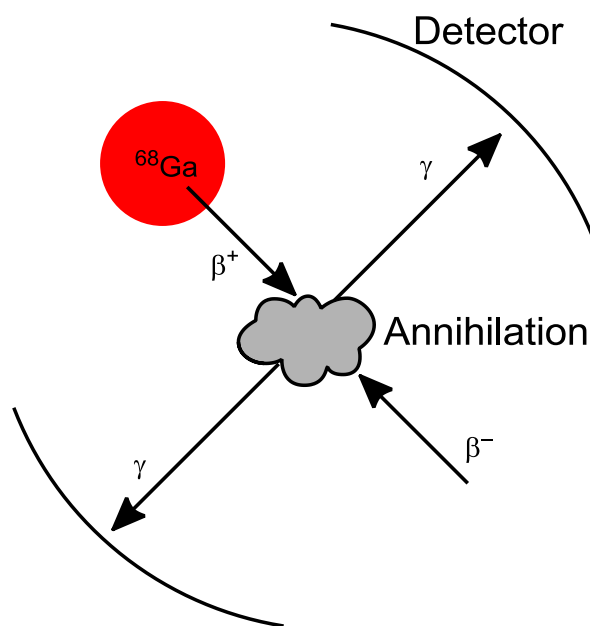
Figure 4 – Schematic representation of the principle behind PET.

Due to the lack of anatomical information of PET, it is routinely coupled with computed tomography (CT), giving an overlaid image which has the high sensitivity of PET with the high resolution of CT.

1.1.1.1.2.1. Non-Metallic radionuclides

Most PET radionuclides are low atomic mass elements (^{13}N, ^{15}O, ^{11}C, ^{18}F) which can directly replace stable analogues without interfering with the biological activity of the molecule. This capability differentiates PET from other imaging techniques where the imaging 'handle' is usually a large molecule which, when attached, sometimes affects its bioactivity.[11]

The half-lives of non-metallic radionuclides are short (2-110mins) which makes them favourable due to minimising the body's exposure to radiation. ^{11}C and ^{18}F decay by pure positron decay, making them suitable for PET and limiting the body's exposure to other decay types.[16] However, this is generally unsuitable for labelling biomolecules (proteins/antibodies) due to the high temperatures needed for standard radiolabelling and the biological half-life commonly being longer than the decay half-life.

Synthetic routes must be designed so that the incorporation of the unstable isotope is carried out at a late stage in the synthesis and therefore maximising the activity of the isotope in the produced imaging agent. In general, the timeframe for synthesis and purification of the radiolabelled compound should be no longer than two to three half-lives.[3,17]

1.1.1.1.2.2. Metal ion radionuclides

Metal ion radionuclides have different advantages and disadvantages when compared with using non-metals. They generally have longer half-lives, see *table 1*, which are favourable when radiolabelling biomolecules which have longer biological half-lives than non-metal radioisotopes,[8] this could also be seen as a disadvantage as this would mean longer radiation exposure to the patient. The long half-lives mean that off-site production and transportation is also possible for some isotopes. The fact that the radioactive decay of metal isotopes is not usually by pure positron emission can be seen as either an advantage or a disadvantage.

1.1.1.1.2.2.1. [64]Cu

[64]Cu has an intermediate half-life (12.7 hours) which allows for production and delivery across different sites and also allows its use with a wide range of biomolecules including antibodies.[16,18]

[64]Cu decays by 18% β^+ which means that the resolution of the image will be decreased or more tracer must be administered and decay by the other pathways can cause both unnecessary radiation to patients and make image reconstruction more challenging when the isotope decays to a gamma product. In some cases this can also be seen as a positive as it also decays by 40% β^- decay which can therefore be used as a simultaneous diagnosis/treatment isotope.

In aqueous environments, copper is generally in the oxidation state II and exhibits Jahn-Teller distortion, as would be predicted for the $3d^9$ electron configuration. Copper(II) is a borderline hard Lewis acid and prefers donors such as nitrogen,[8,19] with a common coordination number of six.[20] Copper(I) is $3d^{10}$ and is therefore much more labile to ligand exchange, therefore kinetic inertness of the copper(II) chelate complex and avoiding reduction to copper(I) are of primary importance for *in vivo* stability.[9,16,21]
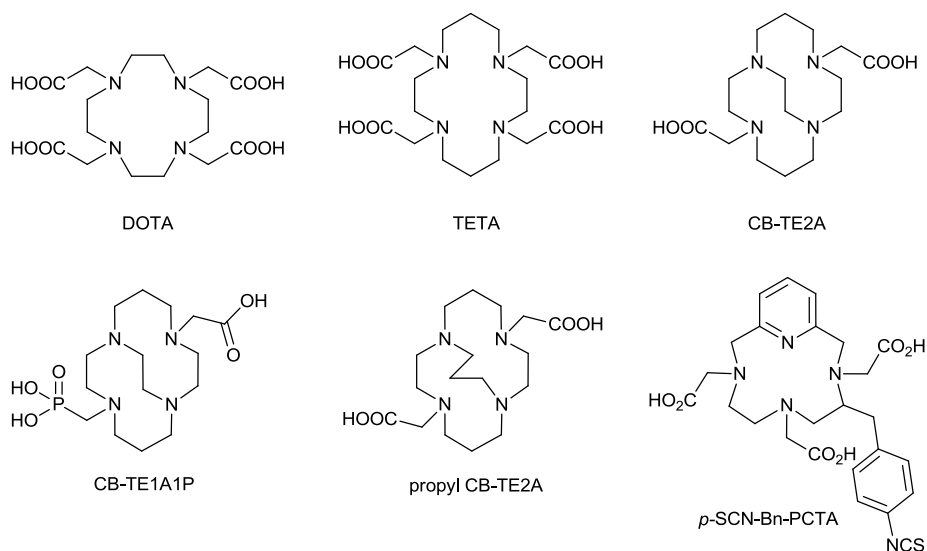
Figure 5 – Chemical structures of known chelators designed for ^{64}Cu complex formation.

The most widely used chelators for ^{64}Cu are tetraazamacrocycles based on cyclam and cyclen, see Figure 5.[19] However, although superior to acyclic derivatives, many macrocyclic copper(II) complexes still suffer from low *in vivo* stability resulting in transmetallation.[22,23] Weisman, Wong and co-workers along with other groups expanded on the chelator library by developing an ethylene cross-bridged cyclam system which has increased stability over non-bridged systems,[24-27] although they generally require elevated temperatures to form complexes, a major drawback for use with temperature sensitive biomolecules.

Recently, Donnelly, Blower and co-workers have conducted a useful study of eight BFCs (including *p*-SCN-Bn-PCTA) for ^{64}Cu for labelling of antibodies, looking at a range of variables.[28] Results show NOTA and a sarcophagine ligand to be among the best when taking account of all the properties assessed, outperforming the commonly used DOTA and these chelators are recommended for use in further studies. Further recent developments in ^{64}Cu chelation chemistry was the synthesis of propyl CB-TE2A, a cross bridged cyclam derivative which has a propyl bridge instead of the commonly used ethyl bridge.[29] This appears to be an important development because the chelator radiolabels at room temperature whilst remaining highly stable, in a similar way to ethyl bridged cyclam although further *in vivo* validation is required. Archibald and co-workers developed a carbon-functionalised CB-TE2A derivative to allow for bioconjugation whilst not compromising coordination number.[30]

Weisman, Wong and co-workers have developed a CB-TE2A derivative in which one acetate arm was replaced with a phosphonate derivative (CB-TE1A1P),[31] which improves ^{64}Cu complexation at room temperature. There is potential to combine these aspects in the synthesis of a propyl cross-bridged cyclam with one or two phosphonate arms and determine its complexation characteristics. Tripier and co-workers have developed macrocycles functionalised with monopicolinate which exhibit fast binding kinetics and form highly stable complexes.[32]

1.1.1.1.2.2.2. [86]Y

[86]Y has a half-life of 14.7 hours which is similar to [64]Cu. Which similarly allows for transport across sites and can be used for biomolecules with longer biological half-lives.[8,9,33] There is also an yttrium isotope used in clinically approved radioimmunotherapy treatments (^{90}Y), see *section 1.3.1.* This means that [86]Y can be used as a direct imaging counterpart of ^{90}Y, giving specific knowledge of where the radioimmunotherapy agent is located *in vivo* without the influence of the metal having a different effect on biodistribution which may be the case with other imaging radioisotopes such as [89]Zr and [111]In.[9,34] [86]Y is produced using a cyclotron from [86]Sr.[8]

Yttrium has properties which are very similar to that of the lanthanides. Yttrium is almost exclusively in the oxidation state III and has a relatively large atomic radius (108 pm), forming complexes with coordination number 7-9.[20] Yttrium(III) is classified as a hard Lewis acid and therefore prefers hard Lewis donors such as oxygen and nitrogen.[8,9]

As yttrium(III) shares many properties with the lanthanides, the chelators used are generally interchangeable, with yttrium(III) forming stable complexes with chelators used in gadolinium(III) MRI contrast agents for example.[8] [86]Y is often used with DOTA (see Figure 5) derivatives, in which it is known to form nine coordinate complexes with the octadentate chelator and the ninth coordination site taken up by a water molecule.[35,36] Yttrium(III) complexes of TETA (see Figure 5) can be formed but are much less stable than the DOTA derivative, with [YTETA] having a complex half-life of only 5 minutes at pH 3.6 and [YDOTA] showing no evidence of decomplexation after 3 months.[37]

1.1.1.1.3. ^{68}Ga

^{68}Ga is unusual as a metallic PET radioisotope for two main reasons; it has a comparatively short half-life (68 minutes) and is produced by radioactive decay of a parent isotope. As a parent isotope, ^{68}Ge has ideal characteristics for generator production, with a half-life of 271 days, ^{68}Ge decays to ^{68}Ga to give a daily supply of the isotope.[8,38]

Efforts in recent years have been focused on developing a commercial system for continuous production of ^{68}Ga for laboratory use over one to two years.[39,40] ^{68}Ga generators are now commercially available and also in clinical use for trials but development in the area of generator production is on-going with improvements required in the areas of; HCl elution, possible metal ion impurities and long-term generator sterility issues.[8] There are currently no FDA-approved generator systems although this is likely to change in the near future with ongoing clinical trials in the USA. However, these limitations do not detract from the overall advantage that ^{68}Ga can be produced on site from a long term generator without the need for a cyclotron on site or daily isotope delivery, a characteristic that could have significant future clinical relevance.[9]

^{68}Ga has an ideal half-life for radiochemistry, being long enough to carry out synthetic procedures but not so long to cause radiosynthetic handling challenges which are a concern for longer lived isotopes. Clinical issues such as unnecessary patient dose are not a major factor with a 68 minute half-life; this is also backed up by ^{68}Ga decaying by 89% positron, avoiding large percentages of more harmful decay types that the patient may receive with other radiometals. The applicability of ^{68}Ga is focused on biomolecules which localise relatively quickly such as small molecules, peptides and antibody fragments.[41,42]

^{68}Ga is exclusively in the oxidation state III in aqueous solution at physiological pH and is generally eluted from a ^{68}Ge/^{68}Ga generator using 0.1M hydrochloric acid,[8,43,44] allowing widespread radiopharmaceutical synthesis. Most synthetic procedures are carried out in the presence of weakly coordinating ligands such as citrate, acetate or oxalate to avoid the formation of insoluble $Ga(OH)_3$ and soluble $Ga(OH)_4^-$, both of which dramatically reduce the kinetics of complex formation.[21] Incorporation of ^{68}Ga into a targeting vector is generally undertaken with the use of a bifunctional chelator (BFC), a molecule which forms complexes

that are stable *in vivo* with a reactive terminating group for bioconjugation. An important condition for a useful BFC is the formation of radiolabelled complexes using mild conditions to avoid degradation of the linked biomolecule and as rapidly as possible due to the short half-life of the radioisotope. For clinical use, a current limitation in comparison to technetium-99m is the frequency that the generator can be eluted relative to the isotopic half-life.

Gallium(III) generally forms six coordinate complexes and is classified as hard Lewis acidic and therefore binds to hard Lewis base donor atoms such as nitrogen and oxygen, which are present in routinely used BFCs.[45,46] Acyclic BFCs are generally less kinetically inert and thermodynamically stable than their macrocyclic counterparts but have the advantage of faster metal ion binding kinetics.[47,48] In contrast to copper(II), gallium(III) may form sufficiently stable complexes with acyclic chelators for *in vivo* use.[49]

Clinically, ^{68}Ga is gaining increased attention, driven largely by the use of DOTA-TOC, DOTA-TATE and DOTA-NOC,[50-52] DOTA-peptide derivatives which are neoendocrine tumour targeting agents. There are also many more ^{68}Ga peptide conjugates at different stages of clinical trials.[42,53] The area was first explored by Maecke and co-workers,[54-56] then recently expanded into further clinical trials by Baum and co-workers.[57-59]

1.1.1.1.3.1. Recent advances in ^{68}Ga chelator design and radiolabelling methodologies

Radiochemical research into ^{68}Ga chelator design in the past few years has been aimed at the development of stable acyclic complexes or rapid room-temperature macrocyclic complex formation to optimise properties for imaging applications.

1.1.1.1.3.1.1. Cyclen

Cyclen (1,4,7,10-tetraazacyclododecane) based BFCs are a popular choice for ^{68}Ga complexation due to the widespread use of DOTA (1,4,7,10-tetraazacyclododecane-1,4,7,10-tetraacetic acid), see Figure 6, based ligands in various applications from targeted MRI contrast agents to radioimmunotherapy, dependent on metal ion selection.[60] Hence, many groups worldwide already have expertise in bioconjugation of DOTA derivatives to different biomolecules; the simple variation of the stable metal to ^{68}Ga is a natural transition into PET radiochemistry. Unfortunately, the preorganisation of DOTA means that

complex formation is generally slow and usually requires conventional or microwave heat, limiting its use to non-heat sensitive biomolecules.[61,62]
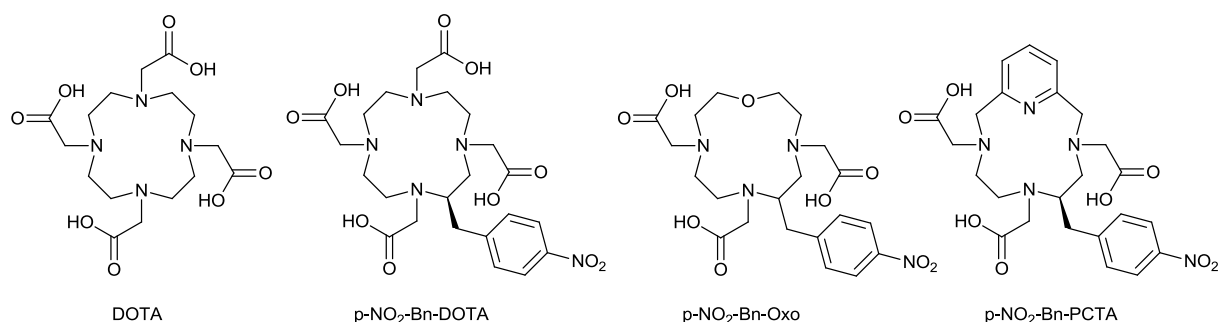
Figure 6 – Chemical structures of cyclen derivatised macrocycles suitable for application to ^{68}Ga radiopharmaceutical formation.

[68]Ga complexation of p-NO$_2$-Bn-DOTA gives the expected requirement of elevated temperatures or long reaction times,[63] with a radiochemical yield (RCY) of 92.5% after 10 minutes at 80°C or 87.5% after 30 minutes at room temperature. There are now however, similar macrocycles which show much more favourable complexation characteristics, with both p-NO$_2$-Bn-Oxo and p-NO$_2$-Bn-PCTA giving higher (<98%) RCYs at room temperature after a reaction time of 5 mins. Although showing similar complexation characteristics, the oxo derivative did not inherit the advantage of kinetic inertness from the parent DOTA, however p-NO$_2$-Bn-PCTA shows both high kinetic inertness and favourable *in vivo* biodistribution characteristics. A study of the oxo derivative also shows inferior *in vivo* characteristics when conjugated to RGD peptides.[64] p-NO$_2$-Bn-PCTA has subsequently been compared to the NOTA derivative for small peptide *in vivo* imaging and has shown to have very similar properties, adding to the library of BFCs suitable for *in vivo* [68]Ga imaging.[65]

1.1.1.1.3.1.2. TACN

TACN (1,4,7-triazacyclononane) based chelators such as NOTA (1,4,7-triazacyclononane-1,4,7-triacetic acid) show favourable characteristics for ^{68}Ga radiolabelling. Chelators based on this backbone generally exhibit fast complexation reaction kinetics, high *in vivo* stability and high selectivity towards gallium(III) due to cavity size.[21,66,67] Recent attention to ligand design has been focused on studying and optimising chelators N-functionalised with three pendant arms containing sites for both coordination and conjugation, see Figure 7.[68-70] This has been used as a way to form trimeric bioconjugate species whilst keeping the

coordinating atoms, with the aim of signal amplification through multivalency.[71,72] A RGD trimer, TRAP(RGD)$_3$, was synthesised and compared to both NODAGA-RGD and DOTATOC showing a 10-20 fold increase in specific activity in comparison, although to achieve this, temperatures of 95°C are required. *In vivo* experiments showed higher affinity when compared with ^{68}Ga-NODAGA-RGD and ^{18}F-galacto-RGD.[73]

A similar system which is based on tri-glutaric acid (NOTGA) has also been developed, see Figure 7.[74] The group synthesised mono-, bis- and trimeric bioconjugates in order to directly link a different number of RGD biomolecules per molecule. The trimeric bioconjugate showed a signal amplification leading to a 54% increase in tumour uptake in comparison to the monomeric version. The effect of different isomers on radiosynthesis was also explored,[74] showing that a diastereomic mixture has no negative effect on biological activity for RGD conjugates. Studies of the influence of metal ion exchange processes showed that the phosphonate donating groups are much less susceptible to transmetallation when compared to acetate donors.[75]

TRAP   NOTGA
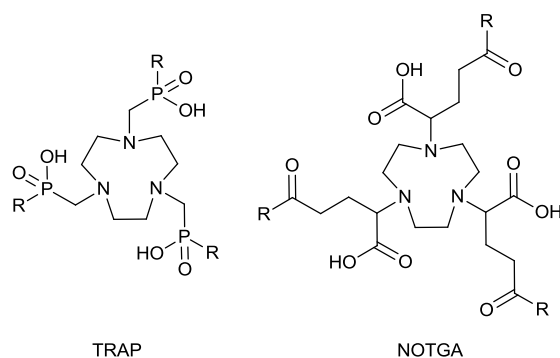
Figure 7 – Chemical structures of TACN derivatives with three conjugation sites to form multivalent derivatives.

1.1.1.1.3.1.3. Other macrocycles

Donnelly and co-workers have translated a well-known ^{64}Cu sarcophagine derivatised chelator to use with ^{68}Ga, see Figure 8.[76] Sarcophagine type chelators have the advantage of forming highly stable complexes in which gallium(III) does not dissociate in the presence of transferrin, a common mechanism for demetallation *in vivo*. The ligand was conjugated with two RGD peptides and showed good *in vivo* characteristics, however further work needs to be carried out with this chelator class to translate labelling to a wider range of biomolecules,

since the harsh (85°C, 30 mins) conditions needed for complex formation are not compatible with proteins and antibodies.

A range of tricarboxylate ligands based on 6-amino-perhydro-1,4-diazepine have been synthesised and both their radiolabelling reactions and stability probed, see Figure 8.[77] The chelators showed good radiochemical characteristics (≥96% RCY, 3 mins reaction time) in a pH range between 4.0 to 6.8 and also showed no demetallation in the presence of transferrin or iron(III) over 2h.

(NHR)$_2$-sar

Perhydro-1,4-diazepine derivatives
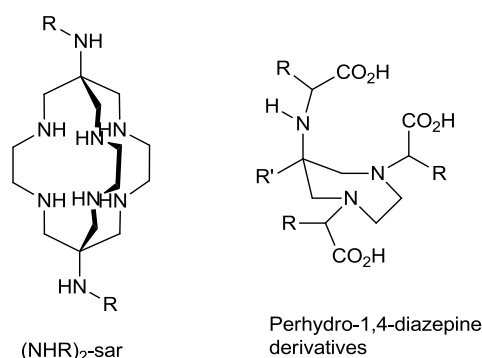
Figure 8 – Chemical structures of new BFC alternatives for ^{68}Ga complexation.

1.1.1.1.3.1.4. Acyclic

Acyclic chelators for ^{68}Ga offer much potential due to the fast kinetics involved in complex formation, recent work in the area is focused on the design of novel chelators which retain the kinetic advantages whilst addressing the issue of low *in vivo* stability, see Figure 9.

Pascu and co-workers have further developed chelators based on the ATSM type thiosemicarbazone structure,[78] which has previously been used for ^{64}Cu peptide labelling.[79,80] The group modified the backbone of the ligand to add aromatic groups, allowing the ligand to be used as a multimodal PET/optical agent with ^{68}Ga and also introducing other functional groups to increase aqueous solubility. The radiolabelling was achieved through transmetallation of the zinc(II) complex with the reactions requiring elevated temperatures for good RCYs. Blower and co-workers have developed a novel chelator; CP256,[48] which shows RCYs of 98-100% after 5 minutes reaction time at room temperature, the reaction also proceeds to ca. 75% RCY at concentrations as low as 1μM, a concentration at which DOTA shows negligible conversion even at 100°C for 30 minutes.

[67]Ga stability studies showed no transchelation after 4 hours with 130-fold excess of iron(II), demonstrating that the complex is highly stable for an acyclic chelator.

Orvig and co-workers have recently been developing DEDPA derivatives.[49] Three versions of the chelator were synthesised; with no reactive groups, a bis-N-functionalised derivative and a C-functionalised derivative, with all three ligands showing quantitative radiolabelling after 10 minutes at room temperature and 97% of the complex remained intact after transferrin challenge experiments. Bis-N functionalised and C-functionalised derivates were also tested as BFCs by conjugating the chelator to RGD.[81] Interestingly, the C-functionalised mono-RGD conjugate showed high stability (92% after 2 hours) whilst the N-functionalised bis-RGD conjugate showed much lower stability (73% after 2 hours). The group also subsequently synthesised a di-azide derivative which can be used for copper(I)-catalysed azide-alkyne cycloaddition (CuAAC) reactions for bioconjugation and showed versatility in forming complexes with a range of radiometals.[82]

aromatic bis(thiosemicarbazonate)   CP256   DEDPA derivatives
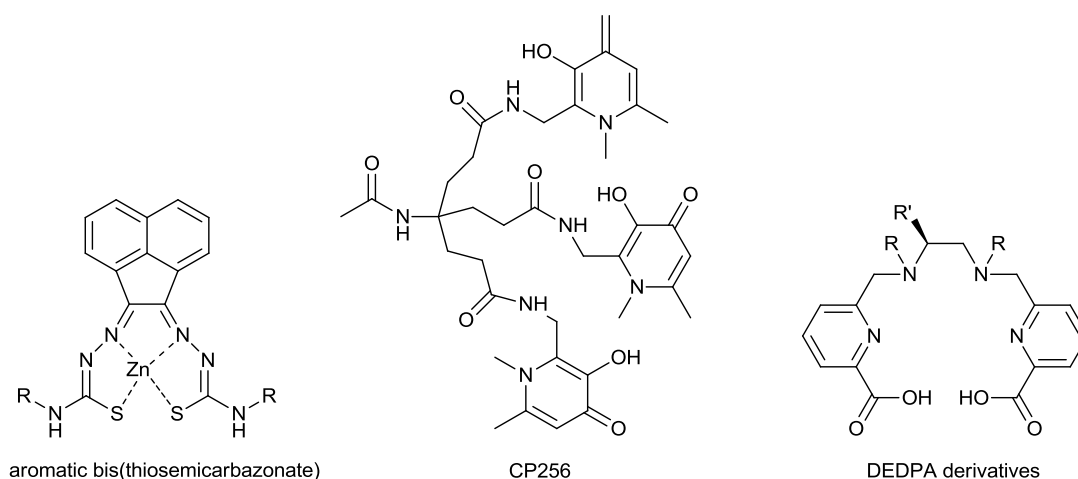
Figure 9 – Chemical structures of recently investigated acyclic chelators for ^{68}Ga radiolabelling.

1.1.1.1.3.1.5. Radiolabelling methodologies

The past few years have seen focus on potential solutions to two key challenges in ^{68}Ga radiochemistry; (1) increasing complex formation reaction rates and (2) suitable methods for translation to a clinical setting. Toth and co-workers have studied a method for the cold synthesis of Ga(NOTA) transmetallation from weak Ga-citrate complexes, see Scheme 1.[83] The developed strategy avoids the formation of hydroxide precipitate and results in much

higher yield of the target complex than the traditional method with an acetate buffer. Although this methodology has not yet been applied to ^{68}Ga radiolabelling.

Zeng *et al*. have developed a microfluidic system for ^{68}Ga complex formation of peptide conjugated NOTA and DOTA derivatives.[84] The group compared their microfluidic system to conventional methods, showing an opportunity in this area for future developments, with the potential to synthesise complexes rapidly in much milder and therefore biomolecule compatible conditions.

Meanwhile Blom *et al*. have combined two techniques for clinical use,[85] incorporating radiosynthesis and steam sterilisation into one method they call autoclabeling. Two peptides; DOTA-TATE and NOC were radiolabelled at 121°C in acetate buffer and showed that the final product was sterile and had no peptide degradation. Although the method is only suitable for biomolecules which are not heat-sensitive, this technique could have clinical relevance for specific applications. Breeman and co-workers have also developed a system that avoids the use of organic solvents during any of the synthetic steps which reduces post-synthesis quality control time by removing the need for gas chromatography.[86] The group have replaced the traditional methods for purification of the obtained [68]GaCl$_4^-$ (elution with HCl and water in commercial cartridges or buffering) for the preconcentration on a solid phase cartridge with a mixture which contains NaCl and HCl. 98% of the activity was eluted from the cartridge using this method and it was shown that it had no detrimental effect on radiochemical synthesis. Recently, Valliant and co-workers have developed an emulsion based method for ^{99m}Tc-complex formation which allows high RCYs at room temperature by a proposed surface concentration mechanism in a method which could be applicable for room temperature ^{68}Ga radiochemistry.[87]
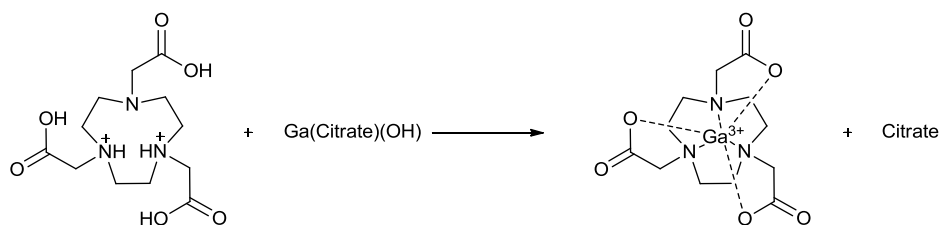
Scheme 1 – Synthesis of [GaNOTA] from Ga-citrate.[83]

1.1.2. Magnetic resonance imaging (MRI)

Magnetic resonance imaging (MRI) is a routine, non-invasive, non-radioactive, high resolution anatomical medical imaging technique which gives a three-dimensional image of internal organs and tissues.[88,89]

Magnetic resonance is founded on the interaction between an externally applied magnetic field and a nucleus which possesses spin, I. An atomic nuclei can interact with a magnetic field if it has an odd atomic weight (I = half integral) or an odd atomic number (I = integral), nuclei which have an even atomic number and an even atomic weight have no spin (I = 0), and do not interact with a magnetic field. ^{1}H is the most commonly analysed isotope as it has many favourable characteristics. It has a nucleus of one proton which makes the spin I = ½ for the ~100% abundant ^{1}H isotope, one of the largest responses to an applied magnetic field in nature and the human body contains primarily water and fats which contain hydrogen, the application of which is the foundation of clinical MRI.[90]
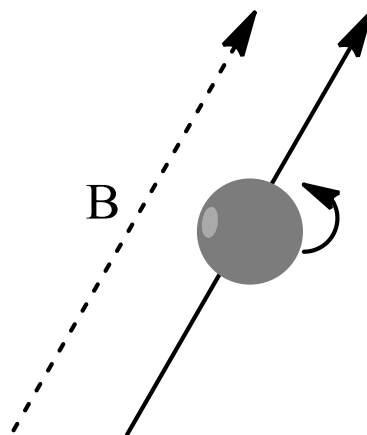
Figure 10 – A positively charged nucleus which produces a magnetic field when the nucleus has spin.

Along with having spin, a proton also has a positively charged nucleus, giving it a local magnetic field. The direction of the magnetic field (B) is parallel to the axis of rotation, see Figure 10, and the changes in the magnetic moment of multiple similar spins is the basis for providing the MR signal. When no external magnetic field is applied, the protons are aligned at random providing zero net magnetisation. When a strong magnetic field is applied, the protons align with the magnetic field (B_0), see Figure 11.

Low energy protons align parallel with the magnetic field (spin up) and high energy protons lie anti-parallel to the magnetic field (spin down). In a clinical setting, the only thing which determines the alignment of specific nuclei is the strength of the external magnetic field.
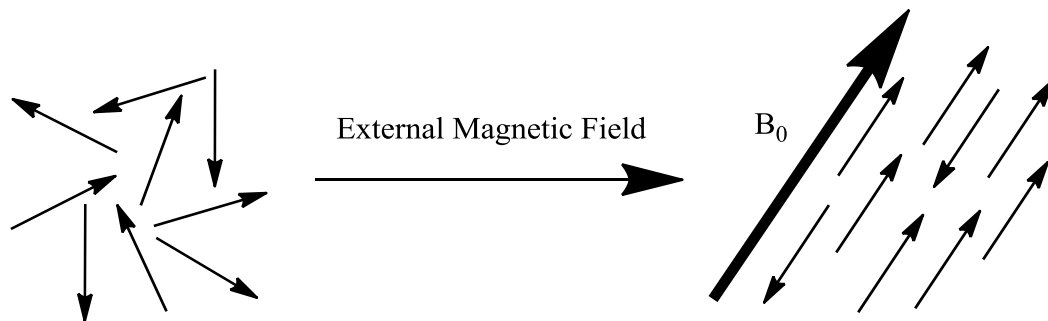
Figure 11 – Schematic of the alignment of randomly arranged protons upon applying an external magnetic field.

There is always an excess of nuclei which align with the magnetic field, and given that all except the excess cancel each other out, this gives a net magnetisation. Increasing the excess of aligned nuclei would improve the net magnetisation and give a higher signal. This can be done by increasing the difference between the energy levels, so fewer nuclei have the energy to reach the high energy level, and can be achieved by using higher magnetic field strengths.[90,91]

The individual protons are not stationary, they begin to rotate, or precess about the magnetic field, see Figure 12. The precession is slightly tilted away from the axis of the magnetic field, being the z direction, the axis of rotation is always parallel to B_0. The speed of precession, known as the precessional frequency, is proportional to the strength of the magnetic field by Larmors equation ($\omega = B_0 \times \gamma$). The precessional frequency given by this equation determines the energy of the radio frequency used.[91]
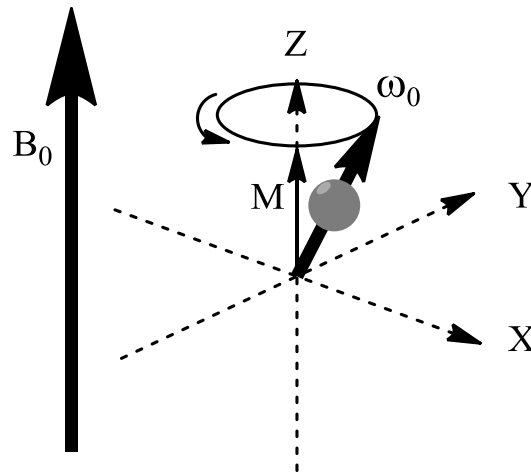
Figure 12 – Precession of protons parallel to the magnetic field (B_0) at larmor frequency (ω_0).

Resonating protons at the precessional frequency by a radio frequency (rf) pulse causes the net magnetisation vector (NMV) to move out of alignment away from B_0, usually at a 90° angle from the longitudinal plane to the transverse plane, see Figure 13, and some protons to gain energy and become anti-parallel to the magnetic field (spin down).
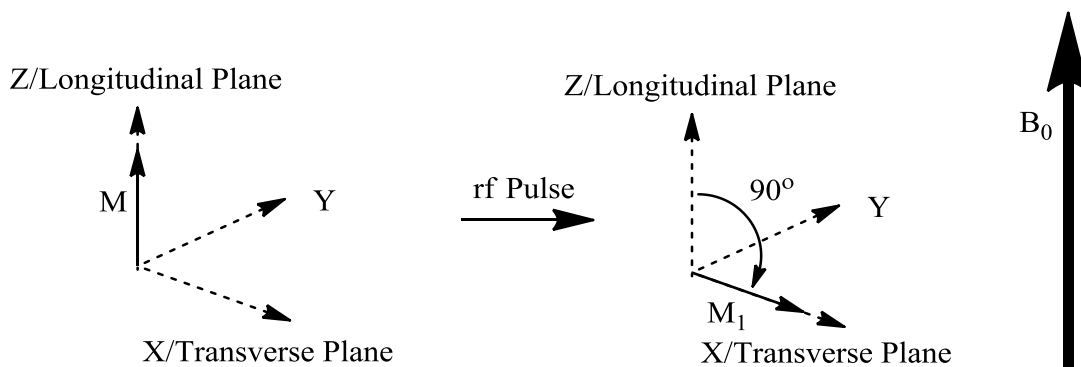
Figure 13 – Diagram to show the rotation of the MNV 90° from B_0 with an rf pulse.

Once the pulse is stopped, the protons begin to realign from M_1 back to their equilibrium orientation, M, emitting energy at the frequency ω_0. The changes in the magnetic field from precession are detected with a receiver coil perpendicular to the transverse plane. The process by which protons equilibrate and energy is lost is called relaxation.[91] The two most important relaxation times for MRI are T_1 and T_2.

1.1.2.1. MRI contrast agents

One of the biggest strengths of MRI over other structural imaging techniques such as CT is the amount of intrinsic contrast between different tissues as a result of differences in T_1 or T_2 relaxation times of the different tissues.[90] In order to increase contrast of specific tissues, an area can be made brighter or darker than the surrounding tissues by use of an MRI contrast agent which are also more versatile and offer fewer side effects than CT contrast agents. MRI contrast agents are categorised as T_1 or T_2 agents based on their primary effect of shortening the respective relaxation times.

1.1.2.1.1. T_1

T_1 relaxation is a mechanism by which nuclei can realign back to the longitudinal plane by giving up their energy to the surrounding environment or lattice, which does not contribute to the overall spin, and is known as spin-lattice relaxation. This is an exponential process and T_1 is the time taken for 63% of nuclei to recover to the longitudinal plane.

In a T_1 weighted image, tissues with short T_1 times (fat) appear bright, and tissues with long T_1 times (water and tumours) appear dark. A T_1 contrast agent is one which shortens the T_1 of the bulk water protons, causing them to appear brighter. The most common type of T_1 agents are gadolinium(III) based due to its highly paramagnetic nature and symmetrical S-state, affecting the local magnetic field, it has seven unpaired electrons and allows rapid exchange of water molecules.[92-95] Gadolinium(III) is toxic due to the similarity of ionic radii to calcium(II), therefore disrupting the calcium signalling pathway, it therefore needs to be chelated by a polydentate ligand.[94]

The acyclic gadolinium(III) complex, Gd-DTPA (Magnevist), see Figure 14, is a commonly used clinical MRI contrast agent, similar to another clinical contrast agent, Gd-DOTA (DOTArem).[96] They are both ionic in nature, and are balanced with meglumine ions, both complexes are eight coordinate and both have one coordination site available for water molecules, allowing them to come into the first coordination sphere of the paramagnetic ion to allow energy transfer. Another FDA approved MRI contrast agent is Gd-HP-DO3A (ProHance), the complex is non-ionic and is seven coordinate, leaving two coordination sites for water binding. The macrocyclic nature of Gd-DOTA and Gd-HP-DO3A gives greater

stability than DTPA, therefore reducing the tendency for release of the toxic gadolinium(III) ion.[91]

Gd-DTPA
Magnevist

Gd-DOTA
DOTArem

Gd-HP-DO3A
ProHance
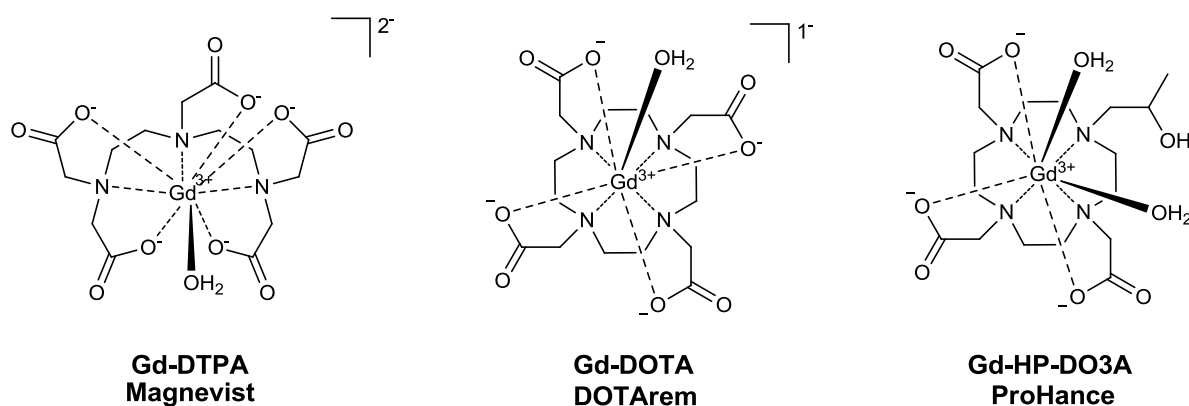
Figure 14 – Chemical structures of FDA approved MRI contrast agents.

1.1.2.1.2. T_2

T_2 decay is caused by nuclei transferring the spin to neighbouring nuclei, resulting in the loss of transverse magnetisation and is known as spin-spin relation, the T_2 relaxation time is the time taken for 63% of the transverse magnetisation to be lost. In a T_2 weighted image, tissues with short T_2 times (water and tumours) appear bright, and tissues with long T_2 times (fat) appear dark.

T_2 contrast agents can be divided into three categories: magnetic oxides, magnetic metal alloys and rare earth metal doped nanoparticles, the most common of these is iron oxide nanoparticle derivatives. Materials of this type are either made from magnetite (Fe_3O_4), maghemite (γ-Fe_2O_3) or a mixture of both, the magnetic properties of which are very similar.[97] Iron oxide materials below 200 nm are known as super-paramagnetic iron oxide nanoparticles.

1.1.2.1.2.1 Super-paramagnetic iron oxide nanoparticles (SPIONs) as T_2 MRI contrast agents.

Magnetic nanoparticles have been used in a range of applications over recent years. With material applications in data storage and as biohybrid materials along with other biomedical applications such as drug delivery, hypothermia agents and imaging as MRI contrast agents.[97]

Due to their small size, iron oxide nanoparticles exhibit super-paramagnetic behaviour and are commonly referred to as super-paramagnetic iron oxide nanoparticles (SPIONs). Their super-paramagnetic nature means that thermal energy is enough to change the magnetisation of individual nanoparticles. Allowing, in the presence of a magnetic field, alignment of magnetisation which can be 10^4 times larger than paramagnetic materials due to the relatively large (compared to atoms) colloidally stable nanoparticles. These nanoparticles are able to create local magnetic fields which shorten relaxation times of local protons. SPIONs generate contrast by both T_1 and T_2 mechanisms but are generally used as T_2 contrast agents due to the larger relaxivity effect. SPIONs are generally composed of a crystalline magnetic iron oxide core coated with a hydrophilic surface layer to allow stable suspension in aqueous environments.

SPIONs are the most commonly used T_2 MRI contrast agents due to having relatively low toxicity[98,99] and a modifiable surface.[100,101] The area is a combination of materials, colloidal, polymeric, organic and inorganic chemistries along with biomedical expertise needed to evaluate applications of synthesised constructs. The size of the SPIONs is important in determining *in vivo* characteristics, needing to be smaller than 200 nm to slow down immune system clearance. Other factors also influence the *in vivo* characteristics of SPIONS such as, size distribution, magnetic susceptibility and surface physiochemical properties. Usually, particles with sizes 40-100 nm are taken up by the reticuloendothelial system (RES) and accumulate in the liver and spleen,[102] and the most commonly used SPIONS are 20-30 nm which have longer blood pool times and are excreted renally.[103] Although, for most applications which do not require brain images, sizes of <150 nm are sufficiently small enough to pass through most endothelial barriers.[104] However, how the size, shape and composition of nanoparticles affect the passing through different endothelial barriers

including the blood-brain barrier is currently a contentious issue which requires more study to develop more robust generalisations.

There are currently a number of SPIONs which have been approved for clinical use, dextran coated Endorem® (Guerbet)[105] for liver and spleen imaging, dextran coated Combidex® (AMAG)[106] for lymph node imaging and silica coated GastroMARK® (AMAG)[102] for gastrointestinal imaging amongst others.

1.1.3. Optical

Optical imaging for biomedical research in the study of mammalian biology has been used widely for many years,[107] allowing the visualisation of cellular processes in living subjects. However, due to limited light penetration through mammalian tissue, its clinical utility is limited and is usually reserved for study of small animals.[108,109] Small molecule optical imaging agents can be generally split into two branches; lanthanide luminescence and organic dyes.

1.1.3.1 Lanthanide luminescence

Lanthanide cations have low absorption coefficients which result in low efficiency in populating the emitting levels by direct excitation, the efficiency of systems is determined by its quantum yield. Solvent coordination to lanthanide ions opens up non-radiative pathways to return to the ground state. These problems can be overcome by coordination of a suitable chromophore antenna. The chromophore absorbs light energy which can then populate the emitting levels of the cation via energy transfer. The ligand would ideally be polydentate, containing at least 8 donor atoms to ensure that the first coordination sphere of the metal ion is full to prevent the binding of solvent molecules which cause quenching of luminescence.[107]

The wavelength that a molecule absorbs energy at is named the 'excitation wavelength', this wavelength is determined by the choice of chromophore on the molecule. The wavelength at which the molecule releases energy is named the 'emission wavelength'. The difference between these wavelengths is called the Stokes shift. During energy transfer between the chromophore and the metal centre energy is lost; therefore the emission energy is always lower than that needed for excitation.[107]

One way to create an appropriate ligand is to attach a chromophore antenna onto a macrocycle, allowing the ligand to absorb energy which can be transferred to the lanthanide ion. When designing a molecule for use in a biological system, competition between biological chromophores is important to avoid, most natural chromophores absorb wavelengths below 300nm, synthetic molecules, therefore, are usually designed to absorb wavelengths above 300nm.

Lanthanides chelates are commonly used due to their large Stokes shift and long fluorescence lifetimes (ca. 0.6 ms for a sensitised europium(III) complex compared to 5 ns for BODIPY derivatives). Their ability to produce fluorescence in a low to zero background region makes lanthanide chelates ideal as contrast agents in multiple biological applications.[110] The most commonly used lanthanides used in luminescence are europium(III) and terbium(III) because they have emission wavelengths in a suitable region (visible) and long lived excited states.[111]

To create an effective molecule there are three main components to incorporate. Firstly the chromophore antenna is attached to the macrocycle which is then complexed with the lanthanide(III) ion to form the luminescent complex. To activate the lanthanide(III) ions to luminescence energy must be absorbed through the chromophore antenna in the antenna-to-cation sensitisation process.[107,112]

1.1.3.2 Optical dyes

Organic optical dyes fluoresce, they absorb light which excites the molecule into a higher energy state, followed by the return of the molecule to the ground state which results in the emission of light. As with lanthanide luminescence, energy is lost in this process and therefore the emission energy is lower than the excitation energy, making the wavelength of emission different from the wavelength absorbed. This process can be repeated by the same molecule in a 'catalytic' nature but photobleaching can occur which leads to degradation of the molecule.[113]
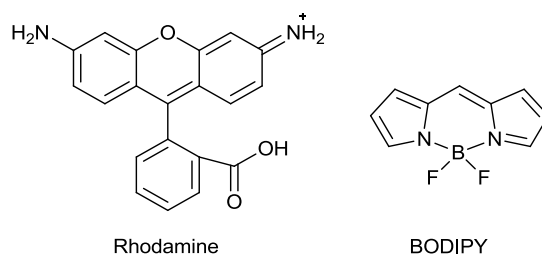
Figure 15 – Chemical structures of commonly used organic dyes rhodamine and BODIPY.

Common dyes used in biomedical applications are rhodamine and boron dipyrromethenes (BODIPY), see Figure 15. These dyes have an added advantage for biomedical applications as they are known to be taken up into cells. Rhodamine agents are hydrophobic cationic which can target mitochondrial function and give apoptotic information using confocal microscopy.[114,115]

1.1.4. Multi-modality

Individual imaging modalities have specific advantages and disadvantages. PET has very high sensitivity but gives limited anatomical information, MRI has very high resolution but low sensitivity, see Figure 16, and for optical imaging, quantification beyond a few millimetres is difficult, and so no single modality is perfect for gaining all necessary information. Multi-modality molecular imaging is the combination of two or more detection techniques, the advantages of multiple techniques can be combined whilst mitigating the disadvantages of each individual modality.[116]

The combination of the high resolution and high sensitivity of MRI and PET can give information respectively on anatomy and function. When applying that to oncology, diagnostic accuracy is increased and future treatment options are better informed. Multi-modal imaging agents have exciting potential as, for example, they can be used in surgery for live imaging (fluorescence), ensuring that all cancerous material has been removed (MRI), and to track and identify tumour cells and cellular processes (PET).

1.1.4.1. PET/MRI

PET alone gives very little information regarding spatial anatomy and is often combined with CT as standard, in a similar way PET can be combined with MRI to give an image with both

the high sensitivity and ability to visualise metabolic changes of PET with the high resolution anatomical images of MRI.[116,117] PET/MRI has some distinct advantages over PET/CT; lower patient radiation dose, increased soft tissue contrast and the ability to use MRI contrast agents which have much higher versatility and applicability than CT contrast agents.[118]

Construction of a working MRI/PET system has been on-going for the past fifteen years,[119] the limitations of developing this system to date has largely been technological because conventional photomultipliers used in PET cannot operate at the high magnetic field strength of MRI.[120]
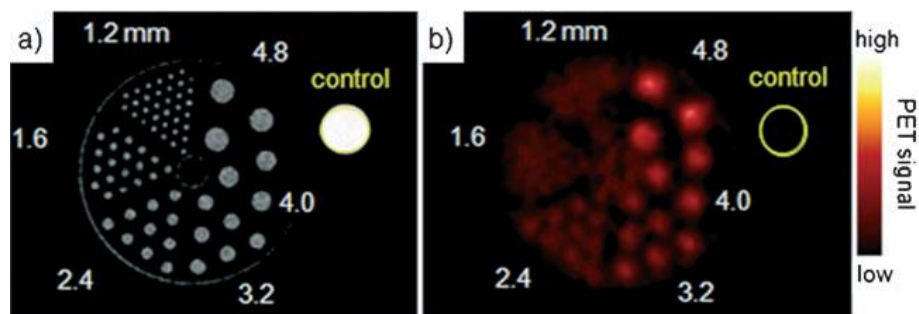
Figure 16 – Comparison of spatial resolution of (a) MRI and (b) PET.[121]

Although still expensive, an integrated MRI/PET system has been constructed over the last five years which does not use silicon based photomultiplier tubes, with a Siemens full body scanner given FDA approval in 2011, see Figure 2.[118,122,123] A pre-clinical version of the scanner has been tested using [^{18}F]-FDG in an *in vivo* pre-clinical study which showed no reduction in quality for either MRI or PET.[124] Although this scanner is still sequential, Lerche and co-workers have been developing a PET insert for a whole body MRI scanner to form a simultaneous device.[125]

A consideration of using a PET/MRI multi-modal agent involves the difference in sensitivities of the two techniques. MRI probes are usually administered in above a thousand-fold higher concentration than PET probes,[116] one way to avoid the approval problems of using a mixture of compounds would be to mix the cold isotope with the hot isotope when radiolabelling so the sample would be identical except for the isotope variation and would therefore have the same pharmacological properties. This can be carried out efficiently

29

using carrier added radiosynthetic procedures (which generally increase radiochemical yield) with specific activity not being a major issue for this type of probe.

Due to the relatively recent commercial availability of clinical and preclinical scanners, there have been very few reported probes which combine a MRI contrast agent with a positron emitting radioisotope, with the majority of these using super-paramagnetic iron oxide nanoparticles (SPIONs) as T_2 MRI contrast agents, see *section 3.1.* Now that suitable technology has been developed there is a wealth of new research opportunities to form MRI/PET probes for multi-modal imaging. One area that needs more research effort is the combination of SPION T_2 contrast agents with positron emitting radioisotopes to form multi-modality imaging probes. Probes of this nature offer a much more sensitive method for quantifying biodistribution of SPIONs *in vivo* as tracking the location of SPIONs is currently very challenging due to the inherent lack of sensitivity to these tracers with MRI. Forming conjugates with positron emitting isotopes can therefore give much greater information on biodistribution and therefore be used to more accurately track how changing of different parameters of the nanoparticles (size, shape, surface coating, targeting agent etc.) affects how they are processed *in vivo*.

1.2. Macrocyclic ligands

Macrocyclic ligands are polydentate ligands which contain donor atoms incorporated into the ring and/or attached to the cyclic backbone. Typically, macrocyclic ligands possess a minimum of nine atoms in the ring, with a least three donor atoms.[126] Macrocycle size and donor atom choice can be tailored for binding different metal ions e.g. transition or lanthanide metal ions. For biological systems, high thermodynamic and kinetic stability is important for a number of reasons. Firstly, the function of the metal complex is lost upon decomplexation, for example if a tumour targeted compound radiolabelled with a radiometal is not stable *in vivo* and some free ion is released, the radiometal is then not targeted to the tumour, causing an increase in background signal. Secondly, some metal ions such as gadolinium(III) can be toxic *in vivo* and using relatively high concentrations of the complexes when they do not have sufficient stability can cause unwanted side effects. Macrocyclic analogues of acyclic counterparts have the desired increase in stability due to the chelate and macrocyclic effect.

1.2.1 The chelate and macrocyclic effect

The chelate effect is the gain of free energy when a polydentate ligand is bound to a metal ion when compared with the corresponding number of unidentate ligands and is driven by a favourable entropic factor. Macrocycles are designed and synthesised with coordination to a metal centre in mind. The macrocycle is preorganised so the metal binding sites are arranged in a position to bind when the molecule is free. Therefore the metal-chelator binding enthalpic energy is minimised when the metal binds to the macrocycle. Macrocycles also possess slow metal dissociation kinetics as the ligands may require major unfavourable rearrangement before dissociation can occur. Overall, this is known as the macrocyclic effect.[127] Therefore cyclen is much more kinetically stable than its open chain counterpart; 2.2.2 tetramine, see Figure 17.
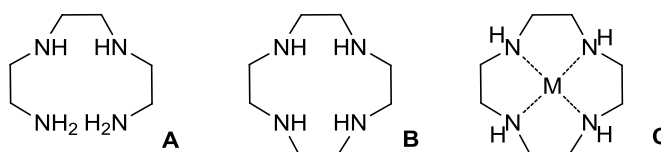
Figure 17 – Chemical structures of (A) 2.2.2 Tetramine, (B) Cyclen (C) Metal co-ordinated cyclen.

31

1.2.2. Bifunctional Chelators

Bifunctional chelators (BFCs) are molecules which comprise a metal binding group and a secondary reactive group. BFCs are used in a wide variety of imaging and therapeutic applications and provide a tool for covalent attachment of a metal complex to a targeting moiety, see Figure 18. Development of suitable BFCs for *in vivo* use requires an in depth knowledge of metal ion coordination chemistry and chelator design.
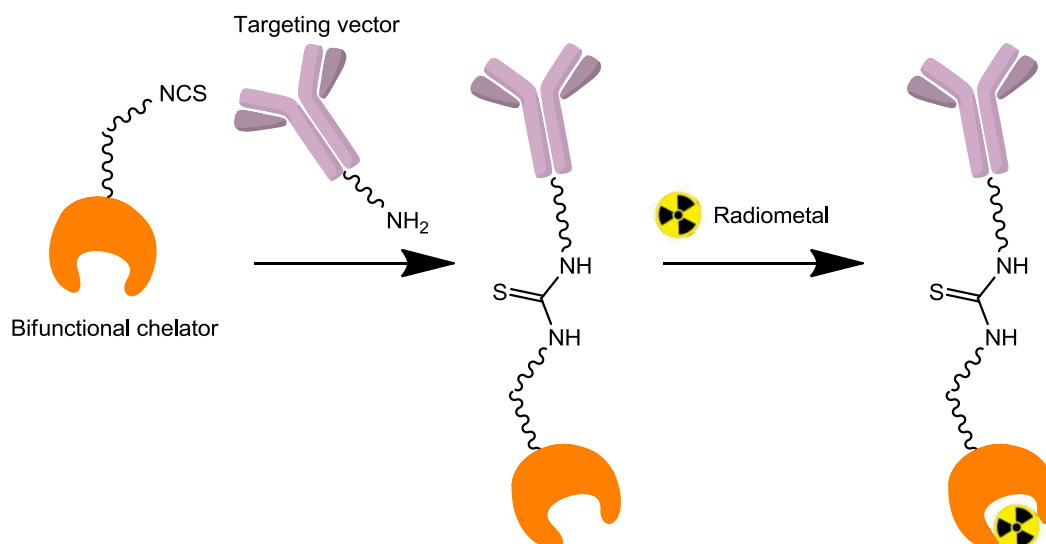
Figure 18 – Schematic representation of a targeted imaging agent using a BFC.

BFCs have characteristic requirements which need to be met to be suitable for *in vivo* use:

- Selectively form a metal chelate complex of the desired metal with both high thermodynamic stability and kinetic inertness; the metal chelate must remain intact under biological conditions to avoid release of the metal ion which may cause an increase in toxicity or increased background signal.

- The formation of the metal complex must be carried out in as short a time as possible in as mild conditions as possible (pH 5-9, <50°C) and at low concentrations (<100 μM). Lengthy or complex radiosynthesis both decreases activity for patient scans and decreases the applicability of the system to a clinical 'kit-like' system. Mild conditions are essential for widespread use as many biomolecules degrade at elevated temperatures (>50°C).

- Ligand synthesis should be cheap, simple and easily scaled up to allow for widespread cost effective application.

Fulfilment of these criteria does not guarantee a useful BFC however, with *in vivo* pharmacokinetics, discerned from lipophilicity and overall charge having a large effect on quality of the images.[21,128,129] It should also be noted that introduction of a BFC to a targeting molecule can have varying effects on the *in vivo* biodistribution of the molecule. The comparative size of the two components is important with the chelator having a greater influence on smaller biomolecules (e.g. peptides) than larger proteins (e.g. monoclonal antibodies).[9]

BFCs can generally be divided into two groups; acyclic and macrocyclic. Broadly speaking, acyclic chelators have faster binding kinetics but form less stable complexes when compared to macrocycles.[130] When selecting or designing a BFC, the characteristics of the metal ion must be assessed. However, some common chelators are used for a range of metal ions, see Figure 19.
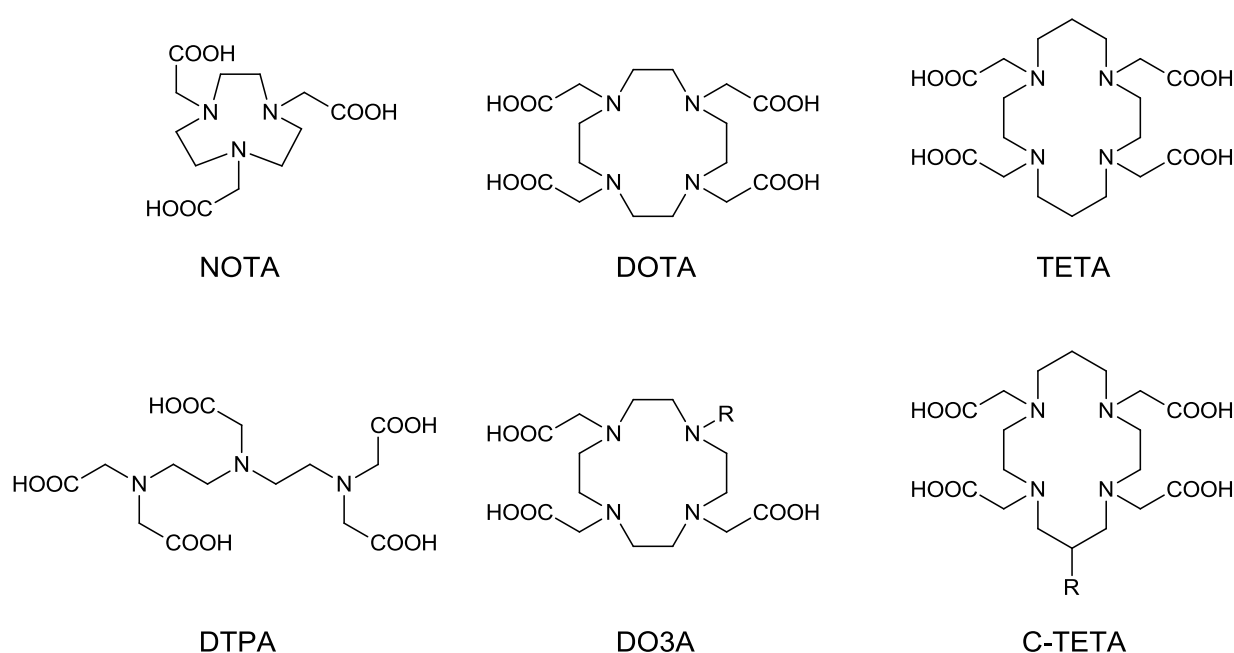
Figure 19 – Selected chemical structures of commonly used BFCs.

Overall, derivatives of DOTA (1,4,7,10-tetraazacyclododecane-1,4,7,10-tetraacetic acid) including replacement of one acetate arm to form DO3A (1,4,7-tris(*tert*-butoxycarbonylmethyl)-1,4,7,10-tetraazacyclododecane) have been the chelators most used in patient scans with ^{68}Ga-DOTA-TOC and ^{68}Ga-DOTA-TATE. [60,131,132] DO3A derivatives are also applicable for a range of applications due to the wide range of metals which can be used with the same chelator.

1.3. Radioimmunotherapy

The use of high energy radiation to kill cancer cells is known as radiotherapy. This is typically carried out using external irradiation with a high energy X-ray beam generated with a linear accelerator. An alternative approach is radioimmunotherapy, in which the therapeutic radiation dose is provided by the systemic administration of a radioisotope targeted to the tissue or tumour (often by conjugation of a chelator to bind a metal ion radioisotope with a monoclonal antibody or peptide). Radioimmunotherapy utilises radioisotopes which decay by α, β^- or Auger electron decay.[16] It is generally used in conjunction with nuclear diagnosis and the radionuclides should therefore have complimentary properties. Emission of the radionuclide should be primarily damaging, with low amounts of penetrating gamma radiation to allow specificity of damage to the local area. However multiple decay pathways can also be seen as an advantage, with ^{64}Cu having applications for both diagnosis and therapy,[8,133,134] see *section 1.1.1.1.2.2.1.* Design of the chelator and specificity of the biomolecule is of upmost importance to reduce destructive non-localised dose. A wide range of radiometals are used in radioimmunotherapy, from heavy metal α emitters such as ^{213}Bi to β emitters such as ^{177}Lu and ^{90}Y.[16]

1.3.1. ^{90}Y

^{90}Y has a half-life of 64 hours, making it a useful radioisotope for radioimmunotherapy (targeted specifically using an antibody) due to the long biological half-lives common with antibodies.[16] A long half life also allows the isotope to be easily transported to clinical locations. Yttrium exists exclusively in oxidation state III and its chemical properties have been discussed previously, see *section 1.1.1.1.2.2.2.* ^{90}Y is generator produced from ^{90}Sr ($t_{1/2}$ = 28.8 years) in high specific activities and decays by pure β^- emission.[135,136] The FDA approved agent named Zevalin® (Spectrum) is a monoclonal antibody for targeting B-cell non-Hodgkin's lymphoma which is labelled with ^{90}Y for radioimmunotherapy or with ^{111}In for diagnosis/treatment progression, the success of which has caused an increase in the number of ^{90}Y clinical trials.[9]

1.4. Developing further medical applications of radiometals

Medical imaging offers the possibility for early stage diagnosis of many diseases, with increasing availability of scanners for various imaging modalities now catching up with the availability of imaging agents. Research in this field requires focus on the development and translation of new imaging agents to rival the $[^{18}F]$-FDG clinical PET impact and the ^{99m}Tc dominance of SPECT. Future developments will offer the clinicians a 'toolkit' of radiotracers to move more towards personalised medicine.

Radiometals fill a specific clinical niche in this area, with their generally longer half-lives ideal for imaging with larger biomolecules. The use of chelators which form highly stable complexes with a range of metals is worthy of future research effort in an attempt to have a single construct which, by varying the metal, can be used in a wide range of imaging modalities and also radioimmunotherapy. The development of new technologies such as PET/MRI clinical scanners offers unique advantages and an opportunity for research scientists to pioneer new imaging agent technologies that maximise the potential of the technique.

1.5. Aims

The aims of this thesis are three fold:

- Design and synthesis of novel benzimidazole DO3A based bifunctional chelators for use with positron emitting radioisotopes such as ^{68}Ga for positron emission tomography (PET), see Figure 20.
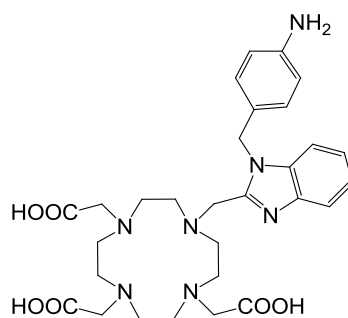
Figure 20 – Chemical structure of example target benzimidazole DO3A derivative.

- Formation of PET/MRI imaging agents derived from surface modification of super-paramagnetic iron oxide nanoparticles (T_2 MRI contrast agents) with macrocycles along with the study of the radiochemical properties of such conjugates with ^{68}Ga, see Figure 21.
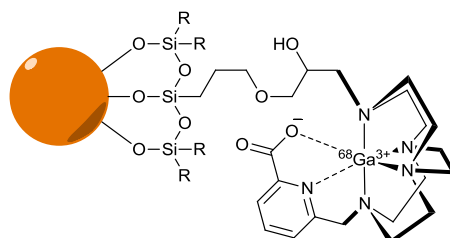
Figure 21 – Example schematic of target PET/MRI imaging agent.

- Further study of the physiochemical characteristics of a benzimidazole DO3A derivative to gain insight into the coordination environment towards future use of [86]Y and ^{90}Y for PET and radioimmunotheraphy respectively, see Figure 22.
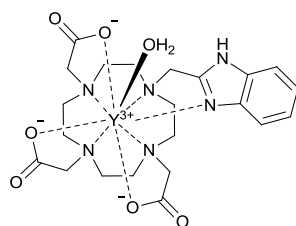
Figure 22 – Chemical structure of yttrium(III) benzimidazole DO3A complex to be studied.

Chapter 2

Synthesis and ^{68}Ga radiolabelling of benzimidazole DO3A derivatives

2. Synthesis and ⁶⁸Ga radiolabelling of benzimidazole DO3A derivatives

2.1. Aims

This chapter reports the synthesis and ^{68}Ga radiolabelling of tetraazamacrocycles for use as bifunctional chelators for PET. The initial step is the synthesis of benzimidazole based precursors, see *section 2.2*, which are then conjugated to a macrocyclic backbone, see *section 2.3,* to form DO3A derivatives. This was followed by ^{68}Ga radiosynthesis optimisation, see *section* 2.4 and radiolabelling of all chelators under the conditions determined, see *section 2.5*.
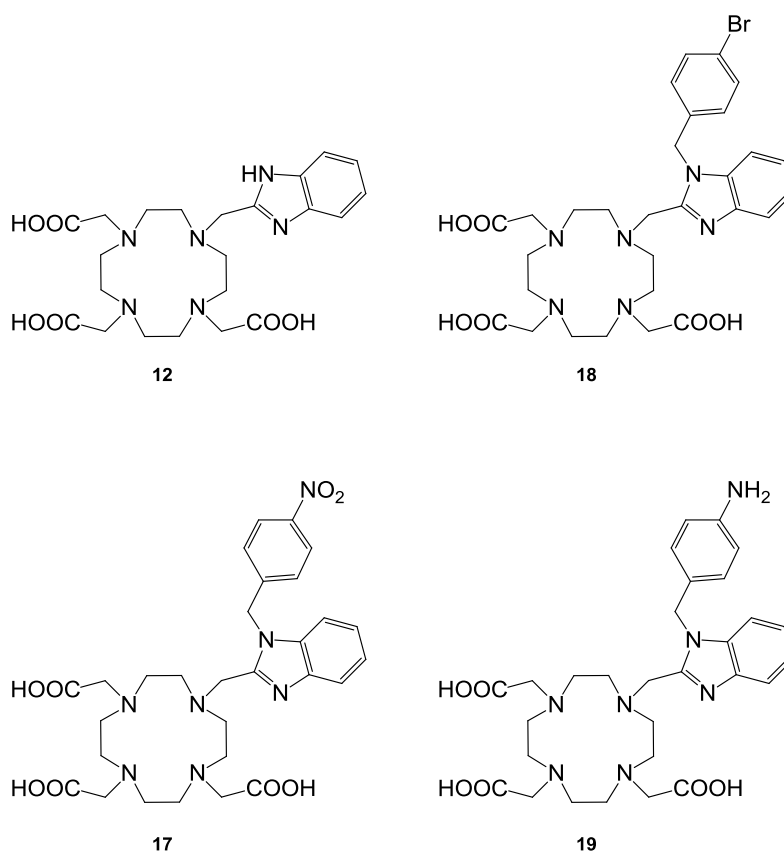
Figure 23 – Chemical structures of the target benzimidazole DO3A derivatives.

Development of novel chelators that can bind ^{68}Ga with properties that also enable them to be used for a range of metals in different applications offers a key advance in this area.

2.2. Synthesis of benzimidazole DO3A precursors

Benzimidazoles are present naturally and are an integral part of the structure of vitamin B$_{12}$.[137] In synthetic drug design, benzimidazole based compounds have been incorporated into pharmaceuticals and have shown high anticancer and antimicrobial activity.[138-140] The absorbance wavelength of benzimidazole overlaps with the range of biological processes (>300 nm), however measurements can be gated to distinguish fluorescence from phosphorescence.

Benzimidazoles have characteristics, see Figure 24, which make them an ideal choice for this work:

1. Highly conjugated π system for use as a chromophore
2. Nitrogen atom for metal coordination
3. The potential to include a reactive carbon group to attach to a chelator
4. Reactive nitrogen position for radiolabelling or bioconjugation

With a view to synthesising macrocyclic benzimidazole DO3A derivatives, this section reports the synthesis of benzimidazole precursors for further modification.
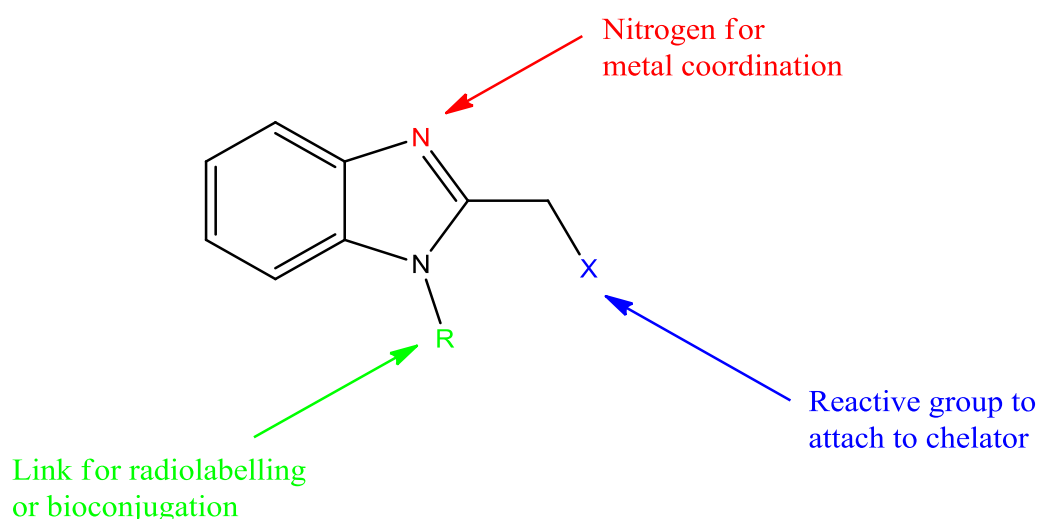
Figure 24 – Annotated molecular structure of benzimidazole precursor.

2.2.1. Methods for N-functional benzimidazole synthesis

The synthesis of multi-functionalised benzimidazole derivatives can be achieved in a two-step process which involves a cyclisation step and a nucleophilic substitution step, either step can be undertaken first, with both routes shown in *Scheme 2.*
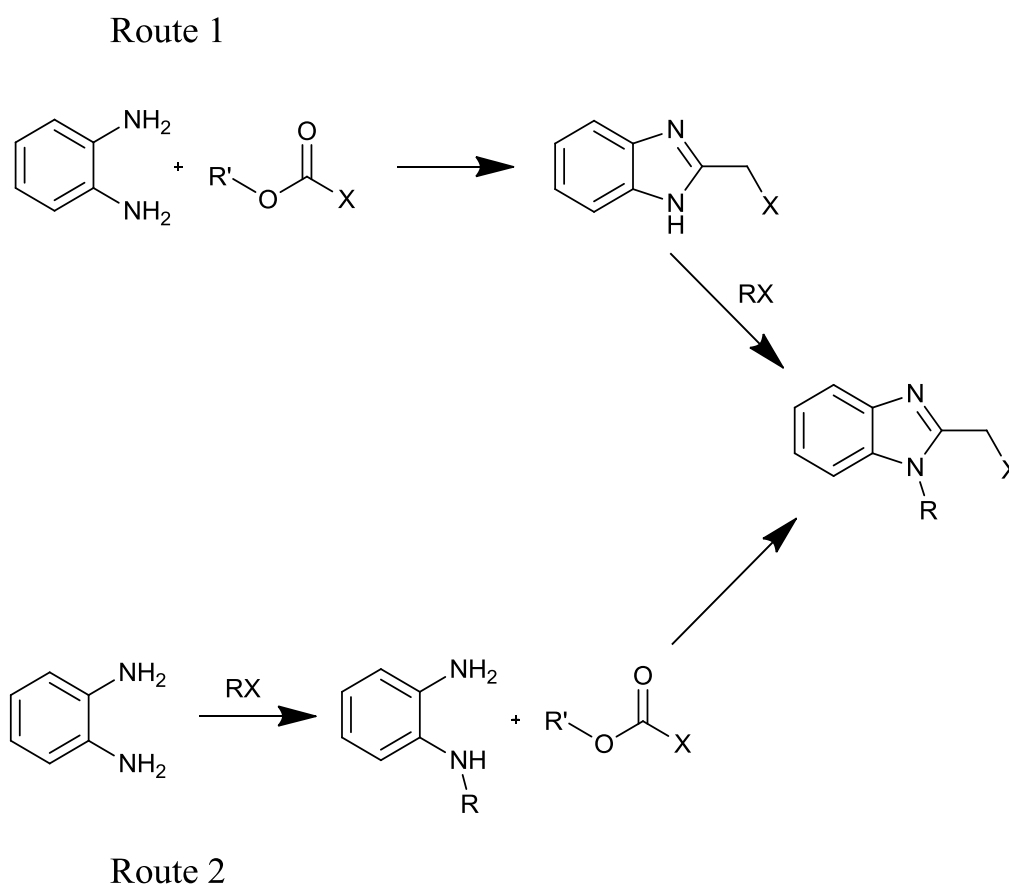
Route 1

Route 2

Scheme 2 – Two potential strategies for synthesis of benzimidazole precursors (R' = H or CH$_2$CH$_3$, X = OH, Cl or Br); route 1 and route 2.

Route 1 involves initial cyclisation to form the benzimidazole unit followed by nucleophilic substitution at the secondary amine on the imidazole to form the target benzimidazole derivative. Route 2 involves the mono substitution of *o*-phenylenediamine followed by the cyclisation step to form the target benzimidazole. Both of these methods have been employed in the literature with varying success that is dependent on the substitution group employed in each method.[141-144] It was also thought possible that a nucleophilic substitution, such as in route 1, could be performed once the benzimidazole has been attached to the macrocyclic chelator, see *section 2.3.6.*

2.2.1.1. Synthesis of N-functionalised benzimidazole derivatives using route 1

Route 1 involves initial cyclisation of the benzimidazole backbone followed by nucleophilic substitution on the secondary amine to form an N-functionalised benzimidazole precursor, see *Scheme 3*. Successful substitution on the imidazole amine depends on the halide leaving group used and the electron withdrawing/donating properties of both reagents, influencing the nucleophilic properties of the electron pair on the imidazole amine.
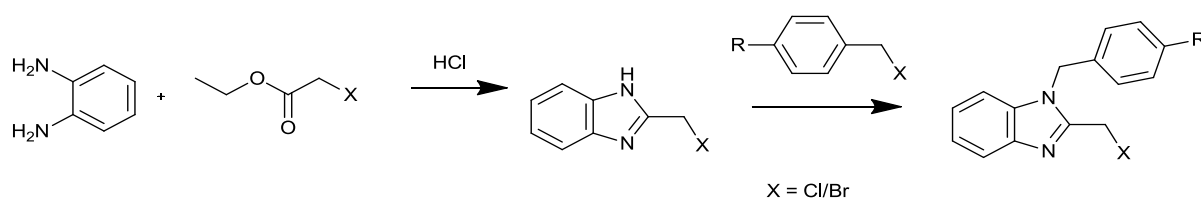
Scheme 3 – Proposed synthetic route to form N functionalised benzimidazole precursors following route 1.

Shi *et al.* used this route to form a dibenzimidazole compound by performing the reaction in a mixture of DMF and H_2O using KOH as a base, see *Scheme 4*.[145] They also surprisingly managed to do a further reaction on the free amine to form the di-quaternary ammonium salt by refluxing the starting material in MeCN, without the need for a base.
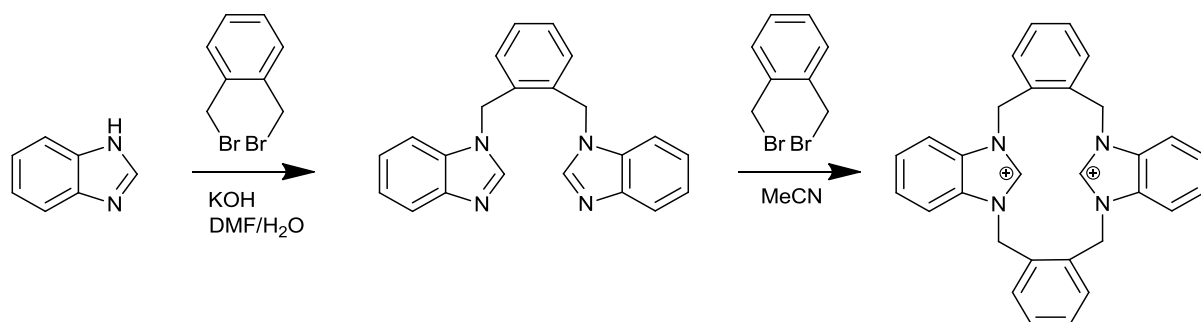
Scheme 4 – Formation of N-functionalised benzimidazole using route 1.[145]

2-(Bromomethyl)-benzimidazole (**1**) was identified as a suitable precursor as it contains a terminal alkyl bromide, a good leaving group for further nucleophilic substitution reactions. This is a useful comparison to the commercially available 2-(chloromethyl)-benzimidazole to see how the choice of halide affects the substitution reactions, see *section 2.3.3.* Reactions to form **1** are well known in the literature and generally involve a condensation reaction between *o*-phenylenediamine and ethylbromoacetate, see *Scheme 5.*[146]
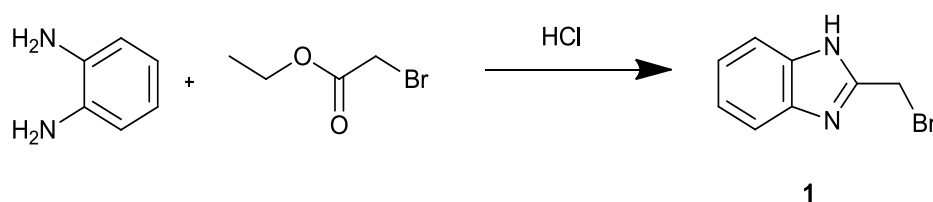
Scheme 5 – Condensation reaction to form 2-(bromomethyl)-benzimidazole.

The 4M HCl solution is heated to reflux followed by a 0°C alkaline work up, causing precipitation of the product. Analytical data confirms the formation of the target compound **1**, albeit in a lower yield (51%) than which was reported (79%).

Protection of the reactive secondary amine was performed to form *tert*-butyl 2-(chloromethyl)-1H-benzo[d]imidazole-1-carboxylate (**2**) in an effort to avoid 'self-reaction' to form a double benzimidazole during further reactions with macrocyclic chelators, see *Scheme 6*. The reaction was carried out using a modified version of standard literature methods for amine protections of this kind.[147] Di-*tert*-butyl dicarbonate (Boc$_2$O) was used to 'boc' protect the secondary amine with triethylamine (TEA) as a base. ^{1}H-NMR, ^{13}C-NMR and MS confirms isolation of the product in a reasonable yield (75%).
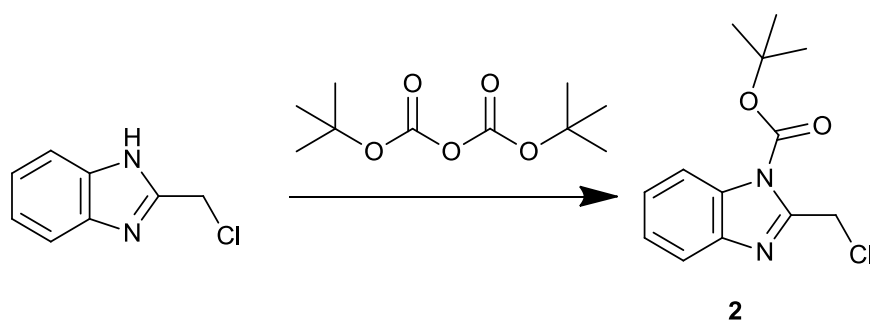
Scheme 6 – Reaction scheme to form boc protected 2-(chloromethyl)-benzimidazole.

Syntheses of 1-(4-bromobenzyl)-2-(chloromethyl)-1H-benzo[d]imidazole (**3**) and 2-(chloromethyl)-1-(4-nitrobenzyl)-1H-benzo[d]imidazole (**4**) were attempted using 4-bromobenzyl bromide and 4-nitrobenzyl bromide as a way to form benzimidazole derivative with a functional group for further reaction, see *Scheme 7*.
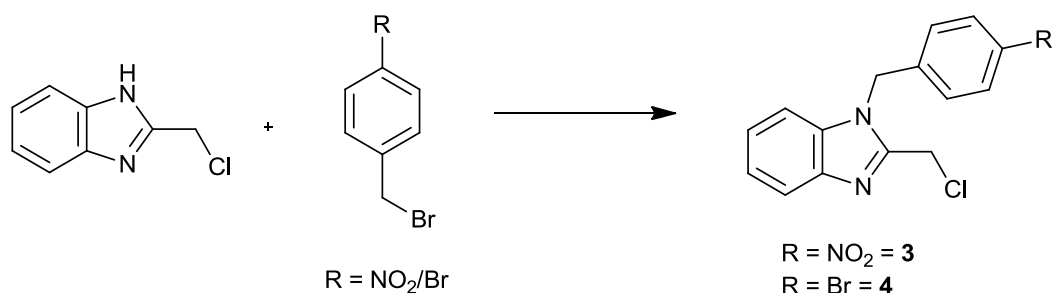
Scheme 7 – Attempted reactions to form N-functionalised benzimidazole derivatives.

The reaction was attempted following a similar method to that used by Thomas *et al.*[148] A polar, aprotic solvent (DMF) was used to facilitate the substitution reaction and potassium carbonate was used as a base. ^{1}H NMR analysis showed that attempts at purification of these compounds using column chromatography were unsuccessful. Previous literature reactions did not include a reactive halide group on the benzimidazole and this may have caused the formation of unwanted side products which were difficult to separate from the desired compounds due to them having similar rf values. Other reaction methods were considered, each of which having limitations when using alkyl halide terminating species. After considering these as possibilities it was thought that employing any of these measures

would cause 'self-reaction' of 2-(chloromethyl)-benzimidazole, an inherent problem of molecules of this nature which also include alkyl halides. With further developments, route 1 may have led to a successful synthesis but route 2 was a known literature method for the formation of 1-(4-bromobenzyl)-2-(chloromethyl)-1H-benzo[d]imidazole (**3**).[143]

2.2.1.2. Synthesis of N-functionalised benzimidazole derivatives using route 2

Route 2 involves an initial alkylation of *o*-phenylenediamine with an alkyl halide derivative followed by a cyclisation step to form an N-functionalised benzimidazole precursor, see *Scheme 8*.
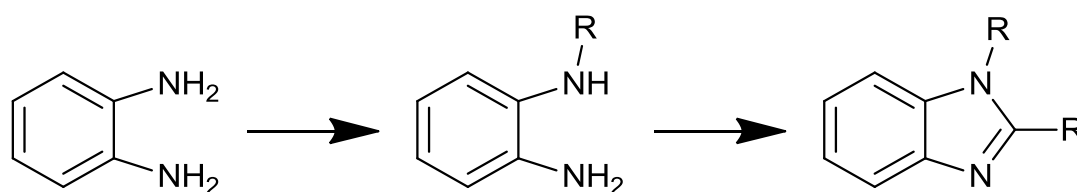
Scheme 8 – General method of N-functionalised benzimidazole synthesis following route 2.

Goker *et al*. used this strategy when synthesising anti-fungal molecules, see *Scheme 9*.[149] In this synthetic method the $Na_2S_2O_5$ adduct of various benzaldehydes in DMF was used to form the benzimidazole backbone after initial alkylation of o-phenylenene diamine.
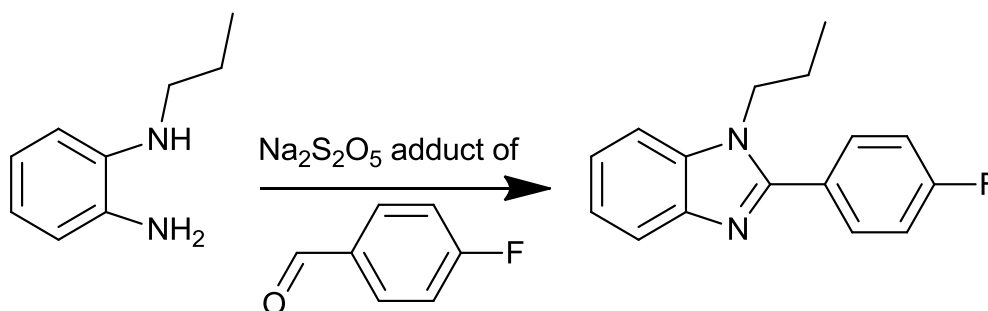
Scheme 9 – Formation of anti-fungal N-functionalised benzimidazole.[149]

Lin *et al.* have also employed this route when synthesising N-functionalised benzimidazoles.[150] Using microwave heating in an attempt to synthesise variations on the

molecules shown in *Scheme 10*, when using P(OPh)₃ as a catalyst the reaction is high

yielding (80-100%) with a variety of different functional groups incorporated.
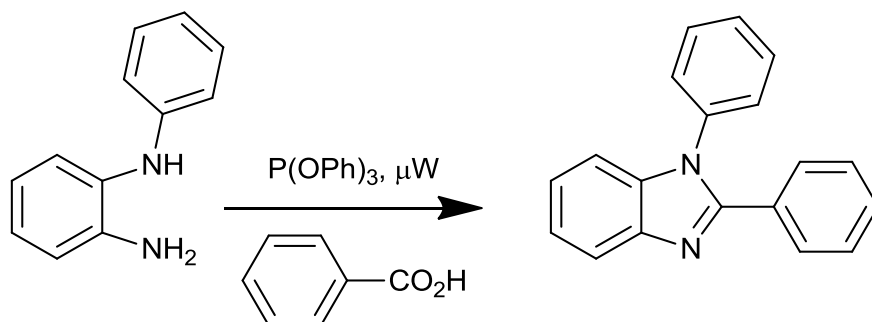
Scheme 10 – Synthesis of N-functionalised benzimidazole using microwave synthesis techniques.[150]

The synthesis in this work was carried out via an initial alkylation of *o*-phenylenediamine

with a para substituted benzyl halide to form **5/6**, this is followed by a cyclisation step to

form the benzimidazole **7/8** and finally conversion of the hydroxyl group into a chloride to

offer a reactive site for further reactions (**3/4**), see *Scheme* 11. All reactions in this scheme

were performed following literature methods.[143,151]
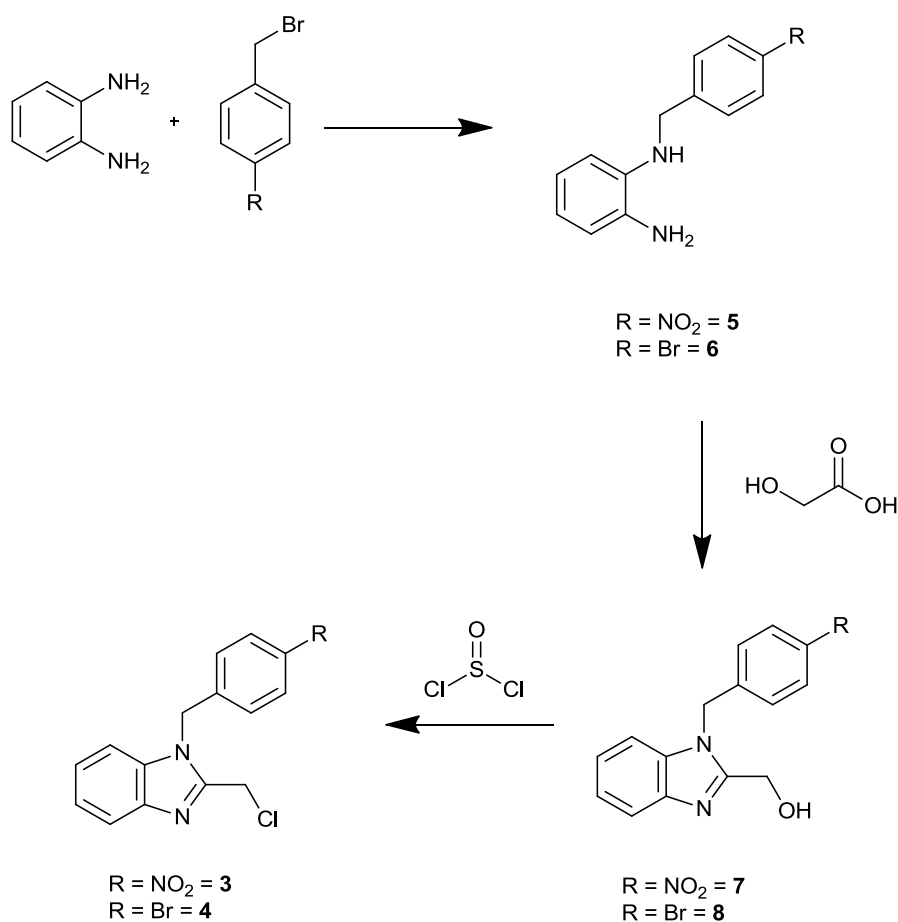
Scheme 11 – Synthetic route to form N-functionalised benzimidazole precursors following route 2.

The initial alkylation was performed by addition of the benzylbromide derivative in methanol drop-wise into a five-fold excess of *o*-phenylenediamine in methanol over 30 minutes. The reaction stirred at room temperature for 4 hours then the solvents were removed. TLC analysis of N1-(4-nitrobenzyl)benzene-1,2-diamine (**5**) showed multiple products with similar rf values and so a recrystallisation step was performed, followed by silica gel column chromatography to give **5** in an 85% yield. The same method was attempted with N1-(4-bromobenzyl)benzene-1,2-diamine (**6**) but the purification by recrystallisation was unsuccessful, however two subsequent separations using silica gel column chromatography resulted in the isolation of pure product in a 67% yield.

Cyclisation reactions of **5** and **6** were performed by dissolving the compounds in 5M HCl and adding a 1.5 molar excess of glycolic acid which were then heated to reflux for 60 hours. A basic work up with sodium hydroxide causes the product to precipitate. The reaction to form (1-(4-bromobenzyl)-1H-benzo[d]ydrophil-2-yl)methanol (**8**) gave pure product by NMR and elemental analysis but in only a 29% yield. NMR and TLC analysis showed (1-(4-nitrobenzyl)-1H-benzo[d]48ydrophil-2-yl)methanol (**7**) required purification, which was achieved using silica gel column chromatography to give **7** in a 52% yield.

The hydroxyl group can then easily be converted to the chloride by treatment with thionyl chloride to give **3** and **4** in 68% and 83% yields respectively. There is a clear downfield shift in the ^{1}H NMR of the CH$_2$ peak, from 4.86 ppm to 6.04 ppm for **3** and 4.82 ppm to 5.83 ppm for **4** due to the increased electron withdrawing properties of the chloride compared with the hydroxyl group.[151] Isolation of the desired products was confirmed using MS analysis. The target compounds **3** and **4** were synthesised in a three step reaction with overall yields of 30% and 16% respectively.

2.2.2. Synthesis of benzimidazole precursors – summary

Four benzimidazole based compounds have been synthesised for attachment to the chelator backbones, see Figure 25. Two routes were investigated in an attempt to synthesise N-functionalised benzimidazole precursors. In route 1, a cyclisation reaction is performed, followed by nucleophilic substitution reaction, however this method was unsuccessful in producing the desired products. 2-(Bromomethyl)-1H-benzo[d]imidazole (**1**) was synthesised to allow the direct substitution of the formed benzimidazole unit in an analogous manner once it is conjugated to a chelator.

2-(Chloromethyl)benzimidazole has also been 'boc' protected to form *tert*-butyl 2-(chloromethyl)-1H-benzo[d]imidazole-1-carboxylate (**2**) to try and avoid possible 'self-reaction' during subsequent functionalisation steps.

In route 2, alkylation of *o*-phenylenediamine is followed by cyclisation in a method which was used successfully to form the desired products, 2-(chloromethyl)-1-(4-nitrobenzyl)-1H-benzo[d]imidazole (**3**), and 1-(4-bromobenzyl)-2-(chloromethyl)-1H-benzo[d]imidazole (**4**) in overall yields of 30% and 16% respectively. **3** and **4** are key precursors in the synthesis of benzimidazole containing BFCs.
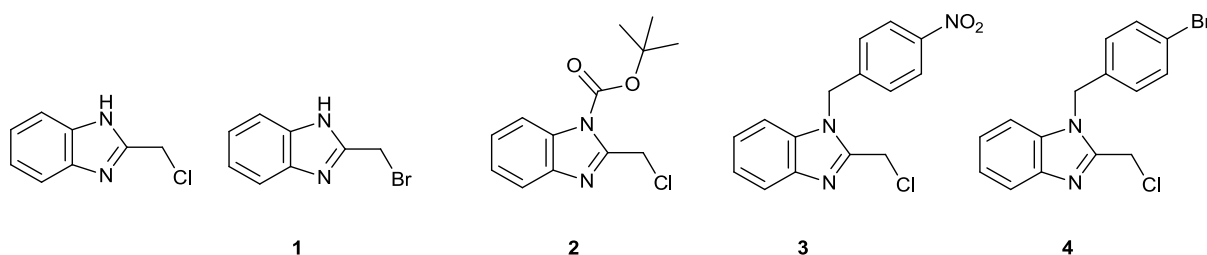
Figure 25 – Chemical structures of the synthesised benzimidazole precursors.

2.3. Synthesis of macrocyclic chelators

2.3.1. Synthetic methodology to form functionalised DO3A derivatives

1,4,7-Tris(*tert*-butoxycarbonylmethyl)-1,4,7,10-tetraazacyclododecane (*t*Bu-DO3A) functionalised derivatives are generally synthesised using one of two possible routes, see *Scheme* 12. Route 1 involves selective triple alkylation of the cyclen ring with *tert*-butyl ester protected carboxylic acids, followed by functionalisation of the remaining secondary amine with a different reactive arm. Route 2 involves formation of a glyoxal bridge, followed by selective alkylation of a single nitrogen which is favoured due to the folded nature of the bridged cyclen causing only two of the nitrogens to be oriented with the lone pairs pointing out of the formed cavity in a suitable orientation for reaction.[152] In addition, selection of a suitable solvent causes the quaternerised amino product to precipitate out of solution and it therefore cannot react beyond a single substitution.[153] The bridge is then removed with hydrazine and the remaining secondary amines can be alkylated in a similar way as route 1 to form the desired 3:1 unsymmetrical product.
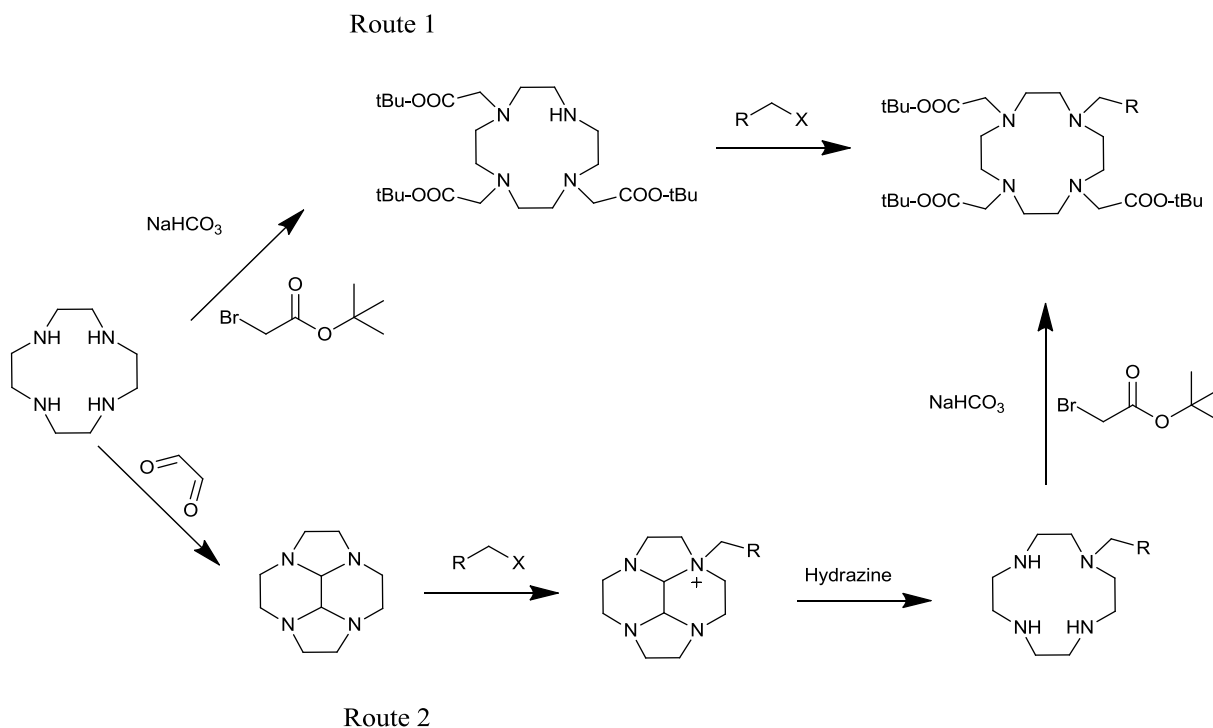
Scheme 12 – Two routes for the synthesis of DO3A derivatives.

Route 2 has the advantage of giving mono-substituted cyclen in high purity, and so no chromatpgraphic separation is required, but has the disadvantage of low overall yields due to the increased number of steps and the variability in yield dependent on pendant arm selection. Route 1 has the advantage of only being a two-step synthesis with little loss of cyclen overall but has the problem of forming mixed arm products in the first reaction which can be challenging to purify. Route 1 was selected as the preferred option and route 2 was not attempted.

2.3.2. Synthesis of 1,4,7-tris(*tert*-butoxycarbonylmethyl)-1,4,7,10-tetraazacyclododecane (*t*Bu-DO3A)

The synthesis of 1,4,7-tris(*tert*-butoxycarbonylmethyl)-1,4,7,10-tetraazacyclododecane (*t*Bu-DO3A) (**9**) was initially attempted following the standard literature procedure,[154] *tert*-butylbromoacetate in a three-fold excess in chloroform is added drop-wise into a stirred solution of cyclen and sodium hydrogen carbonate in chloroform, see *Scheme* 13. The reaction is stirred for 72 hours then the solvents are removed.
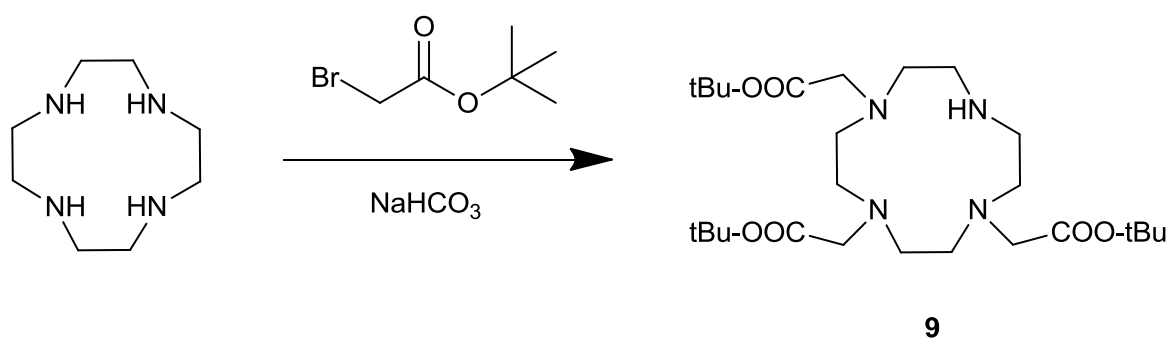
*Scheme 13 – Synthesis of tBu-DO3A (**9**).*

This reaction forms a mixture of multiple arm products, due to selectivity being controlled by stoichiometry, which then need to be separated by silica gel column chromatography to give 1,4,7-tris(*tert*-butoxycarboxymethyl)-1,4,7,10-tetraazadodecane (*t*Bu-DO3A) (**9**). Yields are relatively low (~55%) for this reaction and although ^{1}H and ^{13}C NMR of the product

showed it to be relatively pure, MS confirmed some contamination with tetra substituted cyclen which is very difficult to separate by chromatography. At this stage a new method was sought in an effort to isolate the pure product in higher yields.

An alternative literature method was found which involved a two-step reaction which proceeds through the hydrobromide salt (**10**) before forming *t*Bu-DO3A (**9**), see *Scheme 14*.[155]
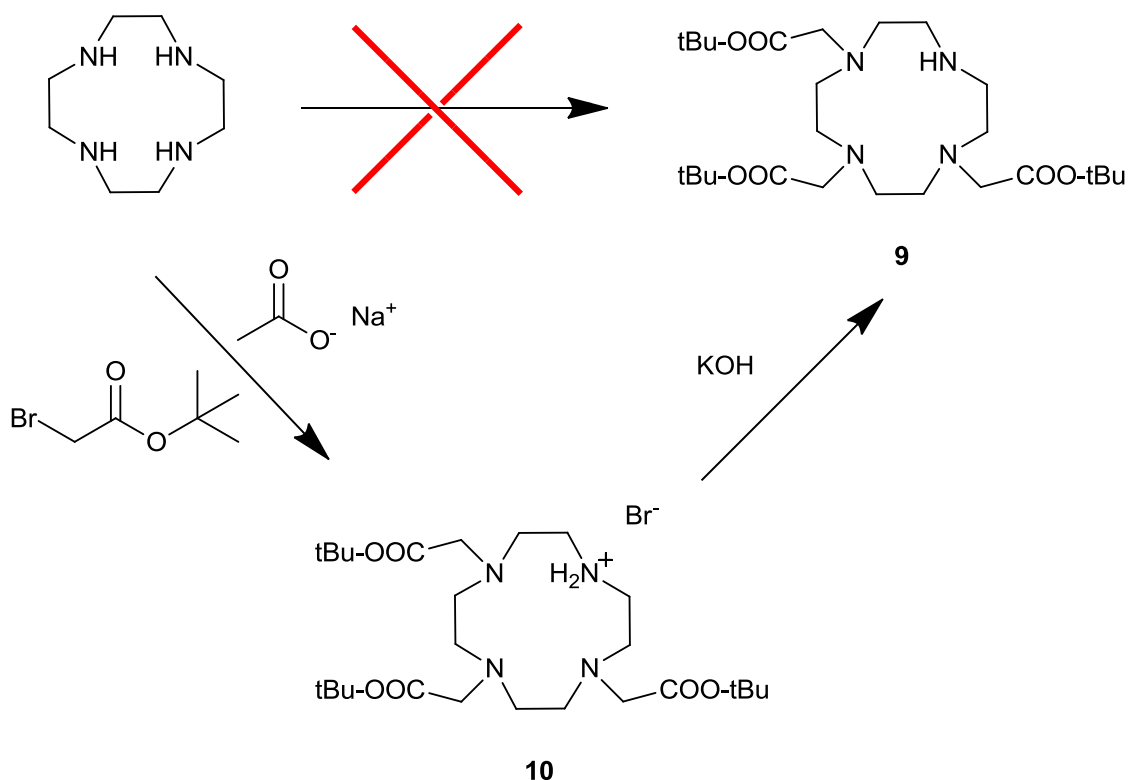
*Scheme 14 – Alternative synthetic route to form tBu-DO3A (**9**).*

The reaction conditions involve changing the solvent to dimethylacetamide (DMA) and using sodium acetate as a base. This results in the formation of 4,7,10-tris(2-(*tert*-butoxy)-2-oxoethyl)-4,7,10-triaza-azoniacyclododecan-1-ium bromide (*t*Bu-DO3A.HBr) (**10**) after 24 hours which, following work up, was isolated in a 78% yield. The hydrobromide salt (**10**) is easily converted into *t*Bu-DO3A (**9**) by dissolving in hot (70°C) water and adding a 10% aqueous solution of potassium hydroxide in a two-fold excess, which causes **9** to precipitate out in near quantitative yield.

The original method gave relatively pure products in *ca.* 55% yields after 72 hours reaction time, purification by silica gel column chromatography and at scales limited to *ca.* 5g of **9.**

The two-step method which goes through a hydrobromide intermediate (**10**) gives high purity compound as characterised by NMR and MS in an overall yield of *ca.* 75% yield in 26 hour reaction times, without the need for chromatography and has been scaled up to form above 11g of **9**.

2.3.3. Synthesis of 1,4,7-tris(*tert*-butoxycarboxymethyl)-10-(2-methylbenzimidazolyl) tetraazadodecane

Once *t*Bu-DO3A (**9**) had been synthesised in high enough purity alkylation of the secondary amine could be performed. Initially, a route which was analogous to the synthesis in *section 2.2.1.1.* was proposed, in which unprotected halide benzimidazole is attached to the macrocycle followed by alkylation of the imidazole secondary amine, see *Scheme* 15.
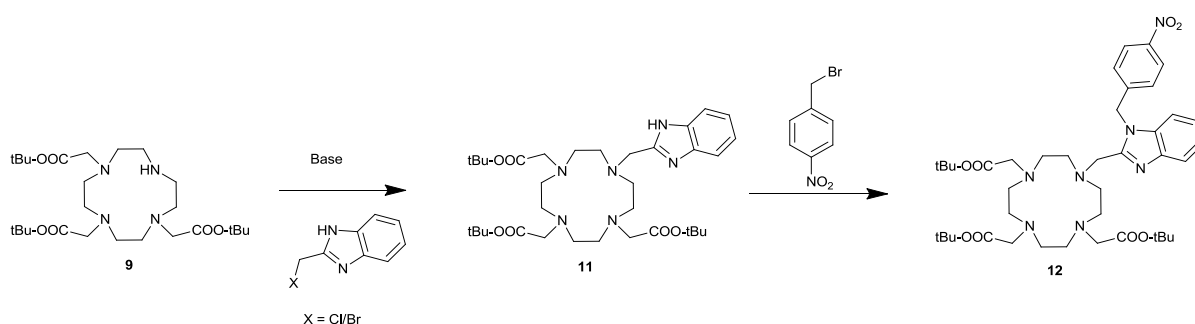
Scheme 15 – Proposed synthetic route to form N-functionalised DO3A derivatives.

The initial conditions attempted for the reaction to form tri-*tert*-butyl 2,2',2''-(10-((1H-benzo[d]ydrophil-2-yl)methyl)-1,4,7,10-tetraazacyclododecane-1,4,7-triyl)triacetate (**11**) used DMF as a solvent, potassium carbonate as a base with catalytic amounts of potassium iodide and a 1.1 excess of benzimidazole and to heat the reaction for 3 hours under reflux.[156] Purification of macrocyclic products from non-macrocyclic products is relatively simple by using a neutral alumina plug, eluting with ethyl acetate for removal of non-

macrocyclic materials then methanol to isolate the macrocyclic components. Purification to separate the different macrocycles is more challenging due to the similar rf values on both alumina and silica stationary phases. ^{1}H NMR and MS analysis of the products from this reaction showed some 'self-reaction' on the benzimidazole (**11a**), see *Scheme 16*.
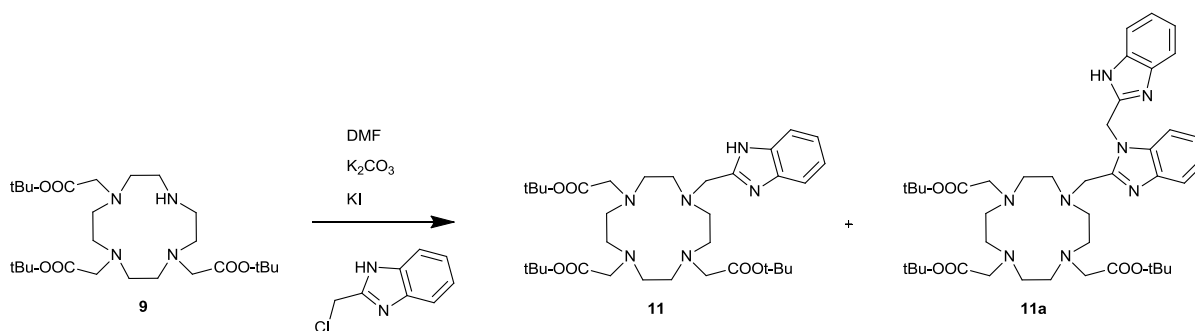
*Scheme 16 – Formation of benzimidazole tBu-DO3A (**11**) and 'self-reaction' product (**11a**).*

It was believed that 'boc' protection of the imidazole amine could offer the advantage of preventing the 'self-reaction', see *Scheme 17*, and the imidazole can then be deprotected concurrently with the *tert*-butyl protecting groups to yield the desired product.
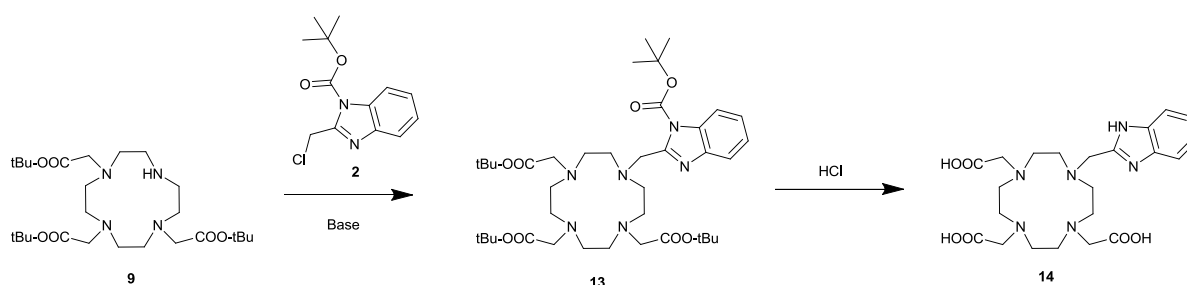
*Scheme 17 – Synthetic route attempted to form **14** via benzimidazole 'boc' protection.*

Conditions for this reaction were varied in an effort to take the reaction to completion as it was observed in the ^{1}H NMR spectrum that protecting the amine was causing a reduction in the reactivity of the benzimidazole halide, even the use of a ten-fold excess of benzimidazole failed to take the substitution reaction to completion. As reaction times and temperatures were increased however other complications arose and evidence of both base catalysed deprotection and polymerisation were seen by MS.

Reaction conditions could not be found to form the desired compound (**13**) and efforts were turned back to tuning reaction conditions in the initial reaction to form **11**, aiming to avoid 'self-reaction'. The solvent was subsequently changed to acetonitrile as it was thought DMF may be facilitating the deprotonation of the benzimidazole proton due to the high polarity of the solvent. Various reaction conditions were tried in an attempt to limit the 'self-reaction'. Using 2-(bromomethyl)-benzimidazole was problematic as the 'self-reaction' is favoured over the reaction with the macrocyclic amine even in stoichiometric amounts. Reaction conditions were developed to synthesise benzimidazole *t*Bu-DO3A (**11**) in very high purity and near quantitative yields, see *Scheme 18*, using a stoichiometric amount of *t*Bu-DO3A (**9**) and 2-(chloromethyl)-benzimidazole. Caesium carbonate was used as a base, with caesium(I) being too large to form macrocycle complex with the metal ion within the macrocyclic cavity. A large amount of dry acetonitrile (*ca.* 400 ml per gram) as the solvent and the reaction stirred at room temperature for 18 hours, increasing reactions time/temperature promoted 'self-reaction'. MS analysis confirms the synthesis of **11** and the absence of peaks for any doubly substituted benzimidazole but interpretation of the NMR spectra at this stage is difficult due to a mixture of protonated and deprotonated benzimidazole in solution. The NMR spectra after deprotection of the *tert*-butyl arms to form the DO3A derivative; 1,4,7-tris(*tert*-butoxycarboxymethyl)-10-(2-methylbenzimidazolyl) tetraazadodecane (**14**) gives a clearer indication of the purity of benzimidazole DO3A derivatives demonstrating that a pure product has been formed.
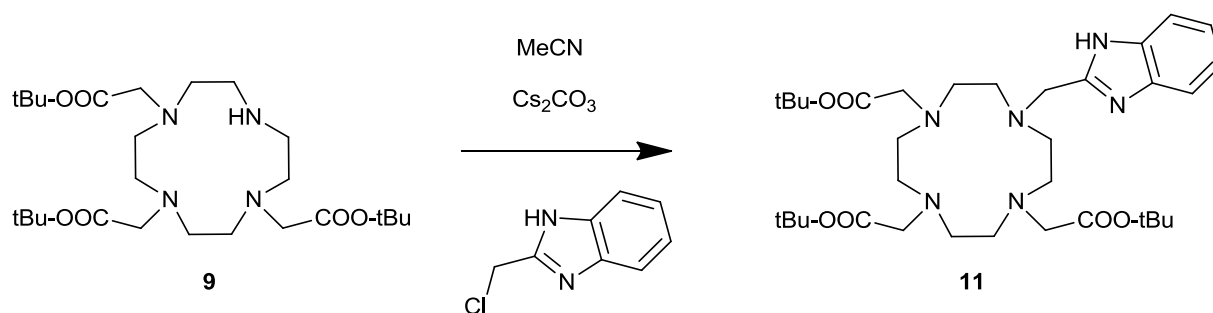
*Scheme 18 – Synthesis of benzimidazole tBu-DO3A (**11**).*

The acid catalysed hydrolysis of esters is a common method used in deprotection of DO3A derivatives and proceeds by heating the reaction mixture to reflux. Deprotection of **11** was initially carried out by dissolving the compound in 6M HCl and heating the reaction mixture to reflux for 18 hours, see *Scheme 19.* After the solvents were removed, ether was added and decanted multiple times to dissolve and remove any ether soluble impurities.
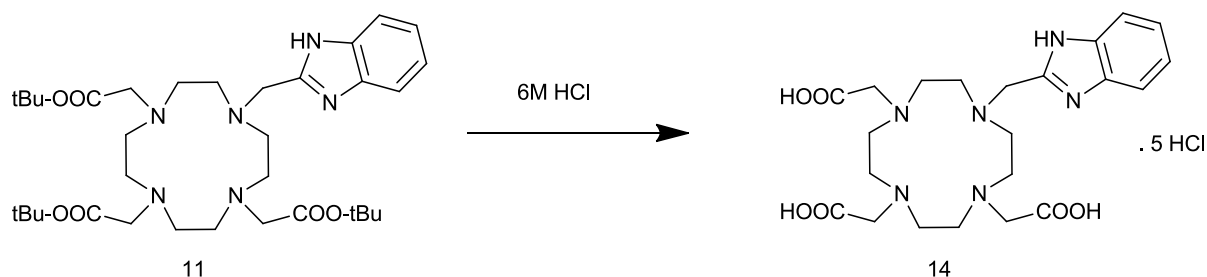
*Scheme 19 – Deprotection reaction to form benzimidazole DO3A (BIDO3A, **14**).*

^{1}H NMR can be used to follow the reaction as the characteristic 'boc' peak at ca. 1.46 ppm disappears. TLC also offers useful *in situ* information due to the large difference in polarity between starting material and product. Using NMR as a tool to determine purity is much easier at this stage of the scheme compared with analysis of the protected version (**11**) as using HCl completely protonates the imidazole, giving a characteristic pattern for the aromatic region and showing that no 'self-reaction' has occurred, see Figure 26. **14** was fully characterised by NMR, MS and elemental analysis which showed that it was the penta HCl salt. HPLC analysis showed the compound to be 93% pure.
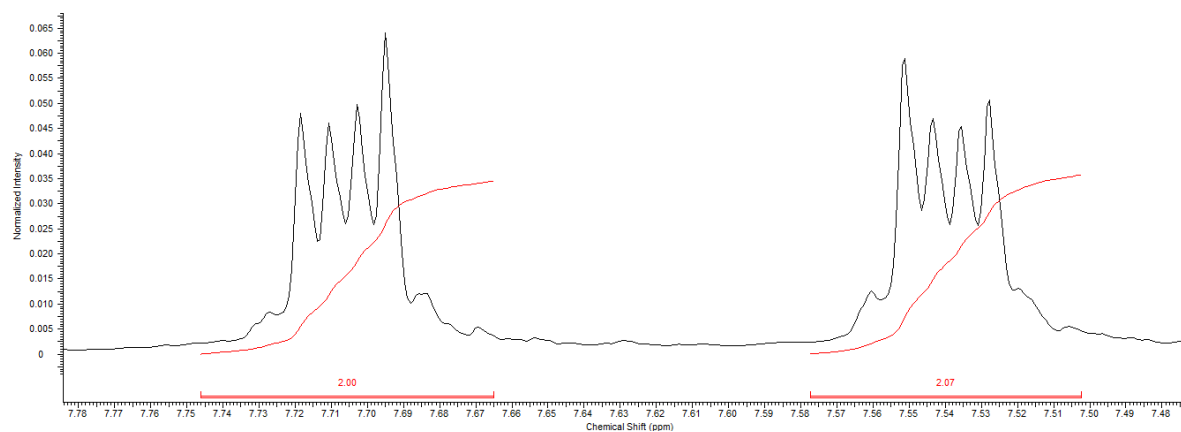
*Figure 26 – Aromatic region of the ^{1}H NMR spectrum of **14** showing characteristic pattern for protonated benzimidazoles.*

In an effort to reduce reaction times, the ester hydrolysis was successfully carried out using a microwave reactor, heating the reaction at 130°C which gives the desired compound in the same levels of purity but reduces the reaction time from 18 hours to 10 minutes. This method is the recommended deprotection method for molecules of this kind due to the very rapid high yielding conversion.

2.3.4. Synthesis of N-Functionalised benzimidazole DO3A

Two routes for the synthesis of N-functionalised benzimidazole DO3A were proposed, see *Scheme 20.* Route 1 involves alkylation of the previously synthesised tri-*tert*-butyl 2,2',2''-(10-((1H-benzo[d]ydrophil-2-yl)methyl)-1,4,7,10-tetraazacyclododecane-1,4,7-triyl)triacetate (**11**). Route 2 involves direct alkylation of *t*Bu-DO3A (**9**) with the previously synthesised N-functionalised benzimidazole derivatives **3** and **4**, see *section 2.2.* Both routes offer a method to synthesise an N-functionalised benzimidazole DO3A derivative with a reactive arm for further bioconjugation.
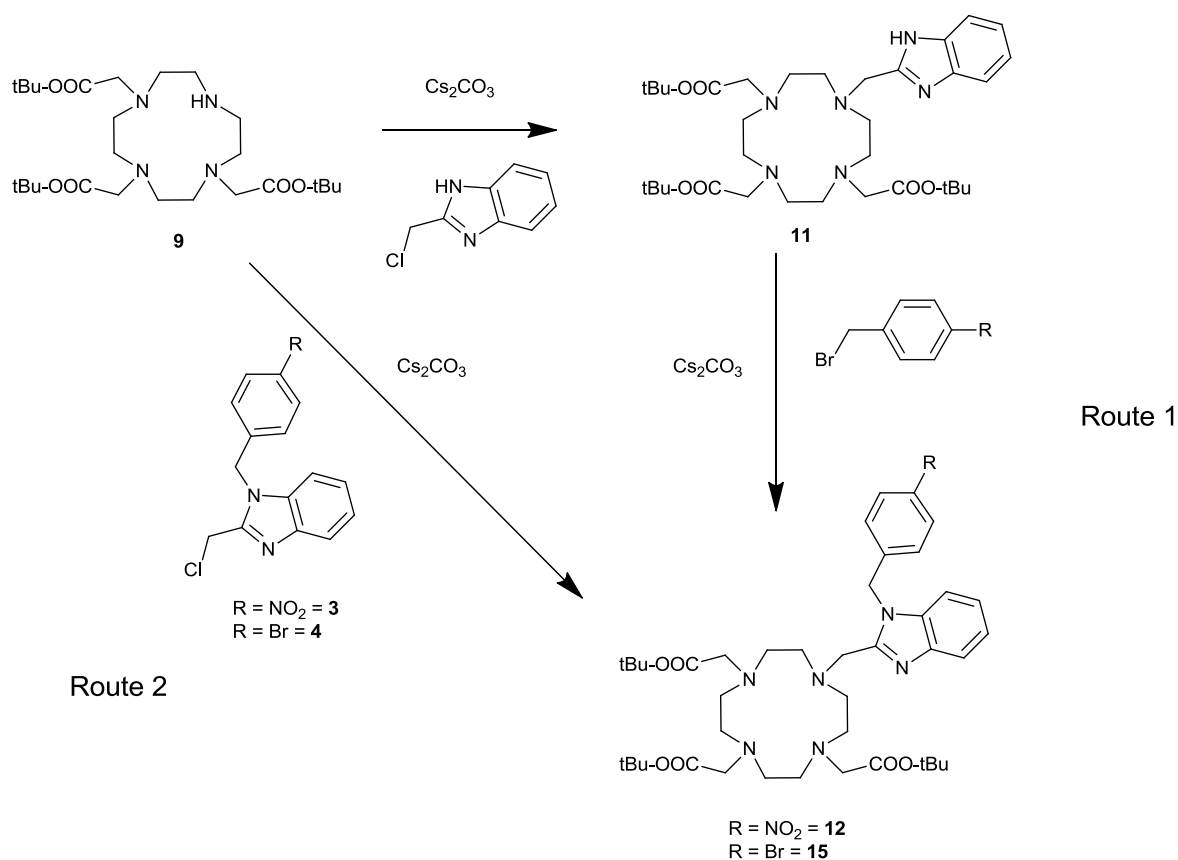
Scheme 20 – Proposed synthetic routes to form N-functionalised benzimidazole DO3A derivatives.

2.3.5. Synthesis of N-functionalised benzimidazole DO3A derivatives using route 1

Route 1 involves alkylation of **11** and was performed in an analogous way to the method described in *section 2.2.1.1.*, see *Scheme* 21*.*
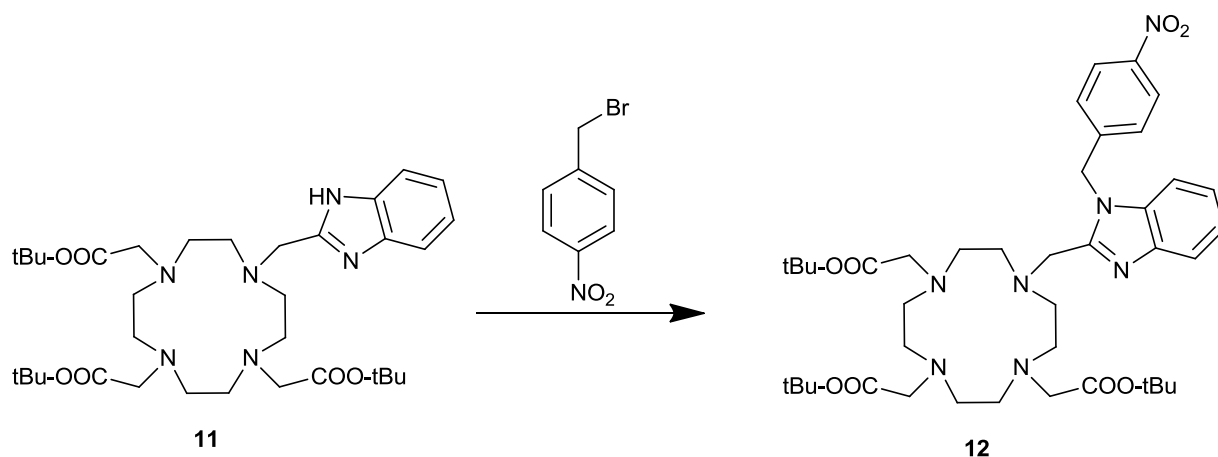
*Scheme 21 – Route 1 used in the attempted synthesis of N-functionalised benzimidazole DO3A (**12**).*

The reaction conditions utilised were the same as those used in an attempt to form **3** described in *section 2.2.1.1.* except the reaction was heated to reflux for 18 hours and 4-nitrobenzyl bromide was used in a 1.1 excess as there is no possibility for 'self-reaction. MS analysis of the crude product from this reaction showed that the desired product had not been formed and efforts turned to using the formed N functionalised benzimidazoles **3** and **4** to alkylate *t*Bu-DO3A (**9**) via route 2.

2.3.6. Synthesis of N-functionalised benzimidazole DO3A derivatives using route 2

Route 2, see *Scheme* 22, involves direct alkylation of *t*Bu-DO3A (**9**) with previously synthesised N-functionalised benzimidazole derivatives **3** and **4**, see *section 2.2*.
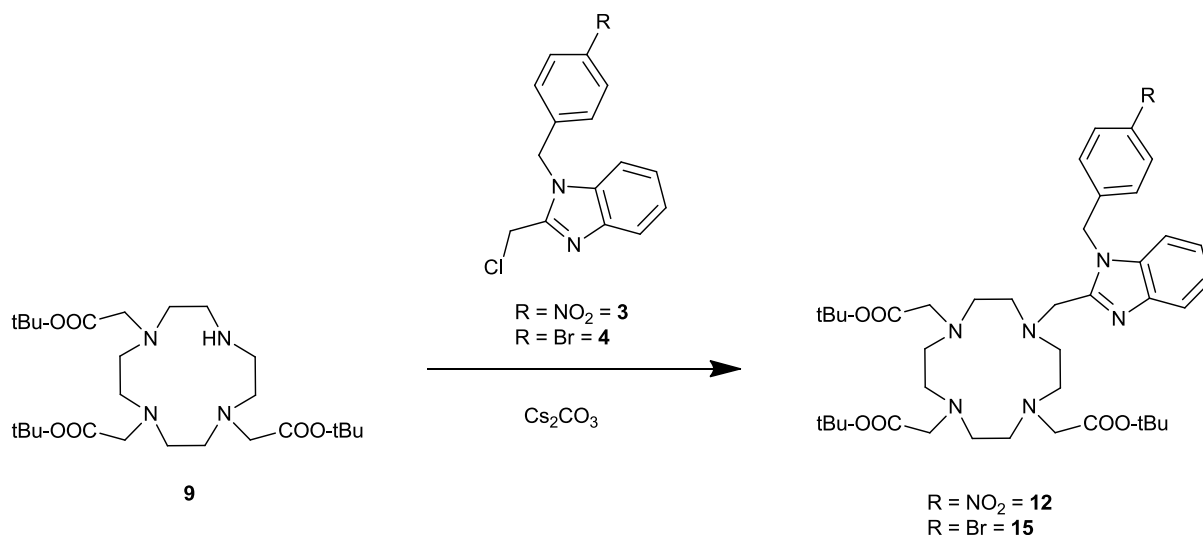
Scheme 22 – Route 2 synthesis of N functionalised benzimidazole DO3A derivatives.

*t*Bu-DO3A (**9**) was reacted with 2-(chloromethyl)-1-(4-nitrobenzyl)-1H-benzo[d]imidazole (**3**) and 1-(4-bromobenzyl)-2-(chloromethyl)-1H-benzo[d]imidazole (**4**) by adding the respective benzimidazole in a 1.1 excess to a stirred solution of *t*Bu-DO3A (**9**) in dry acetonitrile, followed by the addition of a four-fold excess of caesium carbonate. An excess of benzimidazole could be used as there is no possibility of 'self-reaction' on the imidazole. Different temperatures and reaction times were tested for this reaction and the best method was determined to be an 18 hour reflux followed by purification with a neutral alumina plug, eluting with ethyl acetate then methanol. This method gave the desired compounds; 1,4,7-tris(*tert*-butoxycarbonylmethyl)-10-(1-(4-nitrobenzyl)-2-methyl benzimidazole)-1,4,7,10-tetraazacyclododecane (**12**)[151] and 1,4,7-tris(*tert*-butoxycarbonylmethyl)-10-(1-(4-bromobenzyl)-2-methyl benzimidazole)-1,4,7,10-tetraazacyclododecane (**15**) both in 98% yields which were fully characterised by NMR and MS analysis.

2.3.7. Synthesis of 1,4,7-tris(*tert*-butoxycarbonylmethyl)-10-(1-(4-aminobenzyl)-2-methyl benzimidazole)-1,4,7,10-tetraazacyclododecane

The nitro group of **12** can be converted into a more reactive amine group to provide a site for conjugation reactions. Previous work in this area has involved the use of palladium on carbon under a H_2 atmosphere, however it has also been reported that these conditions can cause debenzylation of molecules of this type.[157,158] An alternative literature method for the reduction of nitrobenzyl groups reported by Lalancet *et al.* was used which involves the use of a sulfurated borohydride,[159] see *Scheme* 23, in a procedure which has been carried out successfully in the group previously.[151]
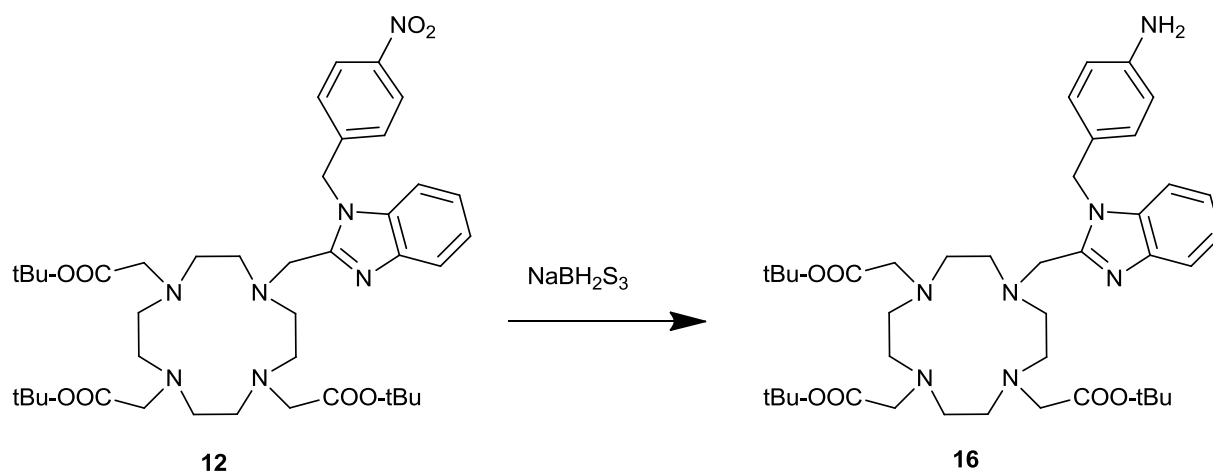
Scheme 23 – Reduction of the nitro group to give an amino benzimidazole DO3A compound 16.

Sulfurated borohydrides are prepared and used *in situ* by stirring together sulphur and sodium borohydride in dry THF for 1 hour under argon before addition of **12** in dry THF which was then heated under reflux for 18 hours. The reaction is then purified via column chromatography to yield the desired product in 50% yield.

2.3.8. Removal of *tert*-butyl protecting groups

The final step in bifunctional chelator synthesis is the removal of the *tert*-butyl protecting groups to form the triacid. Previously developed methods using microwave irradiation were used, see *section 2.3.3*. Deprotection of protected ligands **12, 15** and **16** gave the respective triacids **17-19** in near quantitative yields, see *Scheme 24*.

R = NO$_2$ - **12**
R = Br - **15**
R = NH$_2$ - **16**

R = NO$_2$ - **17**
R = Br - **18**
R = NH$_2$ - **19**
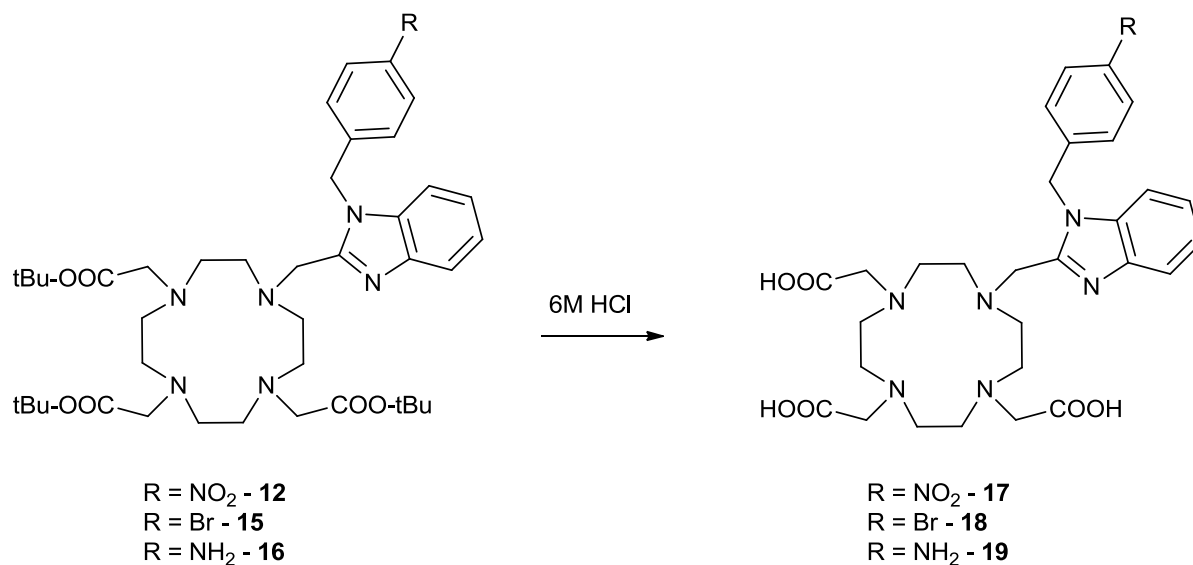
Scheme 24 – Formation of benzimidazole DO3A triacid derivatives by hydrolysis.

Analysis of the chelators using NMR and MS seemed to show all chelates to be successfully synthesised and pure, however by analytical HPLC it was shown that the ligands were 80%, 100% and 90% pure for **17**, **18** and **19** respectively. It was decided that the purity of **18** and **19** was acceptable for further metal complexation reactions but **17** was too low. **17** was purified by semi-prep HPLC to give the desired compound in 100% purity.

2.3.9. Synthesis of macrocyclic chelators – summary

This section details the development of synthetic procedures of N-functionalised DO3A derivatives with reactive arms to allow investigation of conditions for radiolabelling and/or bioconjugation, see Figure 27.
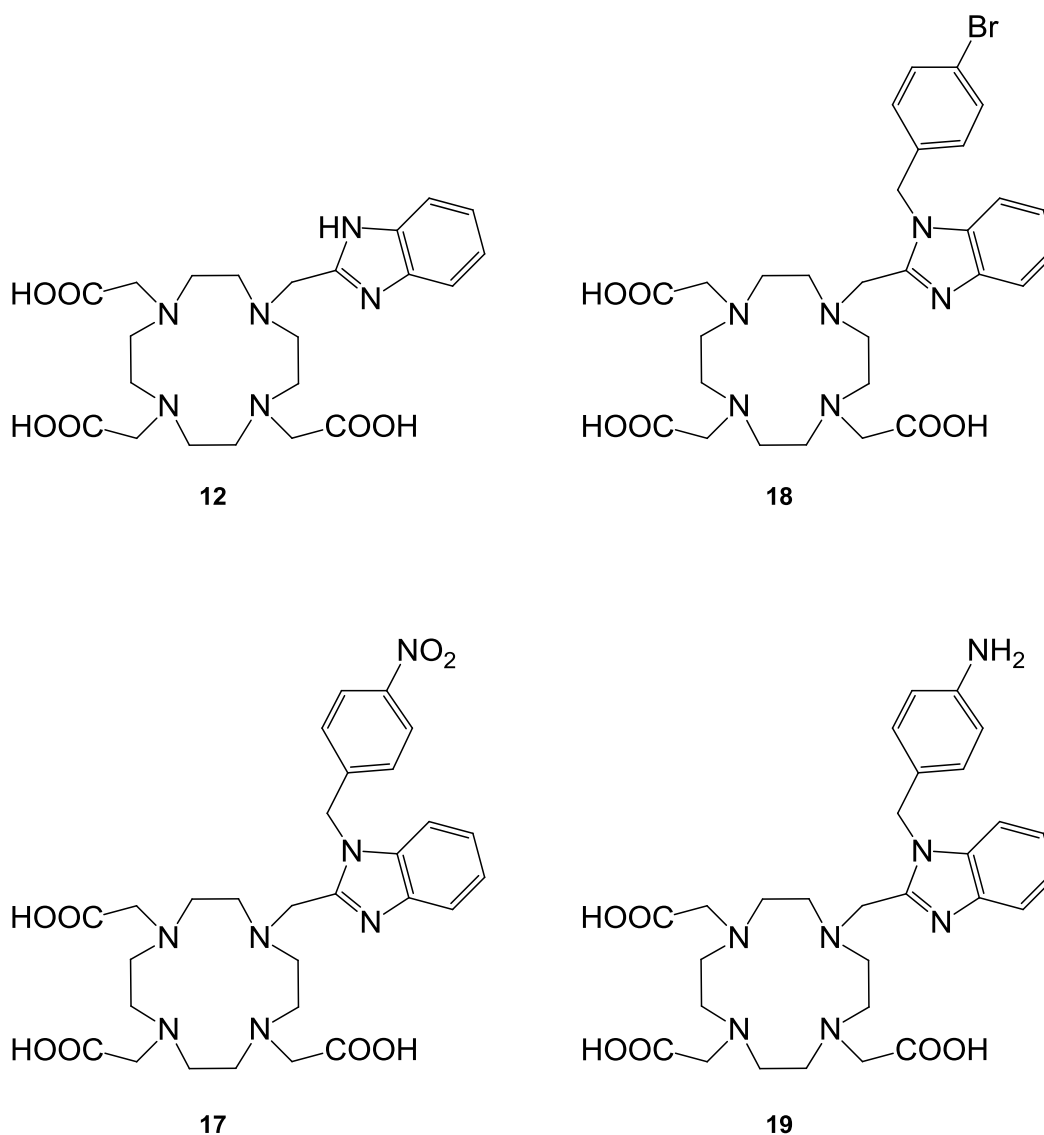
Figure 27 – Library of chelators prepared for ^{68}Ga radiolabelling.

Chelators **12, 17, 18** and **19** have been synthesised in high yields with high purity determined by HPLC ready for radiolabelling with ^{68}Ga.

2.4. $^{69/71}$Ga and $^{63/65}$Cu complex formation

$^{69/71}$Ga and $^{63/65}$Cu complexes of the prepared chelators were synthesised for two reasons. The first reason was to determine the conditions for the formation of $^{69/71}$Ga complexes that can be translated to ^{68}Ga radiolabelling and that, by forming $^{63/65}$Cu complexes, the ligands can also potentially be used with ^{64}Cu. Secondly, cold standards of $^{69/71}$Ga complexes are needed for HPLC identification of radiolabelled species.
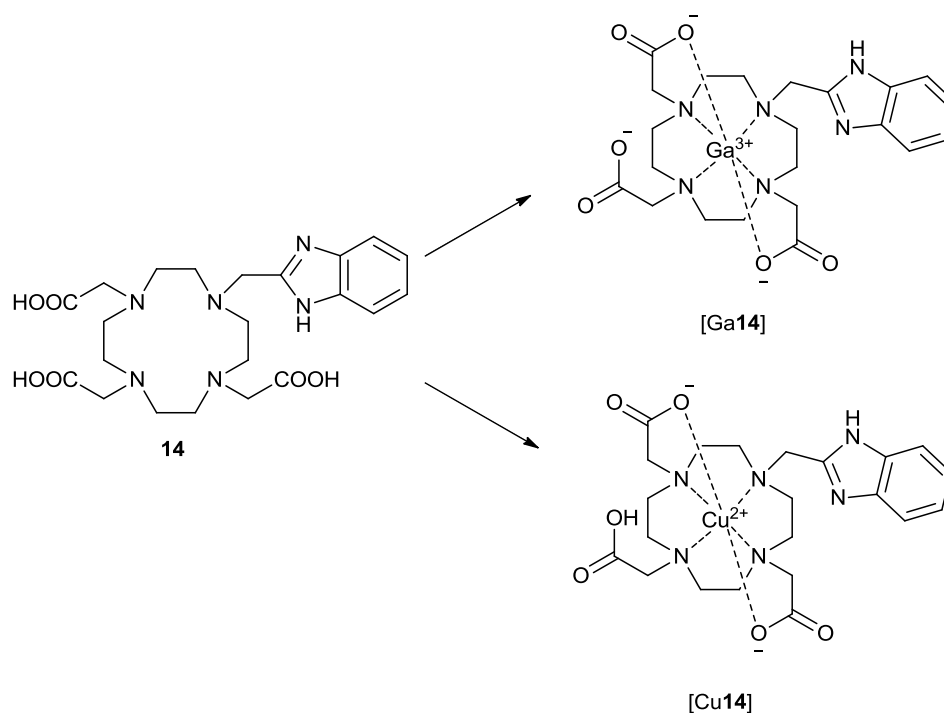
*Scheme 25 – $^{69/71}$Ga and $^{63/65}$Cu complexes formed with **14**.*

Initially, **14** was used in a test reaction on a relatively large scale to see if the proposed methods for complex formation were valid. The reaction to produce the $^{69/71}$Ga complex [Ga**14**] was carried out in ammonium acetate buffer at pH 5 to avoid the formation of hydroxides which reduces the yield, see Scheme 25. The reaction proceeded for 18h at 95°C and was then purified using amberlite XAD16N, eluting first with water to remove inorganic salts, followed by water:acetonitrile (9:1) to elute the compound in a 26% yield.[156] The $^{63/65}$Cu complex [Cu**14**] was formed by reaction of **14** with copper(II) acetate in water with caesium carbonate added as a base and the resulting compound was purified in a similar

manner to [Ga**14**] give a 83% yield. Analysis of the $^{69/71}$Ga and $^{63/65}$Cu complexes was carried out using HRMS and the purity of the compounds was determined using elemental analysis and HPLC. Comparison of the HPLC of the ligand **14** with the complexes gives the cold standard for radiochemistry, with a shift of the product peak retention time from 2.28 mins for **14** to 6.16 and 6.09 mins for [Ga**14**] and [Cu**14**] respectively.

R = NO$_2$ = [Ga**17**]
R = Br = [Ga**18**]
R = NH$_2$ = [Ga**19**]

R = NO$_2$ = **17**
R = Br = **18**
R = NH$_2$ = **19**

R = NO$_2$ = [Cu**17**]
R = Br = [Cu**18**]
R = NH$_2$ = [Cu**19**]
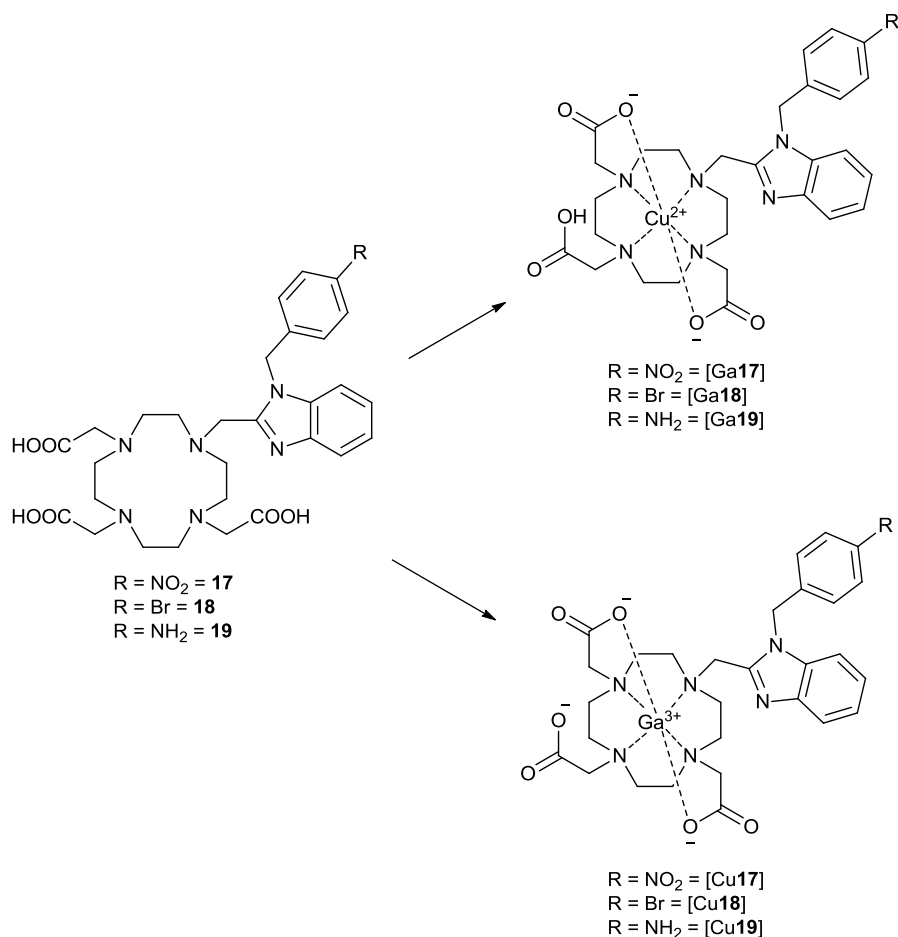
*Scheme 26 – $^{63/65}$Cu and $^{69/71}$Ga complexes formed with **17**-**19**.*

The processes were then applied to chelators **17-19** to give $^{69/71}$Ga and $^{63/65}$Cu complexes, see Scheme 26, on a small scale (ca. 1mg ligand) to produce HPLC standards and allow confirmation of their identity using HRMS. HPLC analysis of all eight complexes showed a complete disappearance of the ligand peak; with a new peak that has a retention time generally ca. 4 minutes later, formation of the desired compound was confirmed by HRMS in all cases.

2.5. ^{68}Ga radiolabelling of 14, 17, 18 and 19

Once cold standards had been successfully synthesised, the chelators could be radiolabelled and analysed. **18** was selected for initial method development.

2.5.1. Method development using 18

Literature research of ^{68}Ga radiolabelling of DOTA type chelators gives some general indications of the best conditions for successful synthesis. When testing and comparing a new chelator, Blower and co-workers performed the radiolabelling reaction with a series of different concentrations for both the novel chelator and as a comparison also investigated the labelling of standard chelators under the same conditions, see Figure 28.[48] This work demonstrated that DOTA could be radiolabelled at 100°C at pH 5 for 30 minutes at 10 μM ligand concentration. However, lowering the concentration to 1μM gave yields lower than 10%.
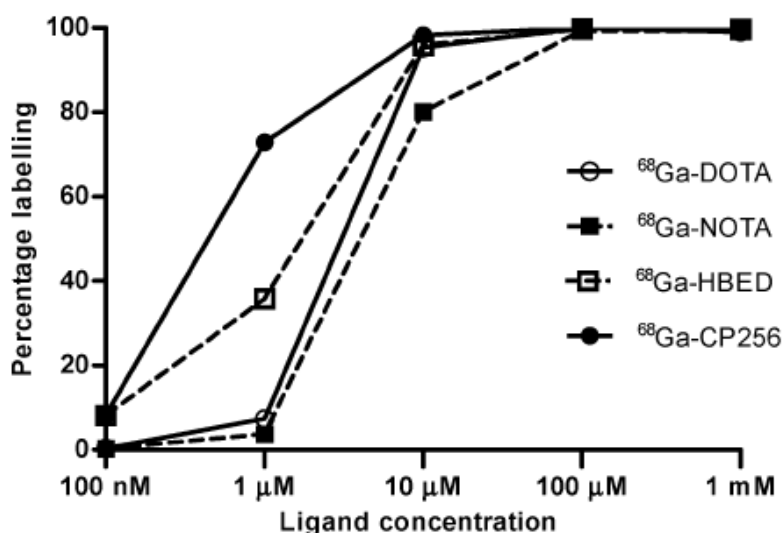
Figure 28 – Radiochemical yields vs. ligand concentration using optimal conditions for a series of standard chelators.[48]

Ferreira *et al*. performed a similar study to determine optimal conditions for radiolabelling a range of chelators.[160] Showing that a C-functionalised DOTA derivative is radiolabelled at

>90% yield at 80°C for 5 minutes at 10 μM ligand concentration, room temperature for 30 minutes gave similar yields of 88%. Similar conditions to those reported were selected for initial labelling reactions. **18** was radiolabelled with ^{68}Ga using 200μl of a 10μM solution in 0.2M ammonium acetate buffer at pH 5, see Scheme 27. Initially, the reaction was carried out at room temperature, with HPLC analysis carried out at 5 minute time points up to 30 minutes.
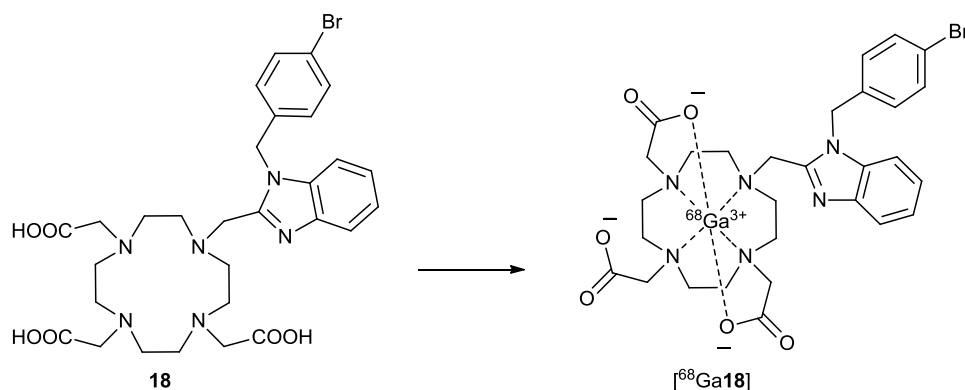
*Scheme 27 – [68]Ga radiolabelling of **18** to form [[68]Ga**18**].*

Using these conditions, HPLC analysis showed that after 5 minutes reaction time, 72% [68]Ga had been incorporated to form [[68]Ga**18**]. Over the following time points there was very little variation up to 25 minutes, with RCYs ranging from 72-80%. After this initially promising result, the reaction temperature was increased to 90°C in an attempt to improve the RCY. This modification gave a yield of 38% after 5 minutes which again showed very little improvement between 5 and 25 minutes, for raw data see *section 6.6.1*.

The reaction was also attempted using microwave synthesis methods, as studies by Velikyan *et al*. show that microwave irradiation of ^{68}Ga complex formation reactions can significantly increase radiochemical yields to mitigate the need for further purification.[161,162] For these experiments, a range of time and temperature points were attempted, see Figure 29. It can be seen from these studies that at 90°C there is an improvement from conventional heating methods, however again there is no improvement observed on increasing the reaction time. Also, increasing the temperature to 130°C had a detrimental effect on the RCY, with only 10% incorporation under these conditions.
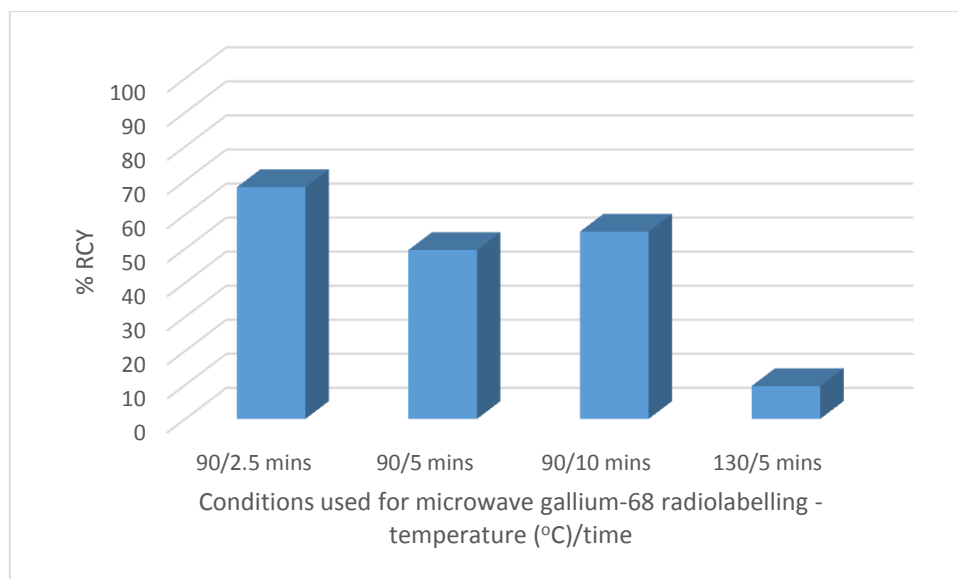
*Figure 29 – Radiochemical yields of microwave irradiated ^{68}Ga radiolabelling of **18**.*

2.5.2. ^{68}Ga complexation of BIDO3A derivatives

From method development, the reaction conditions optimal for this type of chelator would be at room temperature with only a 5 minute reaction time with a concentration of 10μM. Although this did not yield 100% ^{68}Ga incorporation, these conditions were preferred for a number of reasons; a low enough concentration of chelator is used to give high specific activities, a very short reaction time is required and being at room temperature it is applicable to most biomolecules.
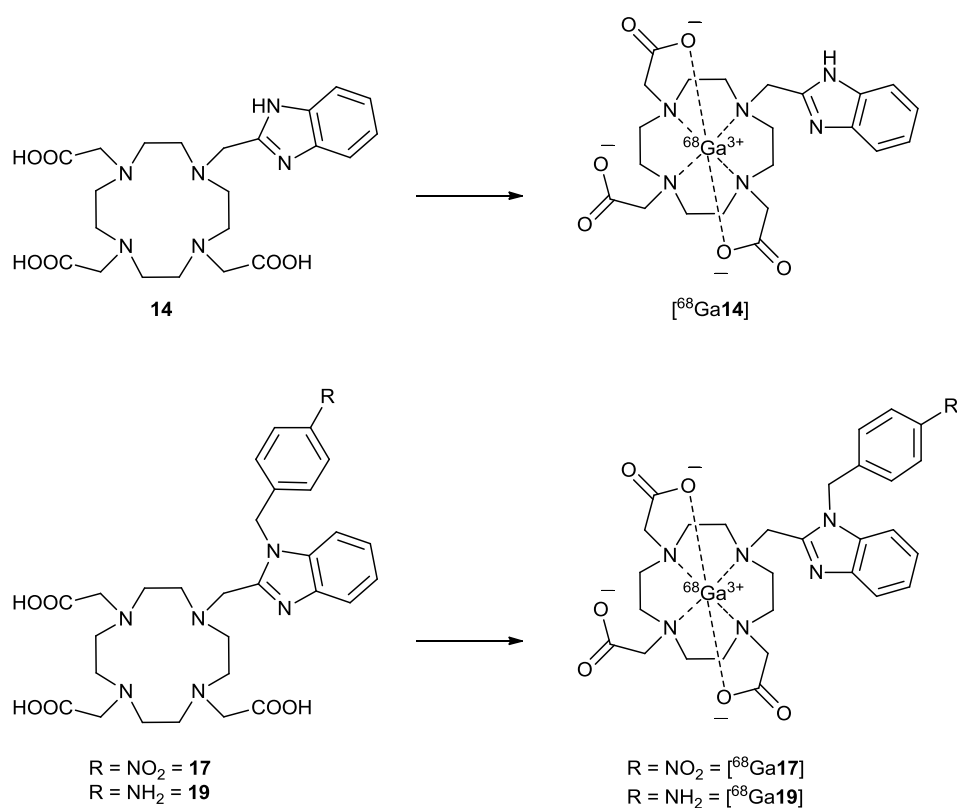
*Scheme 28 – ^{68}Ga radiolabelling of **14**, **17** and **19**.*

These reaction conditions were therefore used to ^{68}Ga radiolabel **14**, **17** and **19** to form [^{68}Ga**14**], [^{68}Ga**17**] and [^{68}Ga**19**] respectively, see Scheme 28. A range of results were observed for the different chelators. **14** showed very similar characteristics to **18**, with a RCY of 73% after 5 minutes. However, **17** and **19** gave RCYs of 33% and 16% respectively. All reactions in this sequence showed the characteristic but unexpected result that increasing reaction time had no positive effect on the formation of the ^{68}Ga complex, with no secondary radiochemical species formed, see *section 6.6.2-6.6.4.*

2.5.3. Metal ion concentration effects – proposed explanation

Recently, two groups have independently considered the problem of metal ion contamination from ^{68}Ge/^{68}Ga generators and how increasing concentration of other metal ions besides ^{68}Ga effects RCY of different bifunctional chelators.[75,163] Chakravart *et al*. conducted a thorough study in which they selected metal ions which were commonly present in ^{68}Ga elution.[163] In one set of studies they looked at a comparable chelator, a

carbon functionalised DOTA derivative, in a similar concentration to that which is used in this work, and showed that without metal ion contamination, the ^{68}Ga complex is generally formed at room temperature following a standard increase in complex formation over 20 minutes. The study was continued by looking at increasing amounts of competition metal ion contamination (1-10ppm) and how that affected RCYs, for all chelators studied, the DOTA derivative was found to be the most sensitive to a range of metals. To back up this data, Šimeček et al. showed that increasing metal ion contamination had a detrimental effect on RCY.[75]

Metal ions (ppb)	Al	Ti	Fe	Zn	Ge
[68]Ga from generator	31031.4	126.97	158.96	110.86	1.03
0.1M HCl control	880.39	8.17	134.22	548.61	2.25
Buffer control	194.96	2.57	13.26	256.28	1.59
[68]Ga processed in 0.1M HCl	644.14	16.14	20156.12	541.88	3.86

Table 2 – ICP-OES of ^{68}Ga elution a different stages of preparation.

ICP-OES was carried out on the decayed ^{68}Ga eluted from the generator used in this work, see Table 2, along with a processed sample identical to those used in the radiolabelling reactions to see if the preparation process was removing some contamination before the ligand was added. Solvents were also tested to see if they were introducing contamination. Studies of the ^{68}Ga generator eluent showed aluminium to be in very large amounts at 31 ppm, according to the literature studies, a concentration of 10 ppm would cause a 50% decrease in RCY.[75,163] However, after processing of the ^{68}Ga, the concentration of aluminium has reduced 5 fold to 0.6 ppm, with literature studies suggesting lower than 1 ppm having negligible influence.[163] The aqueous solvents used during the elution and preparation were shown to not have an influence on contamination. However, after preparation of the ^{68}Ga, there is a dramatic increase in iron concentration up to 20 ppm, with literature suggesting that iron contamination above 10 ppm leads to RCYs of <5% for DOTA.[75,163] It is therefore surprising that the RCYs achieved in this work are as high as they are.

2.6. Conclusions

The synthesis and optimised labelling conditions for ^{68}Ga complex formation of four novel bifunctional chelators was developed, see Figure 30. The initial step in chelator synthesis was the production of benzimidazole units which were developed by exploring two methods. The benzimidazole derivatives were then reacted with azamacrocycles to form four different benzimidazole DO3A derivatives, where two of the macrocyclic compounds have reactive functional groups available for bioconjugation.
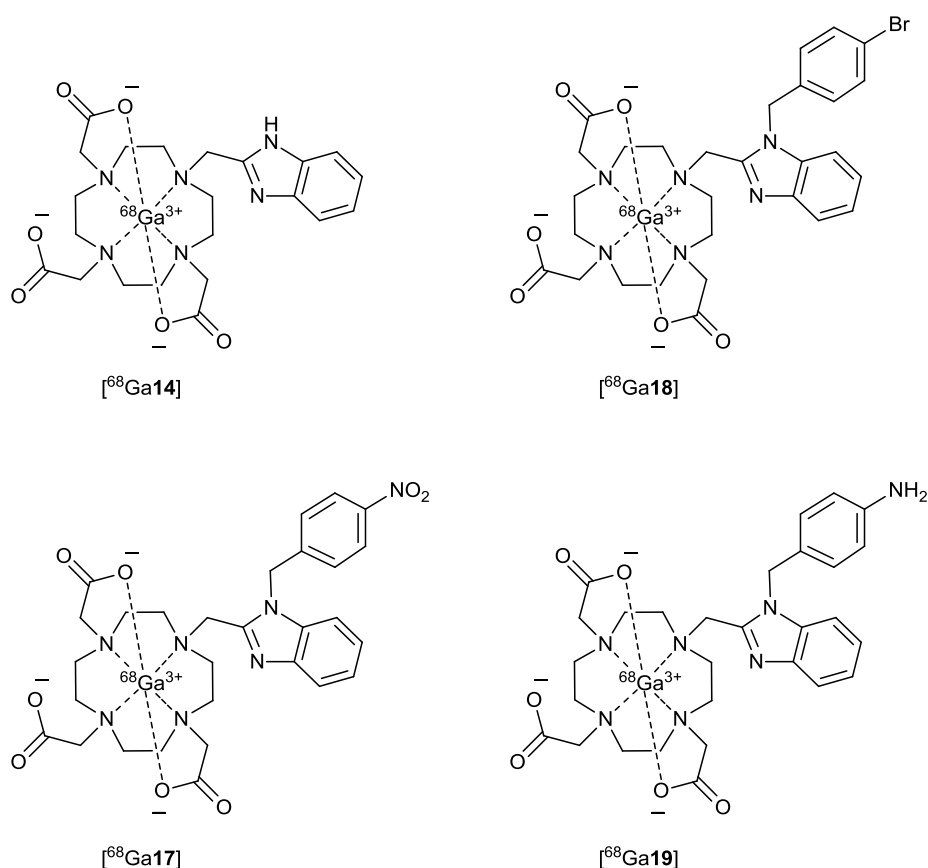
Figure 30 – Synthesised ^{68}Ga BFCs.

$^{63/65}$Cu and $^{69/71}$Ga complexes of four ligands were synthesised and characterised to show the viability of ^{64}Cu and ^{68}Ga radiolabelling for positron emission tomography (PET). This was followed by ^{68}Ga radiochemical synthesis of **18** in which a range of conditions were attempted to optimise the protocol, followed by ^{68}Ga complex formation of **14**, **17** and **19**. In which radiochemical yields of 72%, 73%, 33% and 16% respectively were achieved at 10 µM concentrations at room temperature with reactions times of only 5 minutes.

In order to develop this area of research further investigation is required in a number of areas. The ^{68}Ga radiochemistry requires further study to increase RCYs, efforts should primarily focus on the effect of metal ion contamination and modifications must be made to avoid introduction of other metal ions such as iron. Further studies of the ^{68}Ga complexes would be of interest; specific activities of the chelators could be determined along with *in vitro* and *in vivo* stability studies. For further discussion of proposed future work see *section*s *5.2.1.* and *5.2.2.*

Chapter 3

Synthesis of PET/MRI multi-modal

imaging agents

3. Synthesis of PET/MRI multi-modal imaging agents

3.1. Aims

This chapter reports the synthesis of potential PET/MRI imaging agents. Initial attachment of macrocyclic metal chelating ligands to a siloxane derivative was carried out, *see section 3.4.1*, followed by polymerisation to form a silica shell on super-paramagnetic iron oxide nanoparticles (SPION) that acts as a T_2 MRI contrast agent, *see section 3.4.2.*, followed by deprotection of the macrocycle. The complexation characteristics of siloxane derivatives with $^{69/71}$Ga and $^{63/65}$Cu were studied, *see section 3.4.3.*, followed by radiolabelling of the siloxane derivatives along with bisphosphonate macrocycles with ^{68}Ga, see *section 3.6.* to give PET/MRI imaging agents, see Figure 31.
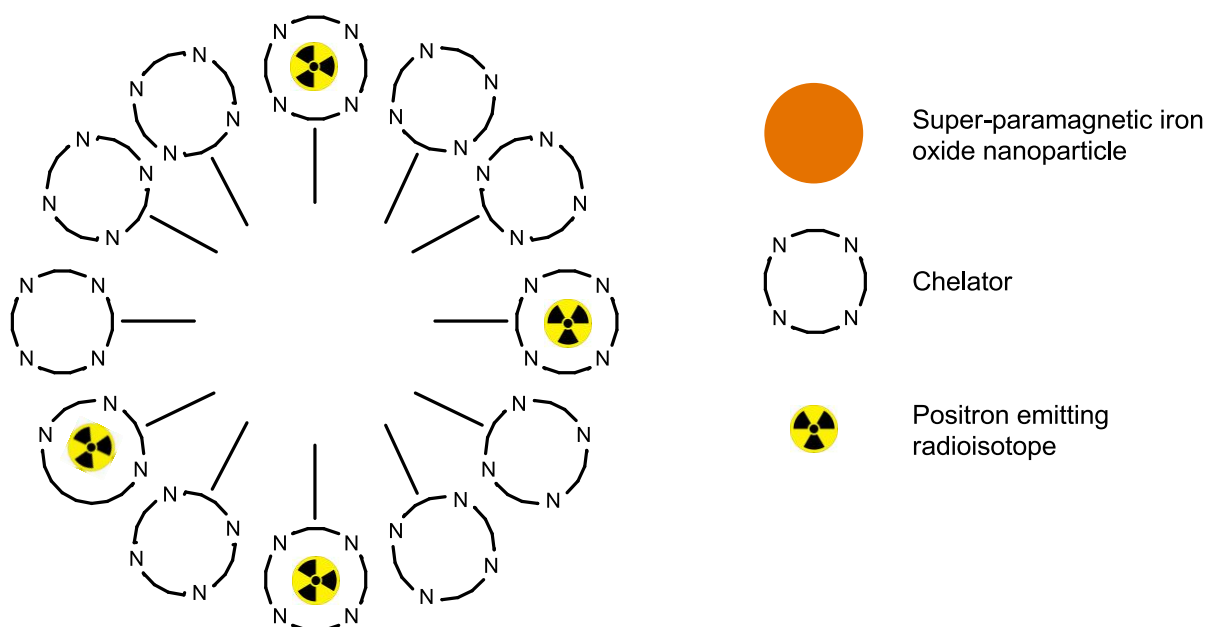
Figure 31 – Schematic representation of SPION containing PET/MRI contrast agent.

Development of combinatorial PET/MRI imaging/contrast agents is a recently emerging field due to the recent development of PET/MRI scanner technology, the clinical applications of which are still unclear. This chapter focuses on the development of the first ^{68}Ga radiolabelled silica coated super-paramagnetic iron oxide nanoparticles for potential use as PET/MRI imaging agents.

3.2. SPION containing MRI/PET agents

The development of MRI/PET agents which contain SPIONs is a recently emerging field which shows big potential for the future of multimodal imaging due to the flexibility of surface modification on the surface of SPIONs.[164,165] Most work in this area to date has focused on DOTA derivatives due to their ease of use and the relative youth of the field.

Jarrett *et al*. have designed dextran coated SPIONs which have aldehyde functions that can be attached to an amine terminating DOTA derivative to give a PET/MRI imaging agent.[166] The group had some problems with conjugation and radiolabelling and found that if DOTA is linked to the nanoparticle followed by ^{64}Cu radiolabelling they saw no radiochemical incorporation, therefore, carrying out the radiochemistry before conjugation was successful but with the anticipated reduction in yields.

Glaus *et al*. developed a similar system but using a PEG coating, see Figure 32,[167] there were no problems of ^{64}Cu radiolabelling in the presence of this coating and they achieved 95% radiochemical purity after only 1 hour reaction time. *In vitro* studies showed high stability over 24 hours with only 2.5% activity lost, *in vivo* biodistribution studies showed promising results with a circulation half-life of 143 minutes.

Patel *et al.* developed a system which modified the surface with DL-DOPA followed by DOTA and copper(II) complexation.[168] They saw that copper complexation caused a decrease in relaxivity of the T_2 contrast agent, speculating that the compound could be used for copper(II) detection *in vivo* for diseases such as Alzheimer's and Menkes disease.

While still using DOTA, Lee *et al.* have also incorporated RDG peptides to target tumour integrin $\alpha_v\beta_3$ expression.[169] The group used polyaspartic acid coated SPIONs which were conjugated to RDG peptides and radiolabelled with ^{64}Cu before being tested *in vivo*. Both pre-clinical PET and T_2 weighted MRI show integrin specific delivery of the nanoparticles to the integrin overexpressing tumours.
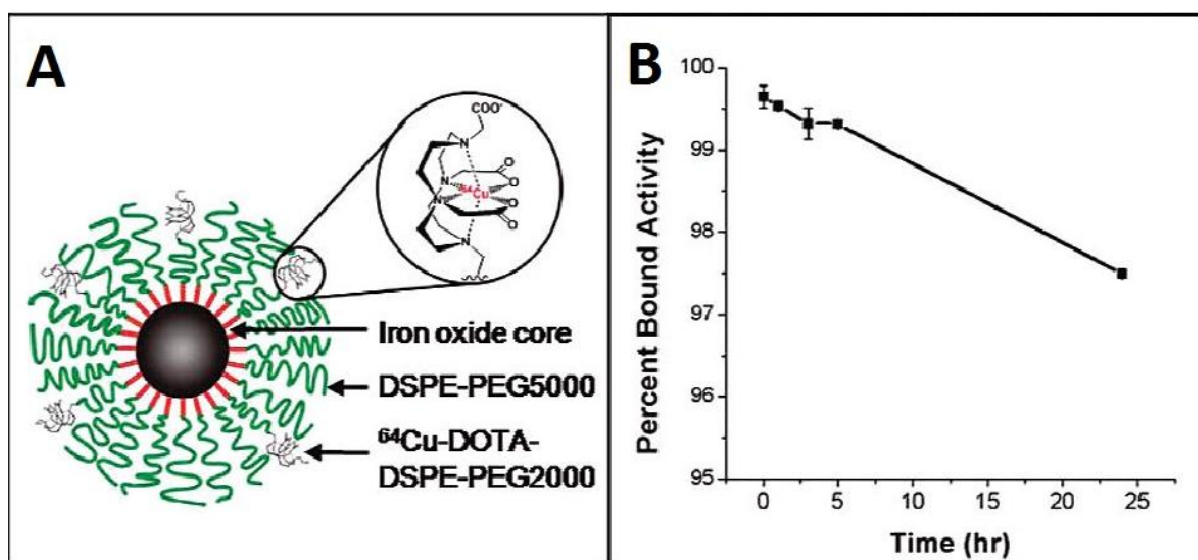
Figure 32 – (A) Schematic representation of dual-modality ^{64}Cu-SPION. (B) In vitro stability of ^{64}Cu-SPION over 24h in mouse serum at 37°C.[167]

Xie *et al.* have used dopamine to modify the surface of the nanoparticles followed by coating with human serum albumin (HSA), a widely used drug carrier.[170] The coated SPIONs were then conjugated with DOTA and cy5.5 dye, forming a structure which can be used as a PET/MRI/NIR agent. Yang *et al.* have also developed a PET/MRI contrast agent which targets integrin $\alpha_v\beta_3$ expression,[171] using PEG coated nanoparticles conjugated to RDG peptides. The group used NOTA as the ^{64}Cu chelator and conjugated an anti-cancer drug which was shown to have pH sensitive release.

Torres and co-workers have developed a non-macrocycle chelator functionalised SPION based PET/MRI contrast agent, see Figure 33.[172] They synthesised a bisphosphonate group for binding to the nanoparticle surface and coupled it to a dithiocarbamate group for ^{64}Cu binding which shows *in vitro* stability for at least 48 hours. The system has the advantage of facile radiolabelling without the need for elevated temperatures.
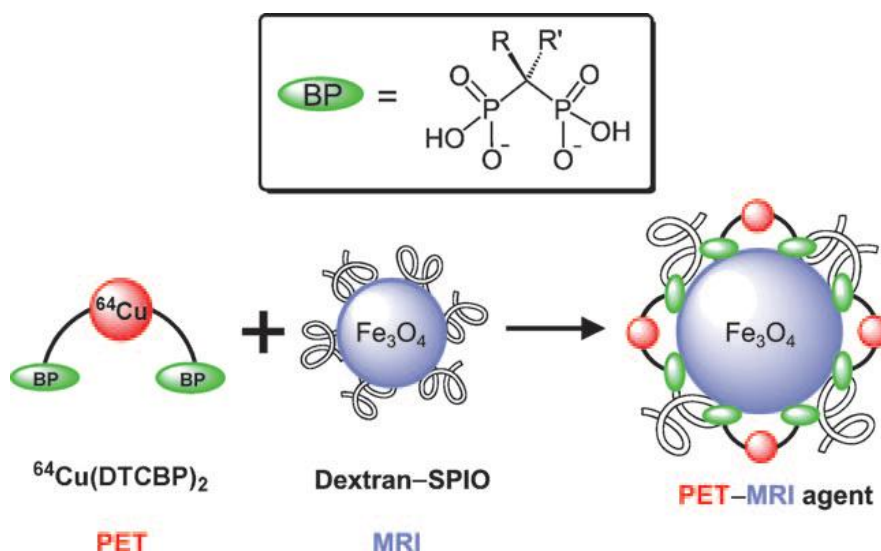
Figure 33 – Schematic representation of a conjugation of a ^{64}Cu-bisphosphonate with a dextran coated SPION to form a PET/MRI imaging agent.[172]

At the time of writing, there is only one published example of a ^{68}Ga labelled SPION.[173] In this study, Stelter *et al.* made no chemical modifications designed for ^{68}Ga radiolabelling in the form of chelator addition. The group used commercially available MagForce®, a PEG coated amine terminating SPION and reacted it with ^{68}Ga in an effort to make stable coordination interactions between the amine surface and the metal ion. Competition assays with DTPA showed >90% of the radioactivity still attached to the nanoparticle. Continuing the remarkable results of this study, *in vivo* results seems to confirm the stability of this construct, with most of the radioactivity seen in the liver and spleen after 50 minutes, a result which is consistent with SPIONs of this size (ca. 100nm).

Spiccia and co-workers conducted a study which used a series of chelators for ^{64}Cu complexation.[174] The group modified three different macrocycles; cyclam, cyclen and 1,4-bis(2-pyridylmethyl)-1,4,7-triazacyclononane (dmptacn), see Figure 34, with a siloxane derivative to give the nanoparticle a silica coating and to test the effect on using different size macrocycles on the ^{64}Cu complexation properties and stability. Dmptacn functionalised SPIONs showed the highest resistance to metal ion leakage in rat plasma. Although initial experiments are promising, conjugation of macrocycles to the nanoparticles caused a large increase in the diameter when determined by NTA (from 7 nm to 170 nm) due to aggregation.
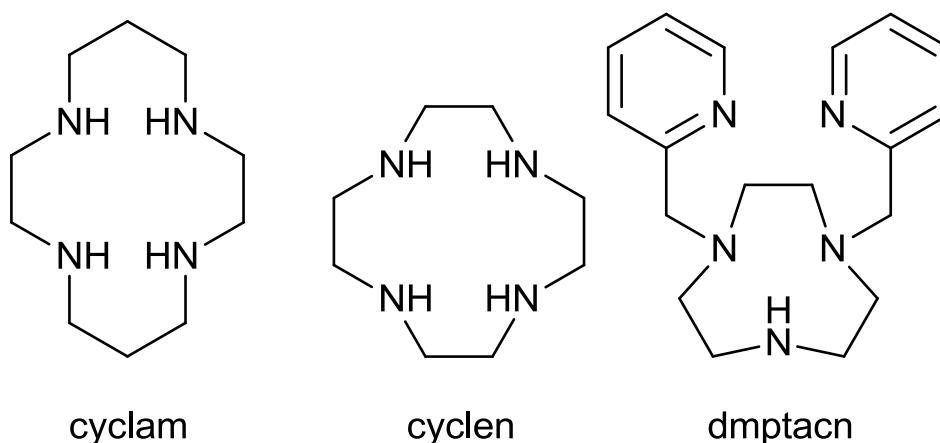
Figure 34 – Three macrocycles used to test complexation properties with ^{64}Cu for attachment to SPIONS.[174]

Combination of SPIONs as T_2 MRI contrast agents with positron emitting radioisotopes offer the potential for much more sensitive quantification of the biodistribution of such conjugates *in vivo*. Offering the potential to accurately see how the variation of different parameters of nanoparticle design affects how the body processes such conjugates.

3.3. Coatings of SPIONs

SPIONs are generally coated for two main reasons; to add functional groups for conjugation and to increase hydrophilicity for colloidal stability (avoid aggregation) which increases blood pool time. The goal is to fulfil these criteria whilst not sacrificing magnetic properties. Coating can be carried out either as part of the NP formation process or post nanoparticle synthesis.[175]

Coating of SPIONs has been developed using a range of different chemical polymers including PEG, chitosan, phospholipids, silica and dextran.[104]

3.3.1. Silica coating

Nanoparticles coated with silica are gaining interest due to its biocompatibility combined with easy covalent functionalisation.[176-178] One commercially available SPION is GastroMARK®,[102] which is formed with a siloxane based polymer over the surface of the nanoparticle. The core size of the SPION is only 10nm but the nanoparticle becomes 300nm due to nature of the coating material. GastroMARK® is used orally for gastrointestinal imaging.

3.3.2. Dextran coating

Dextran is a branched polysaccharide based on glucose which is known to form hydrogen bonds with iron oxide and are generally coated as part of the NP synthesis process.[179] Cross linking of the polymer increases stability beyond that of solely hydrogen bonding. Many clinically licensed SPIONs are coated with dextran due to its high affinity for iron oxide and biocompatibility, an example of which is Endorem®.[105]

3.4. Synthesis of siloxane derivatised macrocyclic ligands

3.4.1. Macrocycle functionalisation

In order to form macrocyclic functionalised magnetic nanoparticles, macrocycles with primary (**21**) or secondary amines (**9**, **11**, **20**) were chosen for epoxide ring-opening reactions in a similar method to that adopted by Spiccia and co-workers, see Figure 35.[174] A hydroxide functionalised macrocycle (**22**) was also investigated due to the related epoxide ring-opening reaction known for this functional group.[180-182] A range of macrocycles were selected in an attempt to study the affect of various characteristics. The effect of different cavity sizes on complexation characteristics can be explored by comparing DO3A derivatives (**9** and **10**) with carbon functionalised TETA derivatives (C-TETA) (**21** and **22**). It is also interesting to study the effect of an ethylene cross-bridge derivative, cross-bridged mono picolinate (CB-MP) (**20**), which are known to affect complexation kinetics and stability.[24,183,184]
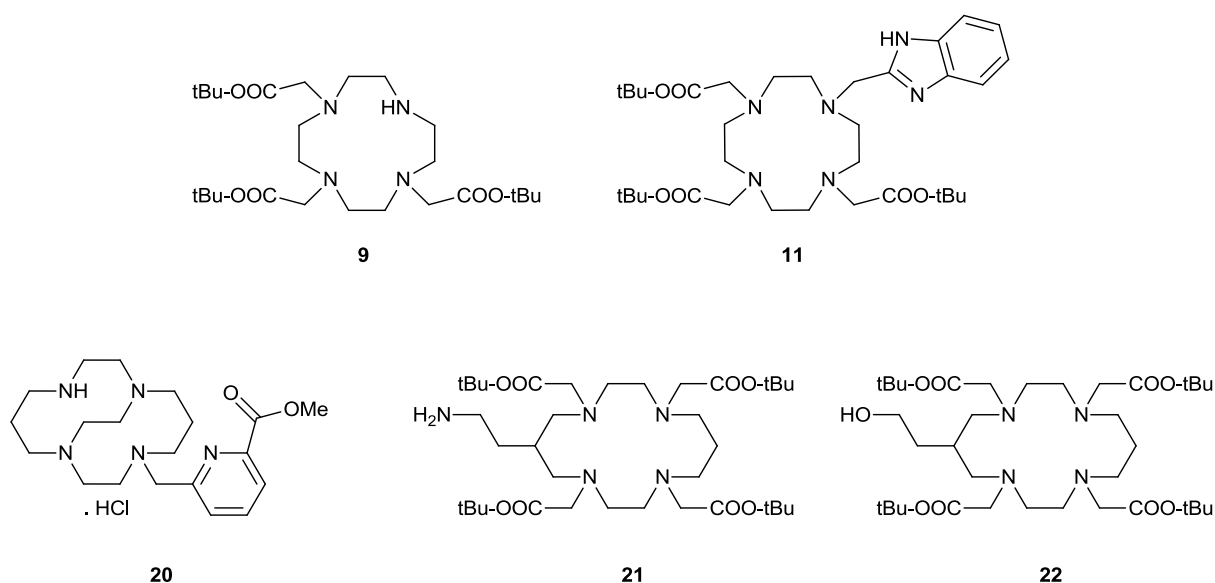
Figure 35 – Macrocyclic chelators selected for nanoparticle conjugation.

*t*Bu-DO3A (**9**) was chosen as one of the initial molecules to optimise for attachment and radiolabelling, due to the similarity with literature compounds that have been previously investigated,[174] along with **11,** which was selected to determine whether a conjugate with a benzimidazole functionality could be formed, see Scheme 29.
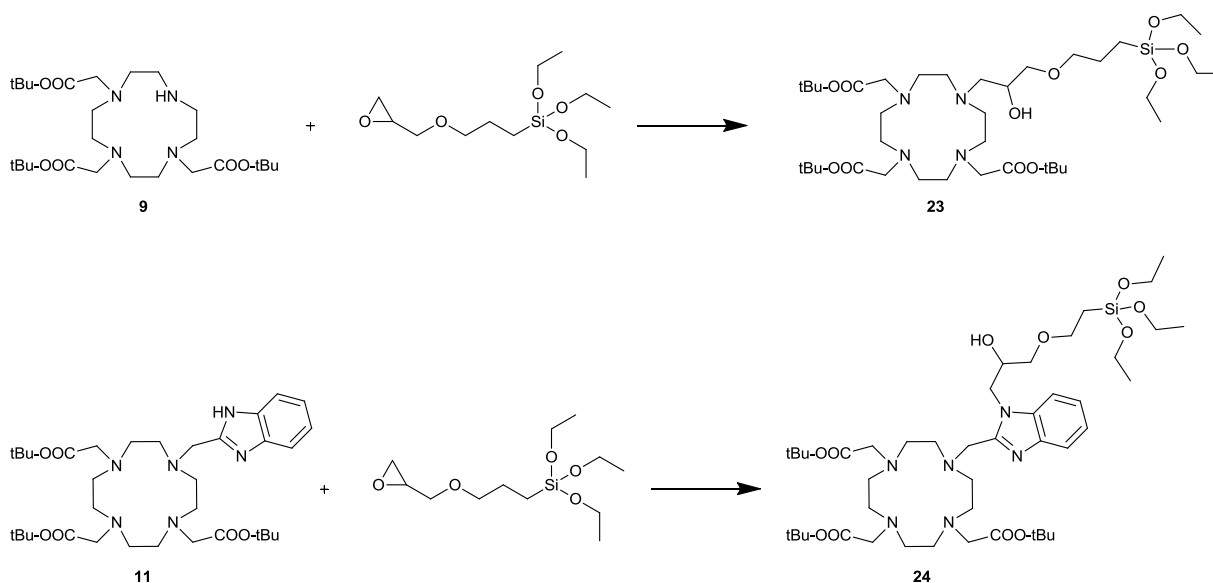
*Scheme 29 – DO3A siloxane derivative reactions attempted to form **23** and **24**.*

Initially, literature methodology was followed directly,[174] heating the macrocyclic starting

material with (3-glycidyloxypropyl)triethoxysilane (GPTES) in a 1:1 ratio in chloroform for 3

days under reflux. The ^{1}H NMR of **23** seemed to show the reaction had gone mostly to

completion, however MS analysis showed a peak at 515.3, corresponding to the starting

material. MS/MS analysis confirmed this peak to be starting material and not fragmentation

of the product. For the reaction to form **24** it appeared that the opposite was true, with the

^{1}H NMR analysis seeming to show only starting materials but there was presence of a small

product peak in MS at 923.5. In an attempt to improve both reactions, the amount of GPTES

was increased to give a 1.5-fold excess, this modification was possible with the molecules

selected due to the presence of only one reactive site, although this seemed to have no

effect on any of the analytical data collected. The reaction was also tried using microwave

irradiation at 90°C for both 30 minutes and 2 hours; these attempts seemed to show slight

improvements on the previous attempts but did not produce sufficient evidence of

feasibility of use in the formation of **24** so the reaction was abandoned at this stage.

Microwave reactions to form **23** gave comparable results to the similar literature methods

so were used for further reactions due to vastly reduced reaction times.
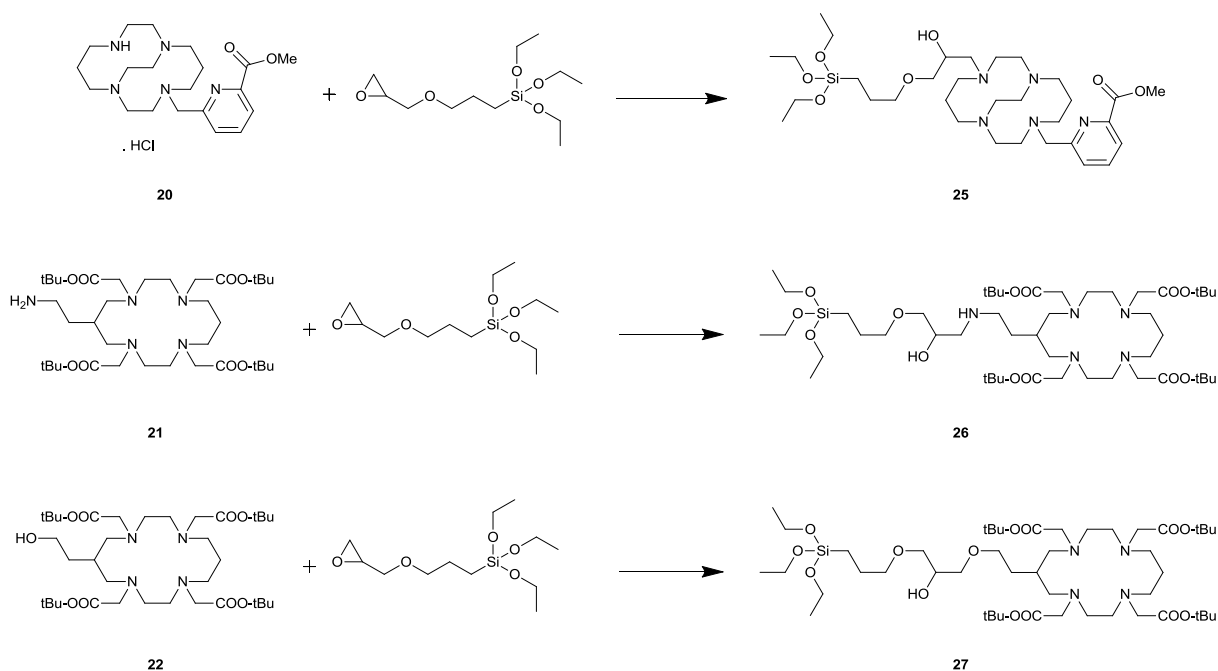
Scheme 30 – Macrocyclic siloxane conjugation to form **25**, **26** *and* **27**.

Initially, reactions to form **25**, **26** and **27** were attempted using the methods developed for **9**, see Scheme 30, heating at 90°C in chloroform using microwave irradiation for 30 minutes with an excess of GPTES. As **21** is a primary amine, the reaction was attempted on both a 1:1 ratio and a 2:1 ratio to see whether di-substitution is possible. Using an excess of GPTES gave evidence of di-substitution when analysed by MALDI MS and therefore it was believed that using a 2:1 ratio would not give a mixture of substituted products and was therefore used. **26** was successfully synthesised and characterised by NMR spectroscopy and MS in a near quantitative yield.

When the reaction was attempted to form **25** the work-up of the reaction was challenging as there was very little material upon completion of the procedure. This may be due to protonation of the macrocyclic amines which is common with CB macrocycles of this type, causing increased water solubility. A common way to avoid this problem is to basify the aqueous layer before extraction,[25,185] however this was thought to be a undesirable for this molecule due to the sensitivity of the siloxane and methyl ester to basic hydrolysis. It was thought that a strict 1:1 ratio of starting materials with no extraction step was the best

method for obtaining the desired compound. Successful synthesis of the desired compound **25** was confirmed by NMR spectroscopy and MS analysis in a 95% yield.

Synthesis of **27** was attempted, although it gives a very similar product to **26**, because the starting material is more readily available, with **21** being produced from **22** in a three step procedure. Epoxide ring-opening reactions with hydroxide groups are reported in the literature but are not as well characterised as with amines and are generally catalysed. Two methods were attempted, method 1 involved the use of an activated charcoal catalyst following related literature procedures.[181] Activated charcoal was acidified with a mixture of nitric and sulphuric acid overnight before being dried and used as a catalyst in similar microwave methods to those described previously for amine terminating macrocycles. MS analysis of the crude compound showed no peak for the desired product. Method 2 involved the use of a copper(I) catalyst, again following literature procedures,[180] crude MS analysis of this reaction showed no peak for the desired product with observed peaks for the starting material and also its copper complex. This is most likely due to oxidation to copper(II) prior to formation of the macrocycle complex, indicating the reason for unsuccessful reaction.

Three siloxane derivatised macrocycles were successfully synthesised for use in nanoparticle conjugation reactions, see Figure 36.
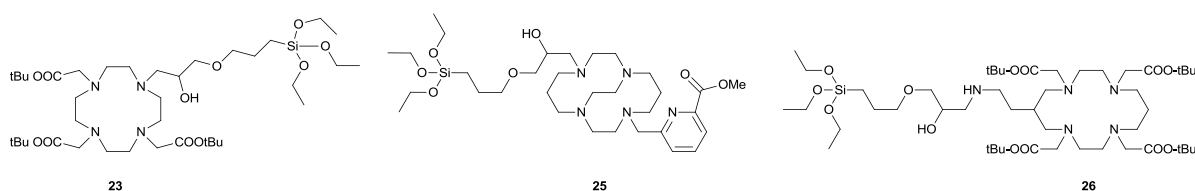
*Figure 36 – Successfully synthesised siloxane macrocycle derivatives **23, 25** and **26**.*

3.4.2. Macrocycle – magnetic nanoparticle conjugation and hydrolysis

Conjugation of synthesised siloxane derivatised macrocycles with super-paramagnetic iron oxide nanoparticles (SPIONs) was carried out in a similar fashion to literature methods.[174] The reaction proceeds in 48 hours at room temperature followed by separation using a strong rare earth magnet, with successive washings using a series of solvents to remove any non-nanoparticle impurities, see Scheme 31.
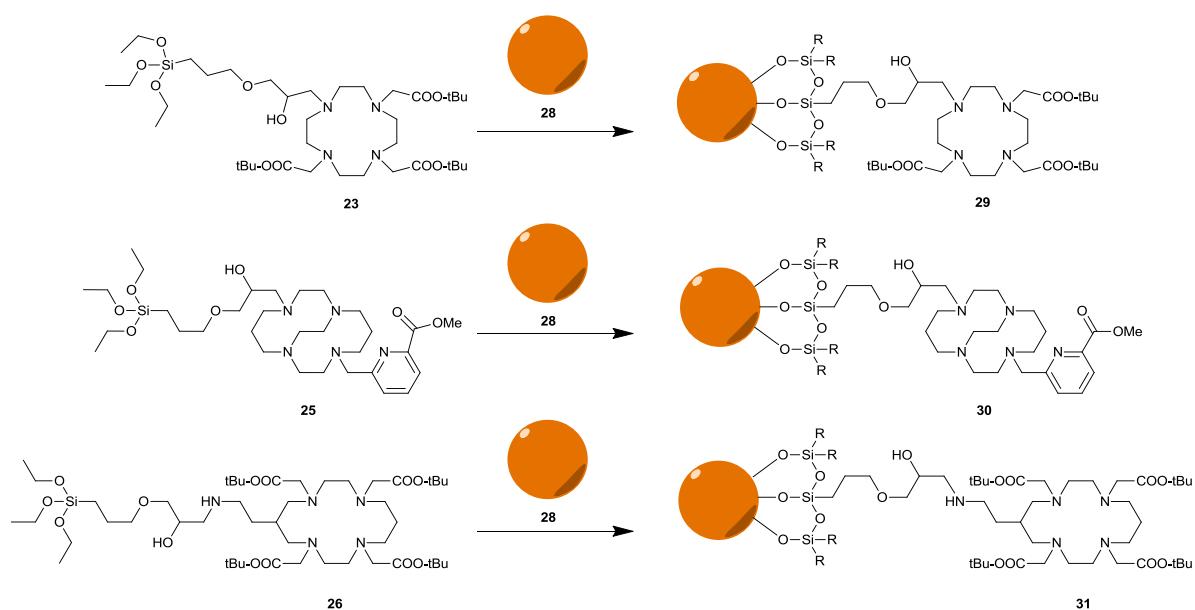
Scheme 31 – Conjugation of siloxane macrocycle derivatives with SPIONs.

Along with the three macrocycles chosen for nanoparticle conjugation, two non-macrocycle siloxane derivatives were selected as controls to study metal incorporation, see Scheme 32. For the controls, previously used siloxane derivative GPTES was used along with triethoxy(ethyl) silane to provide a siloxane surface with macrocyclic chelators.
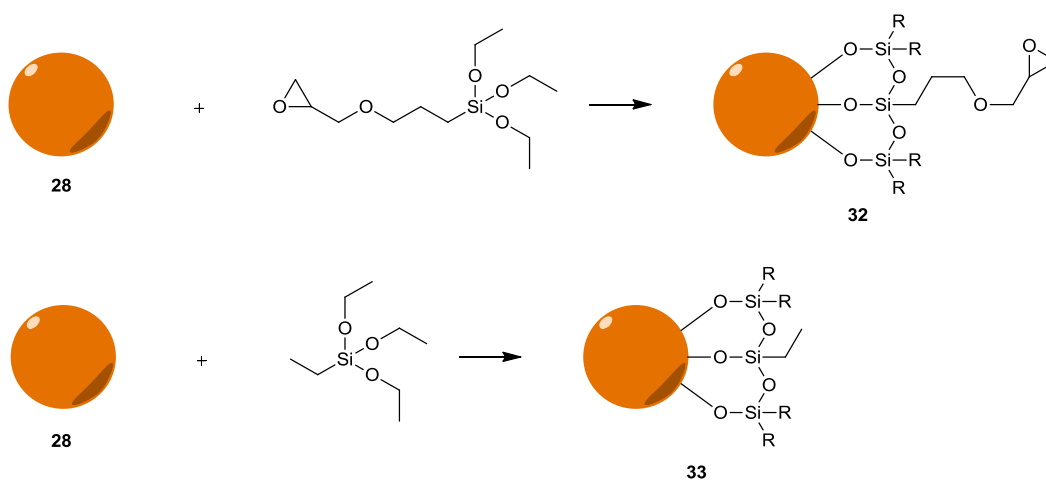
Scheme 32 – Formation of non-macrocyclic siloxane coated nanoparticle controls.

Analysis of structural nanoparticle modifications is challenging due to the inability to use conventional synthetic analytical techniques such as NMR spectroscopy and MS. It was instead decided that a combination of ICP and elemental analysis would be used to determine whether the nanoparticles had been functionalised in the desired manner. All conjugates, to a greater or lesser extent, showed strong evidence that the desired compounds had been isolated, determined by increases in percentage of silicon and carbon for all conjugates. **29** and **32** showed only modest increases in silicon, with amounts of 1.33% and 0.64% respectively. **33** seemed to form an extensive coating with 27.935%. **30** and **31** were consistent with each other at amounts of 15.512% and 13.078% respectively.

Comparison can also be made with the study by Baretto *et al*. which used a similar methodology to synthesise ^{64}Cu agents.[174] After siloxane conjugation of the nanoparticle surface, the group saw elemental analysis results which are similar the results presented here, with their carbon range of 2.67-5.53% comparable to the 2.86-5.67% for these macrocyclic derivatives.

After successful conjugation, hydrolysis of the macrocyclic protecting groups to reveal the free acetate arms must be carried out to form donating groups for metal ion coordination, see Scheme 33. This reaction is even more difficult to follow and formation of the desired product must be inferred by either, how the reaction is known to proceed from literature methods when not attached to the nanoparticle (*t*Bu hydrolysis with TFA/DCM),[186,187] or by test reactions completed with the specific ligand to show method viability (e.g. methyl ester hydrolysis with LiOH).
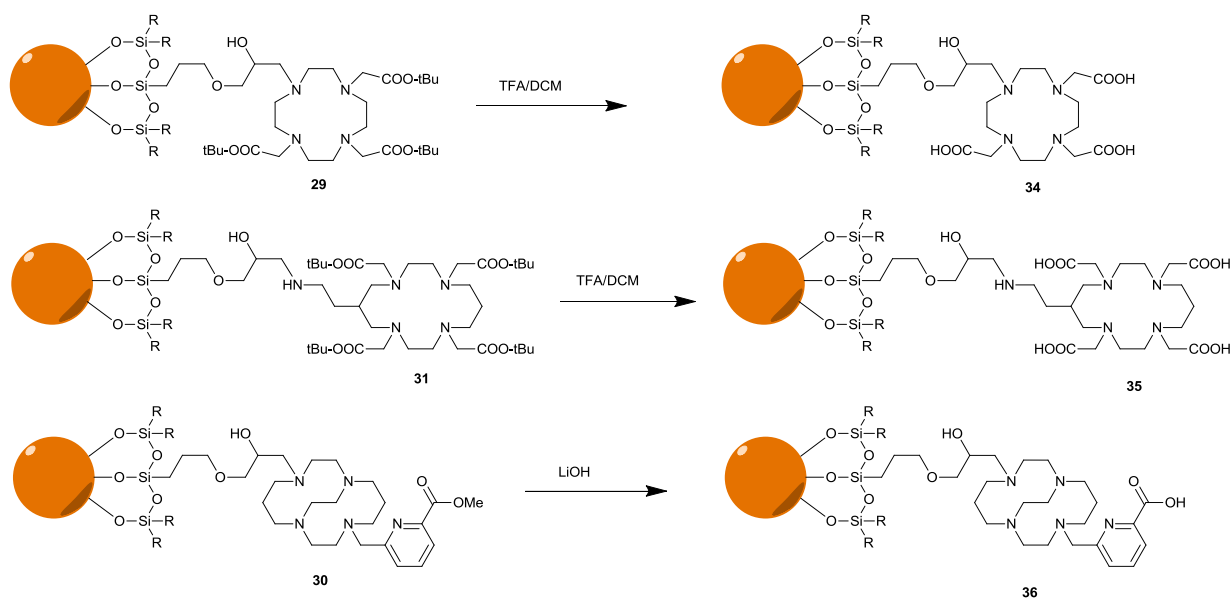
Scheme 33 – Ester hydrolysis of macrocycle-nanoparticle conjugates.

29 and **31** were hydrolysed in a DCM:TFA mixture (10:1) to form **34** and **35** respectively and **30** was dissolved in 60% ethanol and hydrolysed with lithium hydroxide to form **36**, the reactions were mixed at room temperature followed by magnetic separation and successive washings previously described. Although direct analysis is challenging to demonstrate that the reaction has gone to completion, it can be shown by elemental analysis (ICP/CHN) that the organic and silica components are still present on the nanoparticles after reaction and separation.

3.4.3. 'Cold' complexation

In order to study the complexation characteristics of the nanoparticle conjugates prior to radiolabelling (i.e. proof of concept), cold reactions were performed with $^{63/65}$Cu and $^{69/71}$Ga. Both metal ions were reacted with the three macrocycle derivatives, see Scheme 34, along with the two siloxane controls and also the uncoated Fe_3O_4 nanoparticles, see Scheme 35.
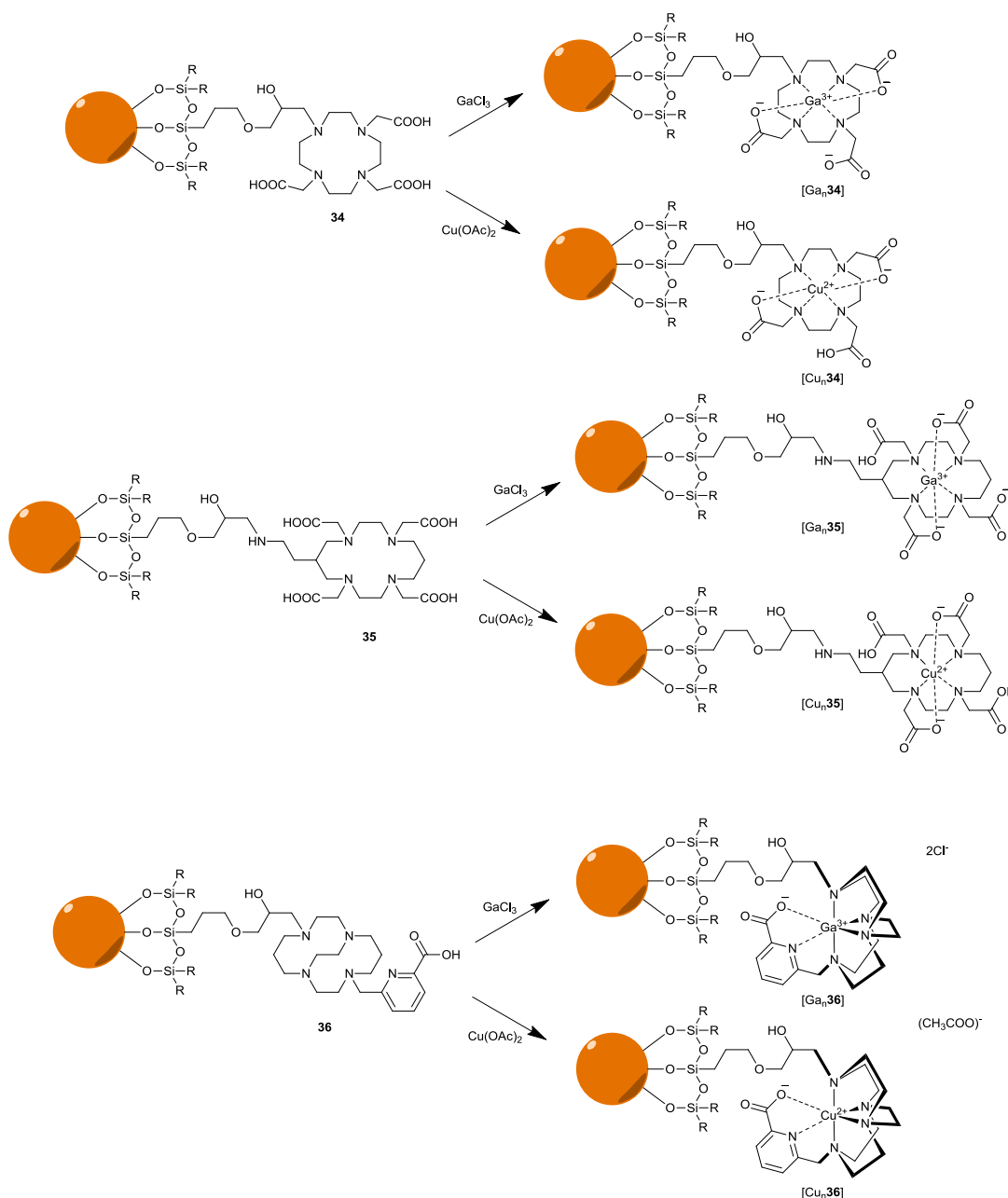
Scheme 34 – Macrocycle-nanoparticle construct $^{69/71}$Ga and $^{63/65}$Cu complex formation.

Complexation reactions were carried out in 60% ethanol solution and purified using a similar method to that described previously, magnetic separation and successive solvent washings.
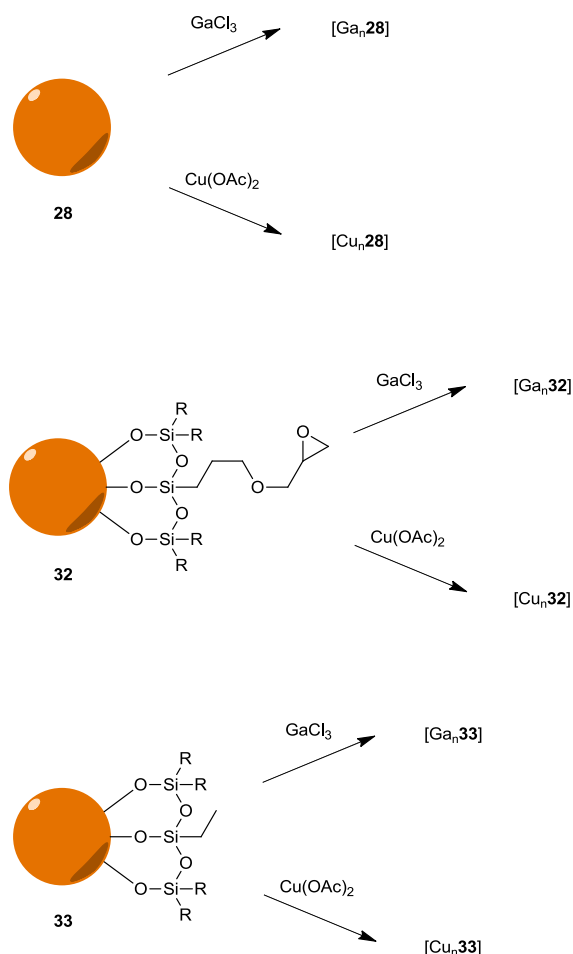
Scheme 35 – Control-nanoparticle $^{69/71}$Ga and $^{63/65}$Cu complex formation.

ICP data for the nanoparticle immobilised complexes was studied to compare the uptake of each of the metal ions and to determine the properties of the different macrocycles and controls. For the $^{69/71}$Ga complexes, it can be seen that all NP immobilised macrocycles and the controls take up gallium(III), see Figure 37. The trend is reproduced in the copper(II) ICP data, see Figure 38. Generally, although it is initially surprising that the uncoated nanoparticles take up both metal ions, it is not a surprise that the percentages are relatively higher than all other samples. This is due to the fact that ICP data is expressed as a mass percentage and for the bare nanoparticles, only oxygen and iron are present, whereas for coated nanoparticles the silica shell will represent a significant percentage of the overall mass, resulting in a lower percentage of metal ion incorporation.
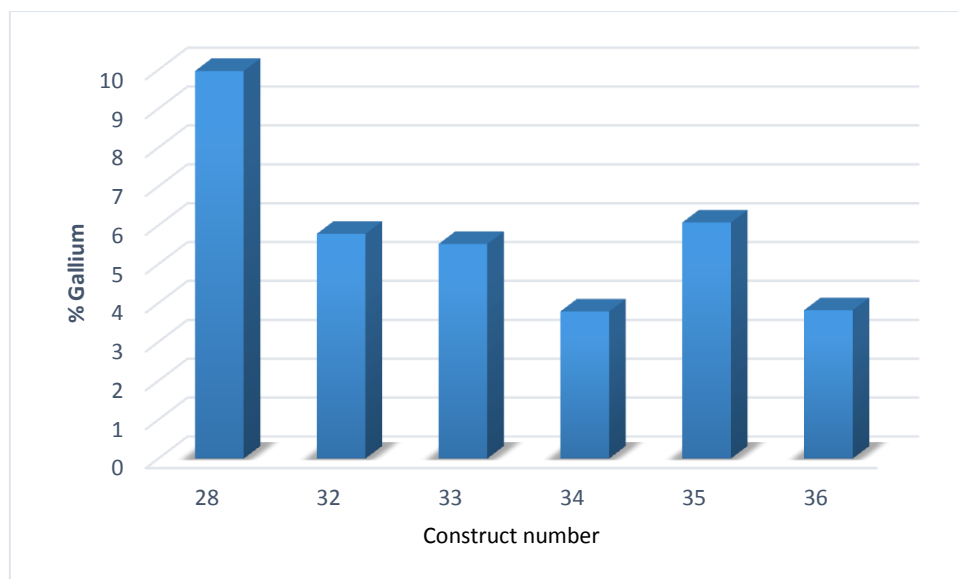
Figure 37 – $^{69/71}$Ga incorporation expressed as a percentage of overall mass for a series of silica coated nanoparticles.

When comparing $^{69/71}$Ga and $^{63/65}$Cu incorporation data it was observed that the macrocyclic derivatives consistently incorporate more $^{69/71}$Ga than $^{63/65}$Cu under the adopted reaction conditions. Hence, the nanoparticles presented in this work are more applicable for ^{68}Ga radiolabelling with the complexation reaction methodology used.
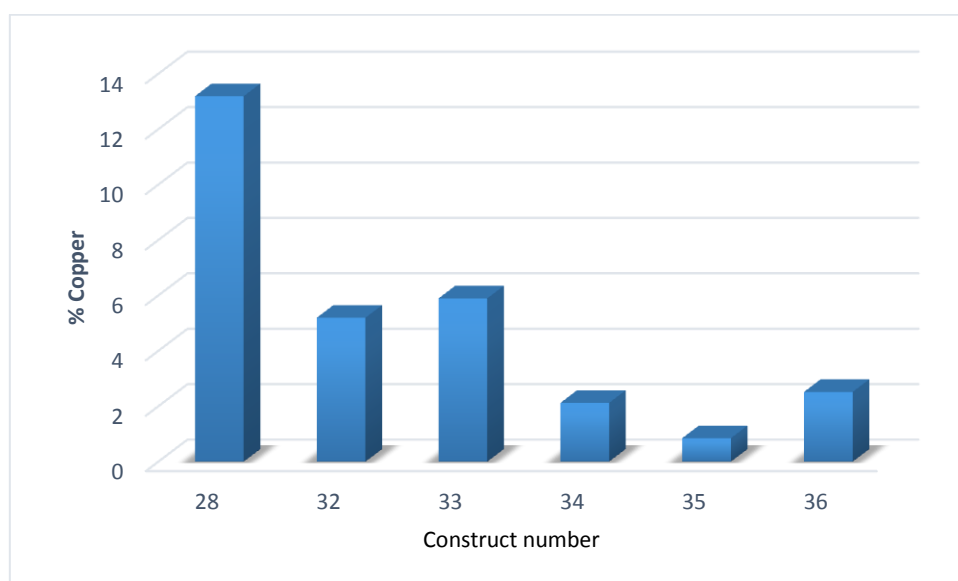
Figure 38 – $^{63/65}$Cu incorporation expressed as a percentage of overall mass for a series of silica coated nanoparticles.

32 contains an epoxide group, which is known to react with alkyl halides to ring-open,[188,189] this could allow coordination interactions with gallium(III) via the alcohol oxygen donor atoms, see Scheme 36, along with the analogous copper(II).
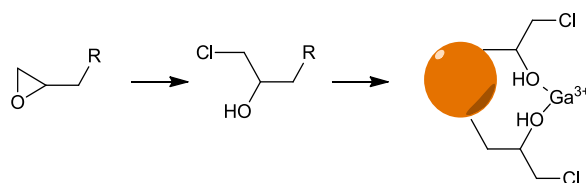
*Scheme 36 – Possible mechanism for the formation of [Ga**32**]*

Due to the unknown effect of the epoxide ring opening reaction of **32**, and the lack of clinical relevance of **28** as it is not biocompatible due to the lack of surface coating, they were not further used as controls. **33** was selected as the control to use in further studies. It was believed that although **33** formed gallium(III) complexes, this was via weak coordination to silica oxygen atoms on the surface and therefore would lead to formation of unstable complexes when compared to macrocycle derivatives, a property which can be studied with the radiolabelled NPs. Regardless of how the controls behaved, the initial aim of this study was to show that as a proof of concept the macrocycle coated nanoparticles could take up gallium(III) and copper(II) before radiochemistry was proved successful.

3.5. Bisphosphonate Endorem conjugation

As an alternative method to silica coatings, bisphosphonate (BP) derivatives were also investigated. BPs are known to form strong interactions with multiple inorganic groups including iron oxide.[172,190-192] Unlike silica derivatives however, using BP as a linker to the chelator does not form a colloidally water stable biocompatible product. BP derivatives either need to be modified with hydrophilic groups such as PEG, or BPs can be used with nanoparticles such as Endorem that have already been surface coateds to make them biocompatible. BP functionalised chelators have been used previously with Endorem, a clinically licensed SPION which is dextran coated.[172,193] BP is proposed to 'burrow' between polymerised dextran to conjugate with the magnetite surface.[193]

To provide a direct comparison to silica coatings, derivatives of the same three macrocyclic ligands were used, see Figure 39.

37 **38** **39**
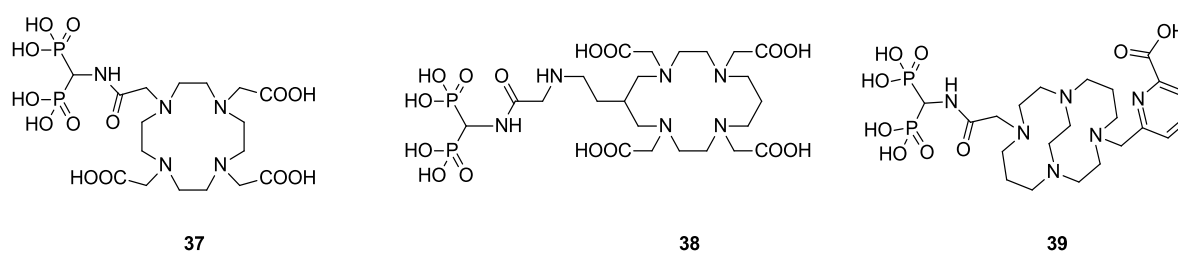
Figure 39 – Bisphosphonate (BP) derivatised macrocycles used for Endorem NP surface attachment.

Bisphosphonate macrocycle derivates (**37**-**39**), along with a non-macrocyclic alkyl control, (1-hydroxydecane-1,1-diyl)diphosphonic acid (**40**) were reacted with Endorem NPs following a modified literature procedure, see Scheme 37.[193] The reaction was performed in aqueous conditions, at a pH of 7; after the reaction was complete the nanoparticles were purified by dialysis with 8-10 kDa cut off. The dextran coating of the nanoparticles causes them to suspend very well in aqueous media, therefore the magnetic separation technique as used for silica derivatives is not applicable. Addition of organic solvent to aid this process was also not desirable and drying and resuspension of the nanoparticles was unnecessary. [68]Ga radiometallation would be carried out in aqueous media and therefore keeping them suspended was preferable.
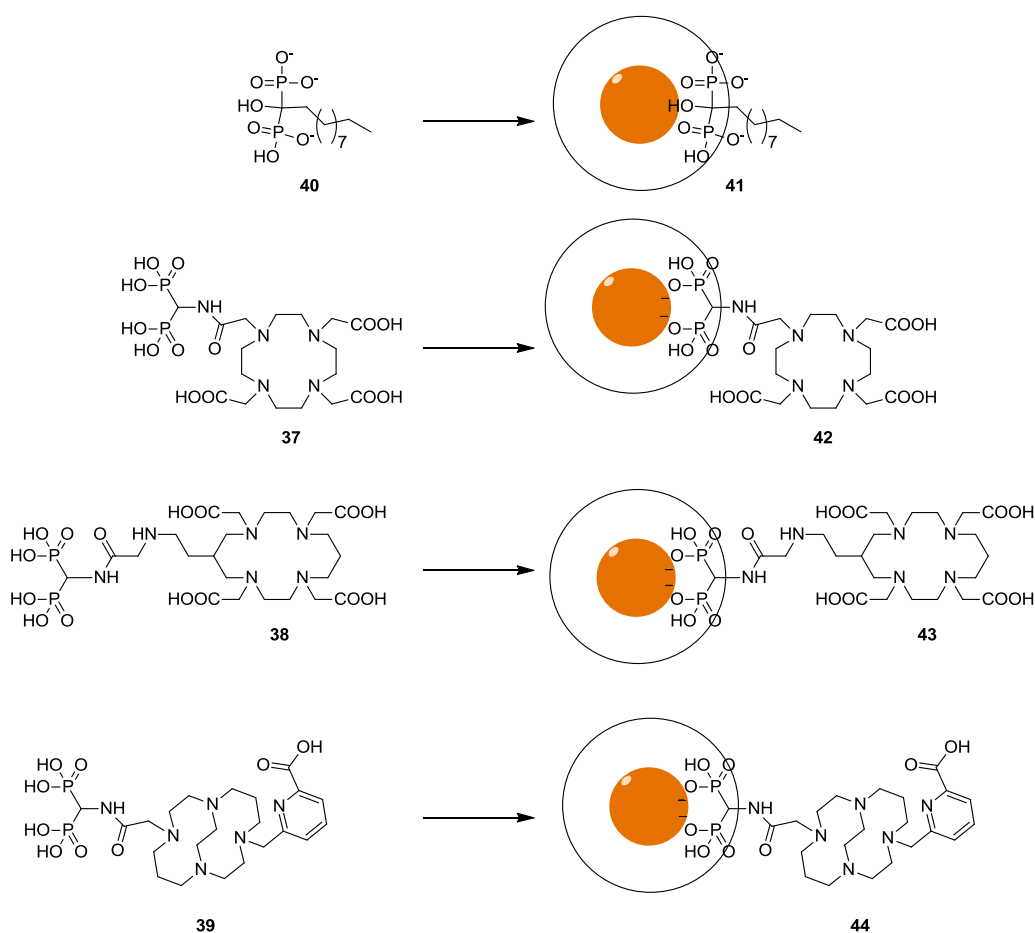
Scheme 37 – Formation of Endorem-bisphosphonate macrocycle derivatives.

Due to the large difference in macrocycle surface concentration between silica and bisphosphonate derivatives along with ICP data collected on the silica based NP derivative giving no indication of surface macrocycle concentration, performing a similar set of cold metal uptake reactions was unlikely to give any indication of metal incorporation into the macrocyclic cavity. CHN data could potentially show some difference as Endorem doesn't contain nitrogen, however, having macrocycles all over the surface on silica derivatives only gives CHN nitrogen percentages in the range of 0.4%, the macrocycle surface concentration for BP derivatives is much lower than this due to the nature of the attachment methodology and therefore CHN is not sensitive enough to give significant data. It was decided that comparison of the radiolabelling properties of the macrocycle NP derivatives (**42-44**) and the control, **41**, would give a good indication of the degree of NP surface functionalisation with the macrocycle bisphosphonate derivatives.

3.6. ^{68}Ga complexation of chelators immobilised on NPs and controls

The range of four bisphosphonate (**41**-**44**) and four siloxane derivatised (**33-36**) macrocycles and controls have been attached to SPIONs, and their complexation properties with ^{68}Ga were explored. Radiochemical complexation reactions were analysed by radio-TLC, eluting with 0.2 M citric acid, with free ^{68}Ga and later ^{68}Ga-EDTA moving with the solvent front and MNPs staying on the baseline of the TLC, see Figure 40.
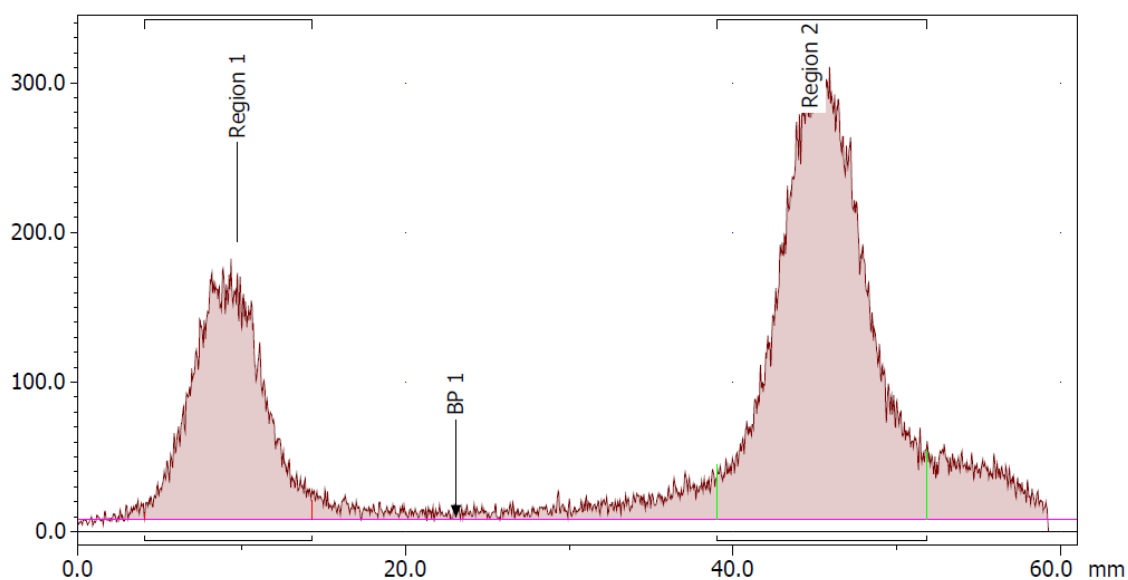
Figure 40 – Example of radio-TLC used to analyse nanoparticle ^{68}Ga conjugation.

Reactions were carried out using 200 µl of 1 mM effective iron concentration with formulated ^{68}Ga, see *section 6.2*, in 20-60 MBq amounts. The reactions were carried out in ammonium acetate buffer (0.2 M) at pH 5 to avoid the formation of unreactive gallium hydroxide species.

Initially, radiolabelling and competition experiments were carried out singularly as a screening method to develop lead compounds, which were subsequently repeated in triplicate to asses reproducibility (*vide infra*).

3.6.1. Bisphosphonate macrocycles immobilised on nanoparticles

Bisphosphonate macrocycle-Endorem NP derivatives were reacted with ^{68}Ga at both RT and 90°C, see Scheme 38.
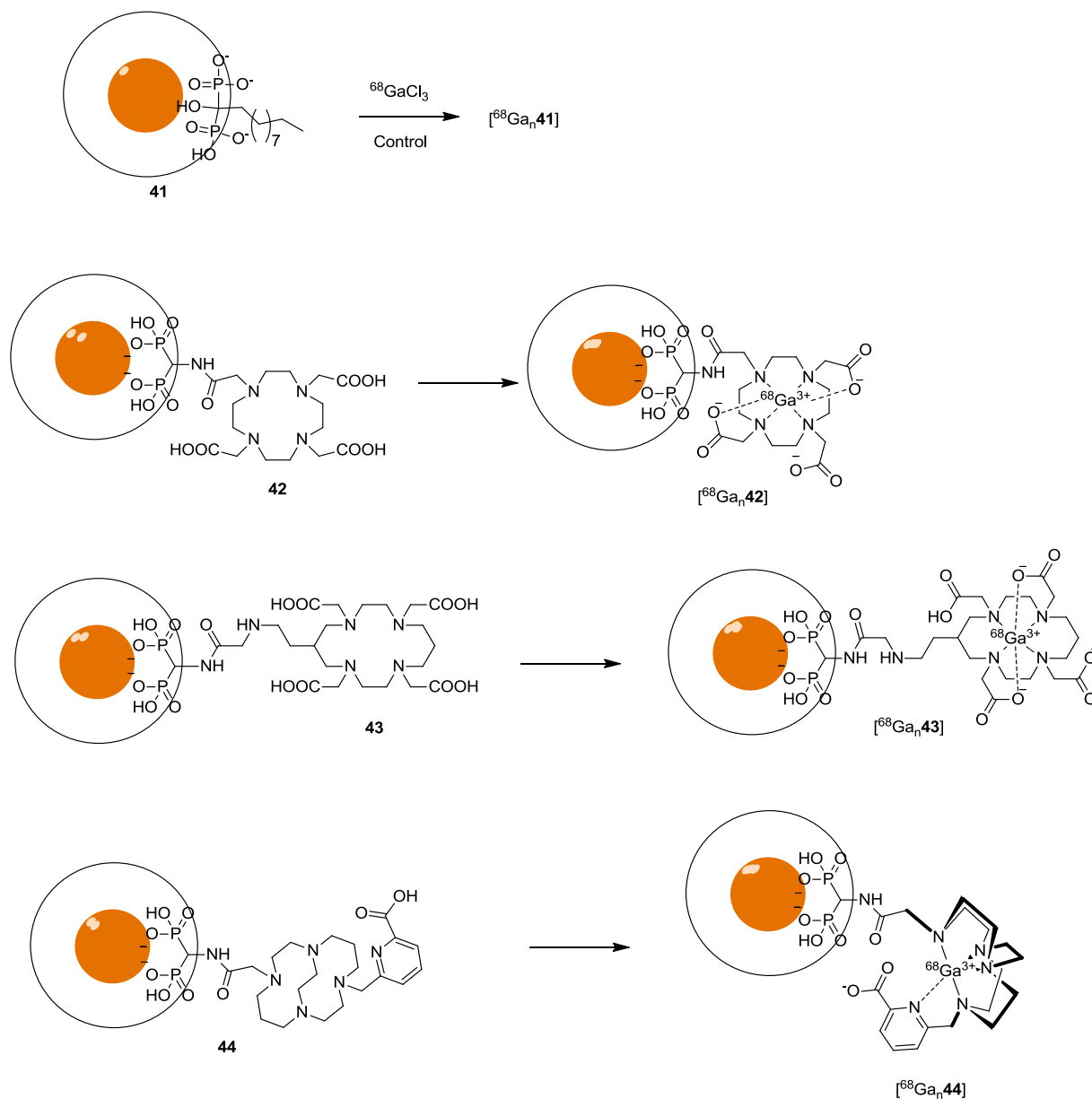
Scheme 38 – Macrocycle bisphosphonate-Endorem ^{68}Ga complex formation.

At room temperature, a considerable amount (40-80%) of ^{68}Ga is incorporated onto the nanoparticle after 5 minutes, see Figure 41.
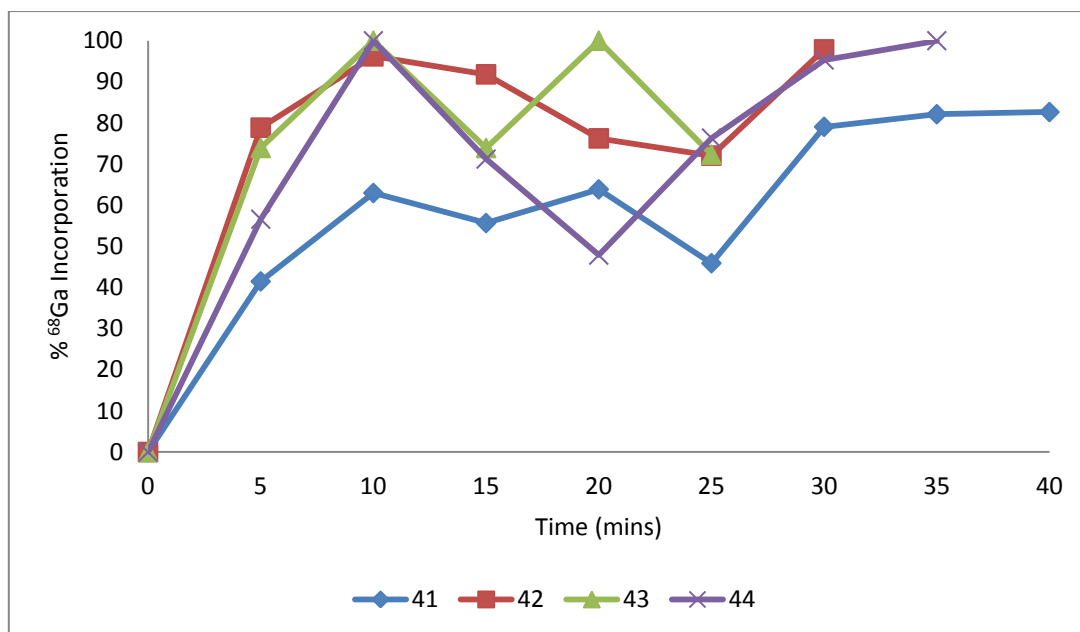
Figure 41 – BP-macrocycle Endorem nanoparticles: ^{68}Ga incorporation at RT.

Over the course of the reaction (30-40 minutes), there is in general a trend towards increasing ^{68}Ga incorporation for all conjugates. However, there is large variation between each time point which could be an indication of weakly coordinated gallium(III) which is in equilibrium between bound and unbound. All of the macrocycle modified NPs (**42**-**44**) give > 95% incorporation, (albeit at different time points) but the control becomes stable at ca. 80% incorporation, for raw data see *sections 6.8.1-6.8.4*.
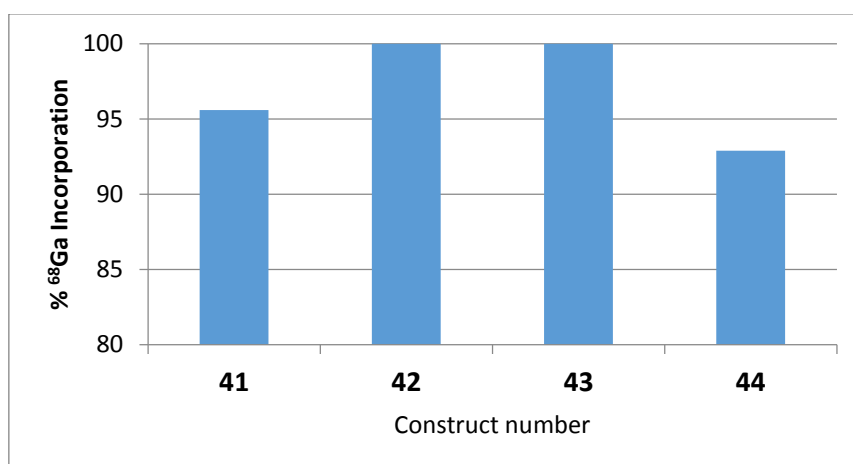
Figure 42 – BP-macrocycle Endorem nanoparticles: ^{68}Ga incorporation at 90°C after 15 minutes.

Increasing the reaction temperature to 90°C causes a consistent and dramatic increase in percentage incorporation of ^{68}Ga, with all four conjugates showing > 90% incorporation after 15 minutes, see Figure 42.

3.6.2. Siloxane derivative NPs

Applying the same method used for the BP-macrocycle Endorem NPs, siloxane-macrocycle coated NPs were reacted with ^{68}Ga at both RT and 90°C, see Scheme 39.
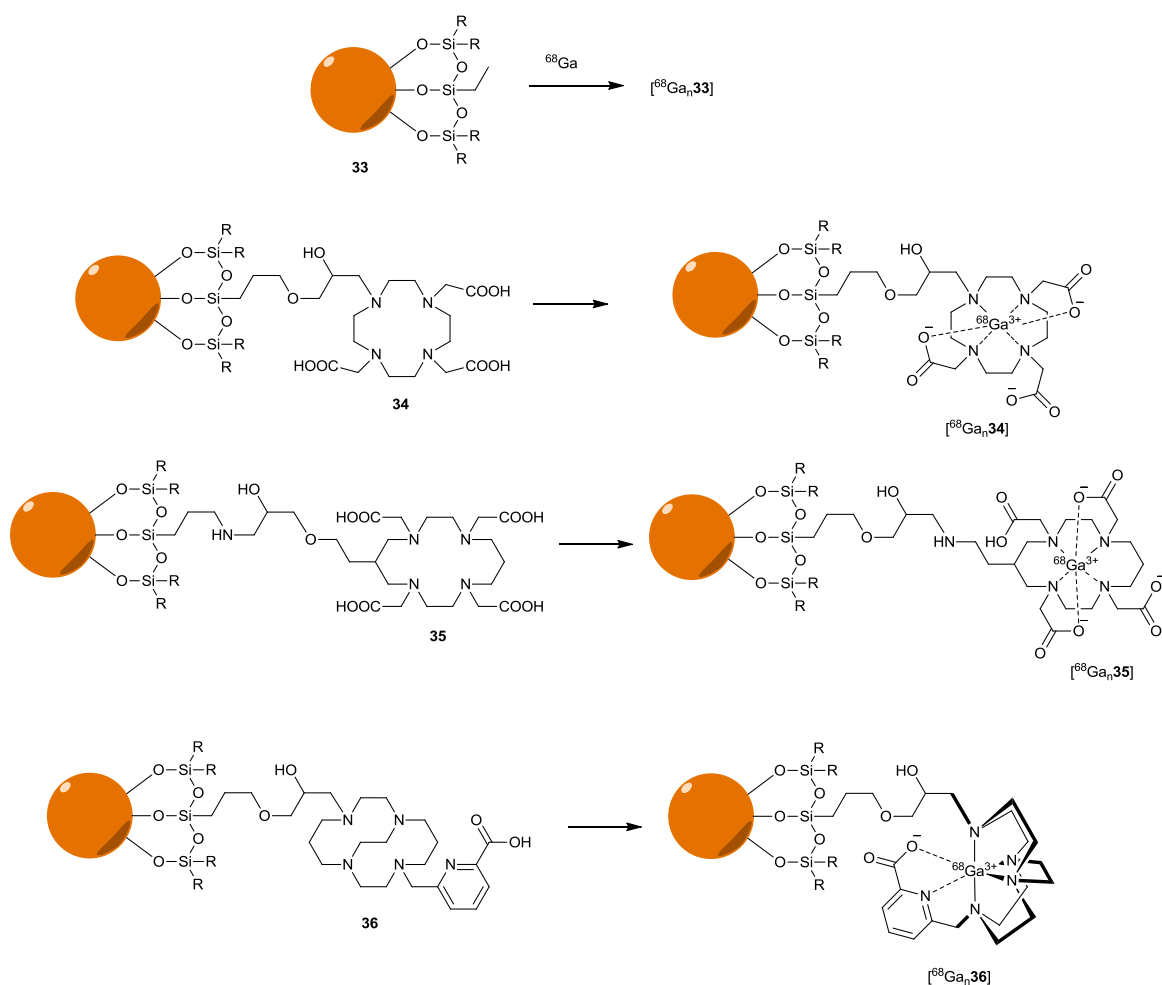
Scheme 39 – Macrocycle siloxane-SPION ^{68}Ga complex formation.

Forming the ^{68}Ga complexes with the nanoparticles at room temperature gave extremely variable results (n=3), see Figure 43, with very large standard deviations observed for each sample (9-20%). The control (**33**) seemed to be the best at incorporating ^{68}Ga under these conditions, consistently giving radiolabelling yields in the 80-100% range after 15 minutes. The three macrocyclic derivatives (**34**-**36**) are largely indistinguishable from each other, and all show poor reproducibility, generally giving between 30-70% incorporation after 15 minutes. In comparison to the bisphosphonates however, the data offers greater consistency. Meaning that within each individual experiment and within the averages, there was largely a steady increase in ^{68}Ga incorporation over time, in contrast to the BP-

macrocycle Endorem NPs which did not show an obvious trend, for raw data see *sections 6.8.5-6.8.8.*
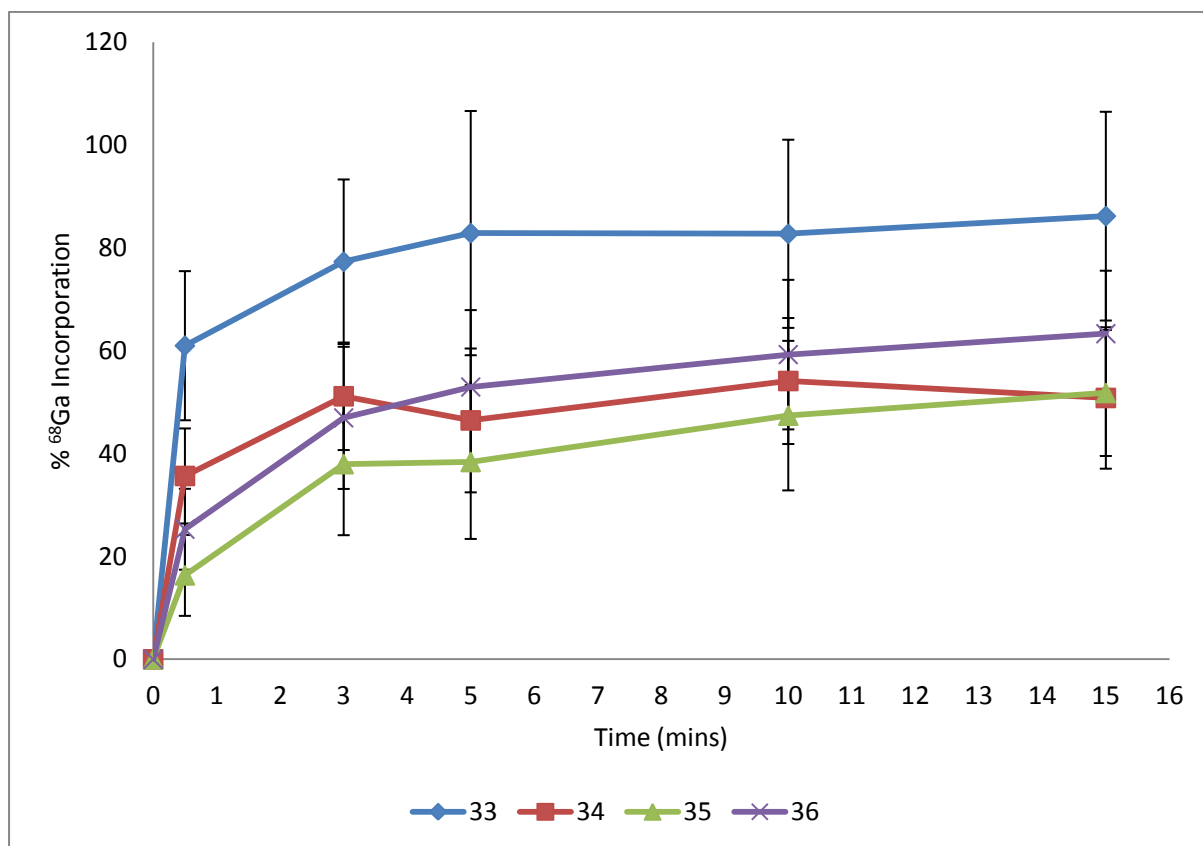
Figure 43 – Siloxane-SPION ^{68}Ga incorporation at RT.

Increasing the reaction temperature to 90°C causes a similar increase in incorporation of the radiolabel to that observed for the bisphosphonate derivatives, see Figure 44, with this data, unlike at RT, showing both internal consistency and cross replication consistency (n=3). As one would expect, there are larger standard deviations at 30s (5-15%) due to the short time point, however after 5 minutes reaction time the RCYs are consistently >95%.
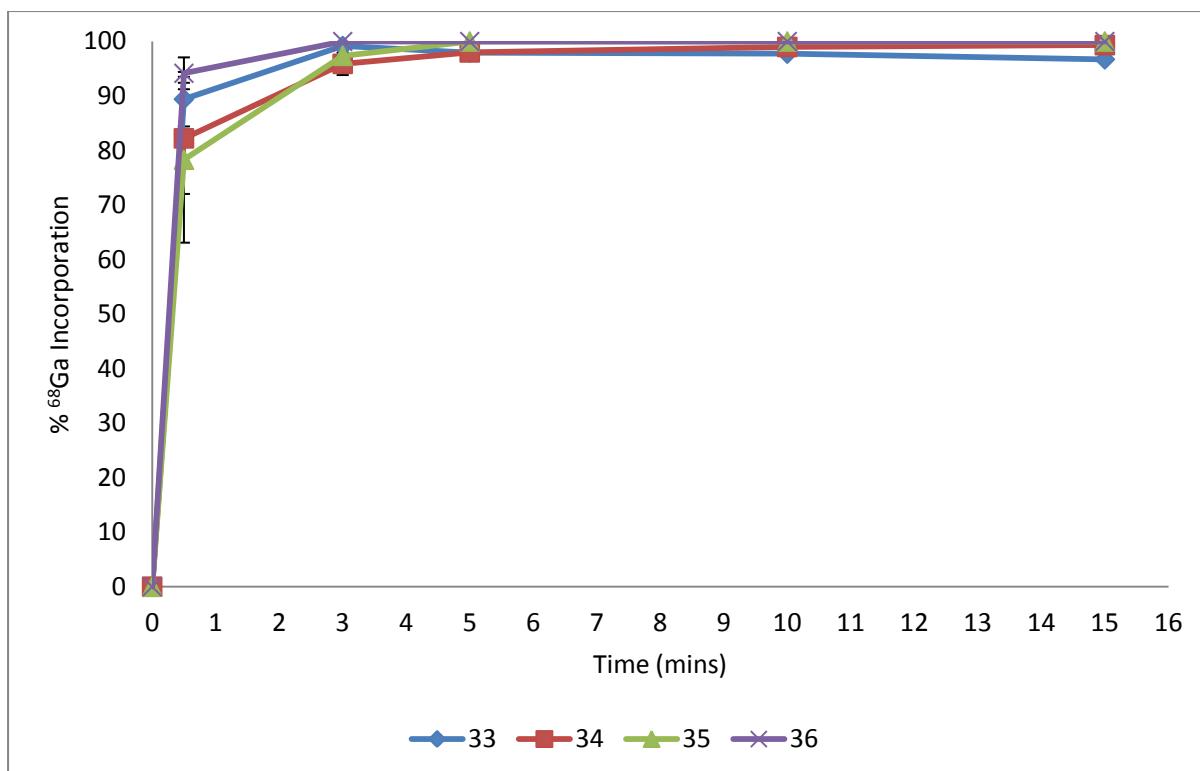
Figure 44 – Siloxane-SPION ^{68}Ga incorporation at 90°C.

3.6.3. EDTA stability

After conditions were determined by which four bisphosphonate NP derivatives ([^{68}Ga$_n$**41**], [^{68}Ga$_n$**42**], [^{68}Ga$_n$**43**] and [^{68}Ga$_n$**44**]) and four siloxane NP derivatives ([^{68}Ga$_n$**33**], [^{68}Ga$_n$**34**], [^{68}Ga$_n$**35**] and [^{68}Ga$_n$**36**]) could be successfully radiolabelled to above 90% yield, competition tests were carried out to determine if ^{68}Ga was weakly or strongly bound to the nanoparticle. Ethylenediaminetetraacetic acid (EDTA) is known to rapidly form complexes with small, charged metal ions,[8,194] and was therefore chosen as a suitable competitor for NP binding. After nanoparticle-^{68}Ga complexation, a 10-fold excess of EDTA (compared to NP iron concentration) was added and the stability challenged at either room temperature or at 90°C. The reaction mixture was again analysed by radio-TLC, with ^{68}Ga-EDTA moving to the solvent front in the same way as free ^{68}Ga (data not shown).
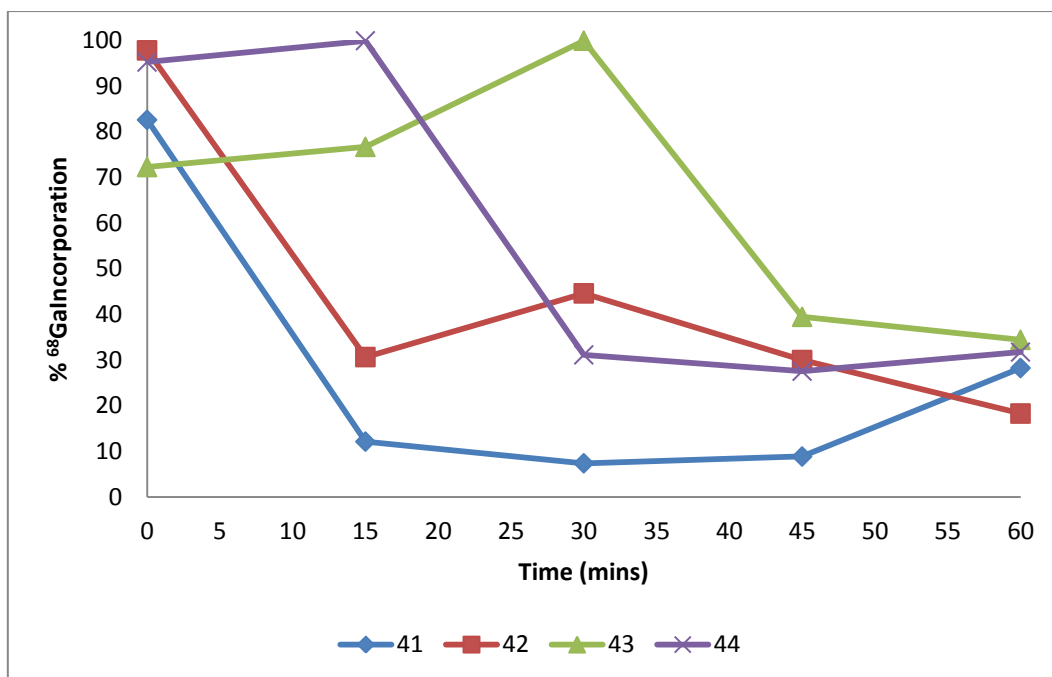
Figure 45 – % Incorporation of ^{68}Ga in bisphosphonate-macrocycle nanoparticles after EDTA competition at room temperature.

The study of bisphosphonate NP derivatives at room temperature shows somewhat inconsistent data, see Figure 45, similar to the formation reaction for these species. The competition with EDTA shows a broad trend of increased label loss with time indicating that the ^{68}Ga may be bound to the NP via weaker coordination interactions, this was consistent across all of the macrocycles (**42**-**44**) and the control (**41**) clearly demonstrating instability over a 1 hour period, for raw data see *sections 6.8.9-6.8.12*.
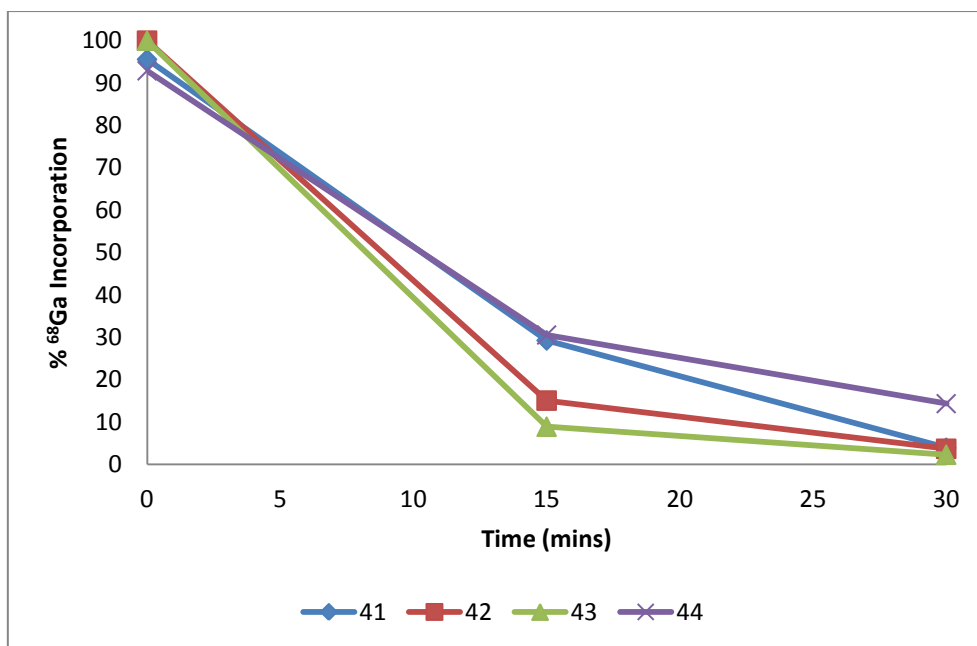
Figure 46 – % Incorporation of ^{68}Ga in bisphosphonate nanoparticles after EDTA competition at $90^{o}C$.

Upon increasing the competition reaction temperature to $90^{o}C$ there is a clear and consistent decrease in stability of all macrocycle derivatised NPs (**42**-**44**) and the control (**41**) bisphosphonate derivatives, see Figure 46, with all four showing >80% loss of bound activity to form the EDTA complex after 30 minutes.
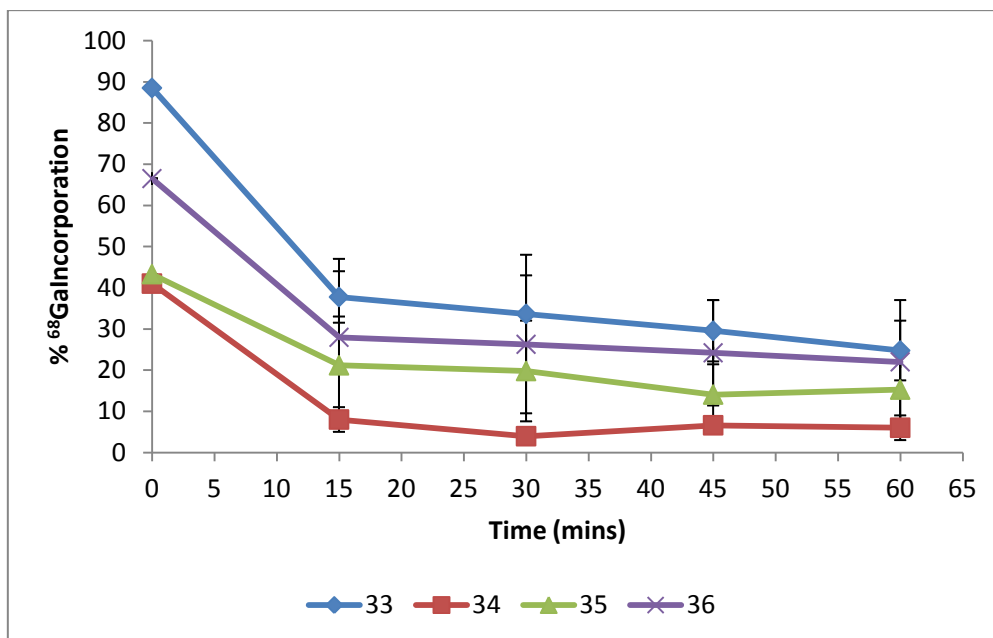
Figure 47 – % Incorporation of ^{68}Ga in siloxane nanoparticles after EDTA competition at RT after radiolabelling at RT.

The same competition experiments were initially attempted with the siloxane derivatives (**33**-**36**), however it was observed that there was variation in the results dependent on whether the nanoparticles had been radiolabelled at RT or at 90°C so the derivatives from each set of labelling conditions were subsequently studied separately and were repeated (n=2/3) to investigate whether the phenomenon was reproducible, for raw data see *sections 6.8.13-6.8.16*.

Initially, siloxane derivatives which had been radiolabelled at room temperature were used in competition with EDTA, see Figure 47. Rapidly (15 minutes), a large percentage of ^{68}Ga was lost from the NP surface/ macrocycles and complexed with EDTA (ca. 50%) however, after this time point, only small amounts of gallium (<10%) was lost over the next 45 minutes. Spiccia and co-workers used a cyclam chelator competition experiment to determine ^{64}Cu-SPION stability.[174] After adding cyclam, 30% of the bound radioactivity was transferred to the cyclam after only 5 minutes. Although this is a significant proportion of activity this can also be used as a purification method before *in vivo* as after separation of the nanoparticles and competition with fresh cyclam only an average of 2.4% ^{64}Cu was lost during the next 60 minutes. This strongly indicates that there is both weakly coordinated metal ions (surface silica) and more stably bound ions (potentially bound to the macrocycle chelators). However, on closer examination of their reported results the loss of radiolabel seems to still be increasing and there is a lack of longer time points which could easily be recorded for this isotope (t$_{\frac{1}{2}}$ = 12.7 h). The percentage of bound radioisotope after 24 h would be very interesting to indicate the potential utility of these derivatised nanoparticles.
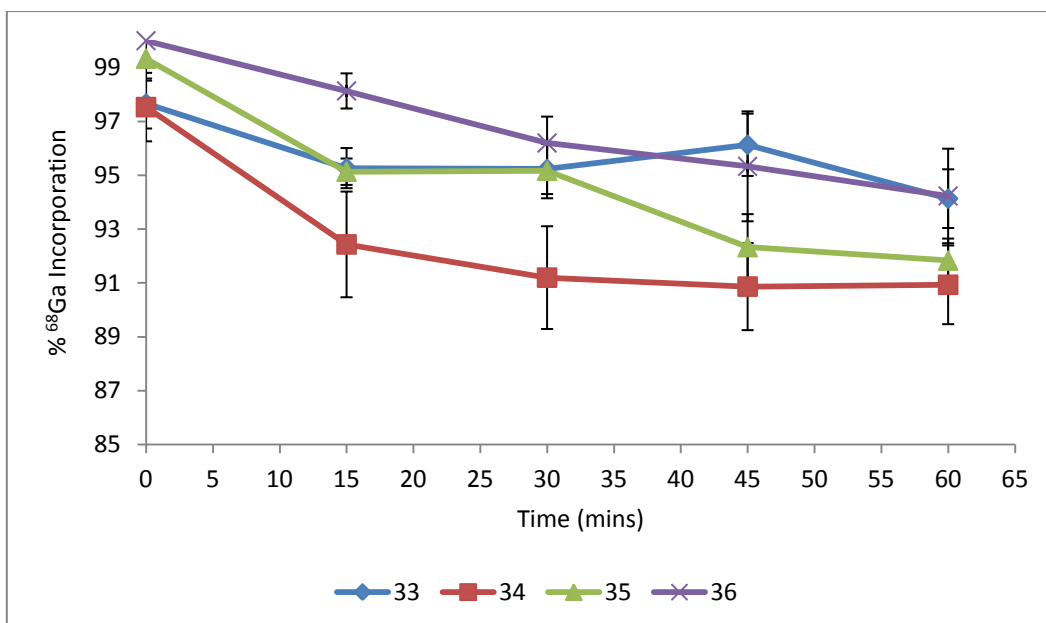
Figure 48 – % Incorporation of ^{68}Ga in siloxane nanoparticles after EDTA competition at RT after radiolabelling at 90°C.

When the same competition experiment was carried out with ^{68}Ga nanoparticles which were synthesised at 90°C the results are very different (n=3), see Figure 48. Consistently between all macrocycles (**34**-**36**) and the control (**33**) there is only a small percentage of radioactivity lost over 60 minutes (<10%) with no dramatic loss after 15 minutes as observed previously.
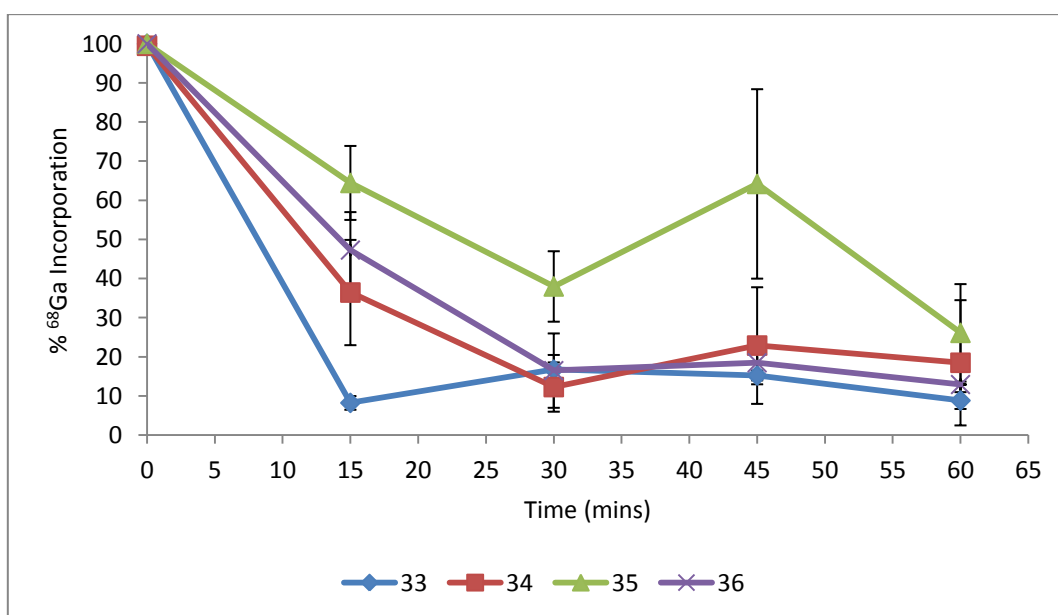
Figure 49 – % Incorporation of ^{68}Ga in siloxane nanoparticles after EDTA competition at 90°C after radiolabelling at 90°C.

However, when the same experiment was carried out (using nanoparticles synthesised at 90$^{\text{o}}$C) but increasing the competition temperature to 90$^{\text{o}}$C most of the ^{68}Ga becomes complexed by EDTA, both after 15 minutes and a steady increase in the loss of the radiolabel up to 60 minutes (n=2), see Figure 49. The control (**33**) rapidly and consistently loses 90% of the ^{68}Ga after 15 minutes competition. Although the macrocycles (**34**-**36**) also lose most of the radioactivity over the course of the experiment, this consistently happens more slowly than is observed for the control. EDTA competition at 90$^{\text{o}}$C is a very harsh competition experiment and lack of stability may not give a useful indication of the *in vivo* stability of the compounds.

3.6.4. Siloxane/Bisphosphonate ^{68}Ga comparison of results and proposed explanation

There are two potential theories to explain the difference between siloxane and bisphosphonate-macrocycle nanoparticle derivatives. A relatively simple explanation for the results could be that the conjugation of the bisphosphonate derivatives with the nanoparticles simply did not work as this reaction is very difficult to analyse. However, this reaction has been carried out successfully on multiple occasions previously by other workers,[172,193] providing evidence to suggest that this method should work as predicted. The second theory is based on surface macrocycle concentration. For nanoparticle synthesis for biomedical applications, the surface of the nanoparticle is functionalised to increase hydrophilicity, forming stable suspensions in water, stopping aggregation and increasing biostability. For siloxane derivatives, the biocompatible nanoparticle coating and the linking group to the macrocycle are the same conjugate, forming a polymerised macrocycle silica layer on the surface of the nanoparticle. For the bisphosphonate derivatives, bisphosphonate itself does not aid with biostability and is therefore used with other coating materials such as dextran coated nanoparticles; Endorem. The bisphosphonate derivatives are thought to then 'burrow' between the gaps in the dextran layer to coordinate to the iron oxide surface.[195]
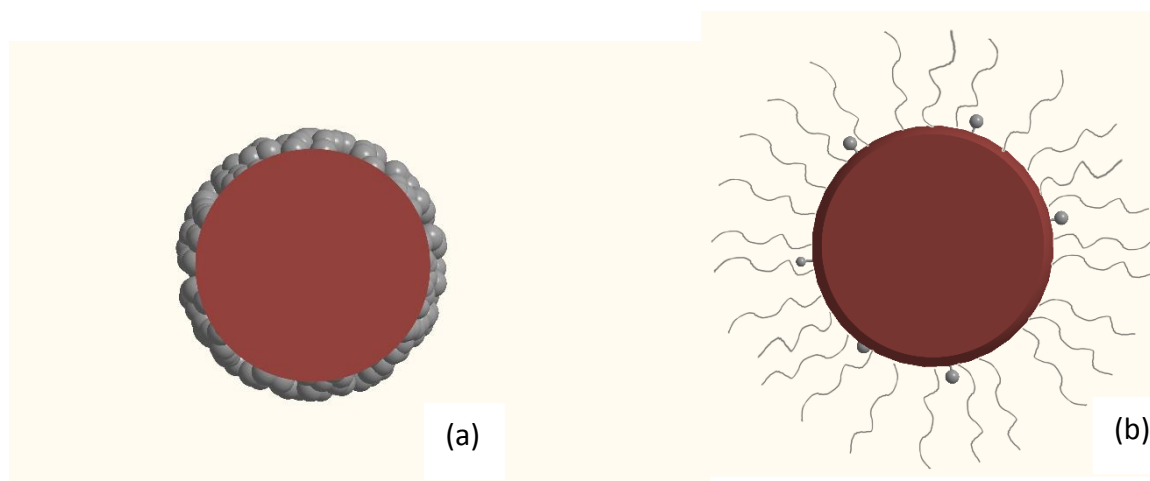
Figure 50 – Visual cross-section representation of (a) siloxane-macrocycle nanoparticle and (b) Endorem-bisphosphonate macrocycle nanoparticle.

This makes the effective macrocycle concentration between each type of nanoparticle dramatically different and also affects the relative accessibility of the macrocycles, see Figure 50. It is observed from all of the controls that ^{68}Ga does react with the nanoparticles without macrocycles present, it is therefore much less likely for the bisphosphonate derivatives to form a macrocyclic ^{68}Ga complex on a concentration basis and hence much of the ^{68}Ga is likely to be forming more weakly bound surface coordination interactions with the nanoparticle or the dextran coating. An effect which may be also observed with siloxane nanoparticles at room temperature, making increased temperatures necessary for macrocyclic complex formation. However this does not explain the stability of the control under the same conditions.

Torres and co-workers have used Endorem and bisphosphonates to form PET/MRI imaging constructs with ^{64}Cu[172] and related SPECT/MRI NP derivatives with technetium-99m.[193] However, the group avoided the problems observed with surface interactions by carrying out the radiochemical reaction using a two-step method. The radiolabelled bisphosphonate derivative was formed prior to attachment of the radiolabelled bisphosphonate molecule to Endorem. However, this method is much more challenging for ^{68}Ga due to the much shorter half-life (1.17h) in comparison to ^{64}Cu (12.7h) and technetium-99m (6h). The two-step procedure is a lengthy process due to the successive centrifuge spin filter washings necessary to separate radiolabelled bisphosphonates which are attached and unattached to the nanoparticle and is therefore not a viable method for use with ^{68}Ga.

Overall this screening of the reactivity of each nanoparticle produced in this work and its stability showed that the bisphosphonate derivatives generally have relatively slow binding kinetics with Endorem and were not found to be sufficiently stable under competition with EDTA, and little difference was observed between the macrocycle functionalised NPs and the control. The siloxane derivatives on the other hand can form strongly bound complexes with ^{68}Ga for all the macrocyclic derivatives and also the control, which are stable under room temperature competition from EDTA. This makes the four silica coated nanoparticle compounds suitable candidates for further study towards *in vivo* use.

3.6.5. Serum stability of silica coated NP derivatives

The four silica based SPIONs radiolabelled with ^{68}Ga at 90°C were studied for stability under condition as relevant to *in vivo* applications. Serum was chosen as the media to construct this experiment, containing multiple species which can complex gallium(III) such as transferrin.[196] The experiments were carried out at physiological temperature (37°C) and were performed on the longest timescale that still gave informative data from radio-TLC (4 hours).
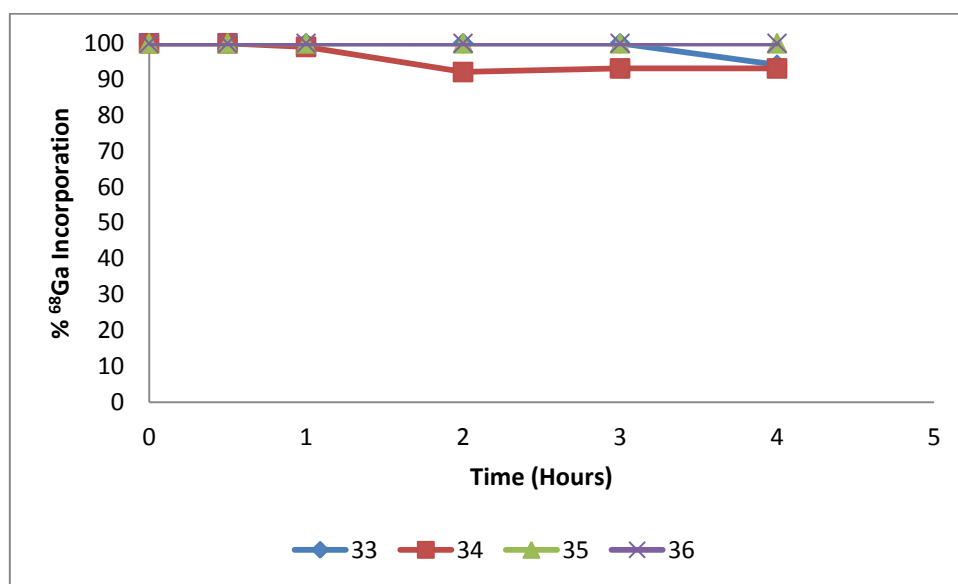
Figure 51 – Graph to show radiochemical stability of ^{68}Ga siloxane SPION conjugates in serum over 4 hours.

Torres and co-workers tested the stability of their ^{99m}Tc-SPIONs and ^{64}Cu-SPIONs by a similar method, but using a centrifuge method instead of radio-TLC for technetium-99m conjugates,[172,193] however both experiments were carried out over the longer time frames possible with these isotopes due to their longer half-lives. Both of which showed no decomposition over the time points measured. A possible limitation with this synthetic and evaluation method is noted however, when the study was developed to PEG conjugated nanoparticles the serum stability gave similar results (94% bound to the SPIONs over 48h).[195] However, when the conjugate was tested *in vivo* there was significant uptake in the knee, evidence for unbound but radiolabelled bisphosphonate, either the BP conjugated to

the nanoparticle is not *in vivo* stable or the analytical/purification methods used were not successful. This however is not a concern for the siloxane derivatives in this study because the radiolabelling is the final step and unbound siloxane macrocycles have already been separated previously, therefore the only positions for ^{68}Ga to be is attached to the nanoparticle, to be present as a 'free' ion or attached to the competition media (EDTA or serum proteins), all of which can be analysed by the methods described. A study which was carried out by Galus *et al*. who suspended synthesised ^{64}Cu-SPIONs in mouse serum at 37°C for 24h,[167] monitoring bound and unbound radioactivity by radio-TLC, showed only a 2.5% loss in bound activity over 24h.

Studies on the radiolabelled nanoparticles in this work showed similar results to the literature, with either little or no loss of activity over 4 hours, see Figure 51. The control [^{68}Ga$_n$**33**] and DO3A [^{68}Ga$_n$**34**] showed a loss of 6% and 7% respectively over the 4 hour period used. C-TETA [^{68}Ga$_n$**35**] and CB-MP [^{68}Ga$_n$**36**] derivatives showed no observable loss in activity, for raw data see *sections 6.8.17*. The control [^{68}Ga$_n$**33**] is therefore still unexpectedly stable under these conditions, however a loss of 6% or 7% of activity is not ideal and C-TETA [^{68}Ga$_n$**35**] and CB-MP [^{68}Ga$_n$**36**] are therefore the lead compounds from these studies.

3.6.6. Nanoparticle size and size distribution

The size and size distribution of nanoparticles is important for application as *in vivo T$_2$* MRI contrast agents as the size of the nanoparticles is direct related to how the body processes and excretes them, if they are too small (<5.5 nm) then they can be excreted through the kidneys.[197] If they are too large (>200 nm) then they can be easily detected by the immune system and excreted via the liver and spleen, resulting in short blood circulation times.[198] The optimal size for most applications is between 10-200 nm. NanoSight® nanoparticle tracking analysis (NTA) is a technique which can determine the size of nanoparticles in aqueous solution by analysis of a video of nanoparticle movement via Brownian motion when illuminated by a laser. The software can then calculate the average size and size distribution of the sample, see Figure 52.
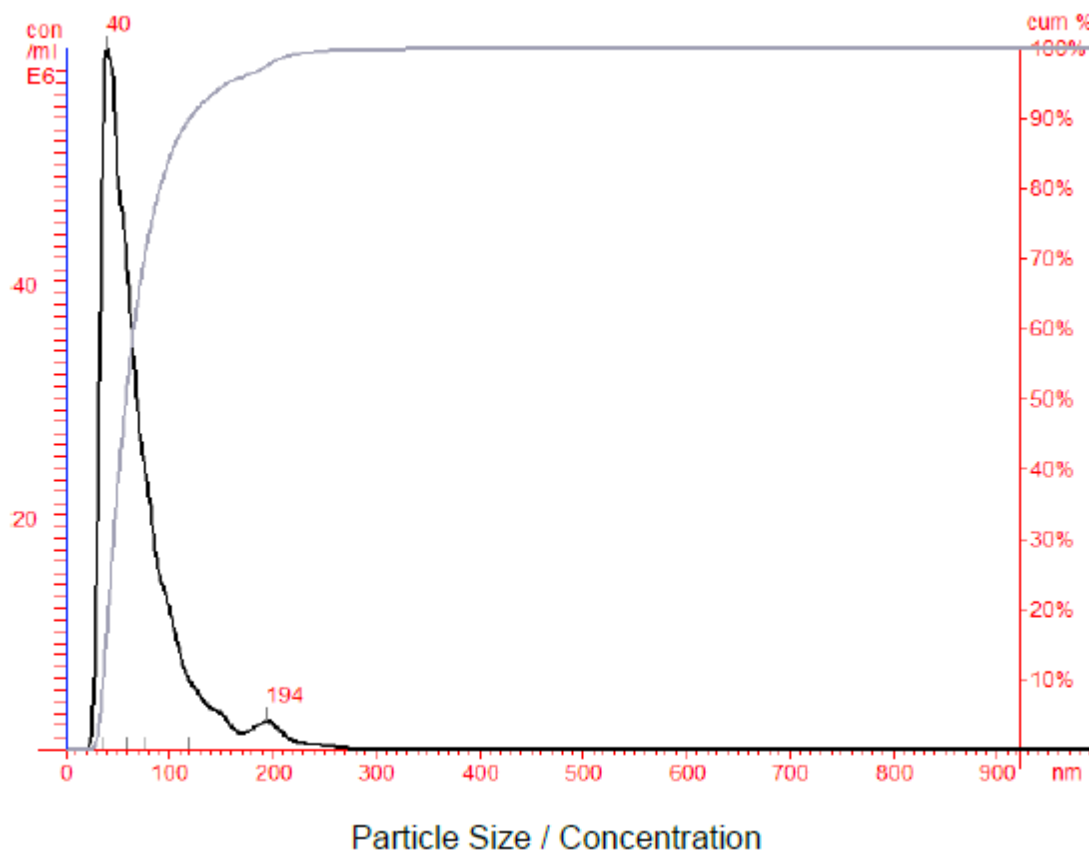
Figure 52 – Example nanosight size distribution graph.

NTA of SPIONs which are coated in siloxane derivatives (**33**-**36**) seem to show large variation between the controls and different macrocycles, see Figure 53. Both the control (**33**) and C-TETA (**35**) forming large agglomerates (<200 nm). DO3A-coated NPs (**34**) have quite a large mean value of 125 nm which is due to the formation of some nanoparticles at around 200 nm that increases the mean value to be much larger than the modal value of only 34 nm. CB-MP (**36**) has the most promising data, with a small enough mean and modal value to be demonstrate suitable parameters for the imaging application (134 nm and 95 nm respectively).
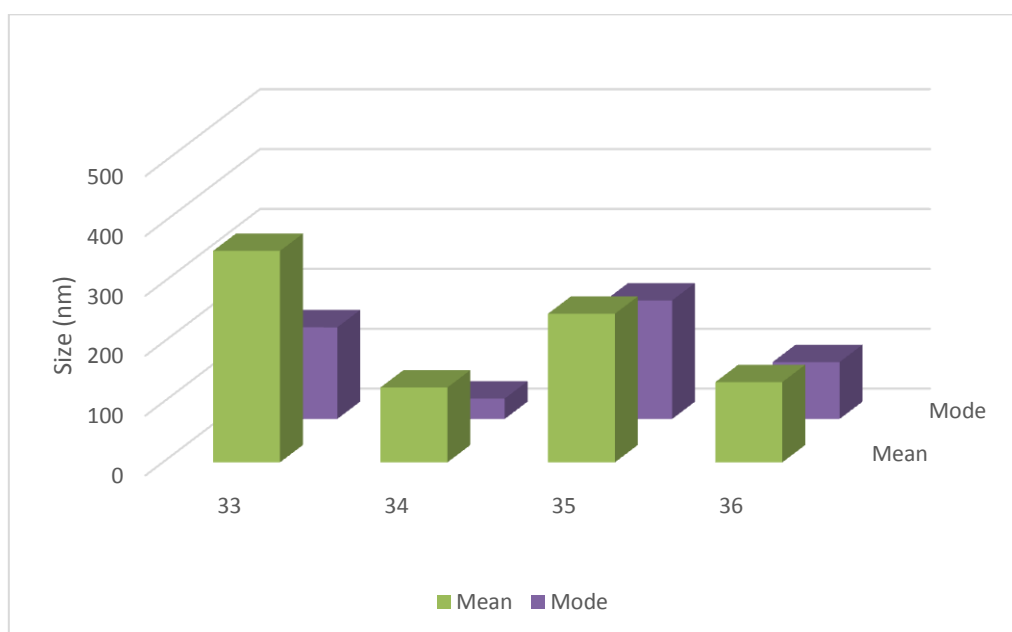
Figure 53 – NTA analysis of siloxane SPIONs showing mean and mode size in nanometres.

After formation of the $^{63/65}$Cu and $^{69/71}$Ga metal complexes NTA was repeated to test if this modification affected aggregation, see Figure 54 and Figure 55. CB-MP (**36**), the most promising of the siloxane chelator derivatives, showed very little difference after both complexes were formed, with mean and modal values still between 40 and 140 nm. C-TETA (**35**) showed slightly inferior characteristics after $^{63/65}$Cu complex formation and a significant size decrease after $^{69/71}$Ga complexation, with a mean value of 103 nm and a modal value of 94nm. The control (**33**) however showed less useful results, with both complexes forming quite large aggregates (200-400 nm).
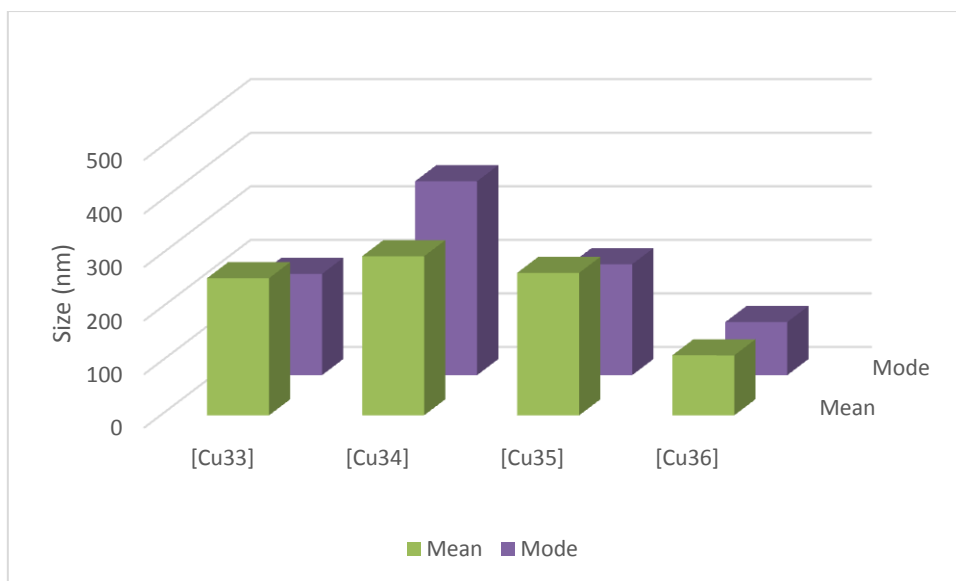
Figure 54 – NTA analysis of $^{63/65}$Cu siloxane SPIONs showing mean and mode size in nanometres
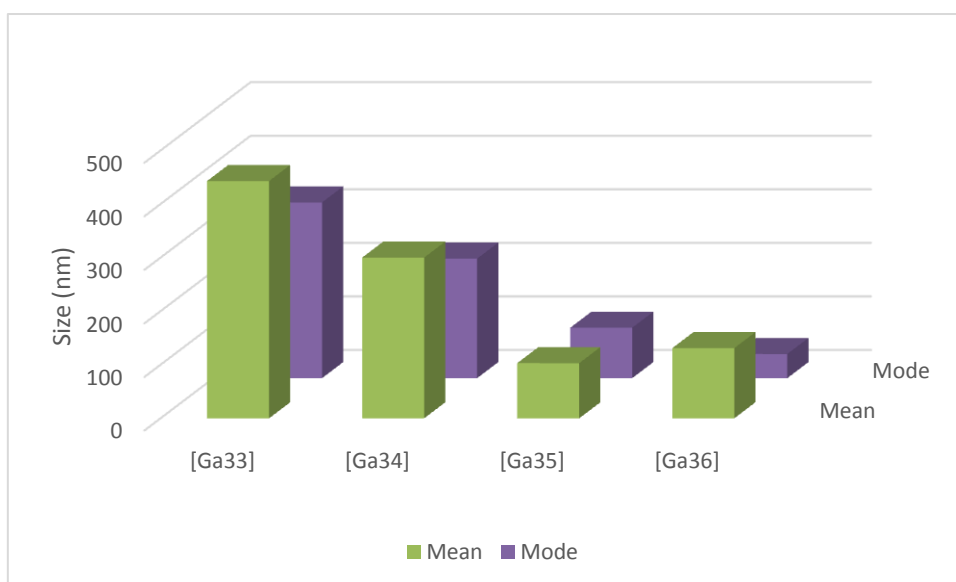
Figure 55 – NTA analysis of $^{69/71}$Ga siloxane SPIONs showing mean and mode size in nanometres

It is assumed however that the nanoparticles formed from $^{69/71}$Ga experiments are not identical to those formed when using ^{68}Ga due to the large difference in metal ion concentration and the fact that the ultimate product after nuclear decay will in fact be a zinc(II) ion complex rather than a gallium(III) ion complex. It was therefore worthwhile to do NTA on nanoparticle samples after radiochemical labelling and subsequent decay, thus testing for concentration effects and also the effect of zinc(II) ion on average nanoparticle size and size distribution.
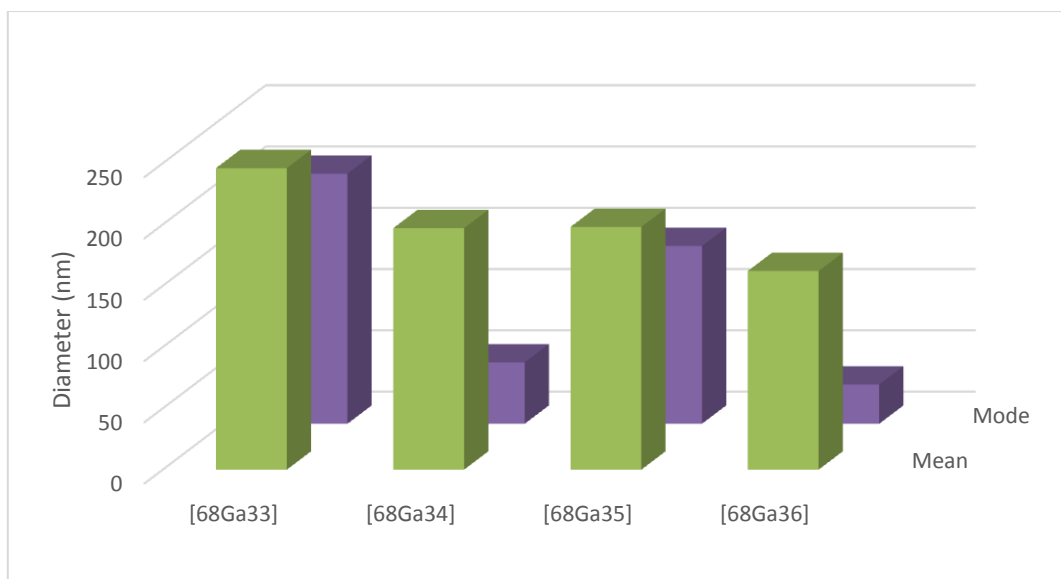
Figure 56 – NTA analysis of ^{68}Ga siloxane SPIONs showing mean and mode size in nanometres.

Encouragingly, NTA of the ^{68}Ga radiolabelled nanoparticle samples gave consistently positive results across all samples, see Figure 56. With all the macrocycles forming nanoparticles below 200 nm mean size, with only the control [^{68}Ga$_n$**33**] being larger at 246nm. The DO3A [^{68}Ga$_n$**34**] and CB-MP NPs [^{68}Ga$_n$**36**] showing potentially useful modal values of 50 and 32 nm respectively. The NTA of radiolabelled samples show some similarities and differences between $^{69/71}$Ga and ^{68}Ga, see Figure 57. Generally, the samples were more consistent with each other after radiolabelling rather than the cold complexation, which would be as expected due to the smaller overall change in structure after doing radiochemical synthesis as only a small amount of the metal ion is available for complex formation.
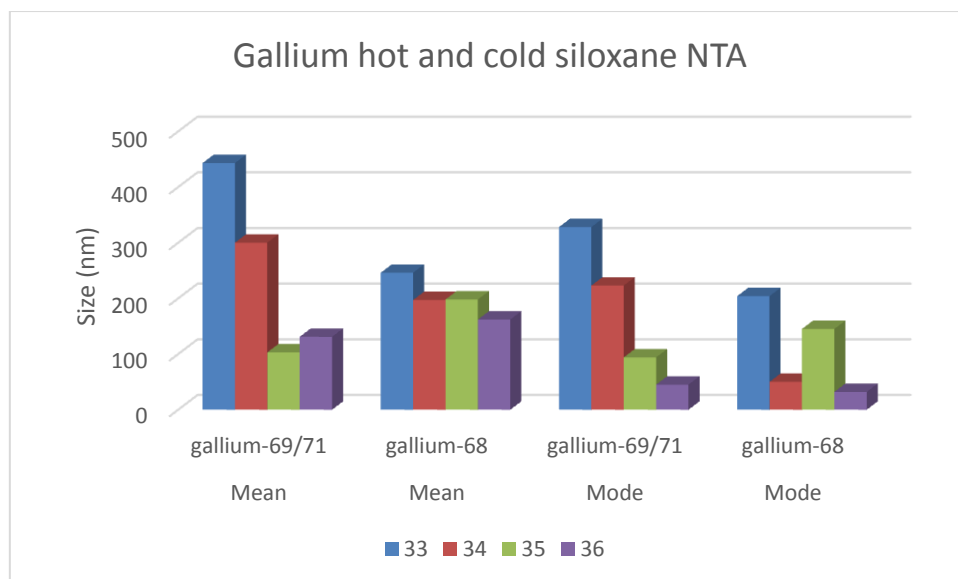
Figure 57 – NTA analysis to compare $^{69/71}$Ga and ^{68}Ga macrocyclic siloxane SPIONs showing mean and mode size in nanometres.

Narrow size distribution is advantageous for *in vivo* applications due to the consistency of properties relating to size, with size distribution referring to the size range between the smallest nanoparticle and the largest. NTA can give information on size distribution in the sample, a useful indicator of *in vivo* applicability. The four silica-SPION ligand constructs (**33-36**) along with $^{69/71}$Ga, ^{68}Ga and $^{63/65}$Cu were analysed, see Figure 58. Throughout all of the control samples, there is a large size distribution (>100 nm). DO3A derivatives (**34**) are the most consistent between samples although the distributions are consistently quite large (100-150 nm). Overall C-TETA (**35**) and CB-MP (**36**) are the most promising candidates, with the lowest size distribution of 40nm for the [Ga$_n$**35**] complex. However, size distributions for [Ga$_n$**36**] and [Ga$_n$**35**] were both better than their radiochemical counterparts. The use of buffer in the radiochemical reaction could be promoting aggregation.
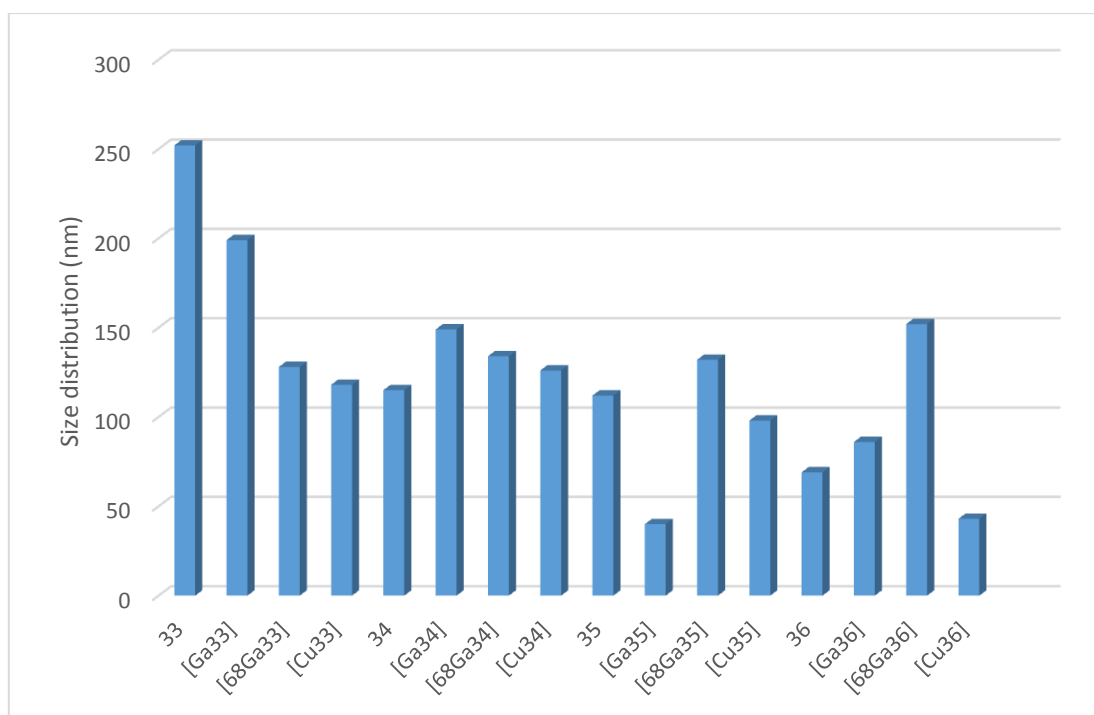
Figure 58 – NTA analysis showing size distribution of SPIONs functionalised with ligands, $^{69/71}$Ga, ^{68}Ga and $^{63/65}$Cu.

NTA gives the value of nanoparticle size in aqueous conditions (hydrodynamic size) which gives predictive behaviour of how the nanoparticles may behave *in vivo* as the whole size of the conjugate determines how it is processed. The use of TEM only has relevance when trying to determine the size of the iron oxide core in order to see the morphology and homogeneity and to predict the magnetic behaviour of the nanoparticles. TEM can therefore not be used to give accurate sizes of nanoparticles in aqueous media and *in vivo* is not valid to determine biodistribution. An example of which is in the study of Spiccia and co-workers,[174] with the group synthesising the nanoparticles in a similar method to those used in this work and coating them with macrocyclic siloxane derivatives. In their studies they show that the nanoparticles functionalised with different macrocycles have an average size of 5-8 nm by TEM, which is similar to **28** (4-8 nm). NTA shows mean values of 164-194 nm, sizes which are nearly identical to the values observed for the radiolabelled macrocycle derivatised nanoparticles (162-197 nm) in this work and very similar to the macrocycle functionalised SPIONs before complexation (125-248 nm). Values which are similar to Endorem, which has a mean hydrodynamic size of 108 nm and a size distribution of 60 nm,[172,193] thus making the nanoparticles in this study an appropriate size and having an adequate size distribution for development towards *in vivo* studies as T_2 contrast agents.

3.7. T_2 analysis

In order to demonstrate the effectiveness of SPIONs synthesised within this work as T_2 MRI contrast agents, T_2 relaxivity and subsequently r_2 values were measured. To this end two samples were selected to be used in this study, one macrocyclic (**36**) and the non-macrocyclic control (**33**). A range of iron concentrations (0.01, 0.025, 0.05, 0.075, 0.1, 0.2, 0.3 mM) were prepared and their T_2 relaxation times (s^{-1}) measured at 11.7 T. These measured T_2 times were plotted against iron concentration to determine r_2 values, see Figure 59 and Figure 60. For both **33** and **36**, a straight line can be fitted to the data to give r_2 values of 598 s^{-1} mM^{-1} and 433 s^{-1} mM^{-1} respectively.
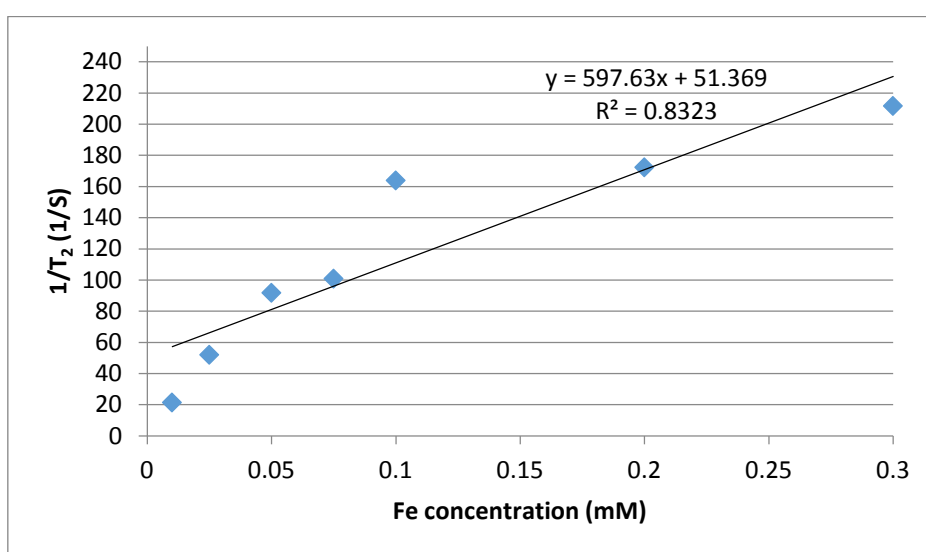
*Figure 59 – Graph of T_2 values across Fe concentration range of **33** to calculate r_2.*
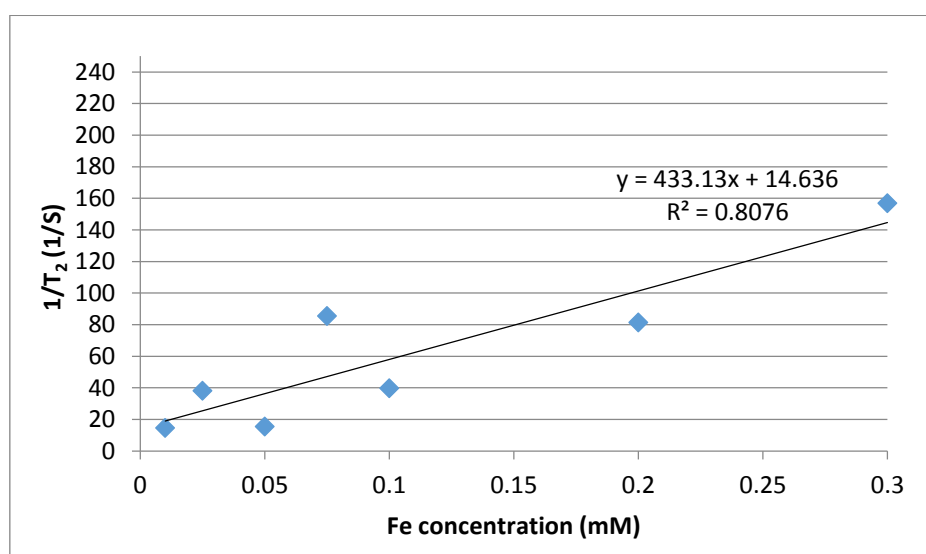
*Figure 60 – Graph of T_2 values across Fe concentration range of **36** to calculate r_2.*

Relaxivity values determined within this work can be compared to a range of other multi-modal SPIONs, see Table 3. The first thing to notice when comparing to similar literature examples is the range of magnetic field strengths used within the literature. This makes direct comparison somewhat challenging, however, studies by Gerion *et al.* showed that an increase magnetic field strength by 640% only causes an increase in r_2 of 23%,[199] direct comparison of r_2 values from these studies can be somewhat misleading however as these nanoparticles are gold based.

More direct comparisons can be made with studies however, with r_2 values generally between 100-350 s^{-1} mM^{-1}.[121,168-171] It appears that this range is consistent for many SPIONs and is generally independent of surface coatings, with a range of different coatings used throughout the different studies. A crude estimate of a 30% reduction of r_2 values for a 3 T NMR can be applied to give values of 303 s^{-1} mM^{-1} and 418 s^{-1} mM^{-1} for **33** and **36** respectively, which would be in the region of values for similar agents. Showing that overall, modifications with siloxane coatings along with macrocycle attachment, has had no detrimental effect on the use of the SPIONs synthesised within this work as T_2 MRI contrast agents.

SPION	Magnetic field strength (T)	Coating	r_2 (s^{-1} mM^{-1})	Reference
RGD-NOTA	4.7	PEG	101	171
RGD-DOTA	1.5	Poly aspartic acid	105	169
Endorem	7	Dextran	126	170
CuMnFe	3	DL-DOPA	148	168
HSA-DOTA	7	Dopamine	314	170
MnFe-QD	1.5	Albumin	321	121
33	11.7	Silica	433	This work
36	11.7	Silica	598	This work
Au-QD-Gd-DOTA	1.4	Silica	2438	199
Au-QD-Gd-DOTA	9	Silica	3004	199

Table 3 – SPION r_2 values at various magnetic field strengths.

3.8. Conclusions

This chapter describes the synthesis and ^{68}Ga radiolabelling of super-paramagnetic iron oxide nanoparticles (SPIONs) to form potential PET/MRI imaging agents. Initially, methods were developed to attach triethoxysilane derivatives onto macrocycles to give a reactive group which can be polymerised to form a silica coating on the surface of the iron-oxide nanoparticles. Three siloxane macrocycles were attached to iron-oxide nanoparticles along with controls and their characteristics towards [69/71]Ga and [63/65]Cu incorporation were probed, see Figure 61.
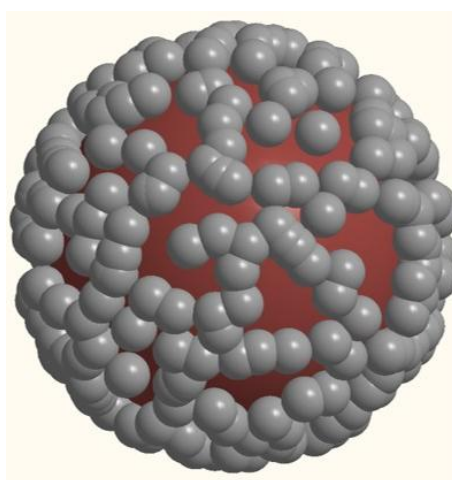
Figure 61 – Schematic representation of a siloxane-macrocycle functionalised SPION.

This was followed up by ^{68}Ga radiolabelling of siloxane derivatives which were compared with a second set of nanoparticles; Endorem® functionalised with bisphosphonate macrocycles. Siloxane derivatives were found to have superior ^{68}Ga complexation characteristics. Siloxane derivatives were also shown to be more stable in competition with EDTA, although there were no significant differences between macrocycle functionalised nanoparticles and control nanoparticles with surface coating but no macrocyclic chelator.

Silica coated derivatives were then taken on for further testing towards *in vivo* use, with serum stability tests showing that carbon functionalised TETA and cross-bridged cyclam monopicolinate macrocycle derivatised nanoparticles had no appreciable loss in the level of activity bound to the nanoparticle after 4 hours. Studies on the DO3A derivative and the

control showed only a moderate loss of activity bound to the nanoparticle after the same time course, with ca. 94% remaining bound.

The size and size distribution were analysed and determined to be within the preferred range to be clinically applicable. However, a key area of proposed future work (*see section 5.2.3.*), involves modifications to increase hydrophilicity and therefore increasing colloidal stability which would be necessary for clinical translation.

Chapter 4

Towards the development of yttrium(III) complexes for PET and radioimmunotherapy

4. Towards the development of yttrium(III) complexes for PET and radioimmunotherapy

4.1. Aims

The study of the physicochemical characteristics of benzimidazole DO3A type ligands is of interest to gain an insight into the modes of coordination with metal ions. A key parameter in the coordination of any chelator to a metal centre is its protonation state. The metal ion must compete with protons for attachment of the donor ligand and the mixture of species present across a pH range can be determined by potentiometry.

Benzimidazole DO3A (**14**) was selected as the most suitable ligand to study due to it having the backbone structure common to ligands presented in this work. The yttrium(III) complex is of interest towards the future development of ^{86}Y and ^{90}Y complexes for PET and radioimmunotherapy respectively.

Potentiometric titrations were carried out in order to determine the speciation and pKa values associated with this ligand. Europium(III) forms a useful luminescent comparator for yttrium(III) and allows the number of bound water molecules to be determined using luminescence lifetime measurements to fully characterise the coordination sphere. The yttrium(III) complex was synthesised and studied using variable temperature (VT) NMR to determine the equilibrium/ donor exchange in solution.

4.2. Yttrium(III) in PET and radioimmunotherapy

Yttrium(III) has radioisotopes which form a unique set in radiometals, having an isotope which can be used in diagnosis and an isotope which can be used in therapy.[9] [86]Y decays by β^+ with a half-life of 14.7 hours, making it a useful PET radioisotope. [90]Y decays by pure β^- and has a half-life of 64 hours, long enough to be used for radioimmunotherapy. The isotopes can be used in a complementary fashion to give a diagnosis/treatment pair which have identical *in vivo* characteristics.[34]

Yttrium(III) shares many characteristics with the lanthanides and is therefore often used with the same chelators, generally forming 7-9 coordinate complexes with hard donor atoms such as nitrogen and oxygen.[8] [86]Y and ^{90}Y have often been used with chelators based on DTPA and DOTA.[200] To give sufficient stability for in vivo applications backbone modifications can be made to DTPA to reduce the release of [90]Y *in vivo* which causes radiation toxicity with bone.[201]

Brechbiel and co-workers developed a chelator based on DTPA which they termed CHX-A''-DTPA, see Figure 62, showing that they ligand can rapidly form stable complexes with [86]Y at room temperature.[202] This chelator was then conjugated to the peptide octreotide for imaging pancreatic tumours, with good tumour selectivity after 4 hours but 75% clearance after 24 hours.[203] The group then went on to study the construct for melanoma imaging using a range of radiometals.[204] CHX-A''-DTPA has also been widely used in conjunction with trastuzumab and cetuzimab for radioimmuno imaging of multiple cancer xenographs with [86]Y.[205]
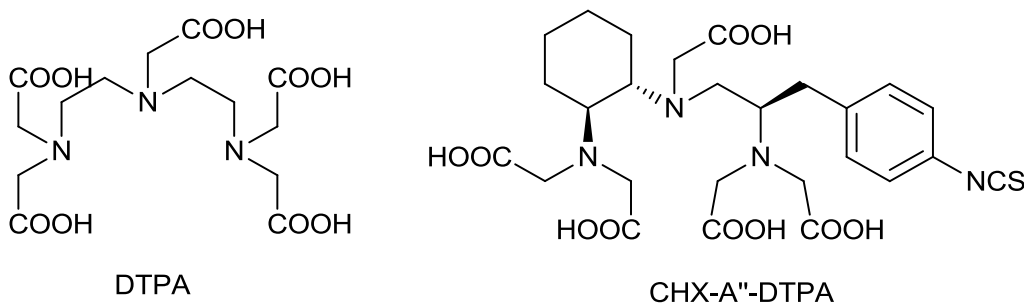
DTPA   CHX-A''-DTPA

Figure 62 – Chelators used in [86]Y PET imaging studies; DTPA and CHX-A''-DTPA.

McQuade *et al*. have used the [86]Y isotope for melanoma imaging, radiolabelling a melanoma targeting hormone derivative with [86]Y-DOTA,[23] biodistribution studies showed the complex to be stable *in vivo* and had high tumour uptake after 30 minutes and 4 hours, however, high clearance was also seen for this complex after 24 hours. C-functionalised derivatives of DOTA offer higher stability complexes as an octacoordinate donating ligand is left intact on conjugation, see Figure 6, and have been used widely for both [86]Y and [90]Y.[16,205,206] A DOTA-octreotide derivative has been used to verify the use of [86]Y as a surrogate for ^{90}Y therapy to determine dose in a clinical setting in patients with metastatic carcinoid tumours.[207]

Zevalin®, a monoclonial antibody agent which targets B-cell non-Hodgkin's lymphoma conjugated to a DTPA derivative, is the only FDA approved ^{90}Y agent used clinically for radioimmunotherapy.[9,208,209] It would be ideal to use [86]Y as the surrogate imaging radioisotope for dosimetry data, however, the biological half-life of the antibody is too long for use with [86]Y. [111]In is more widely available and has a half-life more applicable and is therefore routinely used for imaging with Zevalin®.[210]

The study of novel chelators represents a key area for research to study the properties of both ligands and yttrium(III) complexes in an attempt to fully characterise the coordination sphere to discern *in vivo* characteristics.

4.3. Speciation of benzimidazole DO3A (14)

In an attempt to better understand the nature of the ligands synthesised within this work the protonation pattern of benzimidazole DO3A (14) was determined across a pH range via potentiometric titrations. 14 was selected as the ligand to study as it has the core benzimidazole backbone common to chelators throughout this work. Titrations were carried out using tetramethyl ammonium hydroxide, from which six protonation constants can be determined, see Figure 63. Potentiometric titrations were accompanied by monitoring using UV spectroscopy to follow the absorption peak for benzimidazole that evolves with pH,[211] with a decrease in absorbance with increasing pH due to deprotonation of the imidazole.

In its neutral form, 14 is represented as LH_4. From potentiometry, six protonation constants can be determined, assignment of which can be made by comparison with benzimidazole cyclen, see Figure 64, and benzimidazole (bim), see Table 4.[212,213] The protonation constants for the formation of benzimidazolium ($LH_4 \rightarrow LH_3^-$) are similar between the two macrocycles and are both lower than that for free benzimidazolium. The values for benzimidazolate protonation ($L^{4-} \rightarrow LH^{3-}$) are more similar to free benzimidazole than benzimidazole cyclen, suggesting a possible intramolecular stabilizing hydrogen bond factor between the free acetates and the benzimidazole N-H function. Few other literature examples exist for comparison, with only Sinha and Dogra's study of 2-(aminomethyl)benzimidazole,[214] showing the effect of the amino group on the benzimidazole characteristics.
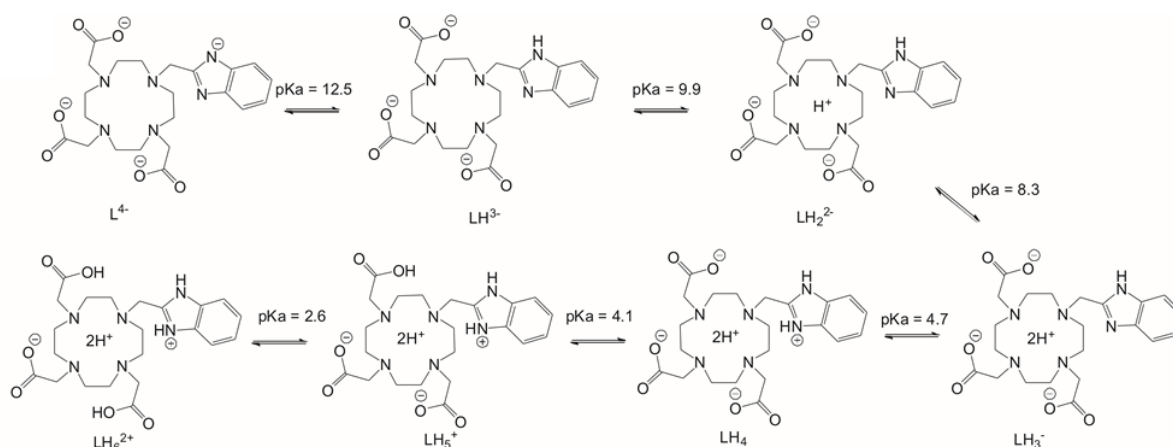
Figure 63 – Protonation patterns of benzimidazole DO3A (14).
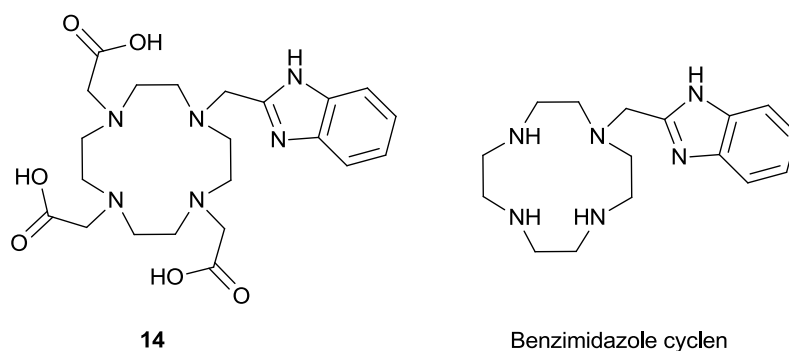
*Figure 64 – Chemical structures of benzimidazole DO3A (**14**) and benzimidazole cyclen.*

The remaining protonation constants are assigned to protonation of the cyclen macrocycle nitrogen atoms and the acetate pendant arms. They can be assigned by analogy to the data for benzimidazole cyclen and the expected pKa values for protonation of amino and carboxylate groups. Slightly lower pKa values are observed for the cyclen ring protonation of **14** when compared with BI cyclen. The highest protonation state that a pKa could be calculated for (LH_6^{2+}) has the benzimidazole, two cyclen nitrogens and two of the carboxylic arms protonated. The speciation diagram shows that the predominant species (LH_3^-) at pH 7.0 has all three carboxylic acids deprotonated, two cyclen ring amines protonated and a neutral benzimidazole.

	14	BI cyclen	bim
$L^{4-} + H^+ \rightleftharpoons LH^{3-}$	12.5	11.1	12.8
$LH^{3-} + H^+ \rightleftharpoons LH_2^{2-}$	9.9	10.2	-
$LH_2^{2-} + H^+ \rightleftharpoons LH_3^-$	8.3	9.0	-
$LH_3^- + H^+ \rightleftharpoons LH_4$	4.7	4.6	5.6
$LH_4 + H^+ \rightleftharpoons LH_5^+$	4.1	-	-
$LH_5^+ + H^+ \rightleftharpoons LH_6^{2+}$	2.6	-	-

*Table 4 – Protonation constants for **14** and literature data for benzimidazole cyclen (BI cyclen) and benzimidazole (bim).*

Along with comparison with literature compounds, the two benzimidazole protonation processes (deprotonation to form benzimidazolate and protonation to form benzimidazolium) can be assigned from UV absorption (overlaid on the speciation diagram), see Figure 65. The UV absorption spectra shows two benzimidazole attributed peaks at 272 and 278 nm, assigned to $\pi^* \leftarrow \pi$ singlet–singlet transitions.[215] By varying the pH it can be seen that imidazolium deprotonation corresponds to a pKa of 4.7, characterised by the decrease in absorbance at 278 nm and the imidazolate formation corresponds to a pKa of 12.5.
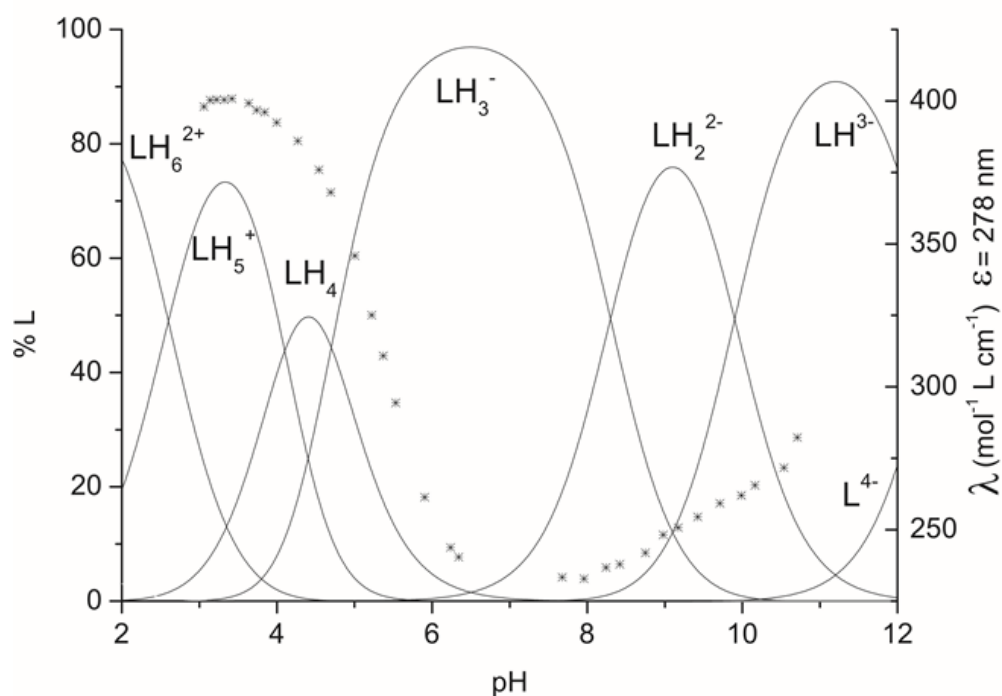
Figure 65 – Speciation diagram of benzimidazole DO3A (**14**) with ε (λ= 278nm) superimposed.

4.4. Speciation and luminescence lifetimes of europium(III) complex of benzimidazole DO3A, [Eu14]

Yttrium(III) complexes are of interest due to the growing field of [86]Y for PET and ^{90}Y for radioimmunotherapy. In order to study the chelators synthesised in the work for use in these applications, a greater insight into the coordination mode of the complex is necessary. Based on the potentiometric titration data for the ligand, it is of interest to study the effect of benzimidazole protonation on metal coordination modes. Europium(III) forms a useful luminescent comparator for yttrium(III) due to their similarities in atomic radius, ionic charge and coordination characteristics. The benzimidazole unit of **14** can be employed to sensitise the lanthanide luminescence process, see *section 1.1.3.1.*

Potentiometric titrations were carried out with **14** (LH_4) in a 1:1 ratio with the europium(III) salt, from which a speciation diagram can be deduced, see Figure 66, with absorbance at 278nm overlaid.
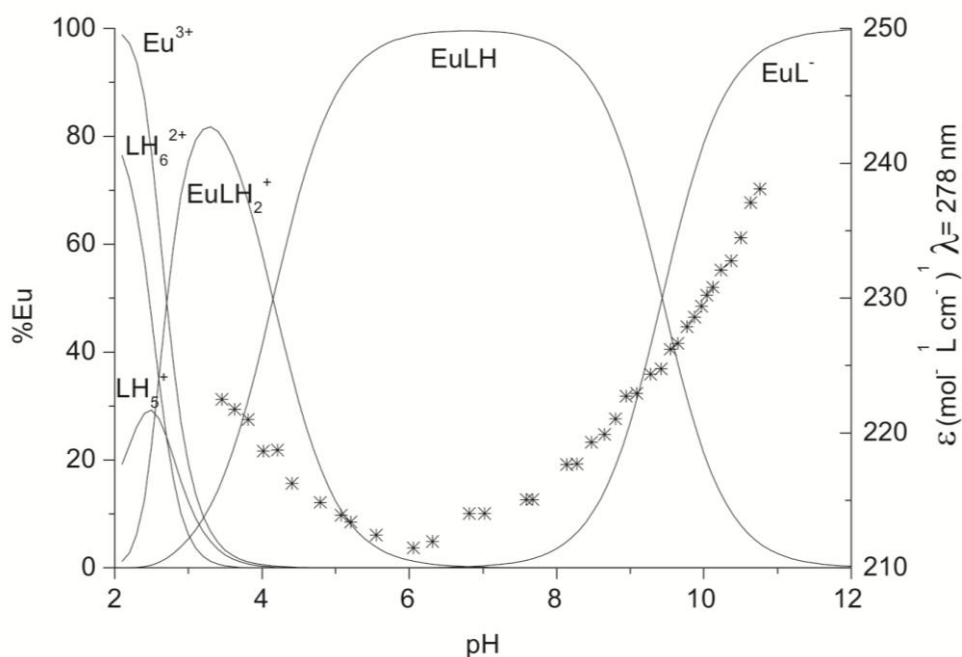
*Figure 66 – Speciation diagram of [Eu**14**] with ε (λ= 278nm) superimposed.*

At acidic pH, the formation of the benzimidazolium ion is observed. When the pH is increased from pH 2, the UV absorbance decreases as the neutral benzimidazole is formed and coordinates to the metal centre, see Scheme 40. In a similar manner to the ligand, when the pH is made increasingly basic, deprotonation of the benzimidazole is indicated by the increase in UV absorbance.
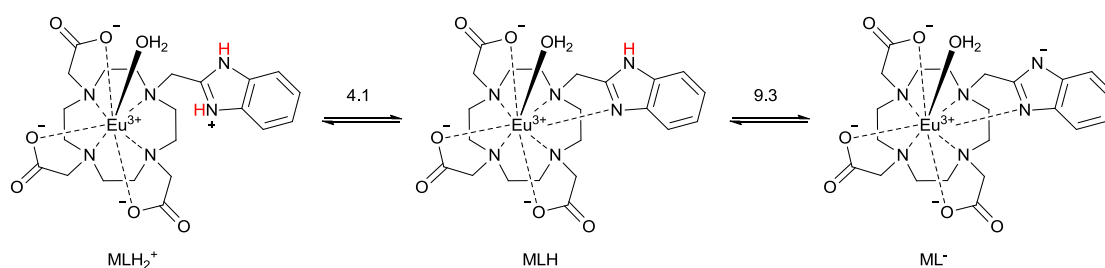
*Scheme 40 – Benzimidazole protonation constants of [Eu**14**].*

Thermodynamic stability can also be assessed using this data, see Table 5. Complexation constants for europium(III) can be compared with zinc(II) due to the high prevalence of zinc(II) *in vivo*, forming a competition ion and causing transmetallation. [Eu**14**] shows a significantly higher stability than [Zn**14**], with a near 100-fold increase. This makes *in vivo* transmetallation to zinc(II) thermodynamically unlikely.

Ligand	europium(III) logK_{ML}	zinc(II) logK_{ML}	Reference
14	21.6	18.8	This work
DOTA	22.9	21.1	[95,216]
DOTP	28.1	24.8	[95,217]
DTPA	22.4	18.3	[216,218]
EDTA	17.3	16.5	[216]
NOTA	13.8	18.3	[95,216]

*Table 5 – Europium(III) and zinc(II) logK_{ML} values for **14** and literature chelators.*

14 can also be compared to other common chelators on the basis of complexation constants for both europium(III) and zinc(II), with a view towards potential transmetallation. Comparisons with DOTA are apt due to the structural similarities, an expected small reduction in stability is noted due to the replacement of a hard acidic donor for a softer nitrogen in **14** and the difference of 1.8 between stability constants for europium(III) and zinc(II) is consistent between the two chelators. This can also be compared to literature values for yttrum(III) complexes of DOTA and DO3A, with equilibrium constants of 24.3 and 21.1 respectively,[219] which are very similar to the europium(III) data. Replacement of acetate arms for phosphonate arms causes a large increase in stability of both complexes and an increase in gap between ions. Acyclic DTPA shows similar binding kinetics to **14** but with a slight increase in preference for the europium(III) ion. Hexacoordinate EDTA and NOTA show the expected lower complexation constants and a more similar result between ions for EDTA, however the small cavity size of NOTA has a detrimental effect for the larger lanthanide and is therefore not useful for this application.

The luminescence lifetime (τ) of [Eu**14**] was determined in order to calculate the number of bound water molecules by measuring the rate constant for depopulation of the excited state in H_2O and D_2O. The luminescence lifetime of [Eu**14**] is 0.63 ms in an aqueous environment, which is typical for a europium(III) complex with a *q* value of 1.1 indicating that the species is nonacoordinate. pH/pD dependence on the number of bound water molecules was also investigated to determine if protonation of the benzimidazole causes it to become non-coordinated to the metal centre. This mechanism causes a decrease in lanthanide luminescence because the efficiency of energy transfer is lost and the metal centre can be quenched more by coordination of a free water molecule on the vacant coordination site. This complex is a pH sensitive lanthanide luminescence probe, an area which has received interest from other research groups.[220-222] However, pH studies of *q* values showed no change in the number of bound waters in the complex at lower pH. This result was surprising as potentiometric titrations showed the benzimidazole is protonated and the decrease in UV absorbance indicating the benzimidazole is no longer coordinated. This can be explained by a structural rearrangement of the complex at lower pH to form an octacoordinate complex with one bound water molecule.

4.5. Synthesis and NMR studies of yttrium(III) complex of benzimidazole DO3A, [Y14]

The yttrium(III) complex can be studied by NMR to gain a greater insight into the different species in solution. Synthesis of the yttrium(III) complex of **14** was carried out using in ammonium acetate buffer at pH 5 using yttrium(III) chloride hexahydrate. Purification was carried out using amberlite XAD16N to remove inorganic salts. Isolation of the pure complex was confirmed using MS and NMR.

Although the structure of yttrium(III) DO3A complexes in the solid state can be of interest,[36,223] the isomers observed can be different to those seen in solution. It can also be that only one isomer is observed (or only one isomer crystallises) in the solid state while more isomers are observed in solution. The solution structure of yttrium(III) complexes of DO3A derivatives has previously been studied by NMR methods,[219,224-226] with studies showing eight coordinate complexes.[227]
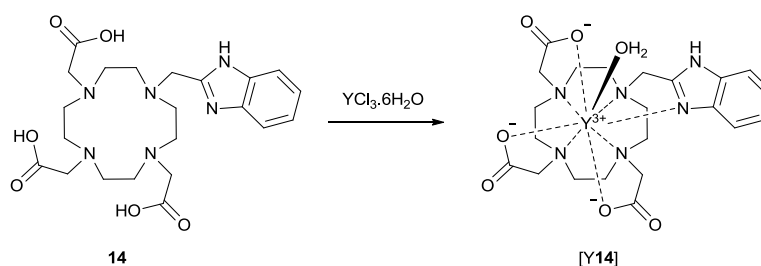
*Scheme 41 – Synthesis of yttrium(III) benzimidazole DO3A [**Y14**].*

^{1}H NMR comparison between the ligand and complex gives evidence of complex formation, see Figure 67, the aryl region of the hydrochloride salt of the ligand contains two peaks due to the symmetrical nature of the imidazolium unit. Upon formation of the yttrium(III) complex, the metal is coordinated to the *N*3 position of the benzimidazole, leading to a loss of symmetry and hence there are four different proton environments, with two peaks overlapping to give the impression of a quintet. However, a similar aryl region could be expected for that of deprotonated ligand, and therefore attention must turn to the alkyl region.
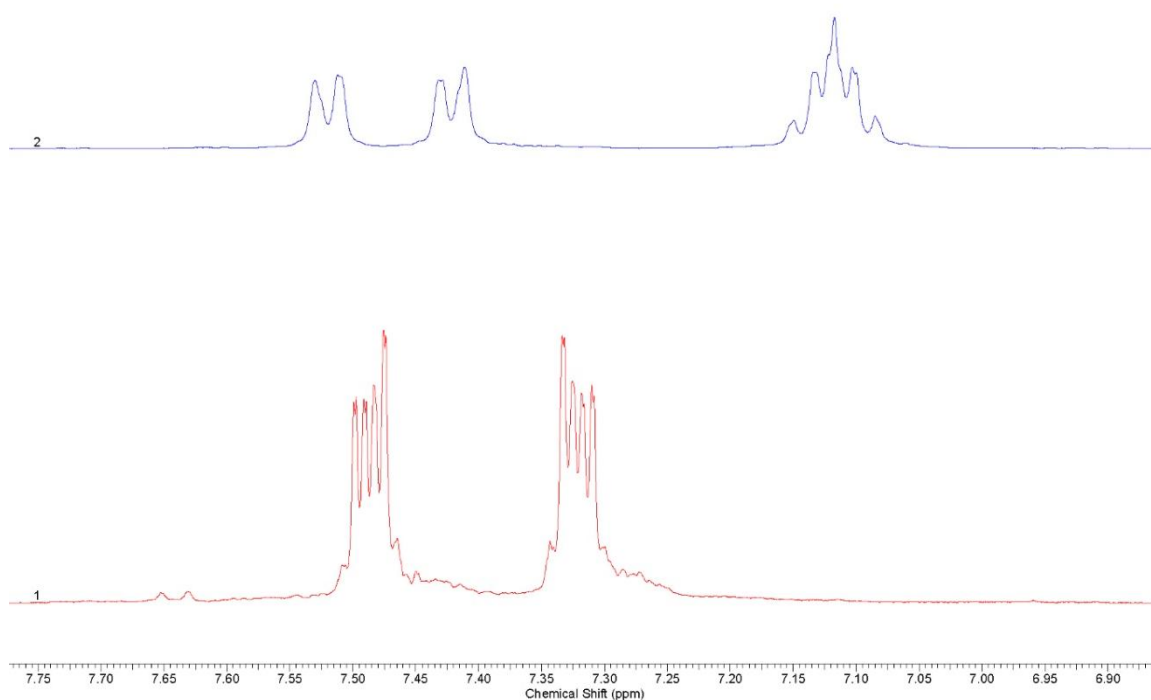
*Figure 67 – Aromatic region expansion of ^{1}H NMR spectra of **14** (red) and [Y**14**] (blue) at 25°C in D$_2$O.*
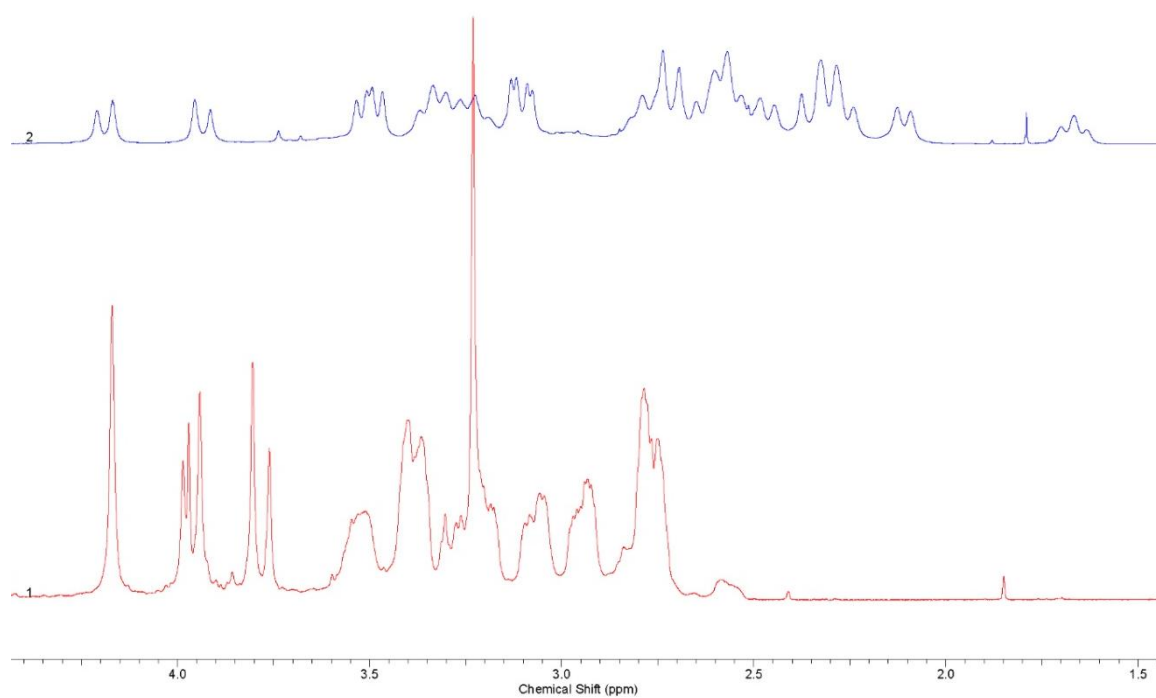
*Figure 68 – Alkyl region expansion of the ^{1}H NMR spectra of **14** (red) and [Y**14**] (blue) at 25°C in D$_2$O.*

Assignment of the alkyl region is somewhat more challenging due to the overlapping macrocyclic CH_2 peaks, however the pattern of resonances can be compared with the ligand, **14**, see Figure 68. From this comparison and with that of [YDOTA]⁻,[225] some assignments can be suggested, see Figure 69. The alkyl region confirms the formation of the yttrium(III) complex when compared with that of the ligand, showing significant structural change. Introduction of the benzimidazole arm introduces asymmetry to the molecule, coordination of the *N*3 position to the metal centre rigidifies the molecule and therefore causes non-equivalence between protons *a* and *b*, causing them to be seen independently as doublets. When this is compared with **14** it can be seen that *a* and *b* are equivalent and are therefore seen as a singlet. The complex is also rigid enough to cause near equivalence of the protons designated *c* that are seen separately from *d*, which is para from the benzimidazole substitution. Assignment of macrocyclic methylene protons is ambiguous and *f* is generally seen in a similar region to that of [YDOTA]⁻. However, *e* is seen as independent due to spatial interactions between methylene protons and imidazole amine, causing a downfield shift. Compared with the ligand, the methylene protons are shifted upfield and there is the introduction of a triplet at 1.70 ppm, which has not been assigned. The comparison of splitting patterns of cyclen methylene protons for [Y**14**] compared with **14** shows a much more complicated pattern which may indicate the presence of multiple species in solution, although little evidence of this is seen is peaks above 3.75 ppm.

Analysis of the ¹³C-NMR gives more clarity on the topic of room temperature isomerism. Showing a total of 19 carbon environments for 22 molecular carbons, see Figure 70. With 10 alkyl environments for the 12 carbons, two of which being unsurprisingly equivalent or overlapping. All peaks are accounted for in the aromatic region and there are 2 peaks for the carbonyl groups, supporting the ¹H NMR evidence of equivalence between two of the acetate arms. It is key to note that there are no observable satellites for different isomers, suggesting that the yttrium(III) complex is either adopting a single orientation at room temperature on the NMR timescale or very rapidly exchanging.
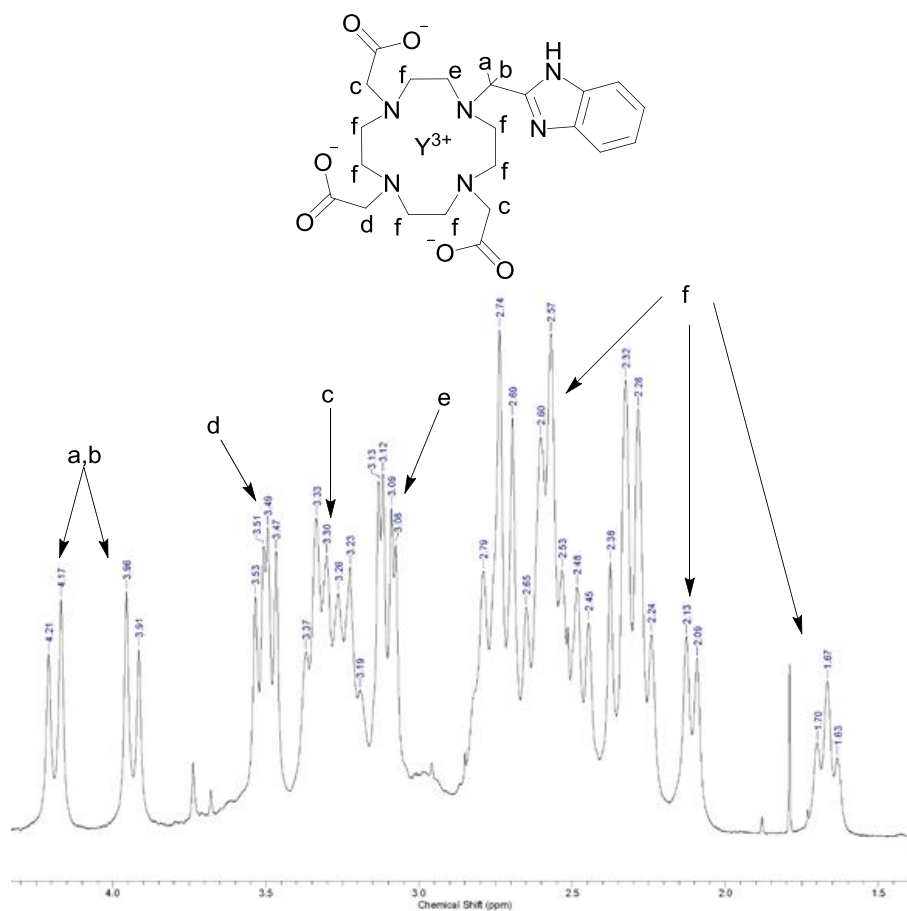
*Figure 69 – ^{1}H NMR spectrum alkyl region assignment for [Y**14**] (coordination bonds omitted from the molecular structure for clarity).*
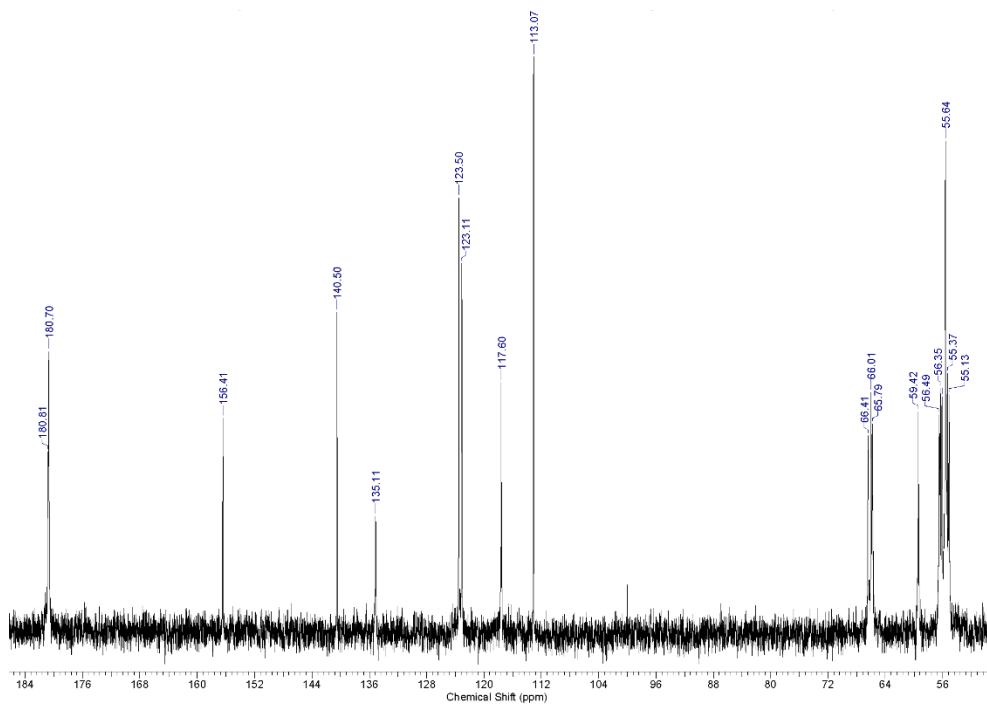
*Figure 70 – ^{13}C NMR spectrum of [Y**14**] at 25^oC in D_2O.*

In order to assess any equilibria or exchange processes of the complex under different conditions, VTNMR experiments were carried out on [Y**14**] in 10°C in increments from 25°C to 85°C, see Figure 71. At 35°C some broadening of alkyl peaks are observed, however, the temperature must be above 45°C to become fluxional and for the peaks to begin to collapse. This observation is very similar to studies carried out by Liu *et al.* on a benzyl [YDO3A]$^{-}$ derivative.[224] Rotation of the acetate and benzimidazole arms and inversion of the ethylene groups at elevated temperatures is relatively fast on the NMR timescale. With four possible isomeric forms for the complex ($\Delta(\delta\delta\delta\delta)$, $\Lambda(\delta\delta\delta\delta)$, $\Lambda(\lambda\lambda\lambda\lambda)$ and $\Delta(\lambda\lambda\lambda\lambda)$) which can interconvert between via arm rotation or ring inversion.[224,228] Steric hindrance is known to inhibit arm rotation and with some complexes, increasing temperature only shows moderate peak collapse,[224,229] an observation which may apply after N-functionalisation of the benzimidazole. Increasing temperature also had the expected broadening affect on the aryl region. The sample was also cooled to room temperature after the VT experiments and the spectrum at 25°C was identical to the spectrum recorded prior to heating, showing that the process is reversible.
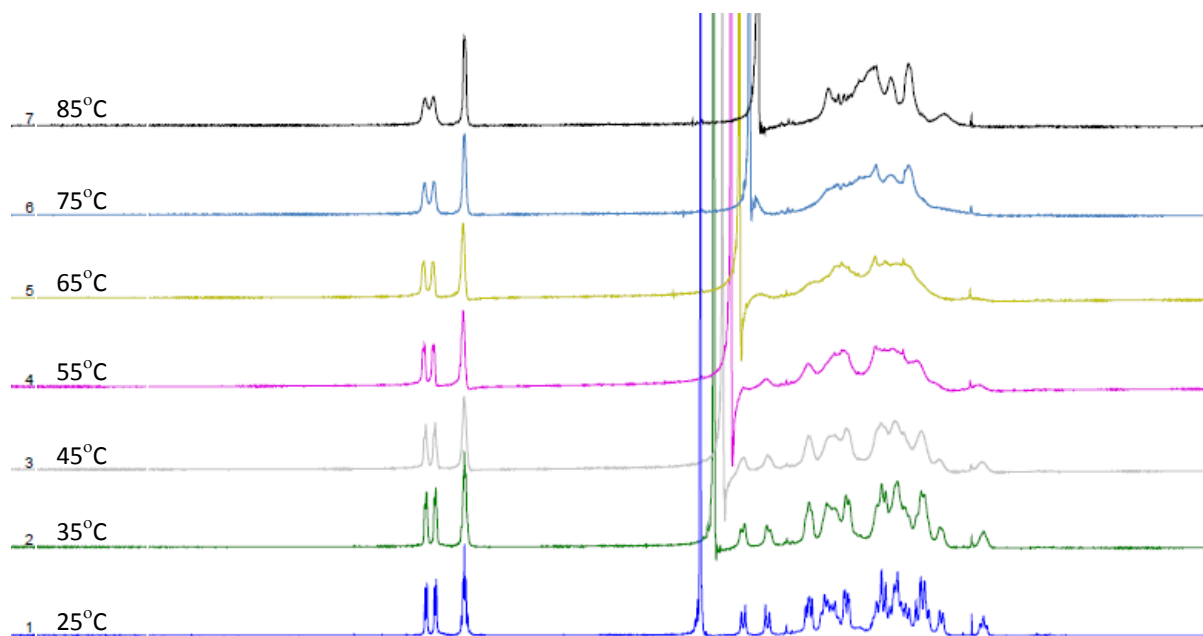
*Figure 71 – VT ^{1}H NMR spectra of [Y**14**] in 10°C increments from 1=25°C to 7=85°C in D$_{2}$O.*

4.6. Chapter conclusions

The development of the chelators synthesised in this work towards use with other metals and applications is of interest, and yttrium(III) complexes are of particular relevance due to the potential application of PET and radioimmunotherapy with [86]Y and ^{90}Y respectively. The study of both the chelator (**14**) and the europium(III) and yttrium(III) complexes increases understanding of how the compounds act under a range of different conditions. The europium(III) complex offers lanthanide luminescence properties and acts as an analogous complex to the yttrium(III) complex. The europium(III) complex was studied using potentiometric titrations accompanied by UV absorbance and luminescent lifetime measurements were carried out. These experiments show that at >pH 5 the complex is nonacoordinate, with eight donor atoms from the chelator and one bound water molecule. As the pH is decreased, the benzimidazole unit protonates and therefore cannot coordinate, the complex changes conformation to give an octacoordinate complex with seven donor atoms from the chelator and no change in the number of bound water molecules.

The yttrium(III) complex was synthesised and NMR studies were carried out to determine the coordination mode of the complex. VT NMR studies demonstrated that it is likely that the complex is not exchanging between isomers at room temperature on the NMR timescale; however increasing the temperature above 45°C caused the peaks to collapse due to rapid exchange of the acetate and benzimidazole arms.

Development of this work should be focused on the study of other N-functionalised benzimidazole DO3A chelators synthesised in this work to determine if modifications to the benzimidazole backbone influence the coordination characteristics of the ligand on binding metal centres. These chelators can also be studied using indium(III) to determine whether they have suitable properties for coordination of the SPECT radioisotope [111]In. This is of importance in predicting *in vivo* characteristics, with ^{111}In often used as a diagnostic surrogate for radioimmunotherapy with [90]Y (e.g. with Zevalin®) it is highly relevant to current clinical practice.

Chapter 5

Concluding Remarks and Future Directions

5. Concluding Remarks and Future Directions

5.1. Conclusions

This work reports the synthesis of bifunctional chelators based on the macrocyclic backbone DO3A and functionalised with benzimidazole arms which offer advantages over DOTA. Benzimidazole has a nitrogen donor for coordination, keeping the chelator octadentate, whilst including a heterocycle N-position for bioconjugation. Benzimidazole is also a chromophore and therefore also has potential applications for lanthanide luminescence sensitisation. The optimised synthesis of four benzimidazole bifunctional chelators is reported along with ^{68}Ga radiolabelling for PET. PET is often combined with CT to give structural information. More recently a PET/MRI scanner has been commercialised which offers advantages over PET/CT. With higher soft tissue contrast, lower overall patient radiation dose and the potential to use MRI contrast agents. This work reports the synthesis of PET/MRI imaging agents which combine macrocyclic ^{68}Ga radiolabelling on the surface of SPIONs, known T_2 MRI contrast agents. These synthesised PET/MRI contrast agents have been studied towards potential *in vivo* use.

In chapter 2, the synthesis and radiolabelling of bifunctional chelators was carried out. This was initially achieved by synthesising N-functionalised benzimidazole derivatives to give a reactive arm for bioconjugation. Although other routes were attempted, this was successfully carried out by the synthesis of preformed N-functionalised benzimidazole precursors due to the lack of reactivity of the benzimidazole NH. Two preformed benzimidazole precursors with nitro- and bromo- functional groups (**3** and **4**) were synthesised in a three step reaction sequence, following alkylation followed by cyclisation, and finally chlorination in overall yields of 30% and 16% respectively.

Attachment of N-functionalised benzimidazole derivatives along with other benzimidazole derivatives including 2-(chloromethyl)benzimidazole to *tert*-butyl protected DO3A were achieved to form macrocyclic bifunctional chelators with eight donor atoms and a potential site for bioconjugation. Synthesis of benzimidazole DO3A (BIDO3A, **11**) was challenging due to 'self-reaction' at the imidazole NH position and the difficulty of separation of the resulting by-products. In an effort to overcome this, a 'boc' protected benzimidazole derivative was also synthesised and the reaction attempted to attach it to the macrocycle.

However this modification caused a decrease in reactivity of the species and therefore the desired product was not formed. BIDO3A was synthesised in a high purity by optimising and controlling reaction conditions. The synthesis of N-functionalised benzimidazole derivatives were attempted by two routes, alkylation at the imidazole NH position which was causing a problem for 2-(chloromethyl)benzimidazole and by using preformed N-functionalised benzimidazole derivatives. Alkylation at the imidazole NH position was challenging and unsuccessful but the desired compounds were synthesised using the preformed N-functionalised benzimidazoles (**12** and **15**). The nitro derivative was converted into a primary amine (**16**) to give a useful reactive group for bioconjugation by reduction using sulphur activated sodium borohydride. All four chelators were finally deprotected to leave three acetate arms for metal complexation (**14**, **17**-**19**), optimised by using microwave irradiation to give reaction times of 10 minutes. Four chelators were synthesised in generally high overall yields (>90%) which incorporate an aromatic benzimidazole unit for coordination and with a secondary position for bioconjugation.

[63/65]Cu and [69/71]Ga complexes of the four chelators were formed as a proof of principle and HPLC of the complexes were compared with the ligands. Radiolabelling of BFCs with ^{68}Ga was developed and one BFC was selected for ^{68}Ga radiolabelling optimisation using different conditions. Surprisingly, increase in temperature or use of microwave irradiation was detrimental to reaction success and the best conditions were 10 μM of chelator at room temperature for 5 minutes, increasing reaction time had no advantage on radiochemical yield for any conditions attempted with metal ion contamination a potential explanation for these anomalous results. The developed conditions were then used to radiolabel the remaining three chelators and form four ^{68}Ga complexes. This study validates the concept that benzimidazole DO3A derivatives can be synthesised and successfully radiolabelled with [68]Ga. The group of chelators have wider potential applications than the related DOTA due to the introduction of the benzimidazole unit. **19**, see Figure 72, is suggested as the lead compound for future study as it has an amine terminating group which is ideal for bioconjugation.
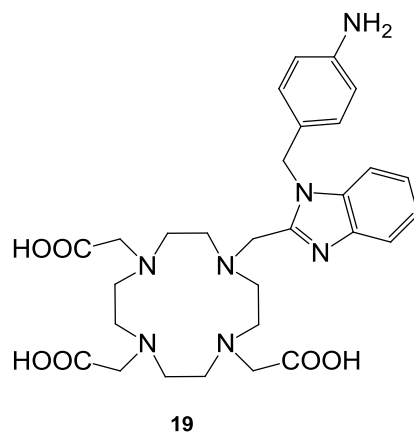
*Figure 72 – Lead BFC synthesised in this work (**19**).*

In chapter 3, PET/MRI multimodal imaging agents were synthesised to develop the knowledge base in a recently emerging area. A range of macrocycles were chosen which had different complexation characteristics with ^{68}Ga, with variations in ring size along with coordination number and macrocyclic rigidity. In order to form PET/MRI imaging agents, the macrocycles were attached to super-paramagnetic iron-oxide nanoparticles (SPIONs), known T_2 MRI contrast agents followed by ^{68}Ga radiolabelling. To facilitate attachment to the nanoparticles the macrocycles were functionalised with siloxane terminating groups, known to react with iron oxide and form a hydrophilic polymeric layer on the iron oxide surface to give colloidally stable nanoparticles in aqueous environments. Two macrocycles were chosen for siloxane reaction optimisation, with one, DO3A, being successful. Once the reaction was optimised, these conditions were used to synthesise a range of three different macrocycles terminating in siloxanes (**23**, **25** and **26**).

Three silica macrocycle derivatives (**34**-**36**) were then attached to the SPIONs forming a hydrophilic layer of siloxane macrocycles on the surface and controls were synthesised without macrocycles. The synthesised nanoparticle derivatives were then studied for their $^{63/65}$Cu and $^{69/71}$Ga complexation characteristics. This study showed that the controls (**28**, **32** and **33**) and macrocycle containing NP derivatives both incorporated each of the metal ions.

The ^{68}Ga radiolabelling characteristics of three macrocyclic (**34**-**36**) and one control (**33**) silica SPION derivatives were assessed along with macrocycle-bisphosphonate nanoparticles synthesised using the commercially available dextran coated nanoparticles Endorem to

137

determine if the coating or the conjugation method had an effect. Conditions were found in which all eight conjugates were successfully radiolabelled at above 90% yield. However, when challenged with an excess of EDTA, the bisphosphonate-macrocycle NP compounds were shown to all have low stability. The silica derivatives were largely stable to EDTA competition at room temperature and the macrocycle NP compounds had superior stability compared to the control at 90°C with EDTA. The variation between the bisphosphonate and silica coated nanoparticles is attributed to the method of attachment of the macrocycles to the nanoparticles, leading to a large difference in the concentration of macrocycles on the surface of the nanoparticles.

The four silica derivatives (**33**-**36**) were therefore taken on to further study to determine the characteristics for *in vivo* application and assess their serum stability, showing that two of the macrocycle NP derivatives showed no appreciable loss of bound activity after four hours. Studies with DO3A NPs and the control showed only modest leaching of ^{68}Ga (ca. 6% lost). Tests were also performed to discern if modification of the surface of the nanoparticle resulted in any issues that would be detrimental for *in vivo* use, either from a size increase or effect on its properties as a MRI contrast agent. It was found that the size of the nanoparticles was still within clinically applicable ranges. The concept was therefore validated that iron oxide nanoparticles can be modified with siloxane-macrocycle derivatives, to give a silica coating on the surface of the NPs, and form stable ^{68}Ga complexes. With overall results offering two lead conjugates for further study, see Figure 73. This is a key development towards the potential *in vivo* application of ^{68}Ga/SPION PET/MRI imaging agents.
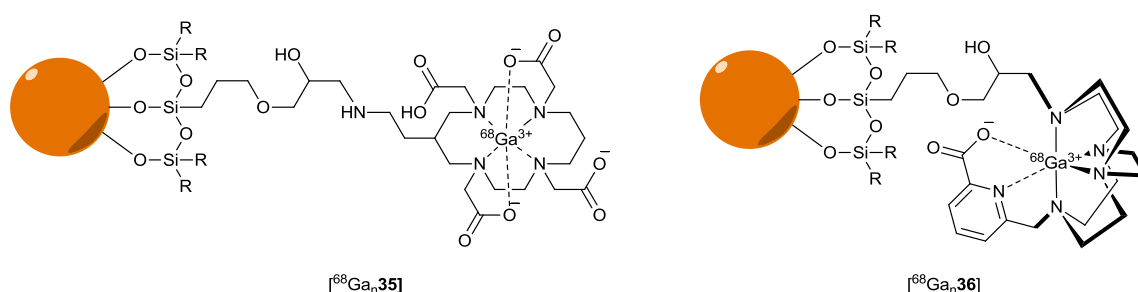
Figure 73 – Lead PET/MRI multi-modal imaging agents for further study.

In chapter 4, further studies of **14** were carried out towards the development of ^{86}Y and ^{90}Y agents for PET and radioimmunotherapy respectively. Potentiometric titrations of **14** were carried out to determine its protonation state over a pH range. Europium(III) was selected as a luminescent comparator for yttrium(III) and the analogous complex with **14** was formed and studied. UV spectroscopic studies of both **14** and [Eu**14**] showed that at low pH, the benzimidazole moiety is protonated, which causes coordination to the metal centre to be inhibited. Luminescent lifetime measurements of [Eu**14**] showed the complex to be nonacoordinate at physiological pH and after benzimidazole protonation at lower pH, there is a structural rearrangement which causes the complex to become octacoordinate. Yttrium(III) complex [Y**14**] was synthesised and studied by variable temperature NMR to study the equilibrium/ exchange of species in solution. In solution at room temperature the complex is rigid in one isomer but rapid rotation of the acetate and benzimidazole arms at increased temperatures causes NMR peaks to collapse.

In conclusion, four benzimidazole DO3A derivatised bifunctional chelators have been synthesised and radiolabelled with ^{68}Ga. Bifunctional chelators have been attached to SPIONs and radiolabelled with ^{68}Ga to form potential PET/MRI imaging agents which show positive radiosynthetic characteristics along with high stability and encouraging characteristics for use *in vivo*. One chelator was studied further towards the potential use with ^{86}Y with PET and ^{90}Y for radioimmunotherapy and its coordination sphere was fully characterised.

5.2. Future directions

Within this research, there is scope for further developments within many areas. This section is intended as a guide to future direction of the respective projects.

5.2.1. Bifunctional chelators – Vary metal ion, vary application

A full study in which both cold and hot metal complexes of the chelators, most notably **19** which with its amine functionality is ideal for bioconjugation, with the following metal ions and respective application. $^{64}Cu/^{86}Y$ (PET), ^{111}In (SPECT), gadolinium(III) (MRI), europium(III)/terbium(III) (lanthanide luminescence) and $^{90}Y/^{177}Lu$ (radioimmunotherapy). This data would validate a chelator system in which varying the metal ion gives access to the widest range of applications. Replication of the studies in chapter 4 with other chelators used in this work would also give an insight to the effect of benzimidazole N-functionalisation on the coordination environment

5.2.2. Bifunctional chelators – Towards *in vivo* applications

The synthesis of the BFCs in this work has been optimised on multigram scale and formation of ^{68}Ga complexes has been successfully achieved as a proof of principle. More effort must now be focused on this area to develop this system for *in vivo* use. In order to do this a range of studies must be complete. Firstly, the complex must be shown to be stable and non-toxic *in vitro* for the duration of an emulated *in vivo* study (ca. 4 hours) to determine if demetallation could occur *in vivo*, therefore causing a background signal increase. This should be followed by a specific activity study, carried out in order to determine how much of the chelator can be radiolabelled at the lowest concentration. This is important for *in vivo* use when the targeted moiety has a relatively low target concentration, therefore causing receptor saturation. Next, the partition coefficient (logP) of the ^{68}Ga complexes should be determined. This information gives insight into the BFC's properties *in vivo* (passage through the epithelium lipid bilayer, non-specific binding etc.). If this study gave acceptable results a biodistribution would be determined in an animal study to assess the *in vivo* characteristics of the complex, stability and excretion pathways. This can be combined with a metabolite study to determine if the complex remains intact.

The reactive groups of the BFC can be assessed, initially to show that the arm is still reactive enough for conjugation and also to demonstrate that the modification does not have a detrimental effect to the radiolabelling. Initially this could be carried out with a small, well characterised biomolecule such as biotin, which can easily be assessed *in vitro* to show that biotin conjugation to the BFC does not interfere with its ability to bind to streptavidin. If these criteria are met then other targeting molecules can be assessed with a view to *in vivo* targeted imaging.

5.2.3. PET/MRI imaging agents – Towards *in vivo* applications

The work presented in chapter 3 shows the possibility of a synthesising a SPION based PET/MRI imaging agent. In order to take this work towards *in vivo* applications further studies can be made. The colloidal stability of SPIONs is of the utmost importance for clinical translation. Initially, some studies of stability can be carried out on the constructs synthesised in this work to determine the colloidal stability under a range of conditions in an attempt to predict *in vivo* behaviour; over a pH range, over a SPION concentration range and in the presence of increasing concentrations of NaCl. These studies can be carried out both qualitatively by observation (precipitation out of solution) and also quantitatively through NTA to determine extent of aggregation. This study should also be carried out at a range of time points, especially for the SPION concentration measurement. This needs to be done to assess clinical applicability, SPIONs are generally commercialised suspended ready for injection, therefore the amount of time the SPIONs can remain stably suspended is very important as a 'use-by' date can be issued after synthesis date. If colloidal stability is a concern for the SPIONs synthesised in this work then simple modifications can be made to increase hydrophilicity. When the SPIONs are coated with macrocyclic siloxane, this can be combined with a hydrophilic siloxane derivative such as PEG siloxane. This study can be carried out using a range of ratios of macrocycle to PEG to determine the optimised formulation to balance colloidal stability with formation of stable ^{68}Ga complexes.

5.2.4. PET/MRI imaging agents – *In vivo* studies and targeting

Once colloidal stability has been engineered, *in vivo* biodistribution studies can be carried out in order to show (a) the radiochemical stability of the constructs and; (b) whether the biodistribution of the SPIONs is as expected for this type of nanoparticle (excreted through liver and spleen). Once this has been successfully carried out, the introduction of a targeting moiety can be achieved in much the same way as the PEG would be attached. Again, a ratio study can be carried out to maximise the balance between biological targeting and the formation of a radiochemically stable construct.

5.2.5. SPIONs – Vary metal ion, vary application

The macrocycle functionalised SPIONs synthesised in this work can be used for different applications, similar but less extensive to those described in *section 5.2.1*. The SPIONs can easily be radiolabelled with ^{111}In to form a MRI/SPECT agent. To the best of my knowledge, at the time of writing there are no SPION/^{111}In based MRI/SPECT based agents reported in the literature. Another clinically useful combination would be the synthesis of gadolinium(III) complexes of the SPIONs, thus forming a T_1/T_2 MRI contrast agent. One advantage over the applications mentioned in *section 5.2.1.*is the ability to form a theragnostic probe. Complexation of ^{90}Y to the constructs synthesised in this work would form an agent which can be used as a T_2 MRI contrast agent, and could also be used for systemically administered radioimmunotherapy.

Chapter 6

Experimental

6. Experimental

6.1. General notes

Bulk solvent was removed by rotary evaporation on a Buchi RE 111 evaporator equipped with a diaphragm vacuum pump, trace solvent was removed on a Schlenk line equipped with an oil pump. Reactions were performed at room temperature (RT) unless otherwise stated. Dialysis was performed using Spectra-Por® Float-A-Lyzer® G2 with 8-10 kDa molecular weight cut off. Speciation, stability and luminescence studies, were carried out by Prof. Françoise Chuburu's group. T_2 experiments were carried out by Dr. Mark Lorch's group. Optical emission ICP was carried out by Dr. Bob Knight. Lanthanide luminescence measurements were carried out by Prof. Stephen Faulker's group. Some ^{68}Ga SPION replication results were carried out by Gonçalo Clemente under my supervision.

6.2. Method used for ^{68}Ga preparation

[68]Ga must be formulated to be in a manner suitable for the radiochemical reaction. [68]GaCl$_3$ is eluted from a 20mCi Eckert & Ziegler IGG100 [68]Ge/^{68}Ga generator in 5ml of 0.1M HCl. This is then loaded on a phenomenex strata X-C solid-phase extraction cartridge. The sample is then eluted using an acetone:0.1M HCl solution (98:2) to give the desired amount of activity for the reaction. The solution is then dried using a heating block at 90°C with a flow of compressed air.

6.3. Materials

Solvents were used as received, except when dry solvents were required. Solvents were dried over activated (oven dried at 200°C for 14 hours) 20Å molecular sieves following literature method.[230] Chemicals were purchased from Sigma-Aldrich, Fisher, Acros, Apollo, Chematech and Strem. Chemicals were used as commercially obtained without any further purification. Magnetite nanoparticles (**25**) were synthesised by Neazar Baghdadi using literature methods.[231] **20**, **21**, **22**, BP-DO3A, BP-C-TETA and BP-CB-MP were synthesised by Prof. Raphael Tripier's group. (R)-(1-(hydrogen phosphonato)-1-hydroxyundecyl)phosphonate was synthesised by Dr. Maelle Monteil. % w/w of elements in nanoparticle samples were determined by a combination of ICP-OES and CHN analysis.

6.4. Instrumentation

6.4.1. NMR spectroscopy

^{1}H NMR and ^{13}C NMR were obtained using a Jeol JNM-LA400 spectrometer at 400 MHz for ^{1}H and 100 MHz for ^{13}C in the solvents indicated, referenced against standard internal TMS or residual non deuterated solvent signal. Chemical shifts (δ) are quoted in parts per million (ppm). Splitting patterns are designated as s (singlet), d (doublet), t (triplet), q (quartet), quin (quintet), m (multiplet) and br (broad). Deuterated solvents were purchased from either Goss chemicals Ltd or Cambridge Isotopes Ltd.

6.4.2. MS

MS was performed using a Finnegan MAT 900 XLT system using electrospray ionisation (ESI). MALDI mass spectra were recorded at the "Services communs" of the University of Brest with an Autoflex MALDI TOF III smartbeam spectrometer. Accurate mass spectrometry measurements were obtained using a LQT Orbitrap XL.

6.4.3. CHN

CHN analysis was performed using a CHN analyser EA1108 (Carlo Erba).

6.4.4. ICP-OES

Inductively Coupled Optical Emission Spectroscopy (ICP-OES) analysis was carried out using a Perkin Elmer Optima 5300 DV. All the samples were in solid state, digested with aqua regia in glass sample vials on a hotplate. Calibration standards were prepared at 1 and 10 ppm from 1000 ppm concentrates of iron, gallium, copper and silicon which were purchased from Romil UK.

6.4.5. Nanosight - nanoparticle tracking analysis (NTA)

Nanoparticle tracking analysis (NTA) was carried out with a LM10-HS microscope from NanoSight using a 75mW laser at 532 nm (green). The concentration of the samples must be adjusted before analysis.

6.4.6. High performance liquid chromatography (HPLC)

High performance liquid chromatography was carried out using either an Agilent 1200 series or an Agilent 1100 series using a Phenomenex Gemini 5u C18 110A, 150x4.60mm column at

1ml/min. Both equipped with a UV detector (series G1314A) and a NaI radiodetector. Data was recorded using Lablogic Laura (version 4.1.13.91)

6.4.6.1. Standard HPLC methods

Method 1: (a) acetonitrile 0.1% TFA (b) water. Gradient from 100% (b) to 40% (b) over 15 minutes follow by returning to 100% (b) after 17 minutes.

Method 2: (a) acetonitrile 0.1% TFA (b) ammonium acetate buffer (0.2M, pH 5). Gradient from 100% (b) to 40% (b) over 15 minutes follow by returning to 100% (b) after 17 minutes.

6.4.7. Radio-Thin layer chromatography (Radio-TLC)

TLCs were ran on 'silica gel 60 on aluminium sheets' (Merck USA), eluting with 0.2M citric acid. Radio-TLC was carried out using a Lablogic Scan-Ram, equipped with a NaI detector at a speed of 10mm/min. Data was recorded using Lablogic Laura (version 4.1.7.70).

6.5. BFC synthesis

6.5.1. Synthesis of 2-(bromomethyl)-1H-benzo[d]imidazole

1
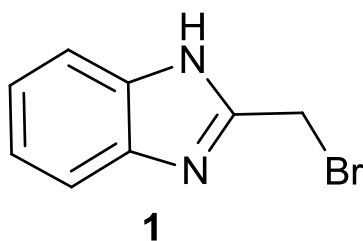
The synthetic procedure was completed following literature methods.[146] A solution of *o*-phenylenediamine (7.0 g, 64.73 mmol) and ethylbromoacetate (14.05 g, 84.15 mmol) in dilute HCl (4 M, 70 ml) was stirred for 4 hours then heated under reflux overnight. The resulting solution was poured into ice water (200 ml) and the pH value adjusted to 9 with 35% ammonia solution. The solid was filtered and washed with water to yield an orange solid (7.0 g, 51%). ^{1}H-NMR (CD$_3$OD): δ 4.83 (s, 2H, CH$_2$-Br), 7.24-7.27 (m, 2H, CH-Ar), 7.54-7.56 (m, 2H, CH-Ar). ^{13}C-NMR (CD$_3$OD): δ 36.82 (CH$_2$-Ar), 114.79 (C-Ar), 122.94 (CH-Ar), 138.12 (CH-Ar), 149.96 (C-Ar). HRMS (ESI): calc. 210.9865 found 210.9859 [M+H]$^+$.

6.5.2. Synthesis of *tert*-butyl 2-(chloromethyl)-1H-benzo[d]imidazole-1-carboxylate

2
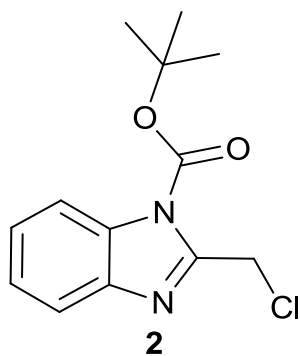
2-(Chloromethyl)-benzimidazole (4 g, 0.024 mol) was dissolved in DCM (30 ml) and methanol (40 ml), di-*tert*-butyl dicarbonate (5.76 g, 0.0264 mol) in DCM (30 ml) was added drop wise followed by triethylamine (1 ml, 0.078 mol) and stirred overnight. Water (10 ml) was added and the product was extracted into DCM (3 x 50 ml), dried (MgSO$_4$), filtered and concentrated *in vacuo* to yield a white solid upon storage at -15°C (4.8 g, 75%). ^{1}H-NMR (CDCl$_3$) : δ 1.69 (s, 9H, C(CH$_3$)$_3$), 4.99 (s, 2H, CH$_2$), 7.32 (m, 2H, CH-Ar), 7.71 (m, 1H, CH-Ar), 7.96 (m, 1H, CH-Ar). ^{13}C-NMR (CDCl$_3$) : δ 28.01 (C(CH$_3$)$_3$), 39.69 (Cl-CH$_2$), 86.57 (C(CH$_3$)$_3$), 115.20 (CH-Ar), 120.53 (CH-Ar), 124.71 (CH-Ar), 125.78 (CH-Ar), 133.41 (C-Ar), 141.72 (C-Ar), 148.13 (C-Py), 150.27 (C=O). HRMS (ESI) calc. 267.0895, found 267.0898 [M+H$^+$].

6.5.3. Synthesis of 2-(chloromethyl)-1-(4-nitrobenzyl)-1H-benzo[d]imidazole
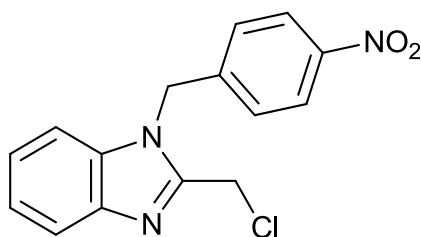
3

Method 1 (Preferred method)

The synthetic procedure was completed following literature methods.[143] Thionyl chloride (10 ml) was added to (1-(4-nitrobenzyl)-1H-benzo[d]imidazol-2-yl)methanol (**7**) (0.5 g, 1.7 mmol) and the reaction stirred under argon for 24 hours. Thionyl chloride was removed *in vacuo*. The solid was redissolved in a minimum amount of MeOH and precipitated using excess diethyl ether which was left to settle then decanted to leave a light brown solid (350 mg, 68%). ^{1}H-NMR (CD$_3$OD): δ 5.37 (s, 2H, CH$_2$), 6.04 (s, 2H, CH$_2$), 7.54-7.74 (m, 5H, CH-Ar), 7.90 (m, 1H, CH-Ar), 8.25 (m, 2H, CH-Ar). ^{13}C-NMR (CD$_3$OD): δ 32.65 (CH$_2$), 48.53 (CH$_2$), 113.69 (CH-Ar), 115.08 (CH-Ar), 124.39 (CH-Ar), 127.84 (CH-Ar), 128.14 (CH-Ar), 128.59 (CH-Ar), 131.02 (C-Ar), 132.74 (C-Ar), 140.92 (C-Ar), 148.66 (C-Ar), 149.44 (C-Ar). HRMS (ESI) calc. 302.0691, found 302.0684 [M]$^{+}$.

Method 2

The synthetic procedure was completed following literature methods.[148] 2-(Chloromethyl)-benzimidazole (2.5 g, 0.015 mol), 4-nitrobenzyl bromide (3.09 g, 0.015 mol) and K$_2$CO$_3$ (0.5 g, 0.06 mol) were dissolved in dry DMF (100 ml) and heated to 100°C for 3 hours then left to cool. Water (100 ml) was added then extracted with DCM (3 x 100 ml) and washed with brine (100 ml), dried (MgSO$_4$), filtered and concentrated *in vacuo* to yield a crude brown solid. Purification was attempted via column chromatography eluting with MeOH in DCM (0-20%). *The desired product was not isolated using this synthetic procedure.*

6.5.4. Synthesis of 1-(4-bromobenzyl)-2-(chloromethyl)-1H-benzo[d]imidazole
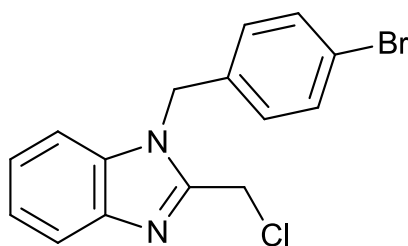
4

Method 1 (preferred method)

The synthetic procedure was completed following literature methods.[143] Thionyl chloride (10 ml) was added to (1-(4-nitrobenzyl)-1H-benzo[d]imidazol-2-yl)methanol (**8**) (0.5 g, 1.58 mmol) and the reaction stirred under argon for 24 hours. Thionyl chloride was removed *in vacuo*. The solid was redissolved in a minimum amount of MeOH and precipitated using excess diethyl ether which was left to settle then decanted to leave a light brown solid (440 mg, 83%). ^{1}H-NMR (CD$_3$OD): δ 5.32 (s, 2H, CH$_2$), 5.83 (s, 2H, CH$_2$), 7.26 (m, 2H, CH-Ar), 7.56 (m, 2H, CH-Ar), 7.60-7.74 (m, 3H, CH-Ar), 7.87 (m, 1H, CH-Ar). ^{13}C-NMR (CD$_3$OD): δ 32.94 (CH$_2$), 49.21 (CH$_2$), 113.99 (CH-Ar), 115.26 (CH-Ar), 123.21 (CH-Ar), 127.83 (CH-Ar), 128.14 (CH-Ar), 129.67 (CH-Ar), 131.50 (C-Ar), 132.84 (C-Ar), 133.04 (C-Ar), 133.28 (C-Ar), 149.48 (C-Ar). MS (ESI): 336 [M+H]$^+$.

Method 2

The synthetic procedure was completed following literature methods.[148] 2-(Chloromethyl)-benzimidazole (2.5 g, 0.015 mol), 4-bromobenzyl bromide (3.75 g, 0.015 mol) and K$_2$CO$_3$ (0.5 g, 0.06 mol) were dissolved in dry DMF (100 ml) and heated to 100°C for 3 hours then left to cool. Water (100 ml) was added then extracted with DCM (3 x 100 ml) and washed with brine (100 ml), dried (MgSO$_4$), filtered and concentrated *in vacuo* to yield a crude brown solid. Purification was attempted via column chromatography eluting with MeOH in DCM (0-20%). *The desired product was not isolated using this synthetic procedure*.

6.5.5. Synthesis of N1-(4-nitrobenzyl)benzene-1,2-diamine
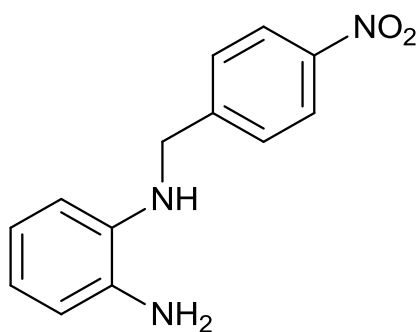
5

The synthetic procedure was completed following literature methods.[143] 4-Nitrobenzyl bromide (5 g, 0.023 mol) in MeOH (300 ml) was added drop wise to a stirred solution of *o*-phenylenediamine (12.51 g, 0.12 mol) in MeOH (400 ml) over 30 minutes. The reaction stirred for 4 hours, concentrated *in vacuo* and recrystallised from EtOH (250 ml) to give a crude solid which was purified via column chromatography, eluting with DCM to yield an orange/red solid (4.75 g, 85%). ^{1}H-NMR (CD$_2$Cl$_2$): δ 3.44 (br s, 2H, NH$_2$), 3.99 (br s, 1H, NH), 4.47 (s, 2H, CH$_2$), 6.49 (m, 1H, CH-Ar), 6.67-6.74 (m, 3H, CH-Ar), 7.56 (d, 2H, CH-Ar, J = 8.8 Hz), 8.18 (d, 2H, CH-Ar, J = 8.8 Hz). ^{13}C-NMR (CD$_2$Cl$_2$): δ 48.06 (CH$_2$), 112.27 (CH-Ar), 117.00 (CH-Ar), 119.50 (CH-Ar), 120.81 (CH-Ar), 124.03 (CH-Ar), 128.36 (CH-Ar), 134.90 (C-Ar), 137.25 (C-Ar), 147.22 (C-Ar), 148.09 (C-Ar). Elemental analysis: (%) calc. for C$_{13}$H$_{13}$N$_3$O$_2$ C 64.19, H 5.39, N 17.27. Found C 64.10 H 5.49 N 16.94. HRMS (ESI) calc. 244.1081 found 244.1077 [M]$^+$.

6.5.6. Synthesis of N1-(4-bromobenzyl)benzene-1,2-diamine

6
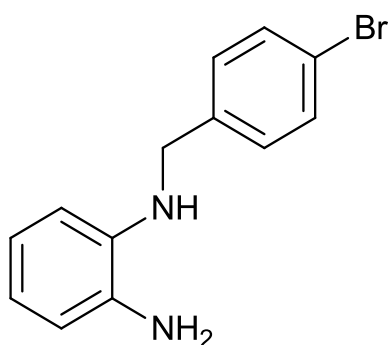
The synthetic procedure was completed following literature methods.[143] 4-Bromobenzyl bromide (5 g, 0.02 mol) in MeOH (300 ml) was added drop wise to a stirred solution of *o*-phenylenediamine (10.82 g, 0.1 mol) in MeOH (400 ml) over 30 minutes. The reaction stirred for 4 hours, concentrated *in vacuo* to give a crude solid which was purified via column chromatography, eluting with 0-50% DCM in hexane to yield an light brown solid (3.70 g, 67%). ^{1}H-NMR (CD$_2$Cl$_2$): δ 3.39 (br s, 2H, NH$_2$), 3.78 (br s, 1H, NH), 4.28 (s, 2H, CH$_2$), 6.54 (m, 1H, CH-Ar), 6.62-6.66 (m, 1H, CH-Ar), 6.69-6.74 (m, 2H, CH-Ar), 7.28 (d, 2H, CH-Ar, J = 8.4 Hz), 7.46 (d, 2H, CH-Ar, J = 8.4 Hz). ^{13}C-NMR (CD$_2$Cl$_2$): δ 47.77 (CH$_2$), 111.96 (CH-Ar), 116.43 (CH-Ar), 118.88 (CH-Ar), 120.42 (CH-Ar), 120.71 (CH-Ar), 129.37 (CH-Ar), 131.57 (C-Ar), 134.54 (C-Ar), 137.31 (C-Ar), 139.01 (C-Ar). MS (ESI): 277 [M$^+$].

6.5.7. Synthesis of (1-(4-nitrobenzyl)-1H-benzo[d]imidazol-2-yl)methanol

7
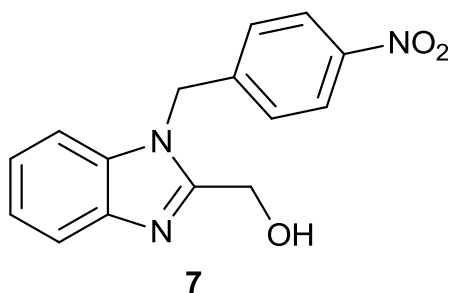
The synthetic procedure was completed following literature methods.[143] 1-(4-Nitrobenzyl)phenylenediamine (**5**) (4.5 g, 0.0185 mol) and glycolic acid (2.11 g, 0.028 mol) were dissolved in 5M HCl (120 ml) and heated under reflux for 60 hours. Cooled to 0°C and made basic with 5% NaOH solution (~700 ml) resulting in a light brown precipitate which was filtered and washed with water (200 ml) and diethyl ether (2 x 100ml) to yield a light brown solid which was purified via column chromatography, eluting with a gradient from DCM to MeOH (5%) to yield a light brown solid (2.7 g, 52%). ^{1}H-NMR (CD$_3$OD): δ 4.86 (s, 2H, CH$_2$), 5.74 (s, 2H, CH$_2$), 7.23-7.32 (m, 3H, CH-Ar), 7.38 (m, 2H, CH-Ar), 7.66 (m, 1H, CH-Ar), 8.16 (m, 2H, CH-Ar). ^{13}C-NMR (CD$_3$OD): δ 46.55 (CH$_2$), 56.62 (CH$_2$), 110.31 (C-Ar), 118.56 (C-Ar), 122.84 (CH-Ar), 123.54 (CH-Ar), 123.59 (CH-Ar), 127.59 (CH-Ar), 143.96 (C-Ar), 147.61 (C-Ar). HRMS (ESI) calc. 284.1030 found 284.1023 [M]$^{+}$.

6.5.8. Synthesis of (1-(4-bromobenzyl)-1H-benzo[d]imidazol-2-yl)methanol
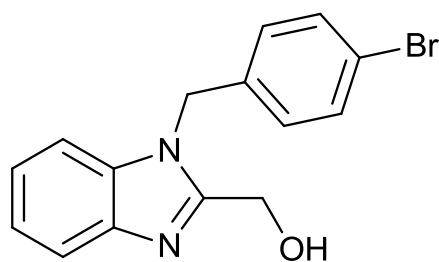
8

The synthetic procedure was completed following literature methods.[143] 1-(4-Bromobenzyl)phenylenediamine (**6**) (3 g, 0.0108 mol) and glycolic acid (1.23 g, 0.0162 mol) were dissolved in 5M HCl (100 ml) and heated under reflux for 60 hours. Cooled to 0°C and made basic with 5% NaOH solution (~700 ml) resulting in a cream precipitate which was filtered and washed with water (200 ml) and diethyl ether (2 x 100 ml) to yield a cream solid (1.0 g, 29%). ^{1}H-NMR (CD$_3$OD): δ 4.82 (s, 2H, CH$_2$), 5.57 (s, 2H, CH$_2$), 7.08 (m, 2H, CH-Ar), 7.23 (m, 2H, CH-Ar), 7.32 (m, 1H, CH-Ar), 7.43 (m, 2H, CH-Ar), 7.65 (m, 1H, CH-Ar). ^{13}C-NMR (CD$_3$OD): δ 46.12 (CH$_2$), 57.95 (CH$_2$), 111.49 (CH-Ar), 119.90 (CH-Ar), 122.60 (C-Ar), 123.63 (CH-Ar), 124.39 (CH-Ar), 129.66 (CH-Ar), 132.84 (CH-Ar), 135.92 (C-Ar), 136.91 (C-Ar), 142.60 (C-Ar), 154.30 (C-Ar). Elemental analysis: (%) calc. for C$_{15}$H$_{13}$BrN$_2$O C 56.80, H4.13, N 8.83. found C 56.97 H 3.85 N 8.89. MS (ESI): 317 [M]$^+$.

6.5.9. Synthesis of 1,4,7-tris(*tert*-butoxycarboxymethyl)-1,4,7,10-tetraazadodecane

9
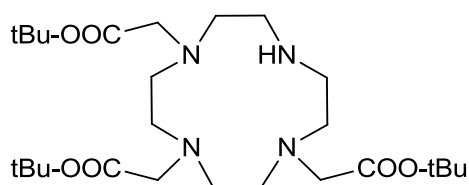
Method 1 (preferred method)

4,7,10-Tris(2-(*tert*-butoxy)-2-oxoethyl)-4,7,10-triaza-azoniacyclododecan-1-ium bromide (**10**) (11 g, 18. 5mmol) was partially dissolved in water (550 ml) at 70°C. The solution was cooled to 40°C after which 10% aqueous solution of KOH (22 ml, 36.96 mmol) was added. The reaction mixture stirred for 15 minutes then filtered to yield a white solid (9.2 g, 97%). ^{1}H-NMR (CDCl$_3$): δ 1.41 (m, 27H, C(CH$_3$)$_3$), 2.50-2.53 (m, 4H, N-CH$_2$), 2.70-2.78 (m, 12H, N-CH$_2$), 3.30 (s, 6H, N-CH$_2$-CO). ^{13}C-NMR (CDCl$_3$): δ 28.29 (C(CH$_3$)$_3$), 28.33 (C(CH$_3$)$_3$), 47.54 (C(CH$_3$)$_3$), 50.81 (N-CH$_2$), 52.33 (N-CH$_2$), 52.39 (N-CH$_2$), 53.07 (N-CH$_2$), 57.31 (N-CH$_2$), 80.87 (N-CH$_2$-CO), 80.92 (N-CH$_2$-CO), 171.17 (C=O), 171.36 (C=O).

Method 2

The synthetic procedure was completed following literature methods.[155] 4,7,10-Tris(2-(*tert*-butoxy)-2-oxoethyl)-4,7,10-triaza-azoniacyclododecan-1-ium bromide (**10**) (5 g, 8.4 mmol) was dissolved in water (250 ml) at 70°C. The solution was cooled to 40°C after which 10% aqueous solution of KOH (9.4 ml, 16.8 mmol) was added. The reaction mixture stirred for 15 minutes then extracted with hexane (3 x 100 ml). The combined extracts were washed with water (3 x 100 ml), dried (MgSO$_4$), filtered and concentrated *in vacuo* to yield a white solid (2.5 g, 61%).^{1}H-NMR (CDCl$_3$): δ 1.41 (m, 27H, C(CH$_3$)$_3$), 2.50-2.53 (m, 4H, N-CH$_2$), 2.70-2.78 (m, 12H, N-CH$_2$), 3.30 (s, 6H, N-CH$_2$-CO). ^{13}C-NMR (CDCl$_3$): δ 28.29 (C(CH$_3$)$_3$), 28.33 (C(CH$_3$)$_3$), 47.54 (C(CH$_3$)$_3$), 50.81 (N-CH$_2$), 52.33 (N-CH$_2$), 52.39 (N-CH$_2$), 53.07 (N-CH$_2$), 57.31 (N-CH$_2$), 80.87 (N-CH$_2$-CO), 80.92 (N-CH$_2$-CO), 171.17 (C=O), 171.36 (C=O).

Method 3

The synthetic procedure was completed following literature methods.[154] A solution of *tert*-butyl bromoacetate (10.00 g, 0.052 mol) in MeCN (300 ml) was added drop wise to a mixture of $NaHCO_3$ (4.39 g, 0.052 mol) and cyclen (3 g, 0.018 mol) in MeCN (900 ml). The solution was stirred for 72 hours. Undissolved material was removed by filtration. The filtrate was concentrated *in vacuo* to yield a crude yellow white solid (~8.5 g). The crude solid was purified using column chromatography, eluting with MeOH in DCM (0-20%) to yield a white solid (4.99 g, 54%). ^{1}H-NMR (CDCl$_3$): δ 1.46 (s, 27H, C(CH$_3$)$_3$), 2.89-2.94 (m, 12H, N-CH$_2$), 3.11 (m, 4H, N-CH$_2$), 3.30 (s, 2H, N-CH$_2$-CO), 3.39 (s, 4H, N-CH$_2$-CO), 10.00 (br s, 1H, NH). ^{13}C-NMR (CDCl$_3$): δ 23.07 (C(CH$_3$)$_3$), 23.37 (C(CH$_3$)$_3$), 42.77 (C(CH$_3$)$_3$), 44.45 (N-CH$_2$), 46.61 (N-CH$_2$), 53.44 (N-CH$_2$), 76.92 (N-CH$_2$), 77.08 (N-CH$_2$-CO), 164.87 (C=O), 165.75 (C=O). *The desired product was synthesised with trace impurities using this synthetic procedure.*

Method 4

The synthetic procedure was completed following literature methods.[154] A solution of *tert*-butyl bromoacetate (13.87 g, 0.0711 mol) in MeCN (400 ml) was added drop wise to a mixture K$_2$CO$_3$ (9.83 g, 0.0711 mol) and cyclen (4.08 g, 0.0237 mol) in MeCN (1.2 L). The solution was stirred for 72 hours. Undissolved material was removed by filtration. The filtrate was concentrated *in vacuo* to yield a crude yellow white solid (~13.2 g). The crude solid was purified using column chromatography, eluting with 0-20% MeOH in DCM (0-20%) to yield a white solid (7 g, 57%). ^{1}H-NMR (CDCl$_3$): δ 1.46 (s, 27H, C(CH$_3$)$_3$), 2.89-2.94 (m, 12H, N-CH$_2$), 3.11 (m, 4H, N-CH$_2$), 3.30 (s, 2H, N-CH$_2$-CO), 3.39 (s, 4H, N-CH$_2$-CO), 9.98 (br s, 1H, NH). ^{13}C-NMR (CDCl$_3$): δ 23.14 (C(CH$_3$)$_3$), 23.49 (C(CH$_3$)$_3$), 42.55 (C(CH$_3$)$_3$), 44.47 (N-CH$_2$), 46.55 (N-CH$_2$), 50.90 (N-CH$_2$), 76.93 (N-CH$_2$), 77.08 (N-CH$_2$-CO), 165.75 (C=O), 168.25 (C=O). *The desired product was synthesised with trace impurities using this synthetic procedure.*

6.5.10. Synthesis of 4,7,10-tris(2-(*tert*-butoxy)-2-oxoethyl)-4,7,10-triaza-azoniacyclododecan-1-ium bromide

10
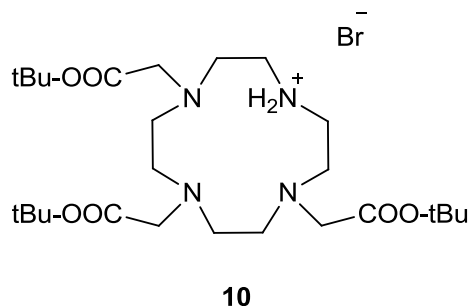
The synthetic procedure was completed following literature methods.[155] To a suspension of cyclen (5 g, 29 mmol) and sodium acetate (7.86 g, 96 mmol) in DMA (60 ml) at -20°C was added to a solution of *tert*-butyl bromoacetate (18.7 g, 14.1 ml, 96 mmol) in DMA (20 ml) drop wise over a period of 30 minutes, during which the temperature was maintained at below -15°C. The reaction was allowed to reach room temperature and stirred for 24 hours. The reaction was then poured into water (300 ml) to give a clear solution. Solid $KHCO_3$ (15 g, 150 mmol) was added portion wise to form a precipitate which was filtered and then dissolved in $CHCl_3$ (250 ml) and washed with water (100 ml), dried ($MgSO_4$), filtered and concentrated to ~25 ml. Diethyl ether (250 ml) was added to form white crystals which were filtered to yield a white solid (13.5 g, 78%). ^{1}H-NMR ($CDCl_3$): δ 1.42 (s, 9H, $C(CH_3)_3$), 1.43 (s, 18H, $C(CH_3)_2$), 2.82-2.92 (m, 12H, N-CH_2), 3.07 (m, 4H, N-CH_2), 3.26 (s, 2H, N-CH_2-CO), 3.81 (s, 4H, N-CH_2-CO), 10.00 (br s, 1H, NH). ^{13}C-NMR ($CDCl_3$): δ 28.26 ($C(CH_3)_3$), 28.30 ($C(CH_3)_3$), 48.57 ($C(CH_3)_3$), 48.90 (N-CH_2), 49.29 (N-CH_2), 51.35 (N-CH_2), 51.44 (N-CH_2), 58.28 (N-CH_2), 81.74 ($C(CH_3)$), 81.90 ($C(CH_3)$), 169.70 (C=O), 170.58 (C=O). MS (ESI): 515.4 [M-Br]$^+$.

6.5.11. Synthesis of tri-*tert*-butyl 2,2',2''-(10-((1H-benzo[d]imidazol-2-yl)methyl)-1,4,7,10-tetraazacyclododecane-1,4,7-triyl)triacetate

11
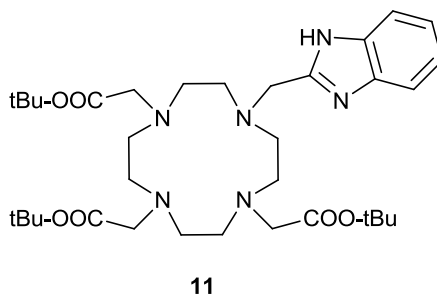
Method 1 (preferred method)

1,4,7-Tris(*tert*-butoxycarboxymethyl)-1,4,7,10-tetraazadodecane (**9**) (3.0 g, 5.83 mmol) was dissolved in dry MeCN (1.2 L), 2-(chloromethyl)-benzimidazole (1.0 g, 5.83 mmol) and Cs_2CO_3 (4.5 g, 23 mmol) was added and the reaction was stirred for 18 hours. The reaction was filtered, concentrated *in vacuo* and purified using a neutral alumina plug, eluting with ethyl acetate (100%) then MeOH (100%) to yield a brown solid (3.7 g, 98%). *The compound was used without analysis.*

Method 2

1,4,7-Tris(*tert*-butoxycarboxymethyl)-1,4,7,10-tetraazadodecane (**9**) 3.00 g, 5.83 mmol), K_2CO_3 (3.22 g, 23.32 mmol) and a trace of potassium iodide were dissolved in DMF (200 ml). 2-(Chloromethyl)-benzimidazole (1.07 g, 6.41 mmol) dissolved in DMF (30 ml) was added drop wise to the stirred solution. The resulting mixture was heated to reflux for 90 minutes. The mixture was filtered and concentrated *in vacuo*. In an attempt to remove residual potassium iodide and K_2CO_3 the solid was subsequently redissolved, filtered and concentrated *in vacuo* in both EtOH and DCM to yield an orange solid (3.76 g). *The desired product was synthesised with trace impurities using this synthetic procedure.*

Method 3

1,4,7-Tris(*tert*-butoxycarboxymethyl)-1,4,7,10-tetraazadodecane (**9**) (3.00 g, 5.83 mmol) was dissolved in DCM (100 ml) and the solution was washed with saturated $NaHCO_3$ solution, the organic layer was isolated, dried (Na_2SO_4), filtered and concentrated *in vacuo* to give a white solid (2.96 g, 5.75mmol). The solid was dissolved in dry MeCN (20 0ml) followed by the addition of 2-(chloromethyl)-benzimidazole (1.05 g, 6.33 mmol) and $NaHCO_3$ (3.7 g, 44

mmol) and heated to 60°C for 48 hours, left to cool, filtered and concentrated *in vacuo* to yield a crude orange solid (3.8 g). The product was purified using column chromatography, eluting with MeOH in DCM (0-20%) then stripped with ethyl acetate:MeOH:ammonia (80:15:5). *The desired product was not isolated using this synthetic procedure*.

Method 4

1,4,7-Tris(*tert*-butoxycarboxymethyl)-1,4,7,10-tetraazadodecane (**9**) (500 mg, 0.97 mmol) was dissolved in dry MeCN (50 ml). 2-(bromomethyl)-1H-benzo[d]imidazole (205 mg, 0.97 mmol) and K_2CO_3 (1.38 g, 10 mmol) was added and the reaction was heated to reflux and monitored by TLC (neutral alumina eluting with ethyl acetate:MeOH (90:10), after 18 hours the reaction was left to cool, filtered and concentrated *in vacuo* to yield a brown solid (580mg). *The desired product was synthesised with trace impurities using this synthetic procedure.*

Method 5

1,4,7-Tris(*tert*-butoxycarboxymethyl)-1,4,7,10-tetraazadodecane (**9**) (0.5 g, 0.97 mmol) was dissolved in dry MeCN (40 ml), 2-(chloromethyl)-benzimidazole (182 mg, 1.1 mmol) and Cs_2CO_3 (1.92 g, 10 mmol) was added to the reaction and the reaction was heated to reflux under argon for 44 hours, filtered and washed with saturated Na_2CO_3 solution, dried (MgSO$_4$), filtered and concentrated *in vacuo* to yield a brown solid (550 mg). *The desired product was synthesised with trace impurities using this synthetic procedure.*

Method 6

1,4,7-Tris(*tert*-butoxycarboxymethyl)-1,4,7,10-tetraazadodecane (**9**) (500 mg, 0.97 mmol) was dissolved in dry MeCN (40 ml), 2-bromomethyl benzimidazole (310 mg, 1.5 mmol) and Cs_2CO_3 (3.25 g, 10 mmol) was added to the reaction and the reaction was heated to reflux for 72 hours, left to cool, filtered and concentrated *in vacuo*. Redissolved in DCM and washed with saturated Cs_2CO_3 solution, dried (MgSO$_4$), filtered and concentrated *in vacuo* to yield a crude orange solid (600 mg). The crude solid was purified via a neutral alumina plug, eluting with ethyl acetate (100%) then MeOH (100%) to yield a brown solid (520 mg). *The desired product was not isolated using this synthetic procedure*.

6.5.12. Synthesis of 1,4,7-tris(*tert*-butoxycarbonylmethyl)-10-(1-(4-nitrobenzyl)-2-methyl benzimidazole)-1,4,7,10-tetraazacyclododecane

12

Method 1 (preferred method)

1,4,7-Tris(*tert*-butoxycarboxymethyl)-1,4,7,10-tetraazadodecane (**9**) (50 mg, 0.097 mmol) was dissolved in dry MeCN (10 ml), 2-(chloromethyl)-1-(4-nitrobenzyl)-1H-benzo[d]imidazole (32 mg, 0.106 mmol) (**3**) and Cs_2CO_3 (75 mg, 0.388 mmol) were added and the reaction was heated under reflux overnight, left to cool then concentrated *in vacuo*. The crude solid was purified via alumina column chromatography, eluting with ethyl acetate (100%) then MeOH (100%) to yield a red solid (75 mg, 98%). ^{1}H-NMR (CDCl$_3$): δ 1.17-1.55 (m, 27H, C(CH$_3$)$_3$), 1.88 (s, 2H, CH$_2$), 2.05-3.25 (br m, 20H, CH$_2$), 5.62 (s, 2H, CH$_2$), 7.11 (m, 1H, CH-Ar), 7.22 (m, 1H, CH-Ar), 7.33 (d, 2H, CH-Ar, J = 8.8 Hz), 7.41 (d, 1H, CH-Ar, J = 7.8 Hz), 7.53 (d, 1H, CH-Ar, J = 7.8 Hz), 8.16 (d, 2H, CH-Ar, J = 8.8 Hz). ^{13}C-NMR (CDCl$_3$): δ 27.08(C (CH$_3$)$_3$), 45.42 (CH$_2$), 48.39 (CH$_2$), 50.56 (CH$_2$), 55,23 (CH$_2$), 81.80 (C(CH$_3$)$_3$), 109.28 (C-Ar), 119.08 (C-Ar), 121.56 (CH-Ar), 122.52 (CH-Ar), 123.75 (CH-Ar), 127.31 (CH-Ar), 135.58 (C-Ar), 142.43 (C-Ar), 144.12 (C-Ar), 147.61 (C=O), 153.49 (C-Ar), 173.24 (C=O). MS (ESI): 802.44 [M+Na$^+$].

Method 2

Tri-*tert*-butyl 2,2',2''-(10-((1H-benzo[d]imidazol-2-yl)methyl)-1,4,7,10-tetraazacyclododecane-1,4,7-triyl)triacetate (**11**) (50 mg, 0.0775 mmol) was dissolved in dry MeCN (10 ml), 4-nitromethyl benzyl bromide (18 mg, 0.0853 mmol) and Cs_2CO_3 (66 mg, 0.34 mmol) was added and the reaction was heated under reflux overnight, left to cool and concentrated *in vacuo. The desired product was not isolated using this synthetic procedure*.

1,4,7-Tris(*tert*-butoxycarboxymethyl)-1,4,7,10-tetraazadodecane (**9**) (50 mg, 0.097 mmol) was dissolved in dry MeCN (10 ml), 2-(chloromethyl)-1-(4-nitrobenzyl)-1H-benzo[d]imidazole (32 mg, 0.106 mmol) (**3**) and Cs_2CO_3 (75 mg, 0.388 mmol) were added and the reaction stirred at room temperature overnight then concentrated *in vacuo*. The crude solid was purified via alumina column chromatography, eluting with ethyl acetate (100%) then MeOH (100%) to yield a red solid (75 mg, 98%).

6.5.13. Attempted synthesis of tri-*tert*-butyl 2,2',2''-(10-((1-(*tert*-butoxycarbonyl)-1H-benzo[d]imidazol-2-yl)methyl)-1,4,7,10-tetraazacyclododecane-1,4,7-triyl)triacetate

13
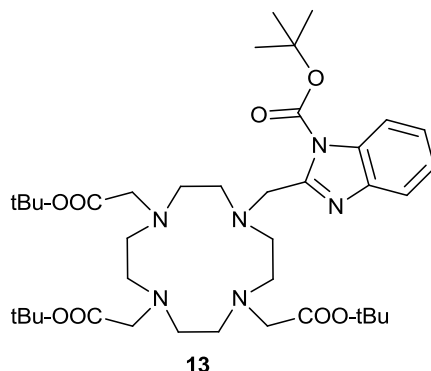
Method 1

1,4,7-Tris(*tert*-butoxycarboxymethyl)-1,4,7,10-tetraazadodecane (**9**) (100 mg, 0.19 mmol) was dissolved in dry MeCN (20 ml), *tert*-butyl 2-(chloromethyl)-1H-benzo[d]imidazole-1-carboxylate (**2**) (62 mg, 0.23 mmol) and Cs_2CO_3 (300 mg, 0.92 mmol) was added and the reaction was stirred at room temperature for 18 hours. The reaction was filtered, concentrated *in vacuo* and purified using a neutral alumina plug, eluting with ethyl acetate (100%) then MeOH (100%) to yield a white solid (120 mg). *The desired product was not isolated using this synthetic procedure*.

Method 2

1,4,7-Tris(*tert*-butoxycarboxymethyl)-1,4,7,10-tetraazadodecane (**9**) (100 mg, 0.19 mmol) was dissolved in dry MeCN (20 ml), *tert*-butyl 2-(chloromethyl)-1H-benzo[d]imidazole-1-carboxylate (103 mg, 0.38 mmol) (**2**) and Cs_2CO_3 (300 mg, 0.92 mmol) was added and the reaction was heated under reflux for 20 hours. The reaction was filtered, concentrated *in vacuo* and purified using a neutral alumina plug, eluting with ethyl acetate (100%) then MeOH (100%) to yield a brown solid (100 mg). *The desired product was not isolated using this synthetic procedure*.

1,4,7-Tris(*tert*-butoxycarboxymethyl)-1,4,7,10-tetraazadodecane (**9**) (50 mg, 0.1 mmol) was dissolved in dry MeCN (20 ml), *tert*-butyl 2-(chloromethyl)-1H-benzo[d]imidazole-1-carboxylate (**2**) (250 mg, 1 mmol) and Cs_2CO_3 (330 mg, 1 mmol) was added and the reaction was stirred for 18 hours. The reaction was filtered, concentrated *in vacuo* and purified using a neutral alumina plug, eluting with ethyl acetate (100%) then MeOH (100%) to yield a white solid (120 mg). *The desired product was not isolated using this synthetic procedure*.

6.5.14. Synthesis of 2,2',2''-(10-((1H-benzo[d]imidazol-2-yl)methyl)-1,4,7,10-tetraazacyclododecane-1,4,7-triyl)triacetic acid

14
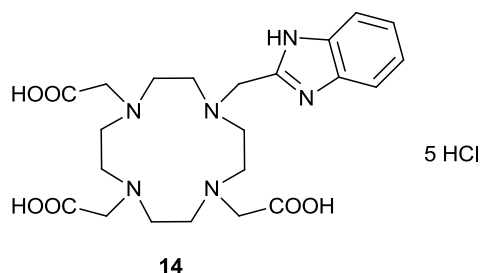
Tri-*tert*-butyl 2,2',2''-(10-((1H-benzo[d]imidazol-2-yl)methyl)-1,4,7,10-tetraazacyclododecane-1,4,7-triyl)triacetate (**11**) (3 g, 4.65 mmol) was dissolved in 6M HCl (200 ml) and heated under reflux for 18 hours. The reaction was then concentrated *in vacuo* and diethyl ether (3 x100 ml) was added and decanted off to remove any impurities to yield a light brown solid (3.0 g, 98%). ^{1}H-NMR (D$_2$O): δ 2.95-2.98 (m, 4H, CH$_2$), 3.12-3.14 (m, 2H, CH$_2$), 3.21-3.30 (m, 2H, CH$_2$), 3.37-3.46 (m, 4H, CH$_2$), 3.51-3.69 (m, 4H, CH$_2$), 3.72-3.83 (m, 2H, CH$_2$), 3.94-4.02 (m, 2H, CH$_2$), 4.09-4.23 (m, 2H, CH$_2$), 4.37 (s, 2H, CH$_2$), 7.49-7.55 (m, 2H, CH-Ar), 7.66-7.72 (m, 2H, CH-Ar). ^{13}C-NMR (D$_2$O) : δ 48.44 (CH$_2$), 48.67 (CH$_2$), 51.21 (CH$_2$), 53.51 (CH$_2$), 54.84 (CH$_2$), 114.58 (CH-Ar), 127.38 (CH-Ar), 130.49 (CH-Ar), 148.08 (C-Ar), 168.71 (CH-Ar), 177.01 (C=O). Elemental analysis for C$_{22}$H$_{45}$Cl$_5$N$_6$O$_{10}$ (L + 4H$_2$O), calc. C 36.15 H 6.21 N 11.50 Cl 24.25. Found C 36.30 H 5.77 N 11.52 Cl 24.30 (Cl found via titration). MS (ESI): 620.8 [M - HCl]. HPLC: Method 2 – retention time = 3:05 mins.

6.5.15. Synthesis of 1,4,7-tris(*tert*-butoxycarbonylmethyl)-10-(1-(4-bromobenzyl)-2-methyl benzimidazole)-1,4,7,10-tetraazacyclododecane
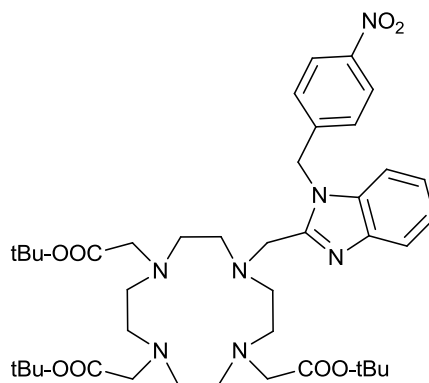

15
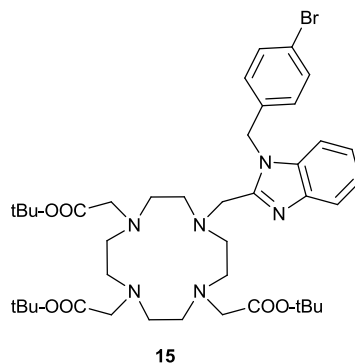
1,4,7-Tris(*tert*-butoxycarboxymethyl)-1,4,7,10-tetraazadodecane (**9**) (1.02 g, 1.98 mmol) was dissolved in dry MeCN (250 ml), 1-(4-bromobenzyl)-2-(chloromethyl)-1H-benzo[d]imidazole (**4**) (800 mg, 2.38 mmol) and Cs_2CO_3 (3.11 g, 9.53 mmol) were added and the reaction was heated under reflux overnight, left to cool then concentrated *in vacuo*. The crude solid was purified via alumina column chromatography, eluting with ethyl acetate (100%) then MeOH (100%) to yield a cream solid (1.58 g, 98%). ^{1}H-NMR ($CDCl_3$): δ 1.39-1.55 (m, 27H, C(CH$_3$)$_3$), 1.97-3.20 (br m, 22H, CH$_2$), 3.41 (s, 2H, CH$_2$), 5.43 (s, 2H, CH$_2$), 7.03-7.13 (m, 3H, CH-Ar), 7.21 (m, 1H, CH-Ar), 7.41-7.44 (m, 3H, CH-Ar), 7.51 (d, 1H, CH-Ar, J = 8.1 Hz). ^{13}C-NMR ($CDCl_3$): δ 27.09(C (CH$_3$)$_3$), 45.44 (CH$_2$), 48.53 (CH$_2$), 50.64 (CH$_2$), 55,25 (CH$_2$), 81.77 (C(CH$_3$)$_3$), 109.35 (C-Ar), 118.98 (C-Ar), 121.35 (CH-Ar), 122.34 (CH-Ar), 128.28 (CH-Ar), 131.77 (CH-Ar), 135.69 (C-Ar), 135.99 (C-Ar), 142.39 (C-Ar), 153.46 (C=O), 173.21 (C=O). HRMS calc. 813.3909, found 813.3895 [M]$^+$.

6.5.16. Synthesis of 1,4,7-tris(*tert*-butoxycarbonylmethyl)-10-(1-(4-aminobenzyl)-2-methyl benzimidazole)-1,4,7,10-tetraazacyclododecane

16

The synthetic procedure was completed following literature methods.[159] NaBH$_4$ (15 mg, 0.384 mmol) and S$_8$ (25 mg, 0.768 mmol) were suspended in dry THF (10 ml) and stirred under argon for 1 hour. 1,4,7-Tris(*tert*-butoxycarbonylmethyl)-10-(1-(4-nitrobenzyl)-2-methyl benzimidazole)-1,4,7,10-tetraazacyclododecane (**12**) (300 mg, 0.384 mmol) in THF (10 ml) was added and the reaction was heated under reflux overnight then left to cool. The resulting solution was washed with 5% NaOH solution (5 x 20 ml), the organic layer was dried (Na$_2$SO$_4$), filtered and concentrated *in vacuo* to yield a crude brown solid (350 mg). The crude solid was purified via column chromatography, eluting with DCM:MeOH (95:5) to yield a brown solid (144mg, 50%). *The compound was used without analysis.*

6.5.17. Synthesis of 2,2',2''-(10-((1-(4-nitrobenzyl)-1H-benzo[d]imidazol-2-yl)methyl)-1,4,7,10-tetraazacyclododecane-1,4,7-triyl)triacetic acid

17
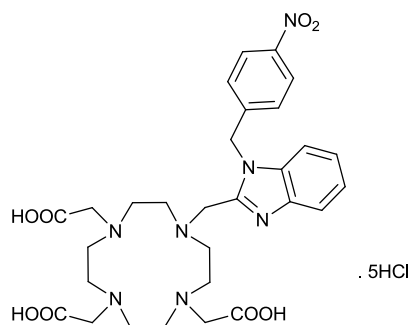
1,4,7-tris(*tert*-butoxycarbonylmethyl)-10-(1-(4-nitrobenzyl)-2-methyl benzimidazole)-1,4,7,10-tetraazacyclododecane (**12**) (1.3 g, 1.67 mmol) was dissolved in 6M HCl (50 ml) and heated under reflux for 18 hours. The reaction was then concentrated *in vacuo* and diethyl ether (3 x100 ml) was added and decanted off to remove any impurities to yield a light brown solid (1.3 g, 98%). ^{1}H-NMR (D$_2$O): δ 2.83-3.72 (m, 20H, CH$_2$), 3.92-3.96 (d, 2H, CH$_2$, J = 16.9 Hz), 4.51 (s, 2H, CH$_2$), 5.98 (s, 2H, CH$_2$-CAr), 7.44 (d, 2H, CH-Ar, J = 8.8 Hz), 7.59-7.73 (m, 3H, CH-Ar), 7.89 (d, 1H, CH-Ar, J = 8.1 Hz), 8.23 (d, 2H, CH-Ar, J = 8.8 Hz). HRMS (ESI) calc. 650.2335 found 650.2237 [M − 5HCl + K$^+$]. HPLC: Method 2 – retention time = 11:34 mins.

6.5.18. Synthesis of 2,2',2''-(10-((1-(4-bromobenzyl)-1H-benzo[d]imidazol-2-yl)methyl)-1,4,7,10-tetraazacyclododecane-1,4,7-triyl)triacetic acid

18
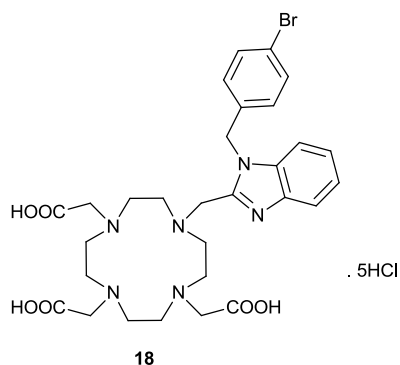
1,4,7-tris(*tert*-butoxycarbonylmethyl)-10-(1-(4-bromobenzyl)-2-methyl benzimidazole)-1,4,7,10-tetraazacyclododecane (**15**) (100 mg, 0.123 mmol) was dissolved in 6M HCl (10 ml) and heated under reflux for 18 hours. The reaction was then concentrated *in vacuo* and diethyl ether (3 x10 ml) was added and decanted off to remove any impurities to yield a red solid (100 mg, 98%). ^{1}H-NMR (D$_2$O): δ 2.51-2.54 (m, 2H, CH$_2$), 2.84-3.02 (m, 6H, CH$_2$), 3.25-3.42 (m, 12H, CH$_2$), 3.70-3.75 (m, 2H, CH$_2$), 4.32 (s, 2H, CH$_2$), 5.65 (s, 2H, CH$_2$-CAr), 7.03 (d, 2H, CH-Ar, J = 8.2 Hz), 7.42-7.52 (m, 4H, CH-Ar), 7.67-7.70 (m, 2H, CH-Ar). ^{13}C-NMR (D$_2$O) : δ 47.63 (CH$_2$), 47.98 (CH$_2$), 48.70 (CH$_2$), 50.38 (CH$_2$), 52.14 (CH$_2$), 53.31 (CH$_2$), 55.80 (CH$_2$), 112.76 (CH-Ar), 115.40 (CH-Ar), 122.54 (C-Ar), 127.20 (CH-Ar), 127.61 (CH-Ar), 128.93 (CH-Ar), 130.06 (C-Ar), 131.78 (C-Ar), 132.45 (CH-Ar), 132.88 (C-Ar), 148.64 (C-Ar), 168.73 (CH-Ar), 176.69 (C=O). HRMS (-ve ESI): calc. 643.1885, found 643.1884 [M − 5HCl − H^{+}]$^{-}$ HPLC: Method 2 – retention time = 12:00 mins.

6.5.19. Synthesis of 2,2',2''-(10-((1-(4-aminobenzyl)-1H-benzo[d]imidazol-2-yl)methyl)-1,4,7,10-tetraazacyclododecane-1,4,7-triyl)triacetic acid
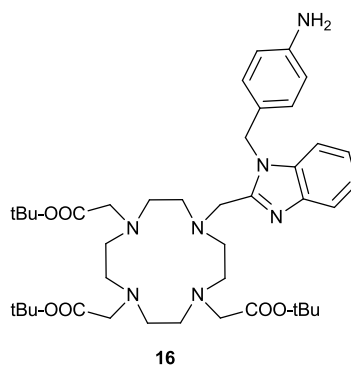

19
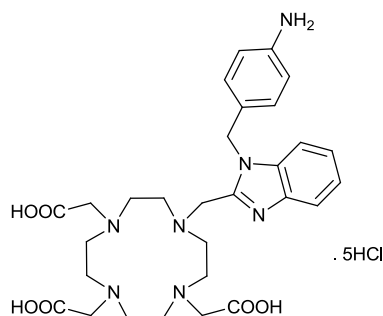
1,4,7-tris(*tert*-butoxycarbonylmethyl)-10-(1-(4-aminobenzyl)-2-methyl benzimidazole)-1,4,7,10-tetraazacyclododecane (**16**) (3 g, 4.65 mmol) was dissolved in 6M HCl (200 ml) and heated under reflux for 18 hours. The reaction was then concentrated *in vacuo* and diethyl ether (3 x100 ml) was added and decanted off to remove any impurities to yield a dark brown solid (3.0 g, 98%). ^{1}H-NMR (D$_2$O): δ 2.64-3.57 (m, 20H, CH$_2$), 3.79-3.83 (m, 2H, CH$_2$), 4.37 (s, 2H, CH$_2$), 5.74 (s, 2H, CH$_2$-CAr), 7.43-7.53 (m, 4H, CH-Ar), 7.61 (m, 2H, CH-Ar), 7.70 (d, 2H, CH-Ar, J = 8.4 Hz). MS (ESI): 582.3 [M + H$^+$]. HPLC: Method 2 – retention time = 8:16 mins.

6.5.20. Synthesis of $^{69/71}$Ga complex of 2,2',2''-(10-((1H-benzo[d]imidazol-2-yl)methyl)-1,4,7,10-tetraazacyclododecane-1,4,7-triyl)triacetic acid

[Ga**14**]

2,2',2''-(10-((1H-benzo[d]imidazol-2-yl)methyl)-1,4,7,10-tetraazacyclododecane-1,4,7-triyl)triacetic acid (**14**) (52 mg, 78.9 μmol) was dissolved in ammonium acetate buffer (pH 5, 0.2 M, 10 ml). To this, gallium(III) chloride (14mg, 78.9μmol) was added drop-wise. The reaction was heated to 95°C for 18 hours then concentrated *in vacuo*. The crude solid was redissolved in water (1 ml) and purified using an Amberlite XAD16N column, eluting with water (100 ml) then water:acetonitrile (9:1, 100 ml) to yield a white solid (12.5 mg, 26%). HRMS calc. 543.1477, found 543.1477 [M+H$^+$]. HPLC: Method 2 – retention time = 7.06 mins.

6.5.21. Synthesis of $^{63/65}$Cu complex of 2,2',2''-(10-((1H-benzo[d]imidazol-2-yl)methyl)-1,4,7,10-tetraazacyclododecane-1,4,7-triyl)triacetic acid

[Cu14]

2,2',2''-(10-((1H-benzo[d]imidazol-2-yl)methyl)-1,4,7,10-tetraazacyclododecane-1,4,7-triyl)triacetic acid (**14**) (32 mg, 48.6 μmol) was dissolved in water (10 ml). To this, copper(II) acetate monohydrate (9.7 mg, 48.6 μmol) and Cs_2CO_3 (79 mg, 0.243 mmol) was added. The reaction was heated under reflux for 18 hours then concentrated *in vacuo*. The crude solid was redissolved in water (1 ml) and purified using an Amberlite XAD16N column, eluting with water (100 ml) then water:acetonitrile (9:1, 100 ml) to yield a green solid (24 mg, 82.8%). HRMS calc. 538.1596, found 538.1595[M+H$^+$]. HPLC: Method 1 – retention time = 5:36 mins.

6.5.22. Synthesis of yttrium(III) complex of 2,2',2''-(10-((1H-benzo[d]imidazol-2-yl)methyl)-1,4,7,10-tetraazacyclododecane-1,4,7-triyl)triacetic acid

[Y14]

2,2',2''-(10-((1H-benzo[d]imidazol-2-yl)methyl)-1,4,7,10-tetraazacyclododecane-1,4,7-triyl)triacetic acid (**14**) (100 mg, 0.25 mmol) was dissolved in ammonium acetate buffer (0.2M, pH 5, 5 ml). To this, yttrium(III) chloride hexahydrate (76 mg, 0.25 mmol) in ammonium acetate buffer (0.2M, pH 5, 5 ml) was added. The reaction was heated under reflux for 18 hours then concentrated *in vacuo*. The crude solid was redissolved in water (1 ml) and purified using an Amberlite XAD16N column, eluting with water (100 ml) then water:acetonitrile (9:1, 100 ml) to yield a white solid (32 mg, 37%). ^{1}H-NMR (D$_2$O): δ 1.63-1.70 (m, 1H, CH$_2$), 2.09-2.85 (m, 15H, CH$_2$), 3.08-3.13 (m, 2H, CH$_2$), 3.19-3.37 (m, 4H, CH$_2$), 3.47-3.53 (m, 2H, CH$_2$), 3.94 (d, 2H, CH$_2$, J = 16.3 Hz), 4.19 (d, 2H, CH$_2$, J = 16.1 Hz), 7.08-7.15 (m, 2H, CH-Ar), 7.41 (d, 1H, CH-Ar, J = 6.9 Hz), 7.52 (d, 1H, CH-Ar, J = 7.1 Hz). ^{13}C-NMR (D$_2$O) : δ 55.13 (CH$_2$), 55.37 (CH$_2$),55.64 (CH$_2$), 56.11 (CH$_2$), 56.35 (CH$_2$), 56.49 (CH$_2$), 59.42 (CH$_2$), 65.79 (CH$_2$), 66.01 (CH$_2$), 66.41 (CH$_2$), 113.07 (CH-Ar), 117.60 (C-Ar), 123.11 (CH-Ar), 123.50 (CH-Ar), 135.11 (C-Ar) 140.50 (CH-Ar), 156.11 (C-Ar), 180.70 (C=O), 180.81 (C=O). HRMS calc. 563.1280 found 563.1288 [M+H$^+$]. Elemental analysis for C$_{22}$H$_{35}$N$_6$O$_9$Y (M + 3H$_2$O), calc. C 42.86 H 5.72 N 13.63. Found C 43.01 H 6.00 N 13.70.

6.5.23. Synthesis of $^{69/71}$Ga complex of 2,2',2''-(10-((1-(4-nitrobenzyl)-1H-benzo[d]imidazol-2-yl)methyl)-1,4,7,10-tetraazacyclododecane-1,4,7-triyl)triacetic acid
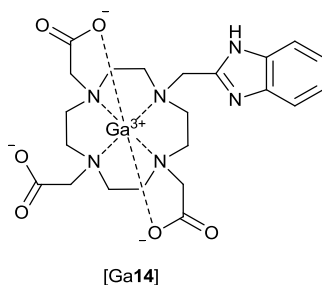

[Ga**17**]

2,2',2''-(10-((1-(4-Nitrobenzyl)-1H-benzo[d]imidazol-2-yl)methyl)-1,4,7,10-tetraazacyclododecane-1,4,7-triyl)triacetic acid (**17**) (1 mg, 1.63 μmol) was dissolved in ammonium acetate buffer (pH 5, 0.2 M, 1 ml). To this, gallium(III) chloride (0.3 mg, 1.63 μmol) was added dropwise. The reaction was heated to 95°C for 18 hours then concentrated *in vacuo*. The crude solid was redissolved in water (1 ml) and purified using an Amberlite XAD16N column, eluting with water (10 ml) then water:acetonitrile (9:1, 10 ml) to yield a white solid (0.8 mg, 67%). HRMS calc. 678.1797, found 678.1794 [M$^+$]. HPLC: Method 2 – retention time = 14:05 mins.

6.5.24. Synthesis of [69/71]Ga complex of 2,2',2''-(10-((1-(4-bromobenzyl)-1H-benzo[d]imidazol-2-yl)methyl)-1,4,7,10-tetraazacyclododecane-1,4,7-triyl)triacetic acid
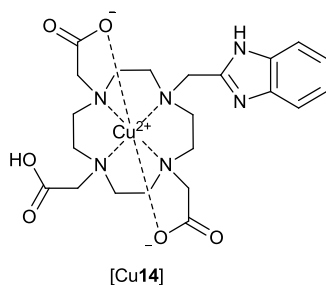

[Ga**18**]

2,2',2''-(10-((1-(4-Bromobenzyl)-1H-benzo[d]imidazol-2-yl)methyl)-1,4,7,10-tetraazacyclododecane-1,4,7-triyl)triacetic acid (**18**) (1 mg, 1.55 μmol) was dissolved in ammonium acetate buffer (pH 5, 0.2 M, 1 ml). To this, gallium(III) chloride (0.2 mg, 1.55 μmol) was added dropwise. The reaction was heated to 95°C for 18 hours then concentrated *in vacuo*. The crude solid was redissolved in water (1 ml) and purified using an Amberlite XAD16N column, eluting with water (10 ml) then water:acetonitrile (9:1, 10 ml) to yield a white solid (0.8 mg, 67%). HRMS calc. 713.1039, found 713.1036. [M$^+$] HPLC: Method 2 – retention time = 15:30 mins.

6.5.25. Synthesis of $^{69/71}$**Ga complex of 2,2',2''-(10-((1-(4-aminobenzyl)-1H-benzo[d]imidazol-2-yl)methyl)-1,4,7,10-tetraazacyclododecane-1,4,7-triyl)triacetic acid**

[Ga**19**]

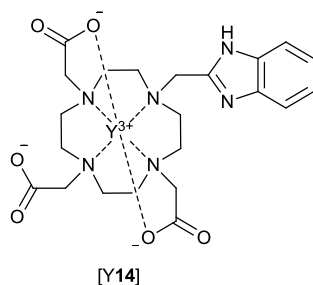2,2',2''-(10-((1-(4-Aminobenzyl)-1H-benzo[d]imidazol-2-yl)methyl)-1,4,7,10-tetraazacyclododecane-1,4,7-triyl)triacetic acid (**19**) (1 mg, 1.72 μmol) was dissolved in ammonium acetate buffer (pH 5, 0.2 M, 1 ml). To this, gallium(III) chloride (0.3 mg, 1.72 μmol) was added dropwise. The reaction was heated to 95$^{\mathrm{o}}$C for 18 hours then concentrated *in vacuo*. The crude solid was redissolved in water (1 ml) and purified using an Amberlite XAD16N column, eluting with water (10 ml) then water:acetonitrile (9:1, 10 ml) to yield a white solid (0.8 mg, 66%). HRMS calc. 648.2056, found 648.2056. [M^{+}]. HPLC: Method 2 – retention time = 10:45 mins.

6.5.26. Synthesis of $^{63/65}$Cu complex of 2,2',2''-(10-((1-(4-nitrobenzyl)-1H-benzo[d]imidazol-2-yl)methyl)-1,4,7,10-tetraazacyclododecane-1,4,7-triyl)triacetic acid
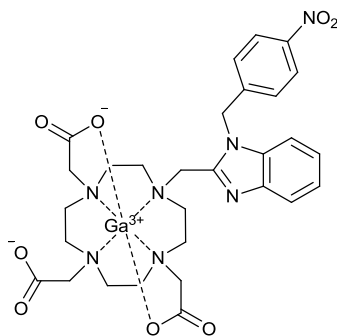

[Cu**17**]

2,2',2''-(10-((1-(4-Nitrobenzyl)-1H-benzo[d]imidazol-2-yl)methyl)-1,4,7,10-tetraazacyclododecane-1,4,7-triyl)triacetic acid (**17**) (1 mg, 1.63 μmol) was dissolved in water (1 ml). To this, copper(II) acetate monohydrate (0.3 mg, 1.63 μmol) and Cs_2CO_3 (2.1 mg, 6.52 mmol) was added. The reaction was heated under reflux for 18 hours then concentrated *in vacuo*. The crude solid was redissolved in water (1 ml) and purified using an Amberlite XAD16N column, eluting with water (10 ml) then water:acetonitrile (9:1, 10 ml) to yield a green solid (0.8 mg, 67%). HRMS calc. 673.1916, found 673.1910 [M$^+$]. HPLC: Method 1 – retention time = 12:31 mins.

6.5.27. Synthesis of $^{63/65}$Cu complex of 2,2',2''-(10-((1-(4-bromobenzyl)-1H-benzo[d]imidazol-2-yl)methyl)-1,4,7,10-tetraazacyclododecane-1,4,7-triyl)triacetic acid

[Cu**18**]

2,2',2''-(10-((1-(4-Bromobenzyl)-1H-benzo[d]imidazol-2-yl)methyl)-1,4,7,10-tetraazacyclododecane-1,4,7-triyl)triacetic acid (**18**) (1 mg, 1.55 μmol) was dissolved in water (1 ml). To this, copper(II) acetate monohydrate (0.3 mg, 1.55 μmol) and Cs_2CO_3 (2 mg, 6.2 mmol) was added. The reaction was heated under reflux for 18 hours then concentrated *in vacuo*. The crude solid was redissolved in water (1 ml) and purified using an Amberlite XAD16N column, eluting with water (10 ml) then water:acetonitrile (9:1, 10 ml) to yield a green solid (0.8 mg, 73%). HRMS calc. 708.1154, found 708.1144. [M$^+$]. HPLC: Method 1 – retention time = 13:51 mins.

6.5.28. Synthesis of [63/65]Cu complex of 2,2',2''-(10-((1-(4-aminobenzyl)-1H-benzo[d]imidazol-2-yl)methyl)-1,4,7,10-tetraazacyclododecane-1,4,7-triyl)triacetic acid

[Cu**19**]

2,2',2''-(10-((1-(4-Aminobenzyl)-1H-benzo[d]imidazol-2-yl)methyl)-1,4,7,10-tetraazacyclododecane-1,4,7-triyl)triacetic acid (**19**) (1 mg, 1.73 μmol) was dissolved in water (1 ml). To this, copper(II) acetate monohydrate (0.36 mg, 1.73 μmol) and Cs_2CO_3 (2.3 mg, 6.92 mmol) was added. The reaction was heated under reflux for 18 hours then concentrated *in vacuo*. The crude solid was redissolved in water (1 ml) and purified using an Amberlite XAD16N column, eluting with water (10 ml) then water:acetonitrile (9:1, 10 ml) to yield a green solid (0.8 mg, 67%). HRMS calc. 655.1991, found 655.1994 [M[+]]. HPLC: Method 1 – retention time = 7:29 mins.
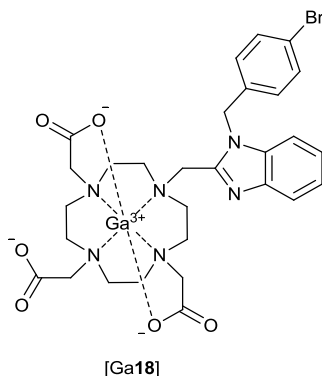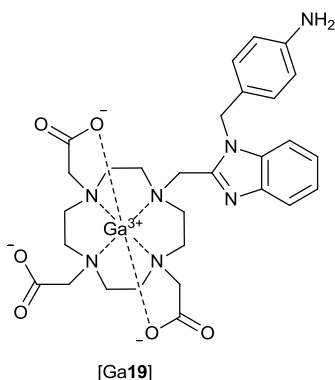
6.6. BFC radiolabelling

6.6.1. Synthesis of ^{68}Ga complex of 2,2',2''-(10-((1-(4-bromobenzyl)-1H-benzo[d]imidazol-2-yl)methyl)-1,4,7,10-tetraazacyclododecane-1,4,7-triyl)triacetic acid

[[68]Ga**18**]
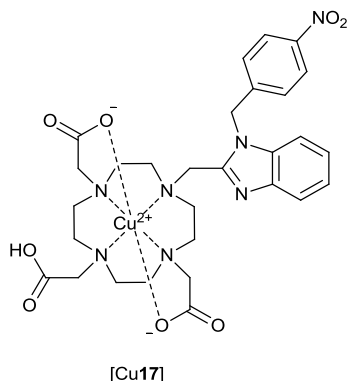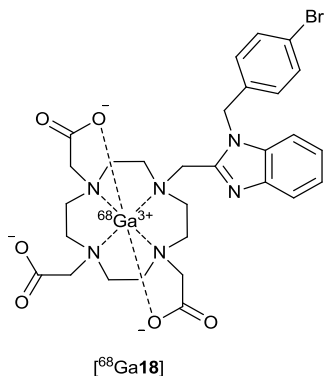
Method 1

2,2',2''-(10-((1-(4-bromobenzyl)-1H-benzo[d]imidazol-2-yl)methyl)-1,4,7,10-tetraazacyclododecane-1,4,7-triyl)triacetic acid (**18**) (200 μl, 10 mM) in ammonium acetate buffer (O.2 M, pH 5) was added to formulated [68]GaCl$_3$ (20-60 MBq) and the reaction was mixed at room temperature using a vortex stirrer for 30 minutes.

Radio-HPLC Time (mins)	% RCY 10mM
5	72.02
10	73.81
15	71.16
20	73.18
25	80.12
30	80.12

Method 2

2,2',2''-(10-((1-(4-bromobenzyl)-1H-benzo[d]imidazol-2-yl)methyl)-1,4,7,10-tetraazacyclododecane-1,4,7-triyl)triacetic acid (**18**) (200 µl, 10 µM) in ammonium acetate buffer (O.2 M, pH 5) was added to formulated ^{68}GaCl$_3$ (80 MBq) and the reaction was heated at 90°C for 30 minutes.

Radio-HPLC	
Time (mins)	% RCY
5	37.78
10	37.61
15	45.40
20	33.22
25	38.13

Method 3

2,2',2''-(10-((1-(4-bromobenzyl)-1H-benzo[d]imidazol-2-yl)methyl)-1,4,7,10-tetraazacyclododecane-1,4,7-triyl)triacetic acid (**18**) (200 µl, 10 µM) in ammonium acetate buffer (O.2 M, pH 5) was added to formulated ^{68}GaCl$_3$ (35-74 MBq) and the reaction was heated using microwave irradiation (see below for temperature and time).

Radio-HPLC	Conditions			
	90°C 2.5 mins	90°C 5 mins	90°C 10 mins	130°C 5 mins
% RCY	68.06	49.60	55.00	9.66

6.6.2. Synthesis of ^{68}Ga complex of 1,4,7-tris(*tert*-butoxycarboxymethyl)-10-(2-methylbenzimidazolyl) tetraazadodecane

[^{68}Ga**14**]
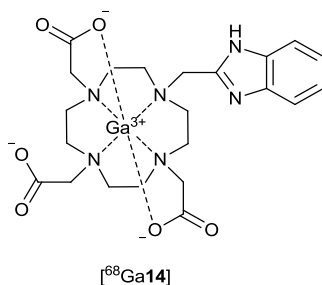
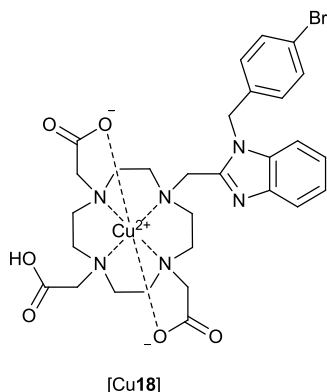1,4,7-Tris(*tert*-butoxycarboxymethyl)-10-(2-methylbenzimidazolyl) tetraazadodecane2,2',2''-(10-((1-(4-bromobenzyl)-1H-benzo[d]imidazol-2-yl)methyl)-1,4,7,10-tetraazacyclododecane-1,4,7-triyl)triacetic acid (**14**) (200 μl, 10μM) in ammonium acetate buffer (O.2 M, pH 5) was added to formulated ^{68}GaCl$_3$ (63-64 MBq) and the reaction was mixed at room temperature using a vortex stirrer for 30 minutes.

Radio-HPLC	
Time (mins)	% RCY
5	73
10	72
15	75
20	72
25	78
30	75

6.6.3. Synthesis of ^{68}Ga complex of 2,2',2''-(10-((1-(4-nitrobenzyl)-1H-benzo[d]imidazol-2-yl)methyl)-1,4,7,10-tetraazacyclododecane-1,4,7-triyl)triacetic acid
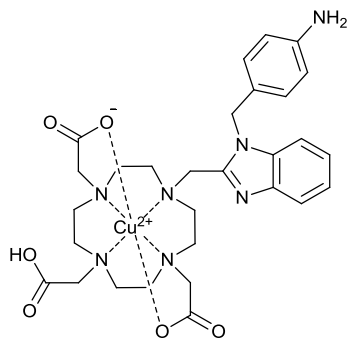

[[68]Ga**17**]
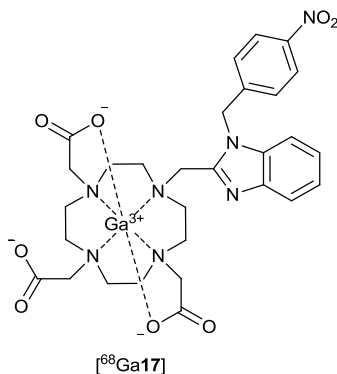
2,2',2''-(10-((1-(4-Nitrobenzyl)-1H-benzo[d]imidazol-2-yl)methyl)-1,4,7,10-tetraazacyclododecane-1,4,7-triyl)triacetic acid (**17**) (200 µl, 10µM) in ammonium acetate buffer (O.2 M, pH 5) was added to formulated [68]GaCl$_3$ (45-58 MBq) and the reaction was mixed at room temperature using a vortex stirrer for 30 minutes.

Radio-HPLC	
Time (mins)	% RCY
5	33
10	33
15	33
20	31
25	29
30	32

6.6.4. Synthesis of ^{68}Ga complex of 2,2',2''-(10-((1-(4-aminobenzyl)-1H-benzo[d]imidazol-2-yl)methyl)-1,4,7,10-tetraazacyclododecane-1,4,7-triyl)triacetic acid

[[68]Ga**19**]
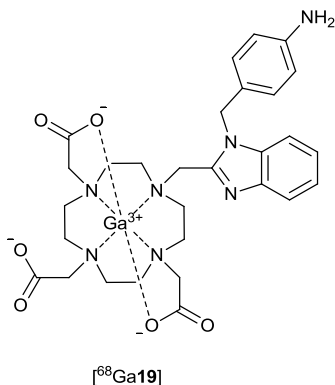
2,2',2''-(10-((1-(4-Aminobenzyl)-1H-benzo[d]imidazol-2-yl)methyl)-1,4,7,10-tetraazacyclododecane-1,4,7-triyl)triacetic acid (**19**) (200 μl, 10μM) in ammonium acetate buffer (O.2 M, pH 5) was added to formulated [68]GaCl$_3$ (45-67 MBq) and the reaction was mixed at room temperature using a vortex stirrer for 30 minutes.

Radio-HPLC	
Time (mins)	% RCY
5	16
10	16
15	15
20	15
25	16
30	17

6.7. MNP synthesis

6.7.1. Methyl 6-(1,4,8,11-tetraazabicyclo[6.6.2]hexadecan-4-ylmethyl)picolinate hydrochloride
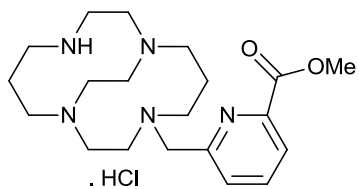
20

20 was synthesised by Prof. Raphael Tripier's group.

6.7.2. Tetra-tert-butyl 2,2',2'',2'''-(6-(2-aminoethyl)-1,4,8,11-tetraazacyclotetradecane-1,4,8,11-tetrayl)tetraacetate
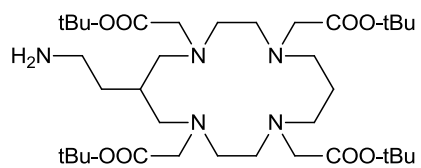
21

21 was synthesised by Prof. Raphael Tripier's group.

6.7.3. tetra-tert-butyl 2,2',2'',2'''-(6-(2-hydroxyethyl)-1,4,8,11-tetraazacyclotetradecane-1,4,8,11-tetrayl)tetraacetate
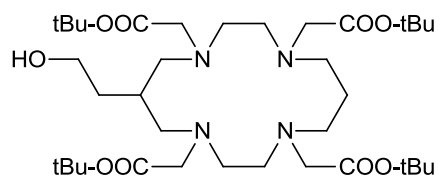
22

22 was synthesised by Prof. Raphael Tripier's group.

6.7.4. Synthesis of tri-*tert*-butyl 2,2',2''-(10-(2-hydroxy-3-(3-(triethoxysilyl)propoxy)propyl)-1,4,7,10-tetraazacyclododecane-1,4,7-triyl)triacetate

23
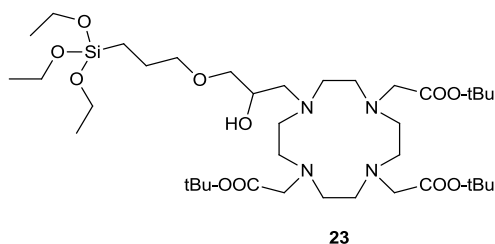
<u>Method 1 (preferred method)</u>

1,4,7-tris(*tert*-butoxycarboxymethyl)-1,4,7,10-tetraazadodecane (*t*Bu-DO3A) (**9**) (1 g, 1.94 mmol) was dissolved in CHCl$_3$ (4ml), (3-glycidyloxypropyl)triethoxysilane (GPTES) (595 mg, 2.13 mmol) in CHCl$_3$ (4 ml) was added dropwise and the reaction was heated with microwave irradiation at 90°C for 2h then concentrated *in vacuo*. The crude oil was redissolved in CHCl$_3$ (10 ml), washed with water (3 x 10 ml), dried (Na$_2$SO$_4$), filtered and concentrated *in vacuo* to yield an off white oil (1.5 g, 97%). ^{1}H-NMR (CDCl$_3$): δ 0.57-0.64 (m, 2H, CH$_2$), 1.18 (t, 9H, CH$_3$), 1.41 (m, 27H, (CH$_3$)$_3$), 1.64-1.69 (m, 2H, CH$_2$), 2.37-2.39 (m, 3H, CH$_2$), 2.56-2.59 (m, 2H, CH$_2$), 2.72-2.86 (m, 14H, CH$_2$), 3.17-3.44 (m, 10H,CH$_2$), 3.78 (q, 6H, CH$_2$). MS (ESI): 793.8 [M+H$^+$].

<u>Method 2</u>

*t*Bu-DO3A (**9**) (93 mg, 0.18 mmol) was dissolved in CHCl$_3$ (5 ml), GPTES (50 mg, 0.18 mmol) in CHCl$_3$ (5 ml) was added dropwise and the reaction was heated under reflux for 3 days then concentrated *in vacuo*. The crude oil was redissolved in CHCl$_3$ (5 ml), washed with water (5 ml), dried (Na$_2$SO$_4$), filtered and concentrated *in vacuo* to yield an off white oil (40 mg, 29%). ^{1}H-NMR (CDCl$_3$): δ 0.57-0.64 (m, 2H, CH$_2$), 1.18 (t, 9H, CH$_3$), 1.41 (m, 27H, (CH$_3$)$_3$), 1.64-1.69 (m, 2H, CH$_2$), 2.37-2.39 (m, 3H, CH$_2$), 2.56-2.59 (m, 2H, CH$_2$), 2.72-2.86 (m, 14H, CH$_2$), 3.17-3.44 (m, 10H, CH$_2$), 3.78 (q, 6H, CH$_2$). MS (ESI): 793.8 [M+H$^+$], 815.6 [M+Na$^+$], 515.3 [*t*Bu-DO3A].

Method 3

*t*Bu-DO3A (**9**) (93 mg, 0.18 mmol) was dissolved in CHCl$_3$ (5 ml), GPTES (75 mg, 0.27 mmol) in CHCl$_3$ (5 ml) was added dropwise and the reaction was heated under reflux for 3 days then concentrated *in vacuo*. The crude oil was redissolved in CHCl$_3$ (5 ml), washed with water (5 ml), dried (Na$_2$SO$_4$), filtered and concentrated *in vacuo* to yield an off white oil (90 mg). ^{1}H-NMR (CDCl$_3$): δ 0.57-0.64 (m, 2H, CH$_2$), 1.18 (t, 9H, CH$_3$), 1.41 (m, 27H, (CH$_3$)$_3$), 1.64-1.69 (m, 2H, CH$_2$), 2.37-2.39 (m, 3H, CH$_2$), 2.56-2.59 (m, 2H, CH$_2$), 2.72-2.86 (m, 14H, CH$_2$), 3.17-3.44 (m, 10H,CH$_2$), 3.78 (q, 6H, CH$_2$). MS (ESI): 793.8 [M+H$^+$], 815.5 [M+Na$^+$], 515.5 [*t*Bu-DO3A].

Method 4

*t*Bu-DO3A (**9**) (93 mg, 0.18 mmol) was dissolved in CHCl$_3$ (5 ml), GPTES (60 mg, 0.20 mmol) in CHCl$_3$ (5 ml) was added dropwise and the reaction was heated with microwave irradiation at 90°C for 30mins then concentrated *in vacuo*. The crude oil was redissolved in CHCl$_3$ (5 ml), washed with water (5 ml), dried (Na$_2$SO$_4$), filtered and concentrated *in vacuo* to yield an off white oil (90 mg 64%). ^{1}H-NMR (CDCl$_3$): δ 0.57-0.64 (m, 2H, CH$_2$), 1.18 (t, 9H, CH$_3$), 1.41 (m, 27H, (CH$_3$)$_3$), 1.64-1.69 (m, 2H, CH$_2$), 2.37-2.39 (m, 3H, CH$_2$), 2.56-2.59 (m, 2H, CH$_2$), 2.72-2.86 (m, 14H, CH$_2$), 3.17-3.44 (m, 10H,CH$_2$), 3.78 (q, 6H, CH$_2$). MS (ESI): 793.7 [M+H$^+$], 815.6 [M+Na$^+$], 515.5 [*t*Bu-DO3A].

6.7.5. Synthesis of tri-*tert*-butyl 2,2',2''-(10-((1-(2-hydroxy-3-(3-(triethoxysilyl)propoxy)propyl)-1H-benzo[d]imidazol-2-yl)methyl)-1,4,7,10-tetraazacyclododecane-1,4,7-triyl)triacetate

24
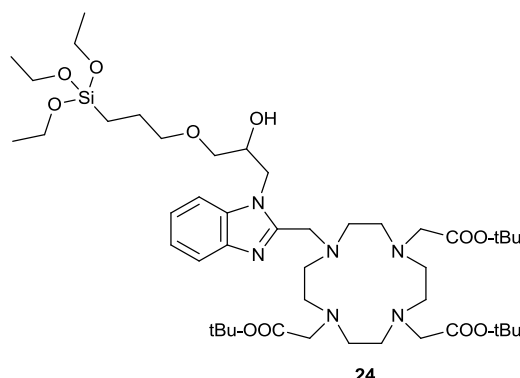
Method 1

tri-*tert*-butyl 2,2',2''-(10-((1H-benzo[d]imidazol-2-yl)methyl)-1,4,7,10-tetraazacyclododecane-1,4,7-triyl)triacetate (**11**) (116 mg, 0.18 mmol) was dissolved in CHCl$_3$ (5 ml), (3-glycidyloxypropyl)triethoxysilane (GPTES) (50 mg, 0.18 mmol) in CHCl$_3$ (4 ml) was added dropwise and the reaction was heated with microwave irradiation at 90°C for 30 mins then concentrated *in vacuo*. The crude oil was redissolved in CHCl$_3$ (4 ml), washed with water (3 x 5 ml), dried (Na$_2$SO$_4$), filtered and concentrated *in vacuo* to yield an off white oil (90 mg). MS (ESI): 923.5 [M+H$^+$].

Method 2

tri-*tert*-butyl 2,2',2''-(10-((1H-benzo[d]imidazol-2-yl)methyl)-1,4,7,10-tetraazacyclododecane-1,4,7-triyl)triacetate (**11**) (116 mg, 0.18 mmol) was dissolved in CHCl$_3$ (5 ml), (3-glycidyloxypropyl)triethoxysilane (GPTES) (60 mg, 0.22 mmol) in CHCl$_3$ (5 ml) was added dropwise and the reaction was heated under reflux for 3 days then concentrated *in vacuo*. The crude oil was redissolved in CHCl$_3$ (5 ml), washed with water (3 x 5 ml), dried (Na$_2$SO$_4$), filtered and concentrated *in vacuo* to yield an off white oil (90 mg). MS (ESI): 923.5 [M+H$^+$].

6.7.6. Synthesis of methyl 6-((11-(2-hydroxy-3-(3-(triethoxysilyl)propoxy)propyl)-1,4,8,11-tetraazabicyclo[6.6.2]hexadecan-4-yl)methyl)picolinate

25
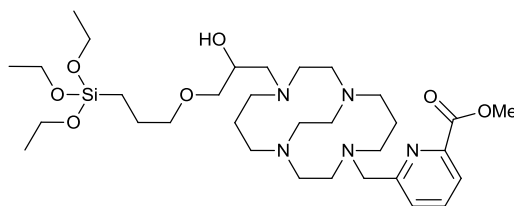
Method 1 (preferred method)

Methyl 6-(1,4,8,11-tetraazabicyclo[6.6.2]hexadecan-4-ylmethyl)picolinate hydrochloride (**21**) (200 mg, 0.485 mmol) was dissolved in $CHCl_3$ (5 ml), GPTES (135 mg, 0.485 mmol) in $CHCl_3$ (5 ml) was added dropwise and the reaction was heated under microwave irradiation at 90°C for 30mins then concentrated *in vacuo* to yield a colourless oil (300 mg, 95%). ^{1}H-NMR (CDCl$_3$): δ 0.40-0.52 (m, 2H, CH$_2$), 1.14 (t, 9H, (CH$_3$)$_3$), 1.63 (m, 5H, CH$_2$), 2.39-3.40 (m, 31H, CH$_2$), 3.58 (q, 6H, CH$_2$-O), 3.95 (s, 3H, CH$_3$), 4.06 (m, 1H, CH$_2$), 7.51 (d, 1H, CH-Ar), 7.87 (m, 1H, CH-Ar), 9.97 (m, 1H, CH-Ar). ^{13}C-NMR (CDCl$_3$): δ 6.33 (CH$_2$-Si), 18.18 ((CH$_3$)$_3$), 21.69 (N-B-CH$_2$), 22.88 (CH$_2$-CH$_2$-Si), 26.53 (N-B-CH$_2$), 44.24 (CH$_2$-O), 44.66 (N-a-CH$_2$), 47.16 (N-a-CH$_2$), 49.94 (N-a-CH$_2$), 50.77 (CH), 52.07 (N-a-CH$_2$), 52.39 (N-a-CH$_2$), 53.23 (CH$_3$-O), 53.59 (N-a-CH$_2$), 55.54 (N-a-CH$_2$), 56.22 (C$_{aminal}$-CH$_2$), 57.15 (C$_{aminal}$-CH$_2$), 58.25 (CH$_2$-N), 63.73 (CH$_2$-N), 71.27 (CH$_2$-O), 73.64 (CH$_2$-O), 124.25 (CH-Ar), 128.81 (CH-Ar), 138.94 (CH-Ar). MS (MALDI-TOF): 654.307 [M+H$^+$].

Method 2

Methyl 6-(1,4,8,11-tetraazabicyclo[6.6.2]hexadecan-4-ylmethyl)picolinate hydrochloride (**21**) (50 mg, 0.121 mmol) was dissolved in $CHCl_3$ (5 ml), GPTES (34 mg, 0.121 mmol) in $CHCl_3$ (5 ml) was added dropwise and the reaction was heated under microwave irradiation at 90°C for 30 minutes then concentrated *in vacuo* to yield a colourless oil (83 mg, 98%). MS (MALDI-TOF): 654.314 [M+H$^+$].

Methyl 6-(1,4,8,11-tetraazabicyclo[6.6.2]hexadecan-4-ylmethyl)picolinate hydrochloride (**21**) (50 mg, 0.121 mmol) was dissolved in $CHCl_3$ (5 ml), GPTES (41 mg, 0.146 mmol) in $CHCl_3$ (5 ml) was added dropwise and the reaction was heated under microwave irradiation at $90^{o}C$ for 30 minutes then concentrated *in vacuo*. The crude oil was redissolved in $CHCl_3$ (5 ml), washed with water (3 x 5 ml), dried (Na_2SO_4), filtered and concentrated *in vacuo* to yield a colourless oil (20 mg). *The desired product was not isolated using this synthetic procedure*.

6.7.7. Synthesis of tetra-*tert*-butyl 2,2',2'',2'''-(6-(4,4-diethoxy-10-hydroxy-3,8-dioxa-12-aza-4-silatetradecan-14-yl)-1,4,8,11-tetraazacyclotetradecane-1,4,8,11-tetrayl)tetraacetate
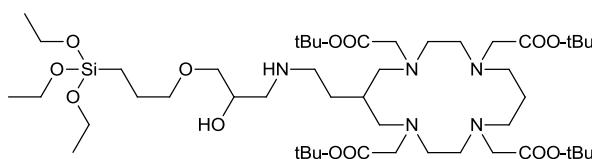
26

Method 1 (preferred method)

Tetra-*tert*-butyl 2,2',2'',2'''-(6-(2-aminoethyl)-1,4,8,11-tetraazacyclotetradecane-1,4,8,11-tetrayl)tetraacetate (**20**) (300 mg, 0.43 mmol) was dissolved in CHCl$_3$ (10 ml) and added dropwise to a solution of GPTES (119 mg, 0.43 mmol) in CHCl$_3$ (10 ml). The reaction was heated under microwave irradiation at 90°C for 30 minutes then concentrated *in vacuo* to yield a colourless oil (419 mg, 99%). ^{13}C-NMR: δ 25.40 (CH$_2$), 28.06 ((CH$_3$)$_3$), 35.13 (CH$_2$), 39.98 (CH$_2$), 51.15 (CH$_2$), 51.76 (CH$_2$), 56.92 (CH$_2$), 57.51 (CH$_2$), 59.72 (CH$_2$), 80.55 ($\underline{C}$-(CH$_3$)$_3$), 170.85 (C=O). MS (MALDI-TOF): 977.579 [M+H$^+$].

Method 2

Tetra-*tert*-butyl 2,2',2'',2'''-(6-(2-aminoethyl)-1,4,8,11-tetraazacyclotetradecane-1,4,8,11-tetrayl)tetraacetate (**20**) (23 mg, 33 μmol) was dissolved in CHCl$_3$ (1 ml) and added dropwise to a solution of GPTES (9 mg, 33 μmol) in CHCl$_3$ (1 ml). The reaction was heated under microwave irradiation at 90°C for 30 minutes then concentrated *in vacuo* to yield a colourless oil (30 mg). MS (MALDI-TOF): 977.588 [M+H$^+$].

Method 3

Tetra-*tert*-butyl 2,2',2'',2'''-(6-(2-aminoethyl)-1,4,8,11-tetraazacyclotetradecane-1,4,8,11-tetrayl)tetraacetate (**20**) (23 mg, 33 μmol) was dissolved in CHCl$_3$ (25 ml) and added dropwise to a solution of GPTES (9 mg, 33 μmol) in CHCl$_3$ (25 ml). The reaction was heated under microwave irradiation at 90°C for 30 minutes then concentrated *in vacuo* to yield a colourless oil (30 mg). MS (MALDI-TOF): 977.579 [M+H$^+$].

Tetra-*tert*-butyl 2,2',2'',2'''-(6-(2-aminoethyl)-1,4,8,11-tetraazacyclotetradecane-1,4,8,11-tetrayl)tetraacetate (**20**) (23 mg, 33 μmol) was dissolved in $CHCl_3$ (1 ml) and added dropwise to a solution of GPTES (18 mg, 66 μmol) in $CHCl_3$ (1 ml). The reaction was heated under microwave irradiation at 90°C for 30 minutes then concentrated *in vacuo* to yield a colourless oil (40 mg). MS (MALDI-TOF): 977.569 [M+H$^+$].

6.7.8. Attempted synthesis of tetra-*tert*-butyl 2,2',2'',2'''-(6-(4,4-diethoxy-10-hydroxy-3,8,12-trioxa-4-silatetradecan-14-yl)-1,4,8,11-tetraazacyclotetradecane-1,4,8,11-tetrayl)tetraacetate
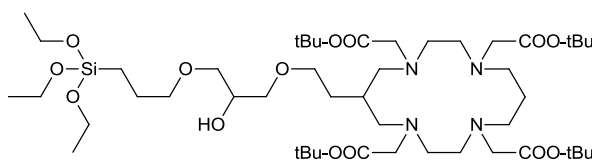
27

<u>Method 1</u>

Cu(CN)$_4$.PF$_6$ (0.71 µmol, 0.2 mg) was added to a solution of tetra-*tert*-butyl 2,2',2'',2'''-(6-(2-hydroxyethyl)-1,4,8,11-tetraazacyclotetradecane-1,4,8,11-tetrayl)tetraacetate (**22**) (50 mg, 71 µmol) and GPTES (24 mg, 86 µmol) in CHCl$_3$ (10 ml) and the reaction was heated under microwave irradiation at 90°C for 30 minutes then concentrated *in vacuo*. The crude oil was redissolved in CHCl$_3$ (5 ml), washed with water (3 x 5 ml), dried (Na$_2$SO$_4$), filtered and concentrated *in vacuo* to yield a colourless oil (20 mg). *The desired product was not isolated using this synthetic procedure*. MS (MALDI-TOF): 763.281 [SM+Cu].

<u>Method 2</u>

Activated charcoal (3 g) was treated with a mixture of concentrated nitric and sulphuric acid (1:1, 30 ml) dropwise over 15 minutes with ice cooling. The reaction then stirred at room temperature for 90 minutes, the liquid was decanted and the solid was resuspended in water (50 ml) and stirred overnight. The reaction was then filtered and concentrated *in vacuo* to yield a black solid (1.5 g). The acid activated charcoal (1 mg) was added to a solution of tetra-*tert*-butyl 2,2',2'',2'''-(6-(2-hydroxyethyl)-1,4,8,11-tetraazacyclotetradecane-1,4,8,11-tetrayl)tetraacetate (**22**) (30 mg, 43 µmol) and GPTES (12 mg, 43µmol) and the reaction was heated at 120°C for 30 minutes. The reaction was then filtered and concentrated *in vacuo* to yield a colourless oil (30 mg). *The desired product was not isolated using this synthetic procedure*.

6.7.9. "Bare" magnetite nanoparticles (data shown for comparison/reference)
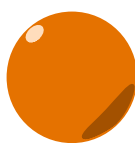
28

Synthesis was carried out by Neazar Baghdadi following literature methods.[231]

<u>NTA</u>
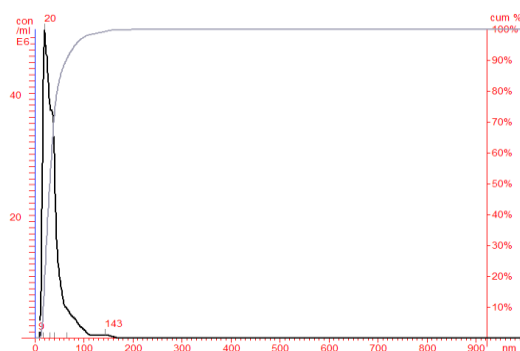
<u>TEM</u>
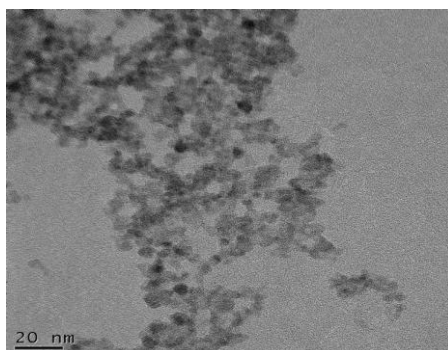
<u>ICP/CHN</u>

Element	% w/w
Si	0.0246
Ga	0.0197
Cu	0.0015
Fe	57.02
C	1.04
H	0
N	0.64

6.7.10. Synthesis of tri-*tert*-butyl 2,2',2''-(10-(2-hydroxy-3-(3-(triethoxysilyl)propoxy)propyl)-1,4,7,10-tetraazacyclododecane-1,4,7-triyl)triacetate functionalised magnetite nanoparticles

29
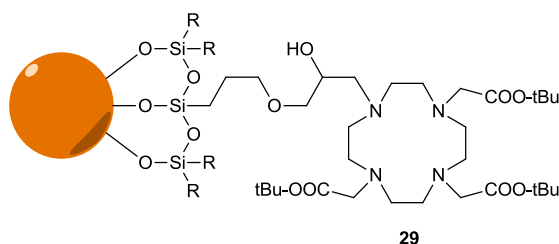
Magnetite nanoparticles (**28**) (280 mg, 1.2 mmol) were suspended in 60% EtOH (25 ml) and 28% ammonia (2.5 ml). To this mixture, tri-*tert*-butyl 2,2',2''-(10-(2-hydroxy-3-(3-(triethoxysilyl)propoxy)propyl)-1,4,7,10-tetraazacyclododecane-1,4,7-triyl)triacetate (**23**) (240 mg, 0.3 mmol) in EtOH (2 ml) was added dropwise and the reaction was stirred at rt under N_2 for 48 hours. The solid was separated using a rare earth magnet, washing successively with 60% EtOH (2 x 25 ml), EtOH (2 x 25 ml), MeOH (20 ml) and ether (20 ml) then concentrated *in vacuo* to yield a black solid (210 mg).

Element	% w/w
Si	0.640
Ga	0.008
Cu	0.004
Fe	62.264
C	5.67
H	1.28
N	0.72

6.7.11. Synthesis of methyl 6-((11-(2-hydroxy-3-(3-(triethoxysilyl)propoxy)propyl)-1,4,8,11-tetraazabicyclo[6.6.2]hexadecan-4-yl)methyl)picolinate functionalised magnetite nanoparticles

30
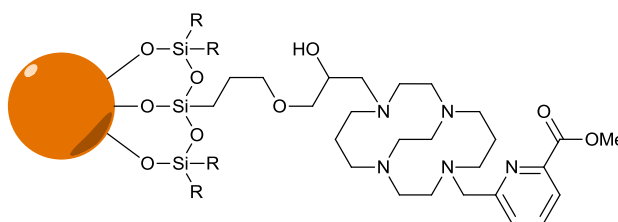
Magentite nanoparticles (**28**) (297 mg, 1.28 mmol) were suspended in 60% EtOH (25 ml) and 28% ammonia (2.5 ml). To this mixture, methyl 6-((11-(2-hydroxy-3-(3-(triethoxysilyl)propoxy)propyl)-1,4,8,11-tetraazabicyclo[6.6.2]hexadecan-4-yl)methyl)picolinate (**25**) (210 mg, 0.32 mmol) in EtOH (2 ml) was added dropwise and the reaction was stirred at rt under N_2 for 48 hours. The solid was separated using a rare earth magnet, washing successively with 60% EtOH (2 x 25 ml), EtOH (2 x 25 ml), MeOH (20 ml) and ether (20 ml) then concentrated *in vacuo* to yield a black solid (240 mg).

Element	% w/w
Si	15.512
Ga	0.000
Cu	0.000
Fe	47.276
C	2.86
H	1.38
N	0.32

6.7.12. Synthesis of tetra-*tert*-butyl 2,2',2'',2'''-(6-(4,4-diethoxy-10-hydroxy-3,8-dioxa-12-aza-4-silatetradecan-14-yl)-1,4,8,11-tetraazacyclotetradecane-1,4,8,11-tetrayl)tetraacetate functionalised magnetite nanoparticles
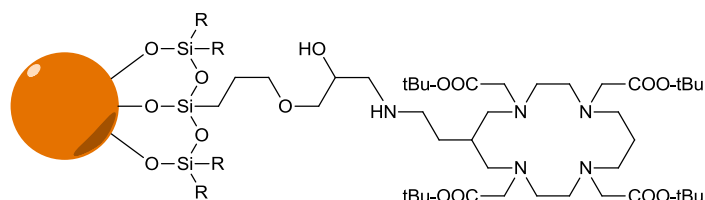

31

Magnetite nanoparticles (**28**) (397 mg, 1.7 mmol) were suspended in 60% EtOH (25 ml) and 28% ammonia (3 ml). To this mixture, tetra-*tert*-butyl 2,2',2'',2'''-(6-(4,4-diethoxy-10-hydroxy-3,8-dioxa-12-aza-4-silatetradecan-14-yl)-1,4,8,11-tetraazacyclotetradecane-1,4,8,11-tetrayl)tetraacetate (**26**) (419 mg, 0.43 mmol) in EtOH (2 ml) was added dropwise and the reaction was stirred at rt under N_2 for 48 hours. The solid was separated using a rare earth magnet, washing successively with 60% EtOH (2 x 25 ml), EtOH (2 x 25 ml), MeOH (20 ml) and ether (20 ml) then concentrated *in vacuo* to yield a black solid (187 mg).

Element	% w/w
Si	13.078
Ga	0.000
Cu	0.000
Fe	50.701
C	3.37
H	1.44
N	0.37

6.7.13. Synthesis of (3-glycidyloxypropyl)triethoxysilane functionalised magnetite nanoparticles

32

Magnetite nanoparticles (**28**) (309 mg, 1.34 mmol) were suspended in 60% EtOH (25 ml) and 28% ammonia (2.5 ml). To this mixture, GPTES (93 mg, 0.335 mmol) in EtOH (2 ml) was added dropwise and the reaction was stirred at rt under N_2 for 48 hours. The solid was separated using a rare earth magnet, washing successively with 60% EtOH (2 x 25 ml), EtOH (2 x 25 ml), MeOH (20 ml) and ether (20 ml) then concentrated *in vacuo* to yield a black solid (282 mg).

Element	% w/w
Si	1.3435
Ga	0.0032
Cu	0.0002
Fe	55.73
C	3.85
H	0.00
N	0.45

6.7.14. Synthesis of triethoxy(ethyl) silane functionalised magnetite nanoparticles
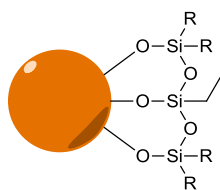
33

Magnetite nanoparticles (**28**) (309 mg, 1.34 mmol) were suspended in 60% EtOH (25 ml) and 28% ammonia (2.5 ml). To this mixture, triethoxy(ethyl) silane (64 mg, 0.335 mmol) in EtOH (2 ml) was added dropwise and the reaction was stirred at rt under N_2 for 48 hours. The solid was separated using a rare earth magnet, washing successively with 60% EtOH (2 x 25 ml), EtOH (2 x 25 ml), MeOH (20 ml) and ether (20 ml) then concentrated *in vacuo* to yield a black solid (235 mg). NTA (nm): mean = 353, mode = 154, SD = 252.

Element	% w/w
Si	27.935
Ga	0.0003
Cu	0.0005
Fe	52.646
C	1.73
H	0.00
N	0.00

6.7.15. Synthesis of 2,2',2''-(10-(3-(3-(dihydroxysilyl)propoxy)-2-hydroxypropyl)-1,4,7,10-tetraazacyclododecane-1,4,7-triyl)triacetic acid functionalised magnetite nanoparticles


34
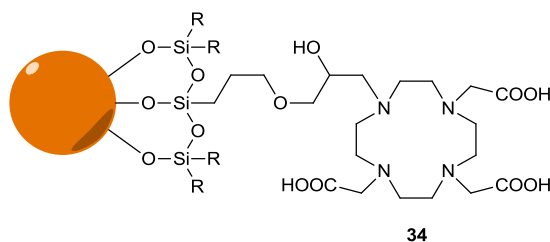
Magnetite nanoparticles functionalised with tri-*tert*-butyl 2,2',2''-(10-(2-hydroxy-3-(3-(triethoxysilyl)propoxy)propyl)-1,4,7,10-tetraazacyclododecane-1,4,7-triyl)triacetate (**29**) (170 mg) was suspended in DCM (20 ml) and added TFA (2 ml) and the reaction was shaken at rt for 24 hours. The solid was separated using a rare earth magnet, washing successively with EtOH (2 x 20 ml), MeOH (20 ml) and ether (20 ml) then concentrated *in vacuo* to yield a black solid (143 mg). NTA (nm): mean = 125, mode = 34, SD = 115.

Element	% w/w
Si	1.976
Ga	0.002
Cu	0.003
Fe	50.648
C	4.87
H	0.86
N	0.43

6.7.16. Synthesis of 2,2',2'',2'''-(6-(2-((3-(3-(dihydroxysilyl)propoxy)-2-hydroxypropyl)amino)ethyl)-1,4,8,11-tetraazacyclotetradecane-1,4,8,11-tetrayl)tetraacetic acid functionalised magnetite nanoparticles

35
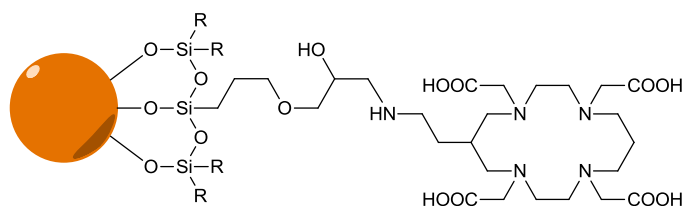
Magnetite nanoparticles functionalised with tetra-*tert*-butyl 2,2',2'',2'''-(6-(4,4-diethoxy-10-hydroxy-3,8-dioxa-12-aza-4-silatetradecan-14-yl)-1,4,8,11-tetraazacyclotetradecane-1,4,8,11-tetrayl)tetraacetate (**31**) (150 mg) was suspended in DCM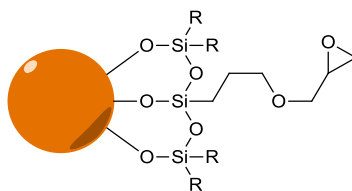 (20 ml) and added TFA (2 ml) and the reaction was shaken at rt for 24 hours. The solid was separated using a rare earth magnet, washing successively with DCM (2 x 20 ml) and ether (20 ml) then concentrated *in vacuo* to yield a black solid (150 mg). NTA (nm): mean = 248, mode = 198, SD = 112.

Element	% w/w
Si	9.724
Ga	0.000
Cu	0.000
Fe	40.585
C	4.80
H	1.14
N	0.24

6.7.17. Synthesis of 6-((11-(3-(3-(dihydroxysilyl)propoxy)-2-hydroxypropyl)-1,4,8,11-tetraazabicyclo[6.6.2]hexadecan-4-yl)methyl)picolinic acid functionalised magnetite nanoparticles

36
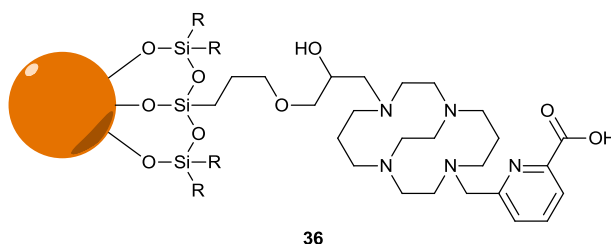
Magnetite nanoparticles functionalised methyl 6-((11-(2-hydroxy-3-(3-(triethoxysilyl)propoxy)propyl)-1,4,8,11-tetraazabicyclo[6.6.2]hexadecan-4-yl)methyl)picolinate (**30**) (100 mg) was suspended in 60% EtOH (15 ml) and added LiOH (6 mg, 0.218 mmol) and the reaction was shaken at rt for 24 hours. The solid was separated using a rare earth magnet, washing successively with 60% EtOH (2 x 20 ml), EtOH (2 x 20 ml), MeOH (20 ml) and ether (20 ml) then concentrated *in vacuo* to yield a black solid (58 mg). NTA (nm): mean = 134, mode = 95, SD = 69.

Element	% w/w
Si	17.731
Ga	0.000
Cu	0.000
Fe	44.194
C	2.60
H	1.32
N	0.24

6.7.18. Synthesis of $^{69/71}$Ga complex of 2,2',2''-(10-(3-(3-(dihydroxysilyl)propoxy)-2-hydroxypropyl)-1,4,7,10-tetraazacyclododecane-1,4,7-triyl)triacetic acid functionalised magnetite nanoparticles

[Ga$_n$**34**]
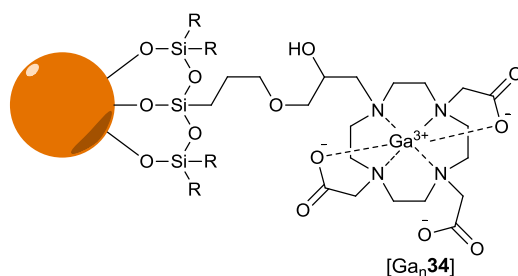
Magnetite nanoparticles functionalised with 2,2',2''-(10-(3-(3-(dihydroxysilyl)propoxy)-2-hydroxypropyl)-1,4,7,10-tetraazacyclododecane-1,4,7-triyl)triacetic acid (**34**) (50 mg, 0.38 mmol) was suspended in 60% EtOH (20 ml) and added GaCl$_3$ (7.4 mg, 42 µmol) and the reaction was shaken at rt for 24 hours. The solid was separated using a rare earth magnet, washing successively with 60% EtOH (2 x 20 ml), EtOH (2 x 20 ml), MeOH (20 ml) and ether (20 ml) then concentrated *in vacuo* to yield a black solid (21 mg). NTA (nm): mean = 300, mode = 223, SD = 149.

Element	% w/w
Si	2.601
Ga	3.784
Cu	0.090
Fe	53.507
C	2.53
H	0.00
N	0.37

### 6.7.19. Synthesis of $^{63/65}$Cu complex of 2,2',2''-(10-(3-(3-(dihydroxysilyl)propoxy)-2-hydroxypropyl)-1,4,7,10-tetraazacyclododecane-1,4,7-triyl)triacetic acid functionalised magnetite nanoparticles

[Cu$_n$**34**]
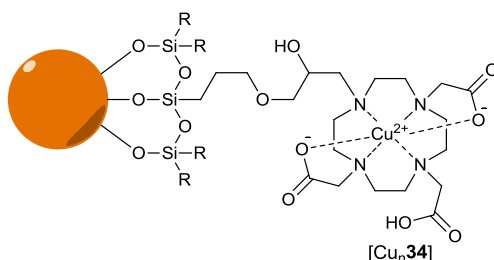
Magnetite nanoparticles functionalised with 2,2',2''-(10-(3-(3-(dihydroxysilyl)propoxy)-2-hydroxypropyl)-1,4,7,10-tetraazacyclododecane-1,4,7-triyl)triacetic acid (**34**) (50 mg, 0.38 mmol) was suspended in 60% EtOH (20 ml) and added Cu(OAc)$_2$.H$_2$O (8.4 mg, 42 µmol) and the reaction was shaken at rt for 24 hours. The solid was separated using a rare earth magnet, washing successively with 60% EtOH (2 x 20 ml), EtOH (2 x 20 ml), MeOH (20 ml) and ether (20 ml) then concentrated *in vacuo* to yield a black solid (24 mg). NTA (nm): mean = 297, mode = 362, SD = 126.

Element	% w/w
Si	2.169
Ga	1.970
Cu	2.119
Fe	55.021
C	3.47
H	0.00
N	0.40

6.7.20. Synthesis of [69/71]Ga complex of 2,2',2'',2'''-(6-(2-((3-(3-(dihydroxysilyl)propoxy)-2-hydroxypropyl)amino)ethyl)-1,4,8,11-tetraazacyclotetradecane-1,4,8,11-tetrayl)tetraacetic acid functionalised magnetite nanoparticles


[Ga_n**35**]
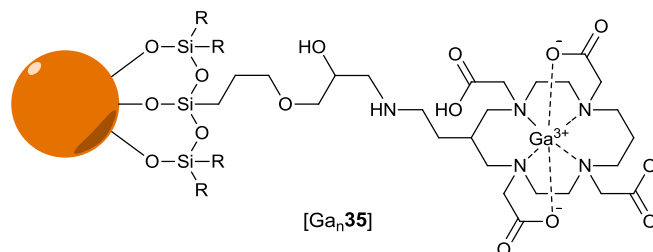
Magnetite nanoparticles functionalised with 2,2',2'',2'''-(6-(2-((3-(3-(dihydroxysilyl)propoxy)-2-hydroxypropyl)amino)ethyl)-1,4,8,11-tetraazacyclotetradecane-1,4,8,11-tetrayl)tetraacetic acid (**35**) (50 mg, 0.30 mmol) was suspended in 60% EtOH (20 ml) and added $GaCl_3$ (6.5 mg, 36 μmol) and the reaction was shaken at rt for 24 hours. The solid was separated using a rare earth magnet, washing successively with 60% EtOH (2 x 20 ml), EtOH (2 x 20 ml), MeOH (20 ml) and ether (20 ml) then concentrated *in vacuo* to yield a black solid (5.2 mg). NTA (nm): mean = 103, mode = 94, SD = 40.

Element	% w/w
Si	33.771
Ga	6.070
Cu	0.026
Fe	38.643
C	3.20
H	0.98
N	0.29

6.7.21. Synthesis of $^{63/65}$Cu complex of 2,2',2'',2'''-(6-(2-((3-(3-(dihydroxysilyl)propoxy)-2-hydroxypropyl)amino)ethyl)-1,4,8,11-tetraazacyclotetradecane-1,4,8,11-tetrayl)tetraacetic acid functionalised magnetite nanoparticles

[Cu$_n$**35**]
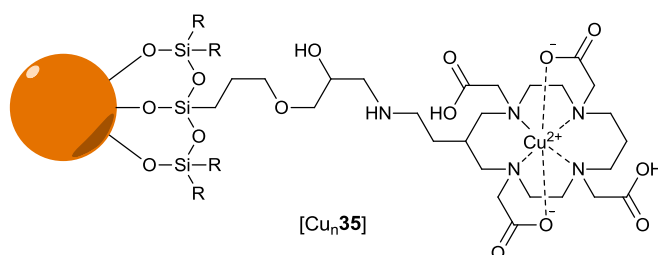
Magnetite nanoparticles functionalised with 2,2',2'',2'''-(6-(2-((3-(3-(dihydroxysilyl)propoxy)-2-hydroxypropyl)amino)ethyl)-1,4,8,11-tetraazacyclotetradecane-1,4,8,11-tetrayl)tetraacetic acid (**35**) (50 mg, 0.36 mmol) was suspended in 60% EtOH (20 ml) and added Cu(OAc)$_2$.H$_2$O (7.2 mg, 36 µmol) and the reaction was shaken at rt for 24 hours. The solid was separated using a rare earth magnet, washing successively with 60% EtOH (2 x 20 ml), EtOH (2 x 20 ml), MeOH (20 ml) and ether (20 ml) then concentrated *in vacuo* to yield a black solid (6.3 mg). NTA (nm): mean = 266, mode = 207, SD = 98.

Element	% w/w
Si	37.285
Ga	0.02
Cu	0.842
Fe	46.154
C	4.43
H	1.37
N	0.36

6.7.22. Synthesis of ^{69/71}Ga complex of 6-((11-(3-(3-(dihydroxysilyl)propoxy)-2-hydroxypropyl)-1,4,8,11-tetraazabicyclo[6.6.2]hexadecan-4-yl)methyl)picolinic acid functionalised magnetite nanoparticles

[Ga$_n$**36**]
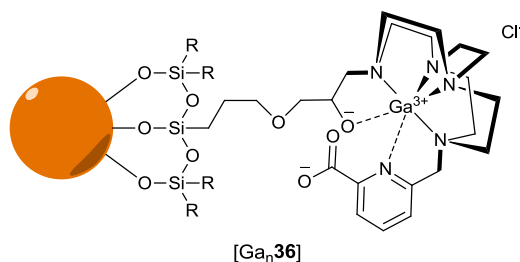
Magnetite nanoparticles functionalised with 6-((11-(3-(3-(dihydroxysilyl)propoxy)-2-hydroxypropyl)-1,4,8,11-tetraazabicyclo[6.6.2]hexadecan-4-yl)methyl)picolinic acid (**36**) (25 mg, 18.6 μmol) was suspended in 60% EtOH (20 ml) and added GaCl$_3$ (3.9 mg, 22.4 μmol) and the reaction was shaken at rt for 24 hours. The solid was separated using a rare earth magnet, washing successively with 60% EtOH (2 x 20 ml), EtOH (2 x 20 ml), MeOH (20 ml) and ether (20 ml) then concentrated *in vacuo* to yield a black solid (8 mg). NTA (nm): mean = 131, mode = 45, SD = 86.

Element	% w/w
Si	13.041
Ga	3.814
Cu	0.025
Fe	31.737

6.7.23. Synthesis of [63/65]Cu complex of 6-((11-(3-(3-(dihydroxysilyl)propoxy)-2-hydroxypropyl)-1,4,8,11-tetraazabicyclo[6.6.2]hexadecan-4-yl)methyl)picolinic acid functionalised magnetite nanoparticles

[Cu$_n$**36**]
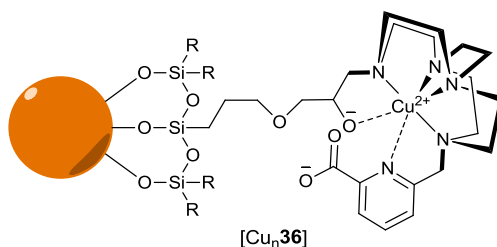
Magnetite nanoparticles functionalised with 6-((11-(3-(3-(dihydroxysilyl)propoxy)-2-hydroxypropyl)-1,4,8,11-tetraazabicyclo[6.6.2]hexadecan-4-yl)methyl)picolinic acid (**36**) (25 mg, 18.6 μmol) was suspended in 60% EtOH (20 ml) and added Cu(OAc)$_2$.H$_2$O (4.4 mg, 22.4 μmol) and the reaction was shaken at rt for 24 hours. The solid was separated using a rare earth magnet, washing successively with 60% EtOH (2 x 20 ml), EtOH (2 x 20 ml), MeOH (20 ml) and ether (20 ml) then concentrated *in vacuo* to yield a black solid (6 mg). NTA (nm): mean = 112, mode = 99, SD = 43.

Element	% w/w
Si	38.676
Ga	0.021
Cu	2.515
Fe	33.601

209

6.7.24. Synthesis of $^{69/71}$Ga complex of magnetite nanoparticles
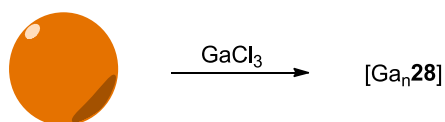
Magnetite nanoparticles (**28**) (100 mg, 0.42 mmol) was suspended in 60% EtOH (20 ml) and added $GaCl_3$ (296 mg, 1.72 mmol) and the reaction was shaken at rt for 24 hours. The solid was separated using a rare earth magnet, washing successively with 60% EtOH (2 x 20 ml), EtOH (2 x 20 ml), MeOH (20 ml) and ether (20 ml) then concentrated *in vacuo* to yield a black solid (62 mg).

Element	% w/w
Si	0.000
Ga	9.968
Cu	0.014
Fe	45.090
C	0.47
H	0.00
N	0.00

6.7.25. Synthesis of [63/65]Cu complex of magnetite nanoparticles
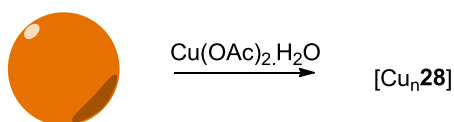
Magnetite nanoparticles (**28**) (100 mg, 0.42 mmol) was suspended in 60% EtOH (20 ml) and added $Cu(OAc)_2.H_2O$ (345 mg, 1.73 mmol) and the reaction was shaken at rt for 24 hours. The solid was separated using a rare earth magnet, washing successively with 60% EtOH (2 x 20 ml), EtOH (2 x 20 ml), MeOH (20 ml) and ether (20 ml) then concentrated *in vacuo* to yield a black solid (48 mg).

Element	% w/w
Si	0.000
Ga	0.000
Cu	13.189
Fe	42.390
C	1.77
H	0.00
N	0.00

6.7.26. Synthesis of [69/71]Ga complex of (3-glycidyloxypropyl)triethoxysilane functionalised magnetite nanoparticles
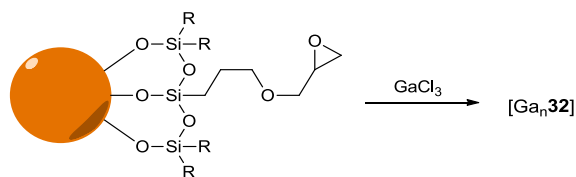
Magnetite nanoparticles functionalised with GPTES (**32**) (100 mg, 0.14 mmol) was suspended in 60% EtOH (20 ml) and added $GaCl_3$ (76 mg, 0.43 mmol) and the reaction was shaken at rt for 24 hours. The solid was separated using a rare earth magnet, washing successively with 60% EtOH (2 x 20 ml), EtOH (2 x 20 ml), MeOH (20 ml) and ether (20 ml) then concentrated *in vacuo* to yield a black solid (59 mg).

Element	% w/w
Si	0.594
Ga	5.779
Cu	0.006
Fe	51.623
C	2.41
H	0.00
N	0.00

6.7.27. Synthesis of $^{63/65}$Cu complex of (3-glycidyloxypropyl)triethoxysilane functionalised magnetite nanoparticles
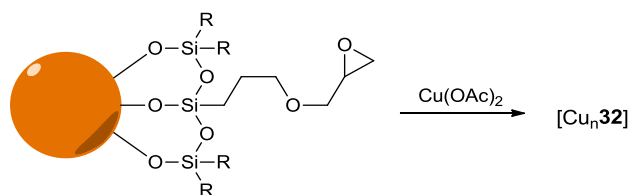
Magnetite nanoparticles functionalised with GPTES (**32**) (100 mg, 0.14 mmol) was suspended in 60% EtOH (20 ml) and added Cu(OAc)$_2$.H$_2$O (86 mg, 0.43 mmol) and the reaction was shaken at rt for 24 hours. The solid was separated using a rare earth magnet, washing successively with 60% EtOH (2 x 20 ml), EtOH (2 x 20 ml), MeOH (20 ml) and ether (20 ml) then concentrated *in vacuo* to yield a black solid (72 mg).

Element	% w/w
Si	0.901
Ga	0.04
Cu	5.193
Fe	52.359
C	3.91
H	0.98
N	0.30

6.7.28. Synthesis of [69/71]Ga complex of triethoxy(ethyl) silane functionalised magnetite nanoparticles
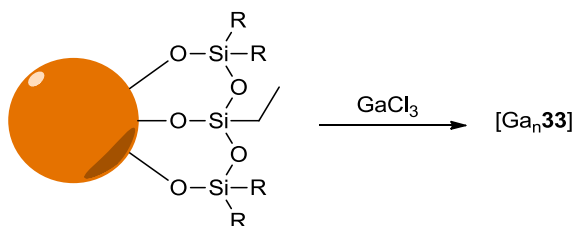
Magnetite nanoparticles functionalised with triethoxy(ethyl) silane (**33**) (100 mg, 0.54 mmol) was suspended in 60% EtOH (20 ml) and added $GaCl_3$ (106 mg, 0.6 mmol) and the reaction was shaken at rt for 24 hours. The solid was separated using a rare earth magnet, washing successively with 60% EtOH (2 x 20 ml), EtOH (2 x 20 ml), MeOH (20 ml) and ether (20 ml) then concentrated *in vacuo* to yield a black solid (20 mg). NTA (nm): mean = 443, mode = 328, SD = 199.

Element	% w/w
Si	13.946
Ga	5.518
Cu	0.000
Fe	41.167
C	3.06
H	0.97
N	0.00

6.7.29. Synthesis of [63/65]Cu complex of triethoxy(ethyl) silane functionalised magnetite nanoparticles
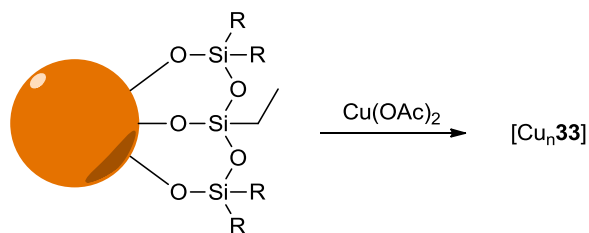
Magnetite nanoparticles functionalised with triethoxy(ethyl) silane (**33**) (100 mg, 0.54 mmol) was suspended in 60% EtOH (20 ml) and added $Cu(OAc)_2.H_2O$ (118 mg, 0.6 mmol) and the reaction was shaken at rt for 24 hours. The solid was separated using a rare earth magnet, washing successively with 60% EtOH (2 x 20 ml), EtOH (2 x 20 ml), MeOH (20 ml) and ether (20 ml) then concentrated *in vacuo* to yield a black solid (56 mg). NTA (nm): mean = 256, mode = 189, SD = 118.

Element	% w/w
Si	15.858
Ga	0.002
Cu	5.891
Fe	34.153
C	2.37
H	0.75
N	0.00

6.7.30. 2,2',2''-(10-(2-((diphosphonomethyl)amino)-2-oxoethyl)-1,4,7,10-tetraazacyclododecane-1,4,7-triyl)triacetic acid
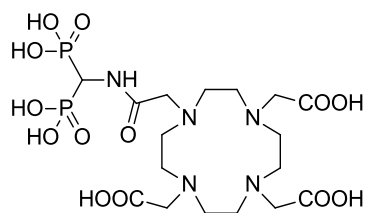
37

37 was synthesised by Prof. Raphael Tripier's group.

6.7.31. 2,2',2'',2'''-(6-(2-((2-((diphosphonomethyl)amino)-2-oxoethyl)amino)ethyl)-1,4,8,11-tetraazacyclotetradecane-1,4,8,11-tetrayl)tetraacetic acid
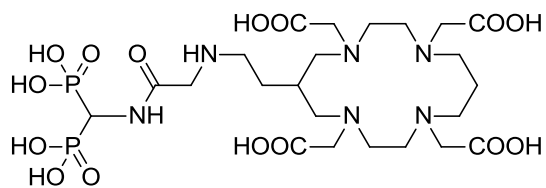
38

38 was synthesised by Prof. Raphael Tripier's group.

6.7.32. 6-((11-(2-((diphosphonomethyl)amino)-2-oxoethyl)-1,4,8,11-tetraazabicyclo[6.6.2]hexadecan-4-yl)methyl)picolinic acid
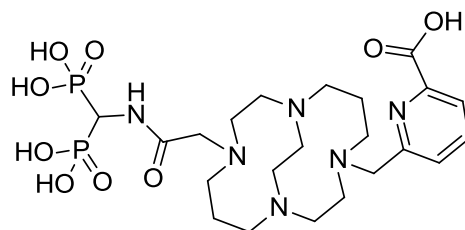
39

39 was synthesised by Prof. Raphael Tripier's group.

6.7.33. (1-(hydrogen phosphonato)-1-hydroxydecyl)phosphonate

$$O=P-O^-$$

with substituents: O^- above, HO and $O=P$ with HO below, chain $(CH_2)_7$ CH$_3$
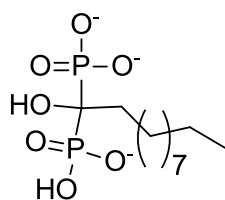
40

40 was synthesised by Dr. Maelle Monteil.

6.7.34. Synthesis of (1-(hydrogen phosphonato)-1-hydroxydecyl)phosphonate derivatised Endorem
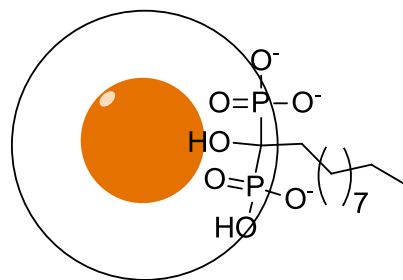
41

(1-(hydrogen phosphonato)-1-hydroxydecyl)phosphonate (**40**) in 0.15M sodium carbonate buffer (pH 7, 9 ml) was added to Endorem (20 mg, 6.4 μmol, 0.33 μM) and the reaction was heated to 100°C for 30 minutes. The vial was then left to cool and dialysed overnight to yield a brown suspension (20 ml, 0.15 μM).

6.7.35. Synthesis of ((2-(4,7,10-tris(carboxymethyl)-1,4,7,10-tetraazacyclododecan-1-yl)acetamido)methylene)bis(hydrogen phosphonate) derivatised Endorem
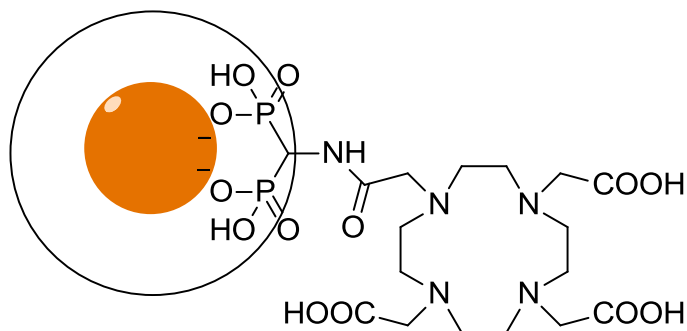
42

((2-(4,7,10-tris(carboxymethyl)-1,4,7,10-tetraazacyclododecan-1-yl)acetamido)methylene)bis(hydrogen phosphonate) (**37**) in 0.15 M sodium carbonate buffer (pH 7, 9 ml) was added to Endorem (20 mg, 6.4 μmol, 0.33 μM) and the reaction was heated to 100°C for 30 minutes. The vial was then left to cool and dialysed overnight to yield a brown suspension (20 ml, 0.15 μM).

6.7.36. Synthesis of ((2-((2-(1,4,8,11-tetrakis(carboxymethyl)-1,4,8,11-tetraazacyclotetradecan-6-yl)ethyl)amino)acetamido)methylene)bis(hydrogen phosphonate) derivatised Endorem

43
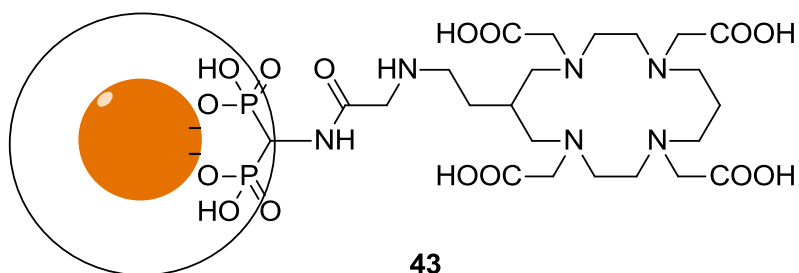
((2-((2-(1,4,8,11-tetrakis(carboxymethyl)-1,4,8,11-tetraazacyclotetradecan-6-yl)ethyl)amino)acetamido)methylene)bis(hydrogen phosphonate (**38**) in 0.15 M sodium carbonate buffer (pH 7, 9 ml) was added to Endorem (20 mg, 6.4 μmol, 0.33 μM) and the reaction was heated to 100°C for 30 minutes. The vial was then left to cool and dialysed overnight to yield a brown suspension (20 ml, 0.15 μM).

6.7.37. Synthesis of ((2-(11-((6-carboxypyridin-2-yl)methyl)-1,4,8,11-tetraazabicyclo[6.6.2]hexadecan-4-yl)acetamido)methylene)bis(hydrogen phosphonate) derivatised Endorem
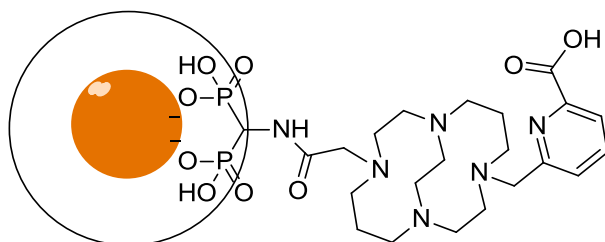
44

((2-(11-((6-carboxypyridin-2-yl)methyl)-1,4,8,11-tetraazabicyclo[6.6.2]hexadecan-4-yl)acetamido)methylene)bis(hydrogen phosphonate) (**39**) in 0.15 M sodium carbonate buffer (pH 7, 9 ml) was added to Endorem (20 mg, 6.4 μmol, 0.33 μM) and the reaction was heated to 100°C for 30 minutes The vial was then left to cool and dialysed overnight to yield a brown suspension (20 ml, 0.15 μM).

6.8. MNP radiochemistry

6.8.1. Synthesis of ^{68}Ga complex of (1-(hydrogen phosphonato)-1-hydroxydecyl)phosphonate derivatised Endorem

41
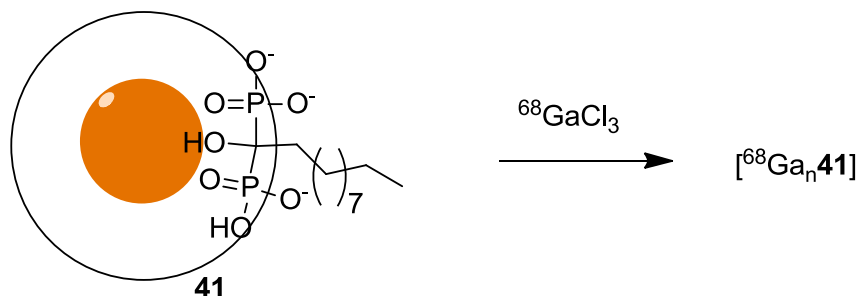
Method 1

(1-(hydrogen phosphonato)-1-hydroxydecyl)phosphonate derivatised Endorem (**41**) (200 μl, 1 mM effective iron concentration) in ammonium acetate buffer (O.2 M, pH 5) was added to formulated ^{68}GaCl$_3$ (75 MBq) and the reaction was mixed at room temperature using a vortex stirrer for 40 minutes.

Radio-TLC	
Time (mins)	% RCY
5	41.48
10	62.98
15	55.67
20	63.86
25	45.91
30	79.06
35	82.12
40	82.65

Method 2

1-(hydrogen phosphonato)-1-hydroxydecyl)phosphonate derivatised Endorem (**41**) (200 μl, 1 mM effective iron concentration) in ammonium acetate buffer (O.2 M, pH 5) was added to formulated ^{68}GaCl$_3$ (30 MBq) and the reaction was heated at 90°C for 15 minutes. RCY (radio-TLC): 95.59%.

6.8.2. Synthesis of ^{68}Ga complex of ((2-(4,7,10-tris(carboxymethyl)-1,4,7,10-tetraazacyclododecan-1-yl)acetamido)methylene)bis(hydrogen phosphonate) derivatised Endorem

$[^{68}Ga_n42]$

Method 1

((2-(4,7,10-tris(carboxymethyl)-1,4,7,10-tetraazacyclododecan-1-yl)acetamido)methylene)bis(hydrogen phosphonate) derivatised Endorem (**42**) (200 µl, 1 mM effective iron concentration) in ammonium acetate buffer (O.2 M, pH 5) was added to formulated ^{68}GaCl$_3$ (77 MBq) and the reaction was mixed at room temperature using a vortex stirrer for 30 minutes.

Radio-TLC	
Time (mins)	% RCY
5	78.86
10	96.20
15	91.82
20	76.25
25	72.06
30	97.88

Method 2

((2-(4,7,10-tris(carboxymethyl)-1,4,7,10-tetraazacyclododecan-1-yl)acetamido)methylene)bis(hydrogen phosphonate) derivatised Endorem (**42**) (200 µl, 1 mM effective iron concentration) in ammonium acetate buffer (O.2 M, pH 5) was added to formulated ^{68}GaCl$_3$ (36.6 MBq) and the reaction was mixed at 90°C for 15 minutes. RCY (radio-TLC): 100%.

6.8.3. Synthesis of ^{68}Ga complex of ((2-((2-(1,4,8,11-tetrakis(carboxymethyl)-1,4,8,11-tetraazacyclotetradecan-6-yl)ethyl)amino)acetamido)methylene)bis(hydrogen phosphonate) derivatised Endorem

$[^{68}Ga_n43]$
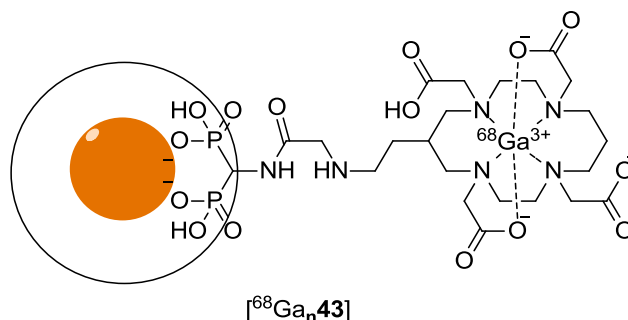
Method 1

((2-((2-(1,4,8,11-tetrakis(carboxymethyl)-1,4,8,11-tetraazacyclotetradecan-6-yl)ethyl)amino)acetamido)methylene)bis(hydrogen phosphonate) derivatised Endorem (**43**) (200 µl, 1 mM effective iron concentration) in ammonium acetate buffer (O.2 M, pH 5) was added to formulated ^{68}GaCl$_3$ (70 MBq) and the reaction was mixed at room temperature using a vortex stirrer for 25 minutes.

Radio-TLC	
Time (mins)	% RCY
5	73.94
10	100
15	73.91
20	100
25	72.31

Method 2

((2-((2-(1,4,8,11-tetrakis(carboxymethyl)-1,4,8,11-tetraazacyclotetradecan-6-yl)ethyl)amino)acetamido)methylene)bis(hydrogen phosphonate) derivatised Endorem (**43**) (200 µl, 1m M effective iron concentration) in ammonium acetate buffer (O.2 M, pH 5) was added to formulated ^{68}GaCl$_3$ (40 MBq) and the reaction was mixed at 90°C for 15 minutes. RCY (radio-TLC): 100%.

6.8.4. Synthesis of ^{68}Ga complex of ((2-(11-((6-carboxypyridin-2-yl)methyl)-1,4,8,11-tetraazabicyclo[6.6.2]hexadecan-4-yl)acetamido)methylene)bis(hydrogen phosphonate) derivatised Endorem

[^{68}Ga$_n$**44**]
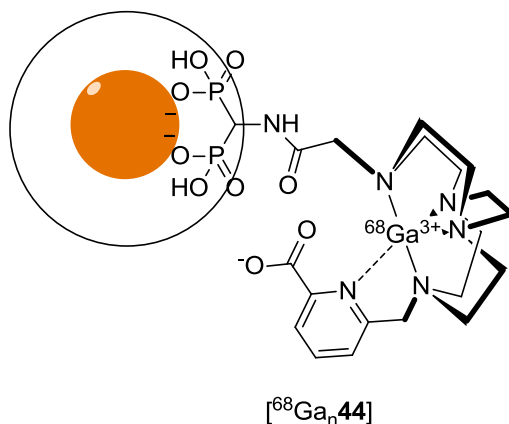
<u>Method 1</u>

((2-(11-((6-carboxypyridin-2-yl)methyl)-1,4,8,11-tetraazabicyclo[6.6.2]hexadecan-4-yl)acetamido)methylene)bis(hydrogen phosphonate) derivatised Endorem (**44**) (200 μl, 1 mM effective iron concentration) in ammonium acetate buffer (O.2 M, pH 5) was added to formulated ^{68}GaCl$_3$ (30.6 MBq) and the reaction was mixed at room temperature using a vortex stirrer for 30 minutes.

Radio-TLC	
Time (mins)	% RCY
5	56.61
10	100
15	71.22
20	47.87
25	76.34
30	95.32

<u>Method 2</u>

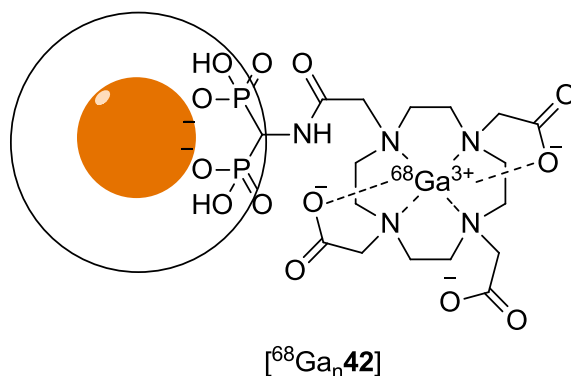((2-(11-((6-carboxypyridin-2-yl)methyl)-1,4,8,11-tetraazabicyclo[6.6.2]hexadecan-4-yl)acetamido)methylene)bis(hydrogen phosphonate) derivatised Endorem (**44**) (200 μl, 1 mM effective iron concentration) in ammonium acetate buffer (O.2 M, pH 5) was added to formulated ^{68}GaCl$_3$ (18.8 MBq) and the reaction was mixed at 90°C for 15 minutes. RCY (radio-TLC): 92.38%.

227

6.8.5. Synthesis of 68Ga complex of triethoxy(ethyl) silane functionalised magnetite nanoparticles
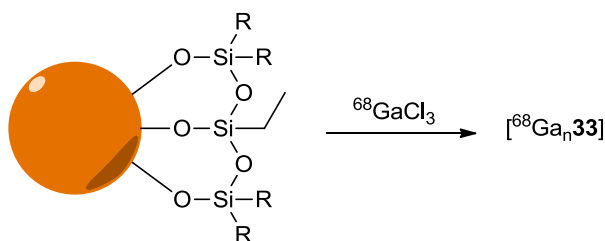
Triethoxy(ethyl) silane functionalised magnetite nanoparticles (**33**) (200 μl, 1 mM effective iron concentration) in ammonium acetate buffer (O.2 M, pH 5) was added to formulated ^{68}GaCl$_3$ (30-79 MBq) and the reaction proceeded at either room temperature or 90°C for 15 minutes.

Radio-TLC	% RCY RT (3 x replication)			% RCY 90°C (3 x replication)		
Time (mins)	1	2	3	1	2	3
0.5	57	62	64	90.76	87.5	90
3	71	82	79	100	99	98.5
5	83	81.2	84.5	94.91	99	100
10	77	87.7	83.6	94.31	99	100
15	79	98	81.6	90.2	100	100

6.8.6. Synthesis of ^{68}Ga complex of 2,2',2''-(10-(3-(3-(dihydroxysilyl)propoxy)-2-hydroxypropyl)-1,4,7,10-tetraazacyclododecane-1,4,7-triyl)triacetic acid functionalised magnetite nanoparticles

$[^{68}Ga_n34]$
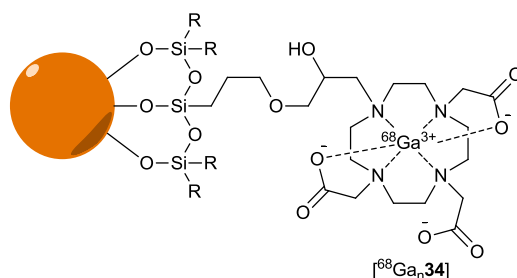
2,2',2''-(10-(3-(3-(dihydroxysilyl)propoxy)-2-hydroxypropyl)-1,4,7,10-tetraazacyclododecane-1,4,7-triyl)triacetic acid functionalised magnetite nanoparticles (**34**) (200 µl, 1mM effective iron concentration) in ammonium acetate buffer (O.2 M, pH 5) was added to formulated ^{68}GaCl$_3$ (32-78 MBq) and the reaction proceeded at either room temperature or 90°C for 15 minutes.

Radio-TLC	% RCY RT (3 x replication)			% RCY 90°C (3 x replication)		
Time (mins)	1	2	3	1	2	3
0.5	35	20	52	100	64.7	82
3	47	35.5	71	100	94	93.7
5	37	28.4	74	100	97	97
10	47	37.4	78	100	98	99
15	41	33.5	78	100	99	99

6.8.7. Synthesis of ^{68}Ga complex of 2,2',2'',2'''-(6-(2-((3-(3-(dihydroxysilyl)propoxy)-2-hydroxypropyl)amino)ethyl)-1,4,8,11-tetraazacyclotetradecane-1,4,8,11-tetrayl)tetraacetic acid functionalised magnetite nanoparticles

$[^{68}Ga_n35]$
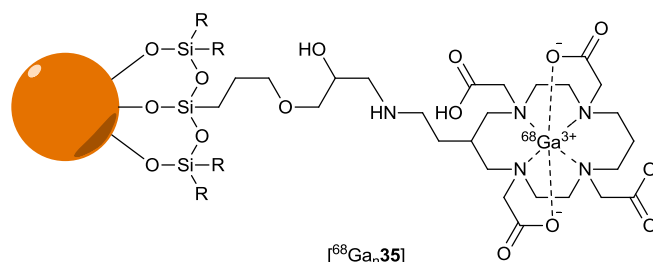
2,2',2'',2'''-(6-(2-((3-(3-(dihydroxysilyl)propoxy)-2-hydroxypropyl)amino)ethyl)-1,4,8,11-tetraazacyclotetradecane-1,4,8,11-tetrayl)tetraacetic acid functionalised magnetite nanoparticles (**35**) (200 µl, 1 mM effective iron concentration) in ammonium acetate buffer (O.2 M, pH 5) was added to formulated ^{68}GaCl$_3$ (34-66 MBq) and the reaction proceeded at either room temperature or 90°C for 15 minutes.

Radio-TLC	% RCY RT (3 x replication)			% RCY 90°C (3 x replication)		
Time (mins)	1	2	3	1	2	3
0.5	6.38	24	18.6	47.94	92	95
3	17.9	42	54	93.14	99	100
5	21.33	46.8	47	100	100	100
10	28.4	55.8	58	100	100	100
15	33.4	63	59	100	100	100

6.8.8. Synthesis of ⁶⁸Ga complex of 6-((11-(3-(3-(dihydroxysilyl)propoxy)-2-hydroxypropyl)-1,4,8,11-tetraazabicyclo[6.6.2]hexadecan-4-yl)methyl)picolinic acid functionalised magnetite nanoparticles

[⁶⁸Ga_n**36**]
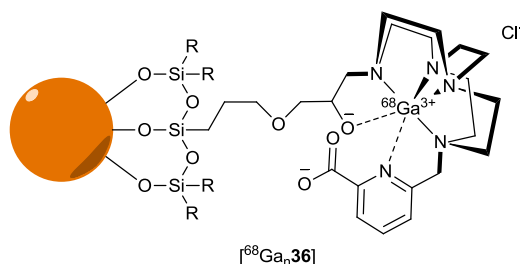
6-((11-(3-(3-(dihydroxysilyl)propoxy)-2-hydroxypropyl)-1,4,8,11-tetraazabicyclo[6.6.2]hexadecan-4-yl)methyl)picolinic acid functionalised magnetite nanoparticles (**36**) (200 μl, 1 mM effective iron concentration) in ammonium acetate buffer (O.2 M, pH 5) was added to formulated ^{68}GaCl$_3$ (31-66 MBq) and the reaction proceeded at either room temperature or 90°C for 15 minutes.

Radio-TLC	% RCY RT (3 x replication)			% RCY 90°C (3 x replication)		
Time (mins)	1	2	3	1	2	3
0.5	10.9	38	27	100	91	91.5
3	25.9	73	42	100	100	100
5	29.9	81	48	100	100	100
10	37.8	87	53	100	100	100
15	46	87	57	100	100	100

6.8.9. EDTA stability of ^{68}Ga complex of (1-(hydrogen phosphonato)-1-hydroxydecyl)phosphonate derivatised Endorem
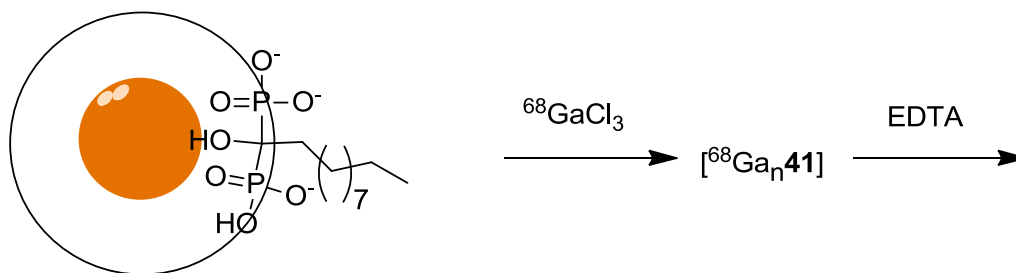
Ethyenediamineteraacetic acid (EDTA) (10 mM, 200 μl) was added to the ^{68}Ga complex of (1-(hydrogen phosphonato)-1-hydroxydecyl)phosphonate derivatised Endorem [^{68}Ga$_n$41] (200 μl, 1 mM effective iron concentration, 44 MBq) and the reaction proceeded at either room temperature or 90°C for 30 or 60 minutes.

Radio-TLC	% [68]Ga attached to nanoparticles	
Time (mins)	RT	90°C
0	82.65	95.59
15	12.13	29.28
30	7.38	3.94
45	8.86	-
60	28.25	-

6.8.10. EDTA stability of ^{68}Ga complex of ((2-(4,7,10-tris(carboxymethyl)-1,4,7,10-tetraazacyclododecan-1-yl)acetamido)methylene)bis(hydrogen phosphonate) derivatised Endorem
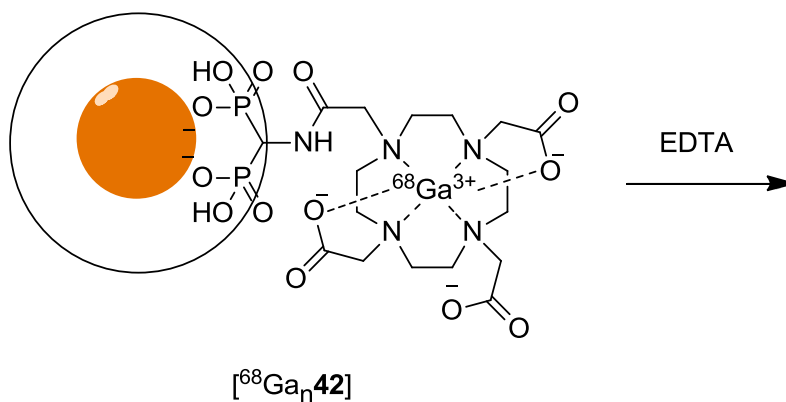
$[^{68}Ga_n\mathbf{42}]$

EDTA (10 mM, 200 µl) was added to the ^{68}Ga complex of ((2-(4,7,10-tris(carboxymethyl)-1,4,7,10-tetraazacyclododecan-1-yl)acetamido)methylene)bis(hydrogen phosphonate) derivatised Endorem $[^{68}Ga_n\mathbf{42}]$ (200 µl, 1 mM effective iron concentration, 34 MBq) and the reaction proceeded at either room temperature or 90°C for 30 or 60 minutes.

Radio-TLC	% ^{68}Ga attached to nanoparticles	
Time (mins)	RT	90°C
0	97.88	100
15	30.66	15.08
30	44.62	3.70
45	30.00	-
60	18.28	-

6.8.11. EDTA stability of ^{68}Ga complex of ((2-((2-(1,4,8,11-tetrakis(carboxymethyl)-1,4,8,11-tetraazacyclotetradecan-6-yl)ethyl)amino)acetamido)methylene)bis(hydrogen phosphonate) derivatised Endorem
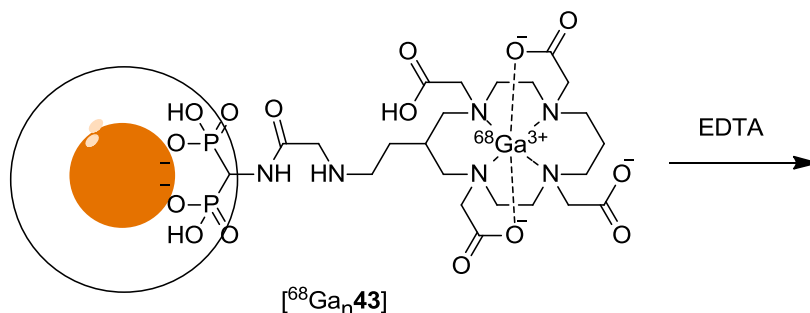
$[^{68}Ga_n\textbf{43}]$

EDTA (10 mM, 200 µl) was added to the ^{68}Ga complex of ((2-((2-(1,4,8,11-tetrakis(carboxymethyl)-1,4,8,11-tetraazacyclotetradecan-6-yl)ethyl)amino)acetamido)methylene)bis(hydrogen phosphonate) derivatised Endorem $[^{68}Ga_n\textbf{43}]$ (200 µl, 1 mM effective iron concentration, 50 MBq) and the reaction proceeded at either room temperature or 90°C for 30 or 60 minutes.

Radio-TLC	[68]Ga attached to nanoparticles	
Time (mins)	RT	90°C
0	72.31	100
15	76.73	9.92
30	100	2.31
45	39.48	-
60	34.44	-

6.8.12. EDTA stability of ^{68}Ga complex of ((2-(11-((6-carboxypyridin-2-yl)methyl)-1,4,8,11-tetraazabicyclo[6.6.2]hexadecan-4-yl)acetamido)methylene)bis(hydrogen phosphonate) derivatised Endorem
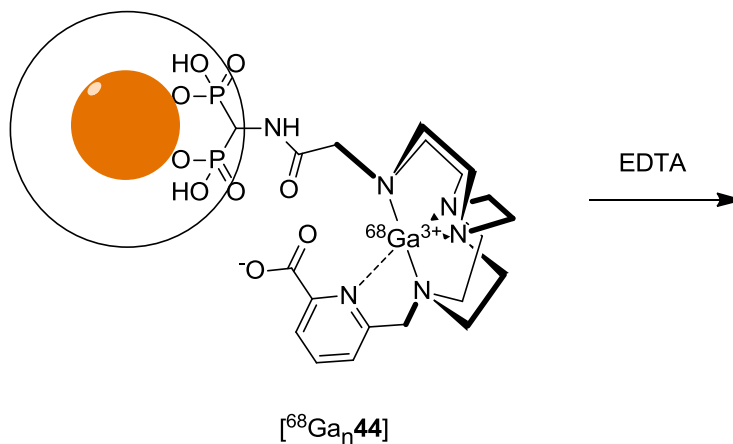
$[^{68}Ga_n\textbf{44}]$

EDTA (10 mM, 200 μl) was added to the ^{68}Ga complex of ((2-(11-((6-carboxypyridin-2-yl)methyl)-1,4,8,11-tetraazabicyclo[6.6.2]hexadecan-4-yl)acetamido)methylene)bis(hydrogen phosphonate) derivatised Endorem $[^{68}Ga_n\textbf{44}]$ (200 μl, 1 mM effective iron concentration, 20 MBq) and the reaction proceeded at either room temperature or 90°C for 30 or 60 minutes.

Radio-TLC	[68]Ga attached to nanoparticles	
Time (mins)	RT	90°C
0	95.32	92.89
15	100	30.56
30	31.14	14.36
45	27.55	-
60	31.75	-

6.8.13. EDTA stability of ^{68}Ga complex of triethoxy(ethyl) silane functionalised magnetite nanoparticles

Method 1

EDTA (10 mM, 200 μl) was added to the ^{68}Ga complex of Triethoxy(ethyl) silane functionalised magnetite nanoparticles synthesised at 90°C [^{68}Ga$_n$**33**] (200 μl, 1mM effective iron concentration, 30-79 MBq) and the reaction proceeded at either room temperature or 90°C for 60 minutes.

Radio-TLC	% inc. RT (3 x replication)			% inc. 90°C (2 x replication)	
Time (mins)	1	2	3	1	2
0	100	94	99	100	100
15	97	92.3	96.5	10	6.5
30	98	91.7	96	13	20.5
45	100	92	96.4	14	16.5
60	95	90	97.4	11	6.7

Method 2

EDTA (10 mM, 200 μl) was added to the ^{68}Ga complex of Triethoxy(ethyl) silane functionalised magnetite nanoparticles synthesised at RT [^{68}Ga$_n$**33**] (200 μl, 1 mM effective iron concentration, 30-79 MBq) and the reaction proceeded at room temperature for 60 minutes.

Radio-TLC	% inc. RT (2 x replication)	
Time (mins)	1	2
0	79	98
15	31.5	44
30	19.3	48
45	22.1	37
60	17.5	32

6.8.14. EDTA stability of ^{68}Ga complex of 2,2',2''-(10-(3-(3-(dihydroxysilyl)propoxy)-2-hydroxypropyl)-1,4,7,10-tetraazacyclododecane-1,4,7-triyl)triacetic acid functionalised magnetite nanoparticles

$[^{68}Ga_n\textbf{34}]$

<u>Method 1</u>

EDTA (10 mM, 200 µl) was added to the ^{68}Ga complex of 2,2',2''-(10-(3-(3-(dihydroxysilyl)propoxy)-2-hydroxypropyl)-1,4,7,10-tetraazacyclododecane-1,4,7-triyl)triacetic acid functionalised magnetite nanoparticles synthesised at 90°C [$^{68}Ga_n\textbf{34}$] (200 µl, 1 mM effective iron concentration, 32-78 MBq) and the reaction proceeded at either room temperature or 90°C for 60 minutes.

Radio-TLC	% inc. RT (3 x replication)			% inc. 90°C (2 x replication)	
Time (mins)	1	2	3	1	2
0.5	99	95	98.6	99	100
3	92.5	95.8	89	23	49.9
5	89.6	95	89	6	18.6
10	90	94	88.6	8	37.8
15	90	93.8	89	2.5	34.5

Method 2

EDTA (10 mM, 200 µl) was added to the ^{68}Ga complex of 2,2',2''-(10-(3-(3-(dihydroxysilyl)propoxy)-2-hydroxypropyl)-1,4,7,10-tetraazacyclododecane-1,4,7-triyl)triacetic acid functionalised magnetite nanoparticles synthesised at RT [^{68}Ga$_n$**34**] (200 µl, 1 mM effective iron concentration, 32-78 MBq) and the reaction proceeded at room temperature for 60 minutes.

Radio-TLC	% inc. RT (2 x replication)	
Time (mins)	1	2
0	41	33.5
15	11	5
30	3.7	4.2
45	8	5.2
60	9	3

6.8.15. EDTA stability of ^{68}Ga complex of 2,2',2'',2'''-(6-(2-((3-(3-(dihydroxysilyl)propoxy)-2-hydroxypropyl)amino)ethyl)-1,4,8,11-tetraazacyclotetradecane-1,4,8,11-tetrayl)tetraacetic acid functionalised magnetite nanoparticles

$[^{68}Ga_n\mathbf{35}]$

Method 1

EDTA (10 mM, 200 μl) was added to the ^{68}Ga complex of 2,2',2'',2'''-(6-(2-((3-(3-(dihydroxysilyl)propoxy)-2-hydroxypropyl)amino)ethyl)-1,4,8,11-tetraazacyclotetradecane-1,4,8,11-tetrayl)tetraacetic acid functionalised magnetite nanoparticles synthesised at 90°C $[^{68}Ga_n\mathbf{35}]$ (200 μl, 1 mM effective iron concentration, 34-66 MBq) and the reaction proceeded at either room temperature or 90°C for 60 minutes.
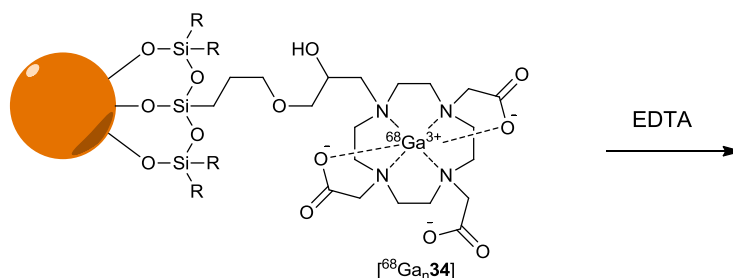
Radio-TLC	% inc. RT (3 x replication)			% inc. 90°C (2 x replication)	
Time (mins)	1	2	3	1	2
0.5	98	100	100	100	100
3	94.6	95.8	95	55	73.9
5	96.5	94	95	29	47
10	90	93	94	40	88.4
15	90	92	93.5	13.7	38.6

EDTA (10 mM, 200 μl) was added to the ^{68}Ga complex of 2,2',2'',2'''-(6-(2-((3-(3-(dihydroxysilyl)propoxy)-2-hydroxypropyl)amino)ethyl)-1,4,8,11-tetraazacyclotetradecane-1,4,8,11-tetrayl)tetraacetic acid functionalised magnetite nanoparticles synthesised at RT [^{68}Ga$_n$**35**] (200 μl, 1 mM effective iron concentration, 34-66 MBq) and the reaction proceeded at room temperature for 60 minutes.
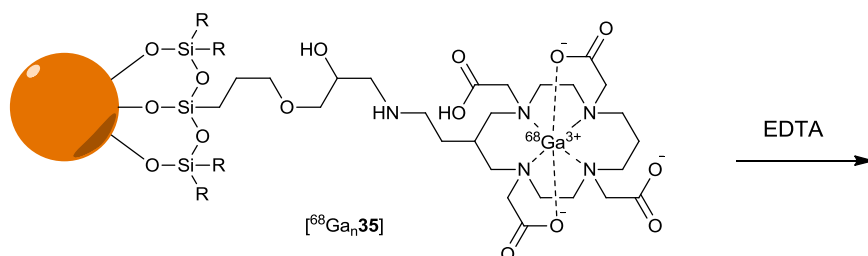
Radio-TLC	% inc. RT (2 x replication)	
Time (mins)	1	2
0	33.4	63
15	9.32	33
30	7.55	32
45	6.72	21.4
60	5.54	25

6.8.16. EDTA stability of ^{68}Ga complex of 6-((11-(3-(3-(dihydroxysilyl)propoxy)-2-hydroxypropyl)-1,4,8,11-tetraazabicyclo[6.6.2]hexadecan-4-yl)methyl)picolinic acid functionalised magnetite nanoparticles

$[^{68}Ga_n36]$

Method 1

EDTA (10 mM, 200 μl) was added to the ^{68}Ga complex of 6-((11-(3-(3-(dihydroxysilyl)propoxy)-2-hydroxypropyl)-1,4,8,11-tetraazabicyclo[6.6.2]hexadecan-4-yl)methyl)picolinic acid functionalised magnetite nanoparticles synthesised at 90°C $[^{68}Ga_n36]$ (200 μl, 1mM effective iron concentration, 31-66 MBq) and the reaction proceeded at either room temperature or 90°C for 60 minutes.

Radio-TLC	% inc. RT (3 x replication)			% inc. 90°C (2 x replication)	
Time (mins)	1	2	3	1	2
0.5	100	100	100	100	100
3	98	96.4	100	37.6	57
5	97	94.6	97	7	26
10	98	93	95	13	24
15	98	93.7	91	13	12.9

Method 2

EDTA (10 mM, 200 μl) was added to the ^{68}Ga complex of 6-((11-(3-(3-(dihydroxysilyl)propoxy)-2-hydroxypropyl)-1,4,8,11-tetraazabicyclo[6.6.2]hexadecan-4-yl)methyl)picolinic acid functionalised magnetite nanoparticles synthesised at 90°C [^{68}Ga$_n$**36**] (200 μl, 1 mM effective iron concentration, 31-66 MBq) and the reaction proceeded at room temperature for 60 minutes.

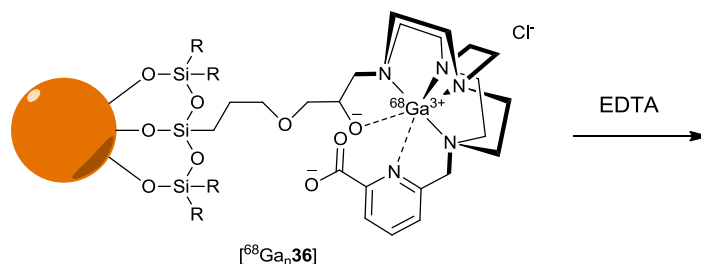| Radio-TLC	% inc. RT (2 x replication)	
Time (mins)	1	2
0	46	87
15	8.9	47
30	9.5	43
45	11.4	37
60	7	37

6.8.17. Saline stability of ^{68}Ga complex of four siloxane functionalised magnetite nanoparticles

Saline (200 μl) was added to the ^{68}Ga complex of siloxane functionalised magnetite nanoparticles ([^{68}Ga$_n$**33**], [^{68}Ga$_n$**34**], [^{68}Ga$_n$**35**] and [^{68}Ga$_n$**36**]) (200 μl, 1mM effective iron concentration, 92-138 MBq) and the reaction was incubated at 37°C for four hours.

Radio-TLC	% ^{68}Ga attached to nanoparticles			
Time (hours)	[^{68}Ga$_n$**33**]	[^{68}Ga$_n$**34**]	[^{68}Ga$_n$**35**]	[^{68}Ga$_n$**36**]
0	100	100	100	100
0.5	100	100	100	100
1	100	99	100	100
2	100	92	100	100
3	100	93	100	100
4	94	93	100	100

6.9 Appendix

6.9.1. NTA of 33

Particle Size / Concentration
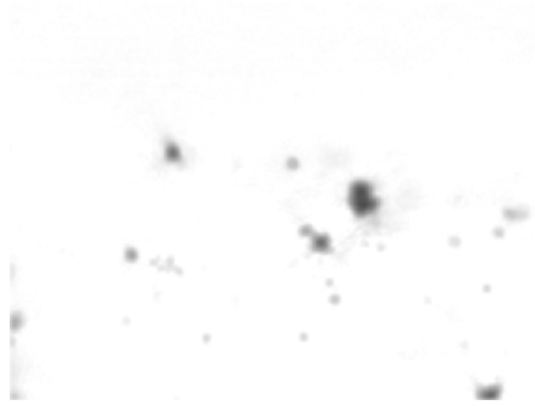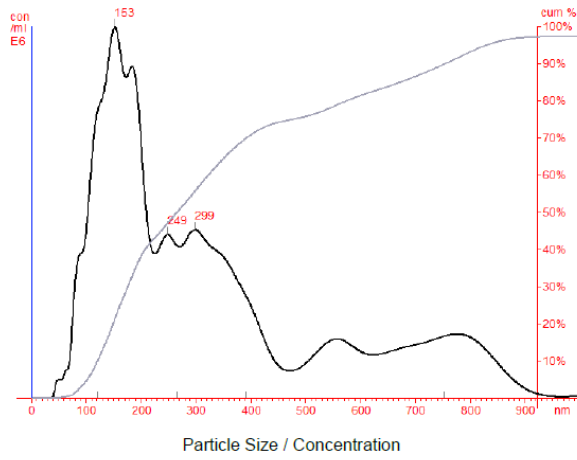
Sample Video Frame

6.9.2. NTA of 34

Particle Size / Concentration
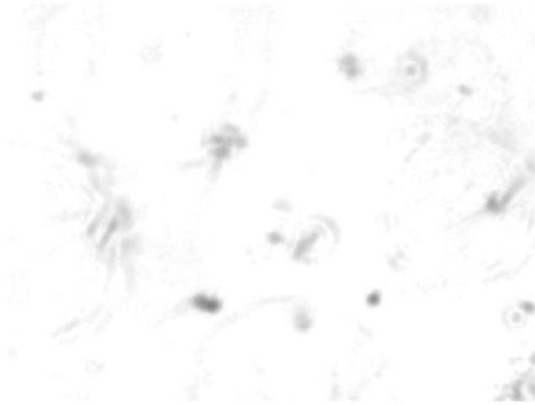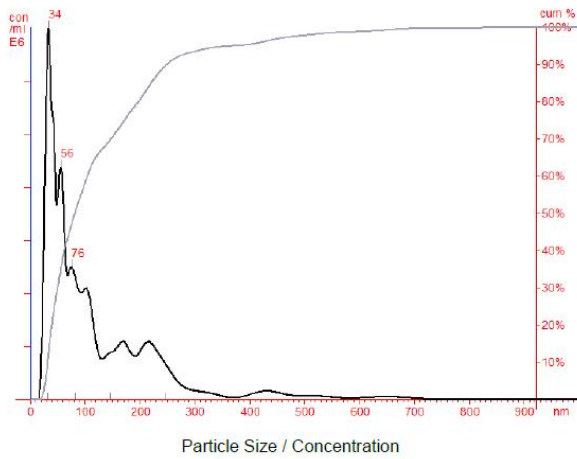
Sample Video Frame

6.9.3. NTA of 35

Particle Size / Concentration
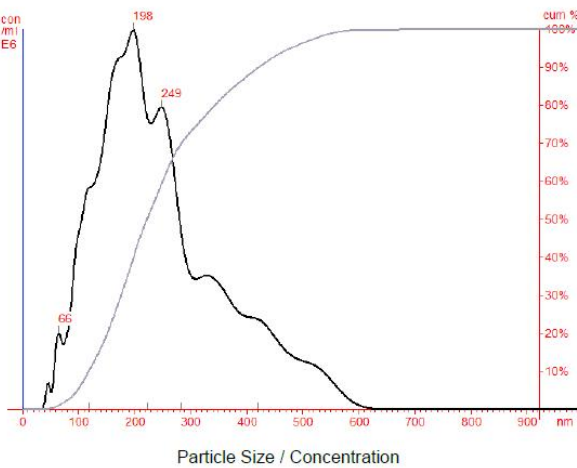
Sample Video Frame

6.9.4. NTA of 36

Particle Size / Concentration
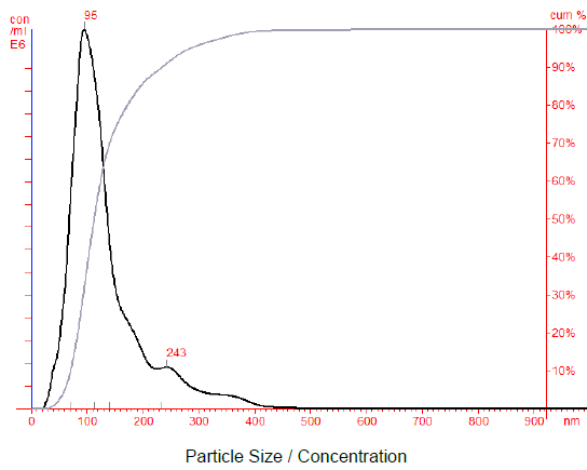
Sample Video Frame

6.9.5. NTA of [Cu$_n$33]

Particle Size / Concentration
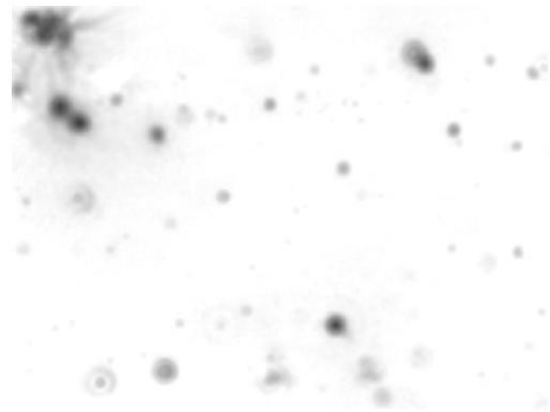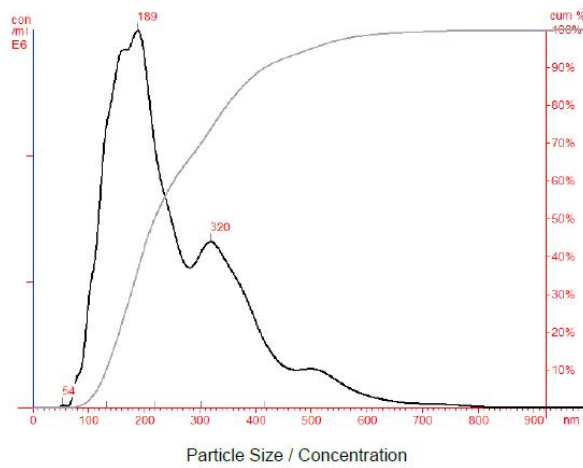
Sample Video Frame

6.9.6. NTA of [Cu$_n$34]

Particle Size / Concentration
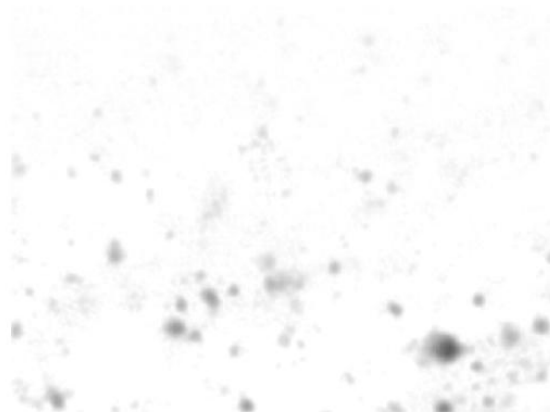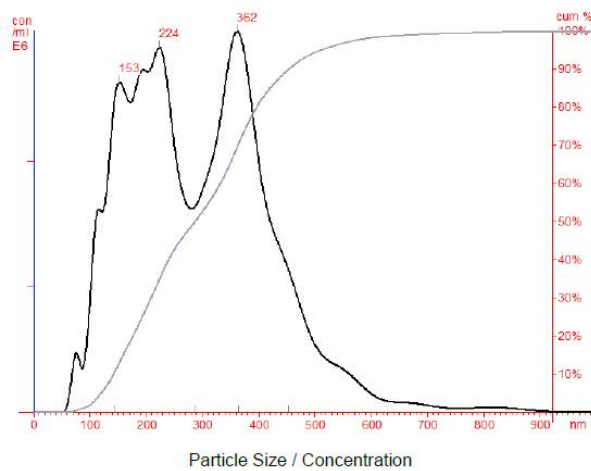
Sample Video Frame

6.9.7. NTA of [Cu$_n$35]

Particle Size / Concentration
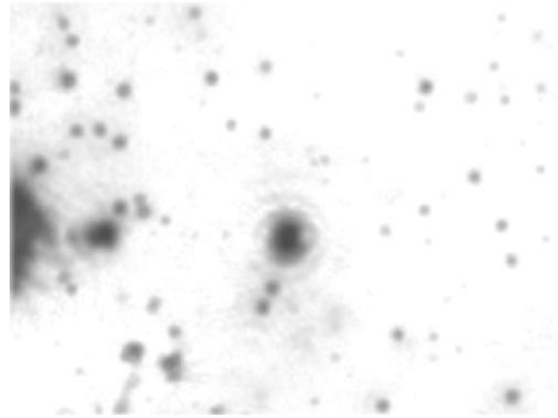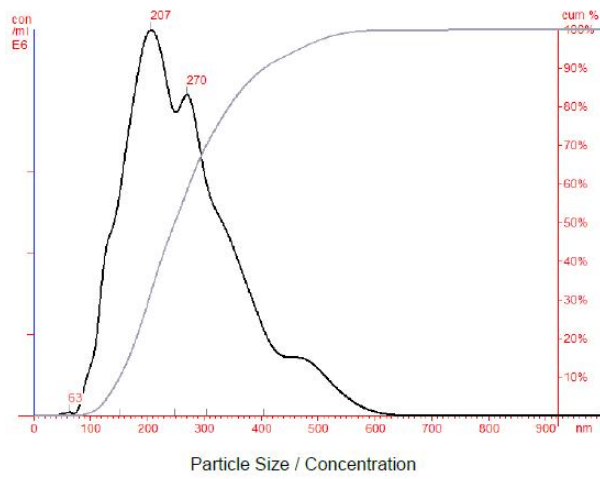
Sample Video Frame

6.9.8. NTA of [Cu$_n$36]

Particle Size / Concentration
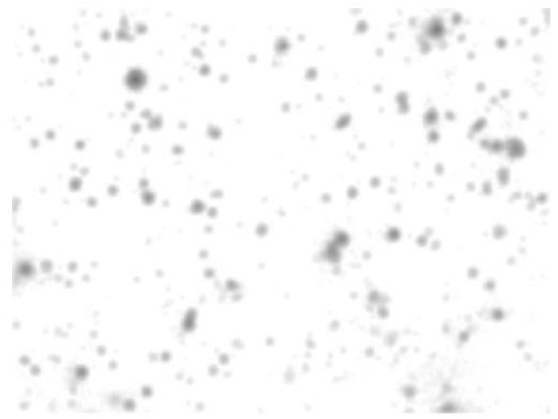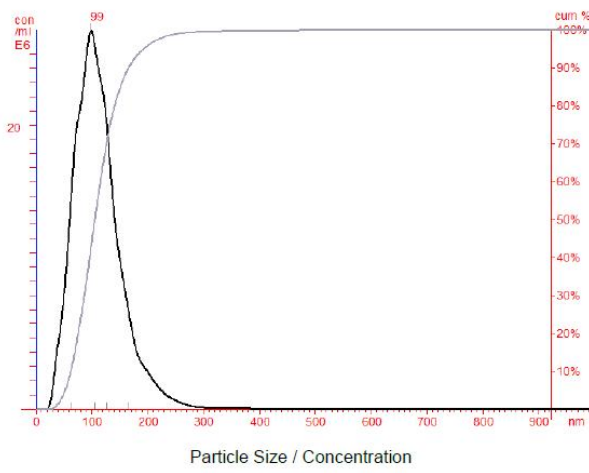
Sample Video Frame

6.9.9. NTA of [Ga$_n$33]

Particle Size / Concentration
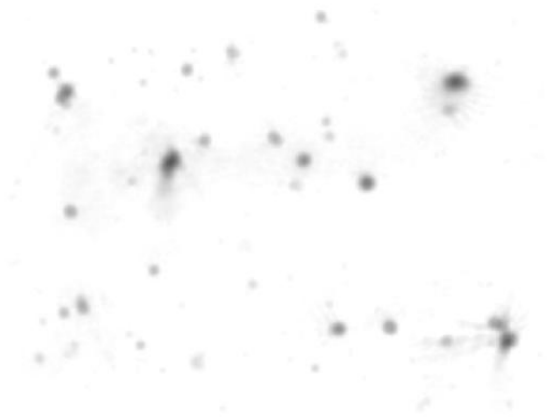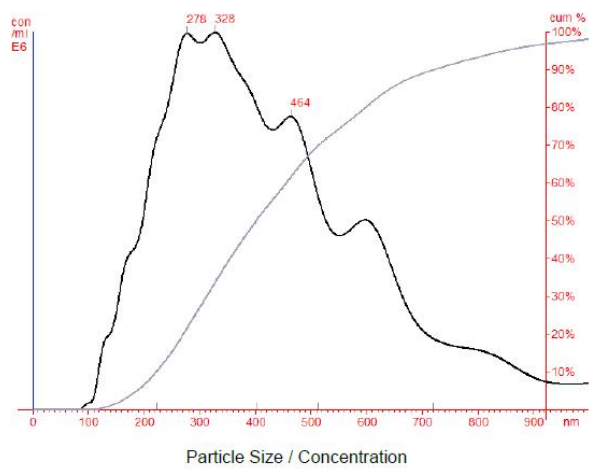
Sample Video Frame

6.9.10. NTA of [Ga$_n$34]

Particle Size / Concentration
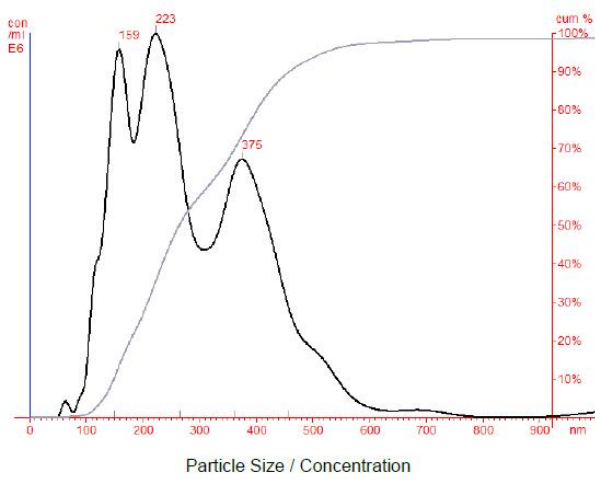
Sample Video Frame

6.9.11. NTA of [Ga$_n$35]

Particle Size / Concentration
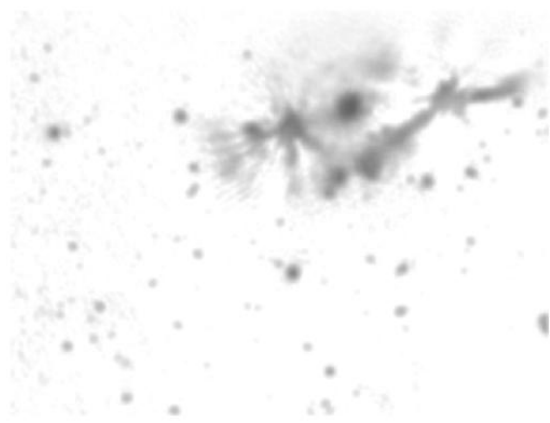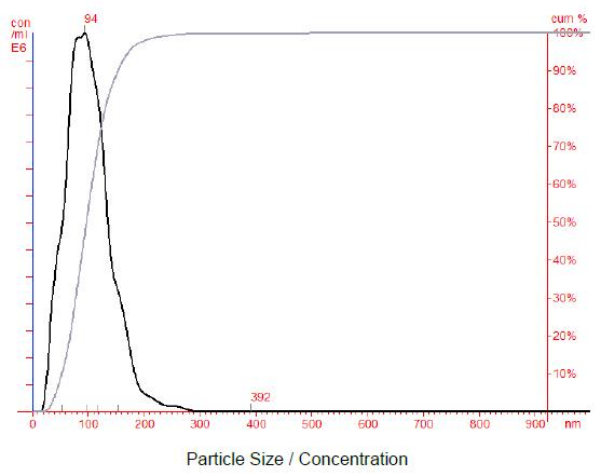
Sample Video Frame

6.9.12. NTA of [Ga$_n$36]

Particle Size / Concentration
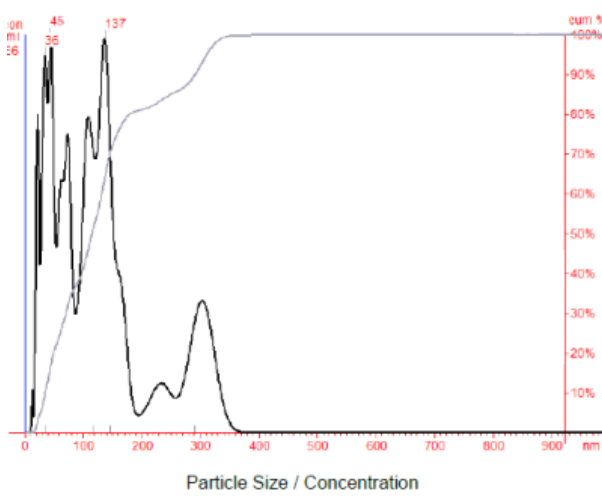
Sample Video Frame

6.9.13. NTA of [^{68}Ga$_n$33]

Particle Size / Concentration
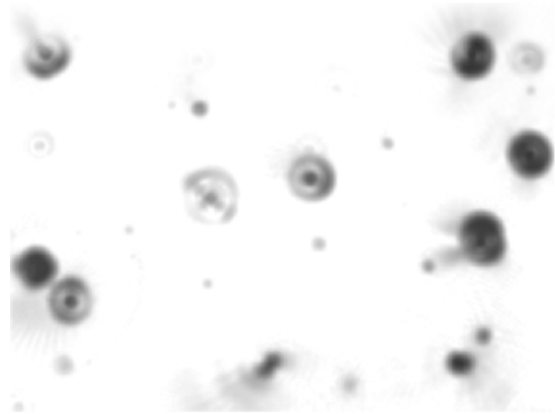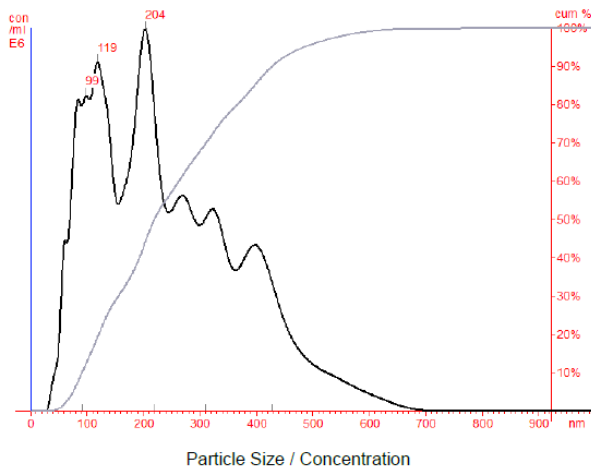
Sample Video Frame

6.9.14. NTA of [^{68}Ga$_n$34]

Particle Size / Concentration
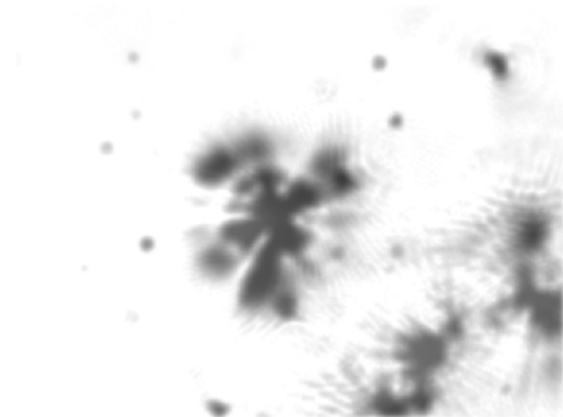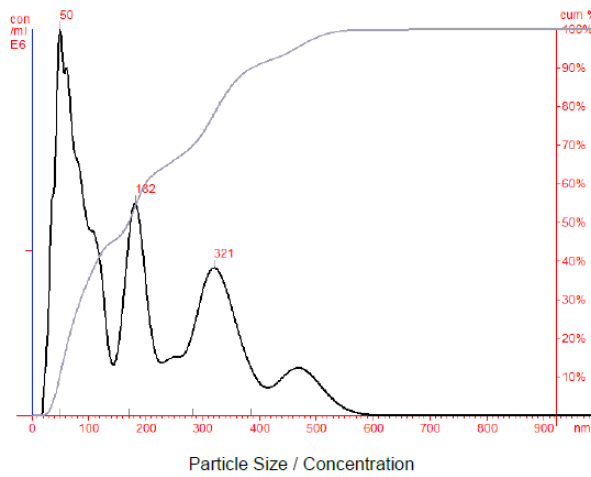
Sample Video Frame

6.9.15. NTA of [^{68}Ga$_n$35]

Particle Size / Concentration
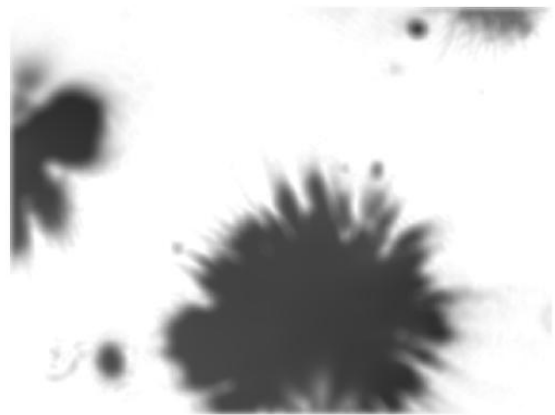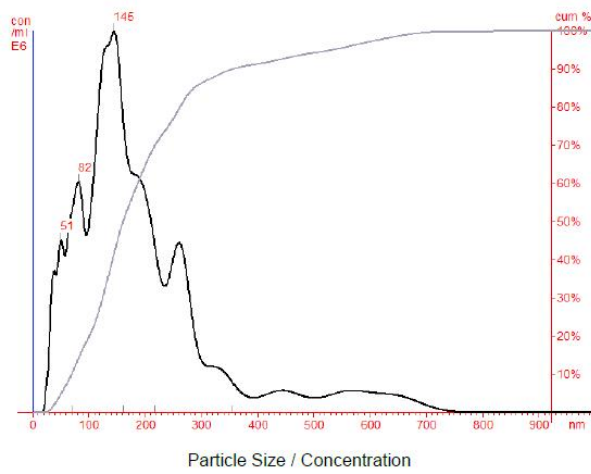
Sample Video Frame

6.9.16. NTA of [^{68}Ga$_n$36]

Particle Size / Concentration
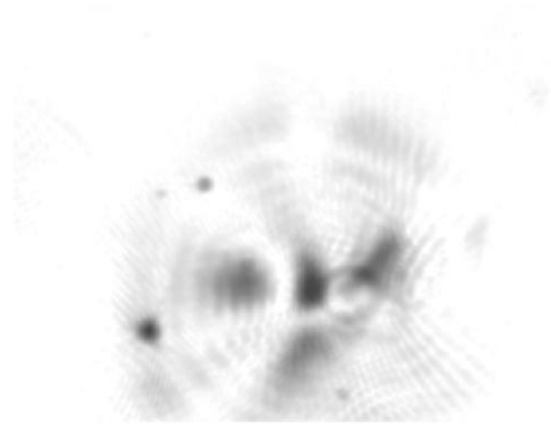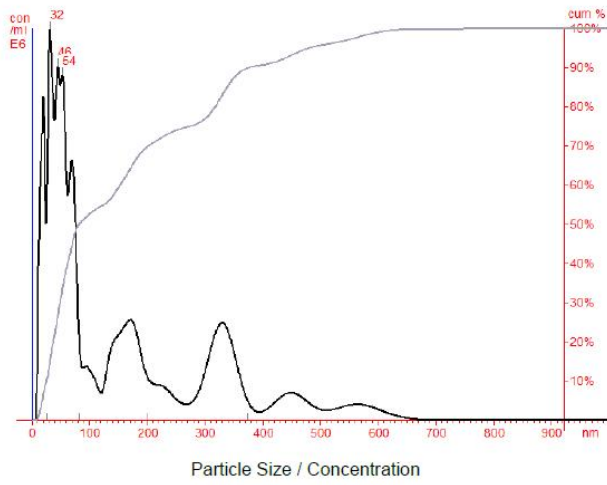
Sample Video Frame

References

(1)   Lee, D. E.; Koo, H.; Sun, I. C.; Ryu, J. H.; Kim, K.; Kwon, I. C. *Chem. Soc. Rev.* **2012**, *41*, 2656.

(2)   http://healthcare.siemens.com/magnetic-resonance-imaging/mr-pet-scanner/biograph-mmr, *26/06/2013*

(3)   Pimlott, S. L.; Sutherland, A. *Chem. Soc. Rev.* **2011**, *40*, 149.

(4)   Rahmim, A.; Zaidi, H. *Nucl. Med. Commun.* **2008**, *29*, 193.

(5)   Bartholomae, M. D.; Louie, A. S.; Valliant, J. F.; Zubieta, J. *Chem. Rev.* **2010**, *110*, 2903.

(6)   Jurisson, S. S.; Lydon, J. D. *Chem. Rev.* **1999**, *99*, 2205.

(7)   Prats, E.; Aisa, F.; Abos, M. D.; Villavieja, L.; Garcia-Lopez, F.; Asenjo, M. J.; Razola, P.; Banzo, J. *J. Nucl. Med.* **1999**, *40*, 296.

(8)   Wadas, T. J.; Wong, E. H.; Weisman, G. R.; Anderson, C. J. *Chem. Rev.* **2010**, *110*, 2858.

(9)   Ramogida, C. F.; Orvig, C. *Chem. Commun.* **2013**, *49*, 4720.

(10)   Li, Z. B.; Conti, P. S. *Adv. Drug Del. Rev.* **2010**, *62*, 1031.

(11)   Miller, P. W.; Long, N. J.; Vilar, R.; Gee, A. D. *Angew. Chem. Int. Ed.* **2008**, *47*, 8998.

(12)   Phelps, M. E. *Proc. Natl. Acad. Sci. U. S. A.* **2000**, *97*, 9226.

(13)   Serdons, K.; Verbruggen, A.; Bormans, G. M. *Methods* **2009**, *48*, 104.

(14)   Sanchez-Crespo, A. *Appl. Radiat. Isot.* **2013**, *76*, 55.

(15)   Le Bars, D. *J. Fluorine Chem.* **2006**, *127*, 1488.

(16)   Bhattacharyya, S.; Dixit, M. *Dalton Trans.* **2011**.

(17)   Contractor, K. B.; Aboagye, E. O. *J. Nucl. Med.* **2009**, *50*, 97S.

(18)   Smith, S. V. *J. Inorg. Biochem.* **2004**, *98*, 1874.

(19)   Shokeen, M.; Anderson, C. J. *Acc. Chem. Res.* **2009**, *42*, 832.

(20)   Shannon, R. D. *Acta Crystallogr. Sect. A* **1976**, *32*, 751.

(21)   Bartholomä, M. D. *Inorg. Chim. Acta* **2012**, *389*, 36.

(22)   Wu, Y.; Zhang, X. Z.; Xiong, Z. M.; Cheng, Z.; Fisher, D. R.; Liu, S.; Gambhir, S. S.; Chen, X. Y. *J. Nucl. Med.* **2005**, *46*, 1707.

(23)   McQuade, P.; Miao, Y. B.; Yoo, J.; Quinn, T. P.; Welch, M. J.; Lewis, J. S. *J. Med. Chem.* **2005**, *48*, 2985.

(24)   Weisman, G. R.; Rogers, M. E.; Wong, E. H.; Jasinski, J. P.; Paight, E. S. *J. Am. Chem. Soc.* **1990**, *112*, 8604.

(25)   Wong, E. H.; Weisman, G. R.; Hill, D. C.; Reed, D. P.; Rogers, M. E.; Condon, J. S.; Fagan, M. A.; Calabrese, J. C.; Lam, K. C.; Guzei, I. A.; Rheingold, A. L. *J. Am. Chem. Soc.* **2000**, *122*, 10561.

(26)   Hubin, T. J.; McCormick, J. M.; Collinson, S. R.; Alcock, N. W.; Busch, D. H. *Chem. Commun.* **1998**, 1675.

(27)   Hubin, T. J. *Coord. Chem. Rev.* **2003**, *241*, 27.

(28)   Cooper, M. S.; Ma, M. T.; Sunassee, K.; Shaw, K. P.; Williams, J. D.; Paul, R. L.; Donnelly, P. S.; Blower, P. J. *Bioconj. Chem.* **2012**, *23*, 1029.

(29)   Pandya, D. N.; Dale, A. V.; Kim, J. Y.; Lee, H.; Ha, Y. S.; An, G. I.; Yoo, J. *Bioconj. Chem.* **2012**, *23*, 330.

(30)   Lewis, E. A.; Boyle, R. W.; Archibald, S. J. *Chem. Commun.* **2004**, 2212.

(31)   Ferdani, R.; Stigers, D. J.; Fiamengo, A. L.; Wei, L. H.; Li, B. T. Y.; Golen, J. A.; Rheingold, A. L.; Weisman, G. R.; Wong, E. H.; Anderson, C. J. *Dalton Trans.* **2012**, *41*, 1938.

(32)   Lima, L. M. P.; Esteban-Gomez, D.; Delgado, R.; Platas-Iglesias, C.; Tripier, R. *Inorg. Chem.* **2012**, *51*, 6916.

(33)   Zeglis, B. M.; Lewis, J. S. *Dalton Trans.* **2011**.

(34)   Perk, L. R.; Visser, G. W. M.; Vosjan, M.; Stigter-van Walsum, M.; Tijink, B. M.; Leemans, C. R.; van Dongen, G. *J. Nucl. Med.* **2005**, *46*, 1898.

(35)   Broan, C. J.; Cox, J. P. L.; Craig, A. S.; Kataky, R.; Parker, D.; Harrison, A.; Randall, A. M.; Ferguson, G. *J. Chem. Soc., Perkin Trans. 2* **1991**, 87.

(36)   Parker, D.; Pulukkody, K.; Smith, F. C.; Batsanov, A.; Howard, J. A. K. *J. Chem. Soc., Dalton Trans.* **1994**, 689.

(37)   Cox, J. P. L.; Jankowski, K. J.; Kataky, R.; Parker, D.; Beeley, N. R. A.; Boyce, B. A.; Eaton, M. A. W.; Millar, K.; Millican, A. T.; Harrison, A.; Walker, C. *J. Chem. Soc., Chem. Commun.* **1989**, 797.

(38)   Al-Nahhas, A.; Win, Z.; Szyszko, T.; Singh, A.; Khan, S.; Rubello, D. *Eur. J. Nucl. Med. Mol. Imag.* **2007**, *34*, 1897.

(39)   Mirzadeh, S.; Lambrecht, R. M. *J. Radioanal. Nucl. Chem. Art.* **1996**, *202*, 7.

(40)   Zhernosekov, K. P.; Filosofov, D. V.; Baum, R. P.; Aschoff, P.; Bihl, H.; Razbash, A. A.; Jahn, M.; Jennewein, M.; Roesch, F. *J. Nucl. Med.* **2007**, *48*, 1741.

(41)   Holland, J. P.; Williamson, M. J.; Lewis, J. S. *Molecular Imaging* **2010**, *9*, 1.

(42)   Fani, M.; Andre, J. P.; Maecke, H. R. *Contrast Media Mol. Imaging* **2008**, *3*, 53.

(43)   Green, M. A.; Welch, M. J. *Int. J. Rad. Appl. Instrum. B* **1989**, *16*, 435.

(44)   Asti, M.; De Pietri, G.; Fraternali, A.; Grassi, E.; Sghedoni, R.; Fioroni, F.; Roesch, F.; Versari, A.; Salvo, D. *Nucl. Med. Biol.* **2008**, *35*, 721.

(45)   Wong, E.; Caravan, P.; Liu, S.; Rettig, S. J.; Orvig, C. *Inorg. Chem.* **1996**, *35*, 715.

(46)   Cox, J. P. L.; Craig, A. S.; Helps, I. M.; Jankowski, K. J.; Parker, D.; Eaton, M. A. W.; Millican, A. T.; Millar, K.; Beeley, N. R. A.; Boyce, B. A. *J. Chem. Soc., Perkin Trans. 1* **1990**, 2567.

(47)   Liu, S.; Edwards, D. S. *Bioconjug. Chem.* **2001**, *12*, 7.

(48)   Berry, D. J.; Ma, Y.; Ballinger, J. R.; Tavare, R.; Koers, A.; Sunassee, K.; Zhou, T.; Nawaz, S.; Mullen, G. E. D.; Hider, R. C.; Blower, P. J. *Chem. Commun.* **2011**, *47*, 7068.

(49)   Boros, E.; Ferreira, C. L.; Cawthray, J. F.; Price, E. W.; Patrick, B. O.; Wester, D. W.; Adam, M. J.; Orvig, C. *J. Am. Chem. Soc.* **2010**, *132*, 15726.

(50)   Oh, S.; Prasad, V.; Lee, D. S.; Baum, R. P. *Int. J. Mol. Imaging* **2011**, 524130.

(51)   Baum, R. P.; Kulkarni, H. R. *Theranostics* **2012**, *2*, 437.

(52)   Buchmann, I.; Henze, M.; Engelbrecht, S.; Eisenhut, M.; Runz, A.; Schaefer, M.; Schilling, T.; Haufe, S.; Herrmann, T.; Haberkorn, U. *Eur. J. Nucl. Med. Mol. Imag.* **2007**, *34*, 1617.

(53)   Smith, D. L.; Breeman, W. A. P.; Sims-Mourtada, J. *Appl. Radiat. Isot.* **2012**.

(54)   Hofmann, M.; Maecke, H.; Borner, A. R.; Weckesser, E.; Schoffski, P.; Oei, M. L.; Schumacher, J.; Henze, M.; Heppeler, A.; Meyer, G. J.; Knapp, W. H. *Eur. J. Nucl. Med.* **2001**, *28*, 1751.

(55)   Henze, M.; Schuhmacher, J.; Hipp, P.; Kowalski, J.; Becker, D. W.; Doll, J.; Macke, H. R.; Hofmann, M.; Debus, J.; Haberkorn, U. *J. Nucl. Med.* **2001**, *42*, 1053.

(56)   Kowalski, J.; Henze, M.; Schuhmacher, J.; Macke, H. R.; Hofmann, M.; Haberkorn, U. *Mol. Imag. Biol.* **2003**, *5*, 42.

(57)   Sainz-Esteban, A.; Prasad, V.; Schuchardt, C.; Zachert, C.; Manuel Carril, J.; Baum, R. P. *Eur. J. Nucl. Med. Mol. Imag.* **2012**, *39*, 501.

(58)   Prasad, V.; Ambrosini, V.; Hommann, M.; Hoersch, D.; Fanti, S.; Baum, R. P. *Eur. J. Nucl. Med. Mol. Imag.* **2010**, *37*, 67.

(59)   Antunes, P.; Ginj, M.; Zhang, H.; Waser, B.; Baum, R. P.; Reubi, J. C.; Maecke, H. *Eur. J. Nucl. Med. Mol. Imag.* **2007**, *34*, 982.

(60)   Stasiuk, G. J.; Long, N. J. *Chem. Commun.* **2013**, *49*, 2732.

(61)   Blom, E.; Langstrom, B.; Velikyan, I. *Bioconjug. Chem.* **2009**, *20*, 1146.

(62)   Decristoforo, C.; Hernandez Gonzalez, I.; Carlsen, J.; Rupprich, M.; Huisman, M.; Virgolini, I.; Wester, H.-J.; Haubner, R. *Eur. J. Nucl. Med. Mol. Imaging* **2008**, *35*, 1507.

(63)   Ferreira, C. L.; Lamsa, E.; Woods, M.; Duan, Y.; Fernando, P.; Bensimon, C.; Kordos, M.; Guenther, K.; Jurek, P.; Kiefer, G. E. *Bioconjug. Chem.* **2010**, *21*, 531.

(64)   Knetsch, P. A.; Petrik, M.; Rangger, C.; Seidel, G.; Pietzsch, H.-J.; Virgolini, I.; Decristoforo, C.; Haubner, R. *Nucl. Med. Biol.* **2013**, *40*, 65.

(65)   Ferreira, C. L.; Yapp, D. T. T.; Mandel, D.; Gill, R. K.; Boros, E.; Wong, M. Q.; Jurek, P.; Kiefer, G. E. *Bioconjug. Chem.* **2012**, *23*, 2239.

(66)   Al-Nahhas, A.; Win, Z.; Szyszko, T.; Singh, A.; Khan, S.; Rubello, D. *Eur. J. Nucl. Med. Mol. Imaging* **2007**, *34*, 1897.

(67)   Velikyan, I.; Maecke, H.; Langstrom, B. *Bioconjug. Chem.* **2008**, *19*, 569.

(68)   Notni, J.; Hermann, P.; Havlickova, J.; Kotek, J.; Kubicek, V.; Plutnar, J.; Loktionova, N.; Riss, P. J.; Roesch, F.; Lukes, I. *Chem. Eur. J.* **2010**, *16*, 7174.

(69)   Simecek, J.; Schulz, M.; Notni, J.; Plutnar, J.; Kubicek, V.; Havlickova, J.; Hermann, P. *Inorg. Chem.* **2012**, *51*, 577.

(70)   Singh, A. N.; Liu, W.; Hao, G.; Kumar, A.; Gupta, A.; Oz, O. K.; Hsieh, J.-T.; Sun, X. *Bioconjug. Chem.* **2011**, *22*, 1650.

(71)   Notni, J.; Simecek, J.; Hermann, P.; Wester, H.-J. *Chem. Eur. J.* **2011**, *17*, 14718.

(72)   Notni, J.; Pohle, K.; Wester, H.-J. *EJNMMI Res.* **2012**, *2*, 28.

(73)   Notni, J.; Pohle, K.; Wester, H.-J. *Nucl. Med. Biol.* **2013**, *40*, 33.

(74)   Gomez, F. L. G.; Uehara, T.; Rokugawa, T.; Higaki, Y.; Suzuki, H.; Hanaoka, H.; Akizawa, H.; Arano, Y. *Bioconj. Chem.* **2012**, *23*, 2229.

(75)   Šimeček, J.; Hermann, P.; Wester, H.-J.; Notni, J. *Chemmedchem* **2013**, *8*, 95.

(76)   Ma, M. T.; Neels, O. C.; Denoyer, D.; Roselt, P.; Karas, J. A.; Scanlon, D. B.; White, J. M.; Hicks, R. J.; Donnelly, P. S. *Bioconjug. Chem.* **2011**, *22*, 2093.

(77)   Waldron, B. P.; Parker, D.; Burchardt, C.; Yufit, D. S.; Zimny, M.; Roesch, F. *Chem. Commun.* **2013**, *49*, 579.

(78)   Arrowsmith, R. L.; Waghorn, P. A.; Jones, M. W.; Bauman, A.; Brayshaw, S. K.; Hu, Z.; Kociok-Kohn, G.; Mindt, T. L.; Tyrrell, R. M.; Botchway, S. W.; Dilworth, J. R.; Pascu, S. I. *Dalton Trans* **2011**, *40*, 6238.

(79)   Paterson, B. M.; Karas, J. A.; Scanlon, D. B.; White, J. M.; Donnelly, P. S. *Inorg. Chem.* **2010**, *49*, 1884.

(80)   Hueting, R.; Christlieb, M.; Dilworth, J. R.; Garayoa, E. G.; Gouverneur, V.; Jones, M. W.; Maes, V.; Schibli, R.; Sun, X.; Tourwe, D. A. *Dalton Trans.* **2010**, *39*, 3620.

(81)   Boros E Fau - Ferreira, C. L.; Ferreira Cl Fau - Yapp, D. T. T.; Yapp Dt Fau - Gill, R. K.; Gill Rk Fau - Price, E. W.; Price Ew Fau - Adam, M. J.; Adam Mj Fau - Orvig, C.; Orvig, C. *Nucl. Med. Biol.* **2012**.

(82)   Bailey, G. A.; Price, E. W.; Zeglis, B. M.; Ferreira, C. L.; Boros, E.; Lacasse, M. J.; Patrick, B. O.; Lewis, J. S.; Adam, M. J.; Orvig, C. *Inorg Chem* **2012**.

(83)   Morfin, J.-F.; Tóth, É. *Inorg. Chem.* **2011**, *50*, 10371.

(84)   Zeng, D.; Desai, A. V.; Ranganathan, D.; Wheeler, T. D.; Kenis, P. J.; Reichert, D. E. *Nucl. Med. Biol.* **2013**, *40*, 42.

(85)   Blom, E.; Koziorowski, J. *Appl. Radiat. Isot.* **2012**, *70*, 980.

(86)   Mueller, D.; Klette, I.; Baum, R. P.; Gottschaldt, M.; Schultz, M. K.; Breeman, W. A. *Bioconjug. Chem.* **2012**, *23*, 1712.

(87)   Simms, R. W.; Kim, D. H.; Weaver, D. M.; Sundararajan, C.; Blacker, M.; Stephenson, K. A.; Valliant, J. F. *Chem.--Eur. J.* **2012**, *18*, 6746.

(88)   Caravan, P. *Chem. Soc. Rev.* **2006**, *35*, 512.

(89)   Bottrill, M.; Nicholas, L. K.; Long, N. J. *Chem. Soc. Rev.* **2006**, *35*, 557.

(90)   Brown, M. A.; Semelka, R. C. *MRI Basic Principles and Applications*; Third ed.; John Wiley & Sons, 2003.

(91)   Westbrook, C.; Kaur, C. *MRI In Practice*; Second ed.; Blackwell Publishing, 1998.

(92)   Wang, X. Y.; Jin, T. Z.; Comblin, V.; Lopezmut, A.; Merciny, E.; Desreux, J. F. *Inorg. Chem.* **1992**, *31*, 1095.

(93)   Aime, S.; Botta, M.; Terreno, E. *Adv. Inorg. Chem.* **2005**, *57*, 173.

(94)   Caravan, P.; Ellison, J. J.; McMurry, T. J.; Lauffer, R. B. *Chem. Rev.* **1999**, *99*, 2293.

(95)   Mewis, R. E.; Archibald, S. J. *Coord. Chem. Rev.* **2010**, *254*, 1686.

(96)   Aime, S.; Botta, M.; Fasano, M.; Terreno, E. *Chem. Soc. Rev.* **1998**, *27*, 19.

(97)   Colombo, M.; Carregal-Romero, S.; Casula, M. F.; Gutierrez, L.; Morales, M. P.; Bohm, I. B.; Heverhagen, J. T.; Prosperi, D.; Parak, W. J. *Chem. Soc. Rev.* **2012**, *41*, 4306.

(98)   Lewinski, N.; Colvin, V.; Drezek, R. *Small* **2008**, *4*, 26.

(99)   Wang, Y. X. J.; Hussain, S. M.; Krestin, G. P. *Eur. Radiol.* **2001**, *11*, 2319.

(100)   Gupta, A. K.; Gupta, M. *Biomaterials* **2005**, *26*, 3995.
(101)   Gupta, A. K.; Naregalkar, R. R.; Vaidya, V. D.; Gupta, M. *Nanomedicine* **2007**, *2*, 23.
(102)   Qiao, R.; Yang, C.; Gao, M. *J. Mater. Chem.* **2009**, *19*, 6274.
(103)   Banerjee, T.; Mitra, S.; Singh, A. K.; Sharma, R. K.; Maitra, A. *Int. J. Pharm.* **2002**, *243*, 93.
(104)   Veiseh, O.; Gunn, J. W.; Zhang, M. Q. *Adv. Drug Del. Rev.* **2010**, *62*, 284.
(105)   Bonnemain, B. *J. Drug Targeting* **1998**, *6*, 167.
(106)   Harisinghani, M. G.; Barentsz, J.; Hahn, P. F.; Deserno, W. M.; Tabatabaei, S.; van de Kaa, C. H.; de la Rosette, J.; Weissleder, R. *New Engl. J. Med.* **2003**, *348*, 2491.
(107)   Bunzli, J. C. G.; Piguet, C. *Chem. Soc. Rev.* **2005**, *34*, 1048.
(108)   Shah, K.; Weissleder, R. *NeuroRx* **2005**, *2*, 215.
(109)   Gross, S.; Piwnica-Worms, D. *Cancer Cell* **2005**, *7*, 5.
(110)   Bornhop, D. J.; Griffin, J. M. M.; Goebel, T. S.; Sudduth, M. R.; Bell, B.; Motamedi, M. *Appl. Spectrosc.* **2003**, *57*, 1216.
(111)   Gunnlaugsson, T.; Leonard, J. P. *Chem. Commun.* **2005**, 3114.
(112)   Bunzli, J. C. G.; Comby, S.; Chauvin, A.-S.; Vandevyver, C. D. B. *J. Rare Earth.* **2007**, *25*, 257.
(113)   Caravan, P.; Parigi, G.; Chasse, J. M.; Cloutier, N. J.; Ellison, J. J.; Lauffer, R. B.; Luchinat, C.; McDermid, S. A.; Spiller, M.; McMurry, T. J. *Inorg. Chem.* **2007**, *46*, 6632.
(114)   Elmore, S. P.; Nishimura, Y.; Qian, T.; Herman, B.; Lemasters, J. J. *Arch. Biochem. Biophys.* **2004**, *422*, 145.
(115)   Scaduto, R. C.; Grotyohann, L. W. *Biophys. J.* **1999**, *76*, 469.
(116)   Jennings, L. E.; Long, N. J. *Chem. Commun.* **2009**, 3511.
(117)   Gerstl, F.; Windischberger, C.; Mitterhauser, M.; Wadsak, W.; Holik, A.; Kletter, K.; Moser, E.; Kasper, S.; Lanzenberger, R. *NeuroImage* **2008**, *41*, 204.
(118)   Raylman, R. R.; Majewski, S.; Lemieux, S. K.; Velan, S. S.; Kross, B.; Popov, V.; Smith, M. F.; Weisenberger, A. G.; Zorn, C.; Marano, G. D. *Phys. Med. Biol.* **2006**, *51*, 6371.
(119)   Shao, Y. P.; Cherry, S. R.; Farahani, K.; Meadors, K.; Siegel, S.; Silverman, R. W.; Marsden, P. K. *Phys. Med. Biol.* **1997**, *42*, 1965.
(120)   Catana, C.; Wu, Y.; Judenhofer, M. S.; Qi, J.; Pichler, B. J.; Cherry, S. R. *J. Nucl. Med.* **2006**, *47*, 1968.
(121)   Choi, J.-s.; Park, J. C.; Nah, H.; Woo, S.; Oh, J.; Kim, K. M.; Cheon, G. J.; Chang, Y.; Yoo, J.; Cheon, J. *Angew. Chem. Int. Ed.* **2008**, *47*, 6259.
(122)   Raylman, R. R.; Majewski, S.; Sendhil Velan, S.; Lemieux, S.; Kross, B.; Popov, V.; Smith, M. F.; Weisenberger, A. G. *J. Magn. Reson.* **2007**, *186*, 305.
(123)   Raylman, R. R.; Majewski, S.; Lemieux, S.; Velan, S. S.; Kross, B.; Popov, V.; Smith, M. F.; Weisenberger, A. G.; Wojcik, R. *Nucl. Instr. Meth. Phys. Res. Sect. A* **2006**, *569*, 306.
(124)   Judenhofer, M. S.; Catana, C.; Swann, B. K.; Siegel, S. B.; Jung, W.-I.; Nutt, R. E.; Cherry, S. R.; Claussen, C. D.; Pichler, B. J. *Radiology* **2007**, *244*, 807.
(125)   Lerche, C. W.; Mackewn, J.; Goldschmidt, B.; Salomon, A.; Gebbhardt, P.; Weissler, B.; Ayres, R.; Marsden, P.; Schulz, V. *Nucl. Instr. Meth. Phys. Res. Sect. A* **2013**, *702*, 50.
(126)   Lindoy, L. F. *The Chemistry of Macrocyclic Ligand Complexes*; Cambridge University Press, 1990.
(127)   Cabbiness, D. K.; Margerum, D. W. *J. Am. Chem. Soc.* **1969**, *91*, 6540.
(128)   Fani, M.; Del, P. L.; Abiraj, K.; Mansi, R.; Tamma, M. L.; Cescato, R.; Waser, B.; Weber, W. A.; Reubi, J. C.; Maecke, H. R. *J. Nucl. Med.* **2011**, *52*, 1110.
(129)   Blom, E.; Velikyan, I.; Monazzam, A.; Razifar, P.; Nair, M.; Razifar, P.; Vanderheyden, J.-L.; Krivoshein, A. V.; Backer, M.; Backer, J.; Langstroem, B. *J. Labelled Compd. Radiopharm.* **2011**, *54*, 685.
(130)   Anderson, C. J.; Welch, M. J. *Chem. Rev.* **1999**, *99*, 2219.
(131)   Eberlein, U.; Lassmann, M. *Appl. Radiat. Isot.* **2013**, *76*, 70.
(132)   Decristoforo, C.; Pickett, R. D.; Verbruggen, A. *Eur J Nucl Med Mol Imaging* **2012**, *39 Suppl 1*, S31.

(133)   Lewis, J. S.; Laforest, R.; Buettner, T. L.; Song, S. K.; Fujibayashi, Y.; Connett, J. M.; Welch, M. J. *Proc. Natl. Acad. Sci. U. S. A.* **2001**, *98*, 1206.

(134)   Obata, A.; Kasamatsu, S.; Lewis, J. S.; Furukawa, T.; Takamatsu, S.; Toyohara, J.; Asai, T.; Welch, M. J.; Adams, S. G.; Saji, H.; Yonekura, Y.; Fujibayashi, Y. *Nucl. Med. Biol.* **2005**, *32*, 21.

(135)   Liu, S. *Adv. Drug Del. Rev.* **2008**, *60*, 1347.

(136)   Xiques Castillo, A.; Perez-Malo, M.; Isaac-Olive, K.; Mukhallalati, H.; Casanova Gonzalez, E.; Torres Berdeguez, M.; Cornejo Diaz, N. *Nucl. Med. Biol.* **2010**, *37*, 935.

(137)   Barker, H. A.; Smyth, R. D.; Weissbach, H.; Toohey, J. I.; Ladd, J. N.; Volcani, B. E. *J. Biol. Chem.* **1960**, *235*, 480.

(138)   Demirayak, S.; Kayagil, I.; Yurttas, L. *Eur. J. Med. Chem.* **2011**, *46*, 411.

(139)   Boiani, M.; Gonzalez, M. *Mini-Rev. Med. Chem.* **2005**, *5*, 409.

(140)   Ozden, S.; Atabey, D.; Yildiz, S.; Goker, H. *Biorg. Med. Chem.* **2005**, *13*, 1587.

(141)   Njoya, Y.; Boufatah, N.; Gellis, A.; Rathelot, P.; Crozet, M. P.; Vanelle, P. *Heterocycles* **2002**, *57*, 1423.

(142)   Charton, J.; Girault-Mizzi, S.; Debreu-Fontaine, M. A.; Foufelle, F.; Hainault, I.; Bizot-Espiard, J. G.; Caignard, D. H.; Sergheraert, C. *Biorg. Med. Chem.* **2006**, *14*, 4490.

(143)   Sparke, A. E.; Fisher, C. M.; Mewis, R. E.; Archibald, S. J. *Tetrahedron Lett.* **2010**, *51*, 4723.

(144)   Dubey, P. K.; Prasada Reddy, P. V. V.; Srinivas, K. *J. Heterocycl. Chem.* **2010**, *47*, 1317.

(145)   Shi, Z.; Thummel, R. P. *J. Org. Chem.* **1995**, *60*, 5935.

(146)   Sheng, C.; Che, X.; Wang, W.; Wang, S.; Cao, Y.; Yao, J.; Miao, Z.; Zhang, W. *Eur. J. Med. Chem.* **2011**, *46*, 1706.

(147)   Indusegaram, S.; Katsifis, A. G.; Ridley, D. D.; Vonwiller, S. C. *Aust. J. Chem.* **2003**, *56*, 819.

(148)   Thomas, A. P.; Allott, C. P.; Gibson, K. H.; Major, J. S.; Masek, B. B.; Oldham, A. A.; Ratcliffe, A. H.; Roberts, D. A.; Russell, S. T.; Thomason, D. A. *J. Med. Chem.* **1992**, *35*, 877.

(149)   Goker, H.; Kus, C.; Boykin, D. W.; Yildiz, S.; Altanlar, N. *Bioorg. Med. Chem.* **2002**, *10*, 2589.

(150)   Lin, S.-Y.; Isome, Y.; Stewart, E.; Liu, J.-F.; Yohannes, D.; Yu, L. *Tetrahedron Lett.* **2006**, *47*, 2883.

(151)   Sparke, A. E. 'PhD thesis', University of Hull, 2008.

(152)   Weisman, G. R.; Ho, S. C. H.; Johnson, V. *Tetrahedron Lett.* **1980**, *21*, 335.

(153)   Rohovec, J.; Gyepes, R.; Cisarova, I.; Rudovsky, J.; Lukes, I. *Tetrahedron Lett.* **2000**, *41*, 1249.

(154)   Dadabhoy, A.; Faulkner, S.; Sammes, P. G. *J. Chem. Soc., Perkin Trans. 2* **2002**, 348.

(155)   Jagadish, B.; Brickert-Albrecht, G. L.; Nichol, G. S.; Mash, E. A.; Raghunand, N. *Tetrahedron Lett.* **2011**, *52*, 2058.

(156)   Fisher, C. M. 'PhD thesis', University of Hull, 2005.

(157)   Mishra, A. K.; Draillard, K.; FaivreChauvet, A.; Gestin, J. F.; Curtet, C.; Chatal, J. F. *Tetrahedron Lett.* **1996**, *37*, 7515.

(158)   Nwe, K.; Richard, J. P.; Morrow, J. R. *Dalton Trans.* **2007**, 5171.

(159)   Lalancet.Jm; Lalibert.M; Brindle, J. R.; Freche, A. *Synthesis* **1972**, 526.

(160)   Ferreira, C. L.; Lamsa, E.; Woods, M.; Duan, Y.; Fernando, P.; Bensimon, C.; Kordos, M.; Guenther, K.; Jurek, P.; Kiefer, G. E. *Bioconjug. Chem.* **2010**.

(161)   Velikyan, I.; Lendvai, G.; Valila, M.; Roivainen, A.; Yngve, U.; Bergstrom, M.; Langstrom, B. *J. Labelled Compd. Radiopharm.* **2004**, *47*, 79.

(162)   Velikyan, I.; Beyer, G. J.; Langstrom, B. *Bioconj. Chem.* **2004**, *15*, 554.

(163)   Chakravarty, R.; Chakraborty, S.; Dash, A.; Pillai, M. R. A. *Nucl. Med. Biol.* **2013**, *40*, 197.

(164)   Welch, M. J.; Hawker, C. J.; Wooley, K. L. *J. Nucl. Med.* **2009**, *50*, 1743.

(165)   Liu, Y. J.; Welch, M. J. *Bioconj. Chem.* **2012**, *23*, 671.

(166)   Jarrett, B. R.; Gustafsson, B.; Kukis, D. L.; Louie, A. Y. *Bioconj. Chem.* **2008**, *19*, 1496.

(167)   Glaus, C.; Rossin, R.; Welch, M. J.; Bao, G. *Bioconj. Chem.* **2010**, *21*, 715.

(168)   Patel, D.; Kell, A.; Simard, B.; Xiang, B.; Lin, H. Y.; Tian, G. H. *Biomaterials* **2011**, *32*, 1167.

(169)   Lee, H.-Y.; Li, Z.; Chen, K.; Hsu, A. R.; Xu, C.; Xie, J.; Sun, S.; Chen, X. *J. Nucl. Med.* **2008**, *49*, 1371.

(170)   Xie, J.; Chen, K.; Huang, J.; Lee, S.; Wang, J. H.; Gao, J.; Li, X. G.; Chen, X. Y. *Biomaterials* **2010**, *31*, 3016.

(171)   Yang, X. Q.; Hong, H.; Grailer, J. J.; Rowland, I. J.; Javadi, A.; Hurley, S. A.; Xiao, Y. L.; Yang, Y. A.; Zhang, Y.; Nickles, R.; Cai, W. B.; Steeber, D. A.; Gong, S. Q. *Biomaterials* **2011**, *32*, 4151.

(172)   de Rosales, R. T. M.; Tavare, R.; Paul, R. L.; Jauregui-Osoro, M.; Protti, A.; Glaria, A.; Varma, G.; Szanda, I.; Blower, P. J. *Angew. Chem. Int. Ed.* **2011**, *50*, 5509.

(173)   Stelter, L.; Pinkernelle, J. G.; Michel, R.; Schwartlaender, R.; Raschzok, N.; Morgul, M. H.; Koch, M.; Denecke, T.; Ruf, J.; Baeumler, H.; Jordan, A.; Hamm, B.; Sauer, I. M.; Teichgraeber, U. *Mol. Imag. Biol.* **2010**, *12*, 25.

(174)   Barreto, J. A.; Matterna, M.; Graham, B.; Stephan, H.; Spiccia, L. *New J. Chem.* **2011**, *35*, 2705.

(175)   Hao, R.; Xing, R. J.; Xu, Z. C.; Hou, Y. L.; Gao, S.; Sun, S. H. *Adv. Mater.* **2010**, *22*, 2729.

(176)   Selvan, S. T.; Patra, P. K.; Ang, C. Y.; Ying, J. Y. *Angew. Chem. Int. Ed.* **2007**, *46*, 2448.

(177)   Gao, J. H.; Gu, H. W.; Xu, B. *Acc. Chem. Res.* **2009**, *42*, 1097.

(178)   Butterworth, M. D.; Illum, L.; Davis, S. S. *Colloids Surf., A* **2001**, *179*, 93.

(179)   Molday, R. S.; Mackenzie, D. *J. Immunol. Methods* **1982**, *52*, 353.

(180)   Torborg, C.; Hughes, D. D.; Buckle, R.; Robinson, M. W. C.; Bagley, M. C.; Graham, A. E. *Synth. Commun.* **2008**, *38*, 205.

(181)   Garcia-Vidal, J. A.; Duran-Valle, C. J.; Ferrera-Escudero, S. *Appl. Surf. Sci.* **2006**, *252*, 6064.

(182)   Zhao, G.; Wang, B.; Yang, W.; Ren, H. *Eur. J. Org. Chem.* **2012**, *2012*, 6236.

(183)   Boswell, C. A.; Sun, X.; Niu, W.; Weisman, G. R.; Wong, E. H.; Rheingold, A. L.; Anderson, C. J. *J. Med. Chem.* **2004**, *47*, 1465.

(184)   Silversides, J. D.; Allan, C. C.; Archibald, S. J. *Dalton Trans.* **2007**, 971.

(185)   Smith, R.; Huskens, D.; Daelemans, D.; Mewis, R. E.; Garcia, C. D.; Cain, A. N.; Freeman, T. N. C.; Pannecouque, C.; De, C. E.; Schols, D.; Hubin, T. J.; Archibald, S. J. *Dalton Trans.* **2012**, *41*, 11369.

(186)   Stasiuk, G. J.; Smith, H.; Wylezinska-Arridge, M.; Tremoleda, J. L.; Trigg, W.; Luthra, S. K.; Iveson, V. M.; Gavins, F. N. E.; Long, N. J. *Chem. Commun.* **2013**, *49*, 564.

(187)   Li, C.; Wong, W.-T. *Tetrahedron Lett.* **2004**, *45*, 6055.

(188)   Kalow, J. A.; Doyle, A. G. *J. Am. Chem. Soc.* **2011**, *133*, 16001.

(189)   Surendra, K.; Krishnaveni, N. S.; Nageswar, Y.; Rao, K. R. *Synth. Commun.* **2005**, *35*, 2195.

(190)   Portet, D.; Denizot, B.; Rump, E.; Lejeune, J. J.; Jallet, P. *J. Colloid Interface Sci.* **2001**, *238*, 37.

(191)   Shafi, K.; Ulman, A.; Yan, X. Z.; Yang, N. L.; Estournes, C.; White, H.; Rafailovich, M. *Langmuir* **2001**, *17*, 5093.

(192)   Lalatonne, Y.; Paris, C.; Serfaty, J. M.; Weinmann, P.; Lecouvey, M.; Motte, L. *Chem. Commun.* **2008**, 2553.

(193)   de Rosales, R. T. M.; Tavare, R.; Glaria, A.; Varma, G.; Protti, A.; Blower, P. J. *Bioconj. Chem.* **2011**, *22*, 455.

(194)   Delgado, R.; Figueira, M. D.; Quintino, S. *Talanta* **1997**, *45*, 451.

(195)   Sandiford, L.; Phinikaridou, A.; Protti, A.; Meszaros, L. K.; Cui, X.; Yan, Y.; Frodsham, G.; Williamson, P. A.; Gaddum, N.; Botnar, R. M.; Blower, P. J.; Green, M. A.; de Rosales, R. T. M. *ACS Nano* **2013**, *7*, 500.

(196)   Harris, W. R.; Pecoraro, V. L. *Biochemistry* **1983**, *22*, 292.

(197)   Choi, H. S.; Liu, W.; Misra, P.; Tanaka, E.; Zimmer, J. P.; Ipe, B. I.; Bawendi, M. G.; Frangioni, J. V. *Nat. Biotechnol.* **2007**, *25*, 1165.

(198)   Chen, L. T.; Weiss, L. *Blood* **1973**, *41*, 529.

(199)   Gerion, D.; Herberg, J.; Bok, R.; Gjersing, E.; Ramon, E.; Maxwell, R.; Kurhanewicz, J.; Budinger, T. F.; Gray, J. W.; Shuman, M. A.; Chen, F. F. *J. Phys. Chem. C* **2007**, *111*, 12542.

(200)   Chong, H.-S.; Song, H. A.; Ma, X.; Milenic, D. E.; Brady, E. D.; Lim, S.; Lee, H.; Baidoo, K.; Cheng, D.; Brechbiel, M. W. *Bioconj. Chem.* **2008**, *19*, 1439.

(201)   Sharkey, R. M.; Mottahennessy, C.; Gansow, O. A.; Brechbiel, M. W.; Fand, I.; Griffiths, G. L.; Jones, A. L.; Goldenberg, D. M. *Int. J. Cancer* **1990**, *46*, 79.

(202) Chong, H. S.; Garmestani, K.; Ma, D. S.; Milenic, D. E.; Overstreet, T.; Brechbiel, M. W. *J. Med. Chem.* **2002**, *45*, 3458.
(203) Clifford, T.; Boswell, C. A.; Biddlecombe, G. B.; Lewis, J. S.; Brechbiel, M. W. *J. Med. Chem.* **2006**, *49*, 4297.
(204) Wei, L.; Zhang, X.; Gallazzi, F.; Miao, Y.; Jin, X.; Brechbiel, M. W.; Xu, H.; Clifford, T.; Welch, M. J.; Lewis, J. S.; Quinn, T. P. *Nucl. Med. Biol.* **2009**, *36*, 345.
(205) Palm, S.; Enmon, R. A.; Matei, C.; Kolbert, K. S.; Xu, S.; Zanzonico, P. B.; Finn, R. L.; Koutcher, J. A.; Larson, S. M.; Sgouros, G. *J. Nucl. Med.* **2003**, *44*, 1148.
(206) Deshpande, S. V.; Denardo, S. J.; Kukis, D. L.; Moi, M. K.; McCall, M. J.; Denardo, G. L.; Meares, C. F. *J. Nucl. Med.* **1990**, *31*, 473.
(207) Jamar, F.; Barone, R.; Mathieu, I.; Walrand, S.; Labar, D.; Carlier, P.; de Camps, J.; Schran, H.; Chen, T.; Smith, M. C.; Bouterfa, H.; Valkema, R.; Krenning, E. P.; Kvols, L. K.; Pauwels, S. *Eur. J. Nucl. Med. Mol. Imag.* **2003**, *30*, 510.
(208) Illidge, T. M.; Brock, S. *Curr. Pharm. Des.* **2000**, *6*, 1399.
(209) Khodjibekova, M.; Szyszko, T.; Khan, S.; Nijran, K.; Tait, P.; Al-Nahhas, A. *Reviews on recent clinical trials* **2007**, *2*, 212.
(210) Wiseman, G. A.; White, C. A.; Stabin, M.; Dunn, W. L.; Erwin, W.; Dahlbom, M.; Raubitschek, A.; Karvelis, K.; Schultheiss, T.; Witzig, T. E.; Belanger, R.; Spies, S.; Silverman, D. H. S.; Berlfein, J. R.; Ding, E.; Grillo-Lopezs, A. J. *Eur. J. Nucl. Med.* **2000**, *27*, 766.
(211) Beeby, A.; Bushby, L. M.; Maffeo, D.; Williams, J. A. G. *J. Chem. Soc., Dalton Trans.* **2002**, 48.
(212) El, M. A.; Cadiou, C.; Dechamps-Olivier, I.; Chuburu, F.; Aplincourt, M. *Eur. J. Inorg. Chem.* **2007**, 5087.
(213) El, M. A.; Cadiou, C.; Dechamps-Olivier, I.; Chuburu, F.; Aplincourt, M.; Tinant, B. *Inorg. Chim. Acta* **2009**, *362*, 1169.
(214) Sinha, H. K.; Dogra, S. K. *Spectrochim. Acta Mol. Biomol. Spectros.* **1985**, *41*, 961.
(215) Krishnamurthy, M.; Phaniraj, P.; Dogra, S. K. *J. Chem. Soc. Perk. Trans. 2* **1986**, 1917.
(216) Cacheris, W. P.; Nickle, S. K.; Sherry, A. D. *Inorg. Chem.* **1987**, *26*, 958.
(217) Sherry, A. D.; Ren, J.; Huskens, J.; Brucher, E.; Toth, E.; Geraldes, C.; Castro, M.; Cacheris, W. P. *Inorg. Chem.* **1996**, *35*, 4604.
(218) Idee, J.-M.; Port, M.; Raynal, I.; Schaefer, M.; Le Greneur, S.; Corot, C. *Fundam. Clin. Pharmacol.* **2006**, *20*, 563.
(219) Kumar, K.; Chang, C. A.; Francesconi, L. C.; Dischino, D. D.; Malley, M. F.; Gougoutas, J. Z.; Tweedle, M. F. *Inorg. Chem.* **1994**, *33*, 3567.
(220) Beeby, A.; Botchway, S. W.; Clarkson, I. M.; Faulkner, S.; Parker, A. W.; Parker, D.; Williams, J. A. G. *J. Photochem. Photobiol. B* **2000**, *57*, 83.
(221) Lowe, M. P.; Parker, D.; Reany, O.; Aime, S.; Botta, M.; Castellano, G.; Gianolio, E.; Pagliarin, R. *J. Am. Chem. Soc.* **2001**, *123*, 7601.
(222) Blair, S.; Lowe, M. P.; Mathieu, C. E.; Parker, D.; Senanayake, P. K.; Kataky, R. *Inorg. Chem.* **2001**, *40*, 5860.
(223) Kotek, J.; Rudovsky, J.; Hermann, P.; Lukes, I. *Inorg. Chem.* **2006**, *45*, 3097.
(224) Liu, S.; Pietryka, J.; Ellars, C. E.; Edwards, D. S. *Bioconj. Chem.* **2002**, *13*, 902.
(225) Keire, D. A.; Kobayashi, M. *Bioconj. Chem.* **1999**, *10*, 454.
(226) Lumata, L.; Merritt, M.; Malloy, C.; Sherry, A. D.; Kovacs, Z. *Appl. Magn. Reson.* **2012**, *43*, 69.
(227) Heppeler, A.; Froidevaux, S.; Macke, H. R.; Jermann, E.; Behe, M.; Powell, P.; Hennig, M. *Chem. Eur. J.* **1999**, *5*, 1974.
(228) Aime, S.; Botta, M.; Ermondi, G. *Inorg. Chem.* **1992**, *31*, 4291.
(229) Woods, M.; Aime, S.; Botta, M.; Howard, J. A. K.; Moloney, J. M.; Navet, M.; Parker, D.; Port, M.; Rousseaux, O. *J. Am. Chem. Soc.* **2000**, *122*, 9781.
(230) Bradley, D.; Williams, G.; Lawton, M. *J. Org. Chem.* **2010**, *75*, 8351.
(231) Ma, M.; Zhang, Y.; Yu, W.; Shen, H. Y.; Zhang, H. Q.; Gu, N. *Colloids Surf., A* **2003**, *212*, 219.